GENERATION OF Eμ-PKCβII TRANSGENIC MICE FOR THE STUDY OF CHRONIC LYMPHOCYTIC LEUKAEMIA (CLL)

Thesis submitted in accordance with the requirements of the University of Liverpool for the degree of Doctor in Philosophy

By

Ali Anvari Azar

Dedication

I dedicate my doctoral dissertation to my parents for their financial and moral supports, for their unconditional devotion, and also to my soul mate Flora for her love and endless patience.

Abstract

The malignant cells of chronic lymphocytic leukemia (CLL) over-express PKCβII, a feature pathogenically important because the TCL1 mouse model of CLL fails to develop disease when PKCβ expression is disrupted. The purpose of this project was to generate transgenic mice in which PKCβII is over-expressed only in B cells. The central hypothesis of this thesis was that over-expression of PKCβII in developing B cells will shift development to favour the generation of the B-1 and MZ B cell populations and eventually lead to the development of a CLL-like disease in the mouse. To construct the expression plasmid, an Eμ promoter was used to direct B cell-specific expression of PKCβII in transgenic mice (Eμ-PKCβII tg mice). PKCβII was tagged with haemagglutination antigen (HA) for identification in Western blots and immunohistochemistry (IHC). Also, mCherry was integrated within the expression plasmid construct in order to visualize transgenic B cells. Over-expressed PKCβII and mCherry fluorescence were detected when this plasmid was tested in A20 cells, a mouse B lymphoma cell line. The construct was then injected into pro-nuclei of fertilized ova isolated from pregnant mice. The injected ova were then transferred to recipient mice to generate potential founder mice. Sequential crossings of transgenic litters born from a single founder mouse led to the generation of homozygous Eμ-PKCβII tg mice. In the spleen of Eμ-PKCβII tg mice, the expression of the transgenic PKCβIIHA was detected and quantification of PKCβII, using Western blotting, showed that PKCβII was over-expressed in Eμ-PKCβII tg mice compared with wild type mice. However, the mCherry could not be detected; this might be due to the fact that expression of the secondary gene(in this case mCherry) was not always efficient because of variable transcription from the IRES sequence. IHC analysis of the spleen of Eμ-PKCβII tg mice confirmed the expression of PKCβIIHA in B cell-rich tissues where the staining for either HA or for PKCβII showed the high expression of these proteins in the white pulp of the spleen specifically to the follicular region. There was no notable development of disease, CLL-like or otherwise in aged Eμ-PKCβII tg mice, but Flow cytometry analysis pointed out that the over-expression of PKCβII resulted in a reduction in the proportion of

follicular B cells and an increase in the proportion of MZ B cells in the spleen, and in B-1 cells in peritoneum and periphery of Eμ-PKCβII tg mice. This expansion of MZ B cells in the spleen was confirmed by H&E stains showing an enlarged marginal zone within the structure of the spleen, and IgM stains showed that this expanded MZ consists mainly of IgM^+ cells. Thus, the generation of a mouse that over-expresses PKCβII specifically within the B cell compartment led to an expansion in the populations of IgM^+ B cells (MZ and B-1 B cells) and a reduction of follicular (mature) B cells. This mouse may be useful for the study of human CLL because of the potential to accelerate disease progression, and would therefore serve as a useful model for drug testing.

Acknowledgments

Firstly, I would like to express my sincere appreciation to my supervisors Dr. Joseph R. Slupsky and Dr. Nikolina Vlatković for their help and supports through my tough journey that I have had during my PhD study. Nikolina has given me a continuous technical support in generation of Eμ-PKCβII tg mice including construction of the expression plasmid and animal screening. Joe has given me an immense support in helping me to improve my scientific writing skill as well as giving me the technical support in designing an appropriate strategy in phenotyping the Eμ-PKCβII tg mice. Surely, I would not been possible to complete this project without their help and supports.

I would also like to thank all the members of the Division of Haematology in the University of Liverpool who have been very generous to extend their help at various phases of my PhD degree, therefore I deeply appreciate them. Finally, I want to extend my especial thanks to Dr. Kathy Till for her guidance particularly in performing Immunohistochemistry (IHC).

Declaration

The work presented in this Thesis is a result of my own work performed during my PhD course between December 2009 and August 2013, apart from pro-nuclei microinjection of transgene into mouse zygotes and subsequent transfer of the injected zygotes into recipient mice to generate potential founder mice, which were performed by Dr. Nikolina Vlatković.

Ali A. Azar

October 2011

Table of contents

List of tables

List of Figures

Abbreviations

µg: Microgram (10-6 grams)

µL: Micro-litre (10-6 litre)

µM: Micro-molar (10-6 molar)

AGC: Super family:

APC: Allophycocyanin

APC-cy7: Allophycocyanin conjugated with cyanine 7 dyes

ALL: Acute lymphocytic leukaemia

AGM: Aorta Gonad Mesonephros

APRIL: A ProlifeRation Inducing Ligand

ATP: Adenosine triphosphate

BAFF: B-cell activating factor

Bcl-2: B-cell lymphoma 2

Bcl-10: B-cell lymphoma 10

BCR: B cell antigen receptor

BLAST: Basic local alignment search tool

BM: Bone marrow

BSA: Bovine serum albumin

Btk: Bruton's tyrosine kinase

CARMA-1: CARD-containing MAGUK protein 1

CD: Cluster of differentiation

CDR3: Complementary-determining regions

CLL: Chronic lymphocytic leukaemia

CLP: Common lymphoid progenitor

CMP: Common myeloid progenitor

CMV: Cytomegalovirus

CT: Control (in labeling the non-littermate wild type control mice)

CT: Threshold cycle

CTP: Cytidine triphosphate

DAB: 3, 3-Diaminobenzidine

DAG: Diacylglycerol

DLBCL: Diffuse large B cell lymphoma

DLEU-2: Deleted In Lymphocytic Leukemia 2

DMEM: Dulbecco's modified Eagle's medium

DNA: Deoxyribonucleic acid

ECL: Enhanced chemi-luminescence

E. coli: *Escherichia coli*

EDTA: Ethylenediaminetetraacetic acid

EGFP: Enhanced Green Fluorescent Protein

ERK: Extracellular signal-regulated kinases

FACS: Fluorescence activated cell sorter

FCS: Fetal calf serum

FITC: Fluorescein isothiocyanate

FO: Follicular

***gapdh*:** Glyceraldehyde 3-phosphate dehydrogenase

GC: Germinal centre

GFP: Green fluorescent protein

GSK3β: Ogen synthase kinase 3β

GTP: Guanosine triphosphate

HA: Influenza hemagglutinin

HBB: HbA-Sen50 beta globin

HCG: Human chorionic gonadotropin

Het: Heterozygous

H&E: Haematoxylin and eosin

HRP: Horseradish peroxidase

Hom: Homozygous

HSCs: Haematopoietic stem cells

HSP90: Heat shock protein 90

KO: Knock out

IHC: Immunohistochemistry

IgG: Immunoglobulin G

IgHV: Variable region of immunoglobulin heavy chain

IgM: Immunoglobulin M

IKK: IκB kinase

IL-7: Interleukin 7

IP3: Inositol-1, 4, 5-triphosphate

IRES: Internal ribosome entry site

JNK: Jun N-terminal kinase

LB: Lysogeny broth

MALT1: Mucosa-associated lymphoid tissue lymphoma translocation protein 1

MAPK: Mitogen activated protein kinase

Mcl-1: Induced myeloid leukemia cell differentiation protein

MSC: multiple cloning sites

M-CLL: Mutated CLL

miR-29: mir-29 microRNA

MDR-KO: Minimal deleted region

mRNA: Messenger Ribonucleic Acid

MZB: Marginal zone B

NFAT: Nuclear factor of activated T cells

NFκB: Nuclear factor κ B

dNTP: Deoxyribonucleotide triphosphate)

PAGE: Polyacrylamide gel electrophoresis

PALS: Peri-arteriolar lymphoid sheath

PB: peripheral blood

PBS: Phosphate buffered saline

PCI: phenol/chloroform/isoamyl alcohol

PCR: Polymerase chain reaction

PDK-1: catalyzed by 3-phosphoinositide-dependent kinase-1

PE: peritoneum

PE: phycoerytherin

PH domain: Pleckstrin homology domain

PHLPP: PH domain leucine-rich repeat protein phosphatases

PI3K: Phosphatidylinositide 3-kinases

PIP2: Phosphatidylinositol 4, 5-bisphophate

PIP3: Phosphatidylinositol-3, 4, 5- trisphosphate

PKC: Protein kinase C

PKCβ: Protein kinase Cβ

PLCγ-2: Phospholipase C-γ2

PMA: Phorbol 12-myristate 13-acetate

PMSG: Pregnant Mare's Serum Gonadotropin

PS: Pseudo-substrate

PVDF: Polyvinylidene fluoride

RT-PCR: Real time PCR

RAG: Recombination activating gene

RelA :v-rel avian reticuloendotheliosis viral oncogene homolog A

RPMI 1641: Roswell Park Memorial Institute 1641

RT: Room temperature

SDS: Sodium dodecyl sulphate

SDS-PAGE: Sodium dodecyl sulphate-polyacrylamide gel electrophoresis

sIgM: Surface IgM

SOC: Super Optimal broth with Catabolite repression

sp: spleen

SSC: Saline-sodium citrate

STAT3: Signal transducer and activator of transcription 3

T-1 B cells: transitional type-1 B cells

TAK1:TGF-beta activated kinase 1

TBS-T: Tris-Buffered Saline and Tween 20

TD: T cell dependent,

TI: T cell independent

tg: transgenic

TNF: Tumor necrosis factors

TRAF-2: TNF receptor associated factor-2

TTP: Thymidine triphosphate

v-d-j: variable (v), diversity (d) and joining (j) region

W: water

WB: Western blotting

WCL: Whole cell lysate

WT: Wild type

XIAP:X-linked inhibitor of apoptosis protein

XID: X-linked immunodeficiency

XLA: X-linked agammaglobulinemia

ZAP70: Zeta-chain-associated protein kinase 70

1 Chapter I: Introduction

1.1 Importance of CLL

Chronic lymphocytic leukaemia (CLL) is considered to be the most common adult leukaemia (Zwiebel and Cheson 1998); it is defined as the proliferation of malignant B lymphocytes with mature appearance in blood and lymphoid organs (Zenz*, et al* 2010). CLL cells are clonal in nature, and fail to undergo terminal differentiation into antibody-secreting cells. Nevertheless, CLL is a heterogeneous disease with respect to disease progression; where some patients have progressive disease while others have indolent disease (Rodriguez-Vicente*, et al* 2013). Many factors are involved in disease pathogenesis of CLL such as genomic aberrations, epigenetic modifications, gene mutations, and deregulated micro-RNA (Zenz*, et al* 2010). In addition, there is defective function in T, NK (natural killer) and dendritic cells in CLL patients, and this leads to the development of hypo-gammaglobulinemia and progressive immunodeficiency.

All CLL cells carry the surface membrane phenotype of antigen experienced ($CD27^+$) and activated ($CD23^+$, $CD25^+$, $CD69^+$, $CD71^+$) B cells. However, CLL cells express much lower levels of surface membrane immunoglobulin and CD19 than do normal B cells. Gene expression analysis shows that CLL cells are more closely related to memory than to naive B cells (Damle*, et al* 2002), and these cells also express CD5 which is an antigen typically expressed by T cells (Seifert and Kuppers 2009). More recently, further gene analysis has revealed that CLL cells originate from a post-germinal centre B cell subset that was previously unrecognized and bore CD5 and CD27 (Seifert*, et al* 2012).

CLL can be subdivided into progressive versus indolent disease (Damle*, et al* 1999). Although there are many methods that can be used to predict disease outcome in CLL, possibly the most powerful and reliable means remains determination of the degree of somatic hyper mutation within the variable regions of the immunoglobulin (Ig) heavy chain (IGHV) genes expressed in the malignant cells. Thus, patients where the IGHV genes retain the germ line sequence, or less than 2% mutational deviation from germ line sequence (so-called un-mutated CLL or U-CLL) generally have a poorer outcome than those patients having IGHV genes containing greater than 2% mutational

deviation (so-called mutated CLL or M-CLL)(Hamblin*, et al* 1999). This relationship between antigen-receptor structure and disease outcome in CLL has an important consequence. Studies have shown that the antigen-binding region of the B cell receptor (BCR) on CLL cells from U-CLL patients has a broader specificity than that of the BCR on CLL cells from M-CLL patients. Thus, interaction with antigen is thought to have a major role in clonal survival and expansion of the malignant clone in U-CLL, and this has become a paradigm of CLL pathogenesis (Stevenson and Caligaris-Cappio 2004).

An additional consideration comes from studies investigating the differences in signals mediated by BCR engagement between M- and U-CLL clones. The signals in M-CLL clones are much weaker than those observed in U-CLL clones. This may be due to the presence of proteins that enhance the BCR signal. For example, expression of tyrosine kinase zeta-associated protein 70 (ZAP-70) is mainly associated with U-CLL clones, and is therefore considered to be a surrogate marker of Ig mutational status (Wiestner*, et al* 2003). More importantly, the presence of this protein within CLL cells has been shown to enhance BCR signaling through a mechanism that is independent of its kinase activity. Thus, the association of ZAP70 expression and poor disease prognosis supports the role of BCR signals in CLL pathogenesis. The initiation of BCR downstream signaling in CLL leads to up-regulation of the anti-apoptotic protein Mcl-1 which has crucial role in survival of CLL cells (Chen*, et al* 2005).

Whether CLL is progressive or indolent, the disease is presently incurable using conventional chemotherapeutic therapies (Binet*, et al* 1977). When the disease is indolent a “watch and wait” approach is taken because the application of therapy here can be worse than the disease itself (Chiorazzi*, et al* 2005). The median life expectancy of CLL patients with indolent disease ranges from 8 to 12 years, and in patients with progressive disease the median life expectancy is much shorter. Therapeutic strategy in CLL mainly focuses on controlling the disease symptoms (Rozman and Montserrat 1995), and current therapy for this disease is based on the use of cytotoxic chemotherapy with agents such as Chlorambucil (alkylating agent) and Fludarabine (purine analogue). These drugs cause apoptosis by inducing DNA damage, but CLL

cells become resistant to these drugs and more aggressive treatment must be used during disease relapse (Rai*, et al* 2000).

1.2 B cell differentiation

In order to understand CLL pathogenesis, an understanding of B cell development is crucial. Figure 1-1 summarizes B cell lineage development.

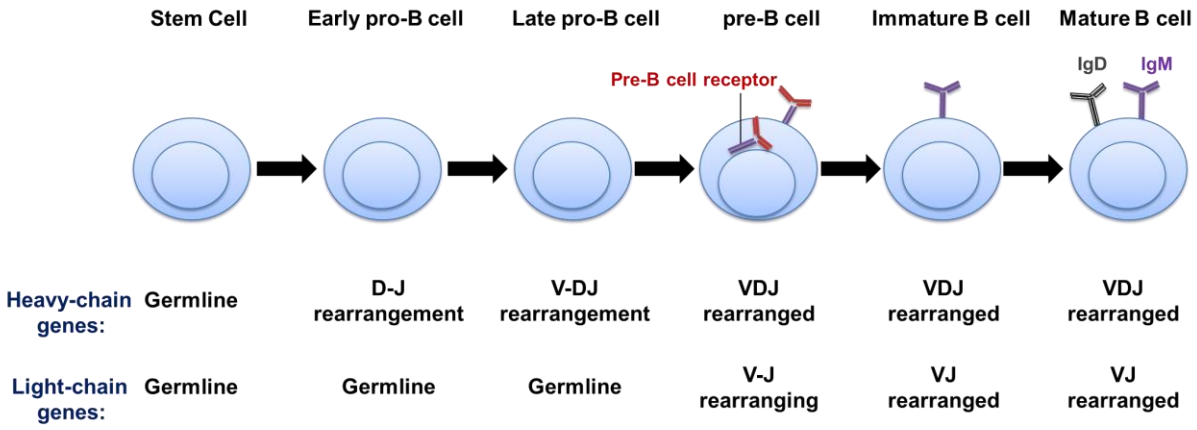

Figure 1-1. The differentiation of hematopoietic progenitor cell into the B-lymphoid lineage; Adapted from (Janeway. 2001). Commitment to B cell differentiation is an irreversible process characterized by activation of the genes regulating expression of the B cell antigen receptor (BCR). These genes include those encoding the µH chain and surrogate L chain of the pre-BCR as well as genes responsible for the rearrangement of the antigen-binding portion of the Ig genes (i.e., RAG-1 and RAG-2).

The development of intra-embryonic from mesenteric cells leads to production of the first haematopoietic progenitor cells called the Hemangioblast. These cells are the common precursor of endothelial and haematopoietic stem cells (HSC) (Munoz-Chapuli*, et al* 1999). HSCs can divide and maintain their stem-cell state of differentiation(Paul 2003). During embryogenesis, HSCs migrate from the Aorta Gonad Mesonephros (AGM) to the foetal liver, thymus, omentum and bone marrow to undergo further differentiation. This localization is based on a specialized program of erythroid, myeloid

or lymphoid differentiation. Haemic cell production continues in these areas until after birth. Within the first four weeks post-partum, the bone marrow becomes the major site of haematopoiesis including B-cell development (Munoz-Chapuli*, et al* 1999). However, recent evidence suggests that B cell development can also take place in the gut lamina propria, and is influenced by microbial colonization(Wesemann*, et al* 2013).

HSCs are responsible for the generation of all haemic cells, the first step of differentiation occurs when these cells form the common lymphoid (CLP) and common myeloid (CMP) progenitor cells. CMP cells then go on to differentiate into the myeloid-derived cells such as megakaryocytic / platelets, neutrophils, monocytes and red blood cells. CLP cells differentiate into lymphoid cells such as natural killer cells, T cells and B cells. The rest of this section is devoted to B cell development (Kondo*, et al* 1997).

In B cell development, each stage of early differentiation represents a change in the immunoglobulin (Ig) genes coding for antibody production (Figure 1-1). CLP cells that express B220 and CD43, but lack expressi3on of HSA and BP-1 are considered to be the earliest B-cell progenitor (Paul 2003). In the presence of Interleukin 7(IL-7), these early B cells give rise to pro-B cells where rearrangement of the variable (v), diversity (d) and joining (j) region genes within the Ig heavy chain initiates (Lee*, et al* 1989). This involves expression of the genes controlling this Ig rearrangement, RAG-1 and RAG-2. When this rearrangement is productive and results in generation of Ig heavy chain protein in combination with surrogate light chains (which serve as templates for Ig light chains and stabilize the Ig heavy chain), pro-B cells then become pre-B cells. At the pre-B cell stage, Ig light chain genes undergo rearrangement to ultimately produce protein that can appropriately combine with Ig heavy chains to construct “good BCRs”. Cells that are able to express good BCRs survive and clonally expand, whereas the cells that are unable to do this undergo apoptosis. In the next step, BCR assemble with the Ig accessory proteins: Igα and Igβ then express on the cell surface as IgM. At this point, pre-B cells become immature B cells. Auto-antigens located in bone marrow interact with surface IgM positive B cells and this plays a crucial role in further differentiation of these cells. Those immature B cells that experience strong stimulation through antigen receptor signaling undergo apoptosis (a process called clonal deletion), those cells that

experience weaker or no interaction with these auto-antigens develop into transitional type-1 B cells (T-1 B cells) that exit the bone marrow and migrate to the spleen where they undergo further development (Hardy and Hayakawa 2001, Paul 2003).

Transitional B cells that enter the spleen localize to the follicle part of the white pulp where they become more responsive to supportive T cell signaling and differentiate to T2 B cells. Here the cells gain surface IgD and CD23. At this point the B cell can experience one of three fates: in the first instance cells that do not experience any stimulation through the BCR undergo apoptosis due to neglect. In the second instance cells that experience strong signals through the BCR, and in conjunction with T cell help within germinal centre further differentiate into antibody-producing plasma cells, or mature memory B cells. Passage through the germinal centre can also stimulate somatic hyper-mutation of Ig gene variable regions through a process called affinity maturation in which antibody affinity to antigen is increased. Also, within germinal centre, the constant region of the Ig heavy chain can undergo a process called class switching from IgM/IgD to IgG, IgA or IgE. The final fate of T2 B cells are marginal zone B cells (MZ B cells). These cells experience low level signals through the BCR, but do not have T cell help. Once MZ B cells become mature they migrate and are retained in the marginal zone of the spleen, and participate in the defence against systemic blood-borne antigens trapped in the spleen. The T2 B cells that experience these fates are known as conventional, or B2 cells. Conventional B cells are considered to be the main B-cell compartment in the adult and mediate adaptive immunity in collaboration with T cells (Carsetti*, et al* 1995, Pillai and Cariappa 2009).

There is another distinct population of B cells known as B-1 cells. These cells can be discriminated from conventional B cells by expression of CD5, which is primarily expressed on T cells, on their surface. B-1 cells locate in pleural cavities and peritoneum, and are responsible for natural antibody secretion (Bos*, et al* 1989, Hardy 2006). Unlike B-2 cells, which have an extremely diverse BCR repertoire that reflects broad usage of v d j gene rearrangement, the BCR on B-1 cells is more restricted and this is reflected in the usage of v d j genes which are typically associated with this B cell

subtype (Hardy 2006). The origin of B1 cells is controversial; in the lineage model, B1 cells arise from the transitional B cells I have so far described and are the result of normal haematopoiesis (Witt*, et al* 2003) (Figure 1-2). In contrast, in the induced differentiation model, B-cell commitment to B1 or B2 occurs during embryogenesis at the point where pro-B cells are generated from the fetal liver progenitor.

Subsequent differentiation of B cells destined to become mature B1 cells is then similar to that of conventional B cells, and the total population is supported by an ability of these cells to self-renew (Hardy and Hayakawa 1991, Lam and Rajewsky 1999). It is important to note that in this model production of B1 cells never switches to the bone marrow. Because the B1 population cannot be easily reconstituted in adult mice, the induced differentiation model of B1 ontogeny is favoured. However, it was recently proposed that the lineage and induced differentiation models of B1 cell development are not mutually exclusive, and that both pathways exist in order to ensure that the B1 population is preserved. The reason why B1 cell production is inhibited within the lineage model is because B1 cells of foetal origin act within adult mice to severely suppress de novo production of B1 cells within the bone marrow (Hardy 2006).

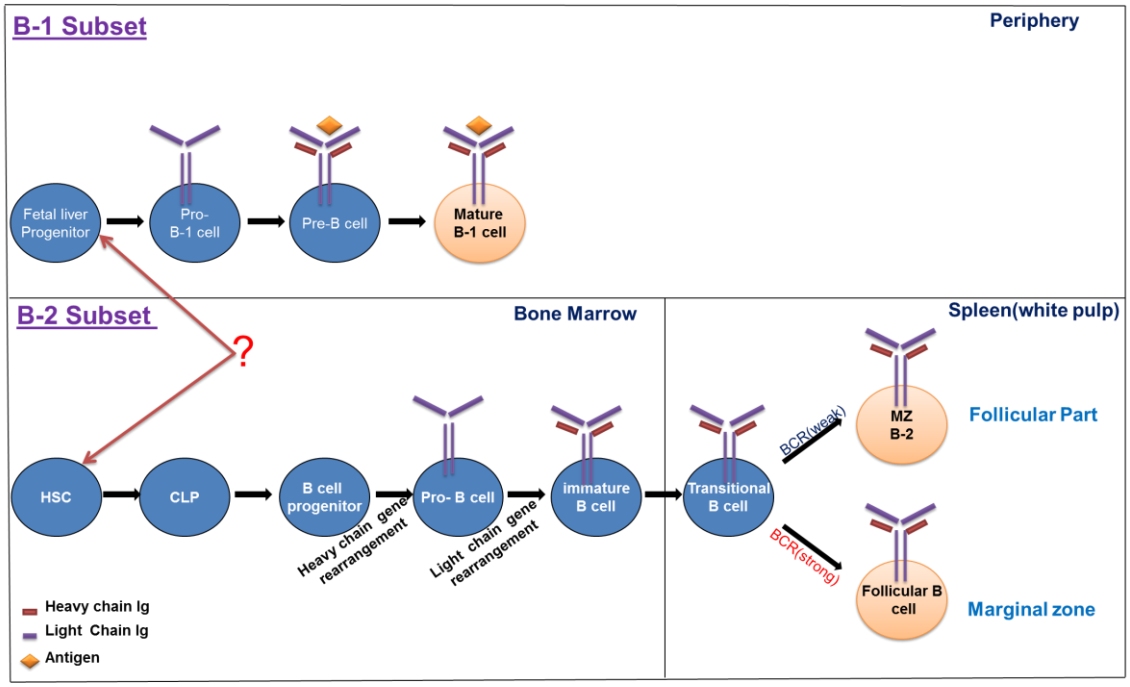

Figure 1-2. Lineage model of differentiation for B-1 and B-2 B cells. The lineage model suggests that B-1 B cells originate from foetal liver progenitor cells during embryogenesis whereas B-2 B cells originate from progenitor cells located in the bone marrow.

B1 cells function in a T cell-independent manner and because of this they bypass the GC reaction in the follicular part of the spleen. B1 cells can be induced to proliferate and differentiate into plasma cells outside the GC microenvironment. This B cell subset is thought to act as a bridge between innate and adaptive immunity, and dysfunction of B-1 cells is associated with auto-immunity and leukaemia (Martin*, et al* 2001).

1.3 CLL origin

The normal B cell that transforms to become a CLL cell has not been characterized. Gene expression analysis of CLL cells show that they have a distinct pattern of gene expression that distinguishes them from the cells of other B cell malignancies. When this pattern is compared with that of normal B cells, it is suggested that CLL cells are more closely related to memory (cells that are antigen-experienced)

than to naive B cells (Klein*, et al* 2001), and to a subset of previously uncharacterized $CD5^{+}CD27^{+}$ B cells (Seifert*, et al* 2012). This observation leads to a principal question: How do CLL cells arise from their normal counterpart?

Do CLL cells arise from single or from multiple cell clones? In the case of CLL originating from a single clone, all genetic events causing the transformation into CLL cells would happen in a distinct subset of B cells at a specific stage of differentiation. If this is the case, genetic changes would occur in a distinct sequence, and would likely follow a standard model of carcinogenesis. If CLL cells arise from multiple clones, genetic lesions can happen in B cells at different stages of development, but the final nature and structure of CLL is determined by a combination of these lesions with exposure to particular factors at particular times to give the transformed cell a growth and survival advantage over other cells. Evidence for this latter model of CLL development has recently come to light. The development and number of CLL-like cells increases with age in adults; such cells are the likely source of the malignant clone. Furthermore, in some patients the presence of multiple CLL-cell clones, each bearing different usage of Ig genes, has been noted. Finally, whole genome analysis of CLL-cell clones indicates that mutations within NOTCH1 and XPO1 are associated with U-CLL whereas mutations in MYD88 and KLHL6 are associated with M-CLL. This could mean that U-CLL and M-CLL are dependent on different signaling pathways for survival (Balatti*, et al* 2012) (Chen*, et al* 2005).

With regard to the normal counterpart of CLL cells, there is much controversy that is likely to arise from our lack of understanding of whether CLL develops from single or multiple clones. Two B cell subtypes have been put forward as likely normal counterparts of CLL; MZ and B1 cells. MZ B cells are antigen experienced and behave in a T cell independent manner (Weill*, et al* 2009). More importantly, the BCR of MZ B cells is known to undergo somatic hyper-mutation the outside germinal centre, and this might explain the genesis of U- and M-CLL (Chiorazzi and Ferrarini 2003). However, MZ B cells do not have quite the same phenotype as CLL cells, particularly with respect to the expression of CD5. With B1 B cells, these cells are phenotypically more similar to CLL than are MZ B cells. These cells express CD5, and the BCR of B1 B cells uses V, D

and J segments and possess complementary-determining regions (CDR3) that are highly similar to those used by CLL cells, particularly U-CLL cells(Messmer*, et al* 2004). However, only 30% of CLL cases carry this stereotypical structure of the BCR (Rossi*, et al* 2013). Furthermore, B1 B cells have only been well characterized in the mouse, and only recently has evidence been generated that potentially establishes a human counterpart (Seifert*, et al* 2012). CD5 positive B cells are known to be present in humans, but the function and nature of these cells needs further characterization (Zenz*, et al* 2010). That CLL cells bear a gene expression profile relating them to human B-1-like B cells provides further evidence for their existence in health and disease. Whether B1 B cells of either human or mouse origin can undergo somatic hyper-mutation of the Ig genes is not known (Fischer*, et al* 1997). Nevertheless, further evidence for a B1 B cell of origin for CLL comes from mouse studies. All of the existing mouse models for CLL-like disease derive from B1 B cells (Oppezzo 2012). Figure 1-3 summarizes the germinal centre reaction and normal B cell counterpart of CLL (Zenz*, et al* 2010).

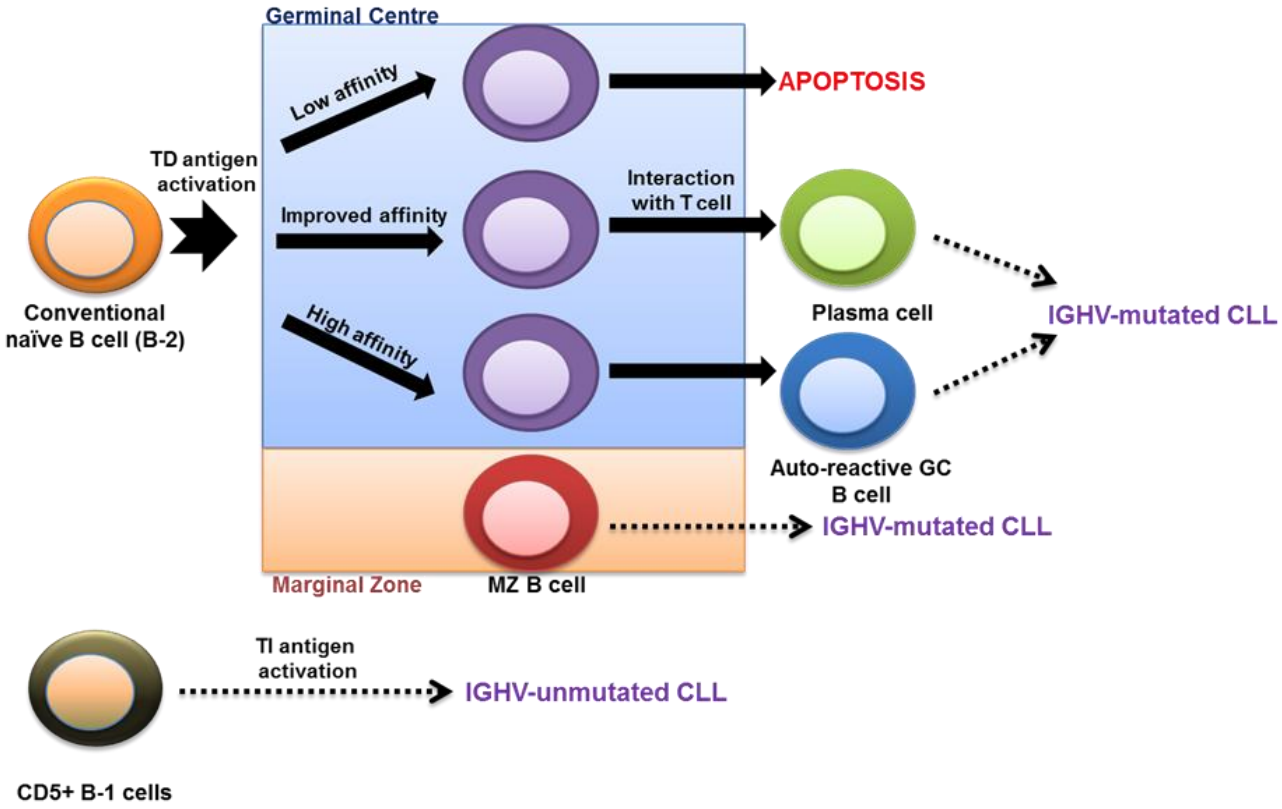

Figure 1-3. Origin of M- and U-CLL cells. (**Adapted from (Zenz*, et al* 2010)).** Based on current paradigms CLL cells can arise from CD5+ B cells (B-1a) and marginal zone (MZ)-like B cells or the mature B cells experience the germinal centre.(**TD:** T cell dependent, **TI:** T cell independent, **IGHV:** Immunoglobulin heavy chain, **MZ:** marginal zone).

1.4 Current mouse models for CLL

The main reason for studying a mouse model of CLL is to gain insight into the factors that are important for disease pathogenesis and progression. Such insight can lead to the development of better systems to test therapeutic treatments for the disease. The first mouse model for CLL was described in a New Zealand black mouse that spontaneously developed a CLL-like disorder. Here, the malignant cells of this condition resemble those of human CLL (Phillips*, et al* 1992). Importantly, this model provides key evidence to explain a genetic component within human disease (Oppezzo 2012).

However, the CLL-like disease suffered by the mice is indolent in nature, and does not give insight into progressive disease.

A second important model of CLL was derived by transgenic expression of TCL1. Here, expression of the TCL1 oncogene is placed under the control of the immunoglobulin gene promoter (IgH-Eμ enhancer) so that over expression appears only in B cells. Thus, the TCL1 transgenic mouse develops a CLL-like disease where the malignant cells result from polyclonal proliferation of $IgM^{+}CD5^{+}$ B cells (Bichi*, et al* 2002). TCL1 expression is important to human disease pathogenesis because high expression levels of this oncogene are correlated to progressive disease(Narducci*, et al* 2000). Indeed, the CLL-like disease associated with the TCL1 transgenic mouse has many features that are associated with the aggressive form of human CLL (Herling*, et al* 2009). For example, the CLL-like cells from the TCL1-transgenic mouse bear un-mutated IgHV genes, and are stereotypic in terms of the HCDR3 gene sequences used (Yan*, et al* 2006). This implicates BCR signaling as an important contributor to the pathogenesis of the CLL-like disease in the TCL1-transgenic mice. Furthermore, constitutive activation of Akt is an important factor in the patho-physiology of aggressive disease in human CLL, and TCL1 may play a role in this activation by interacting with the phosphatidylinositol 3-kinase–Akt pathway leading to enhanced cell survival (Longo*, et al* 2007, Pekarsky*, et al* 2000). However, the argument against this model is that it does not truly represent CLL because the TCL1 transgenic mouse develops other B lympho-proliferative disorders with high frequency.

A second transgenic model of aggressive CLL has been developed by transgenic co-expression of Bcl-2 with a RING and zinc finger mutant of TNF receptor associated factor-2 (TRAF-2) (Zapata*, et al* 2004). TRAFs are adaptor proteins that connect tumour necrosis factor (TNF)-family receptors (TNFRs) to intracellular signal transduction (Zapata*, et al* 2007). Up regulation of TRAF family proteins, particularly TRAF1 has been observed in CLL cells, and TRAF1 expression is associated with chemo-refractory disease in CLL (Michie*, et al* 2007, Munzert*, et al* 2002). TRAF2 which lacks the RING and zinc finger domains located within its N terminus (TRAF2DN) is structurally similar to TRAF1, and targeted over expression of TRAF2DN in mouse B

cells leads to the development of low-grade B cell malignancies. The same is true for Bcl-2, targeted over expression of this protein in B cells leads to the development of low-grade malignancy of this cell type in mice. This is relevant for human CLL because the malignant cells of this disease typically over express Bcl2. When TRAF2DN and Bcl2 transgenic mice are crossed together a CLL-like disease develops, and the malignant cells are phenotypically similar to human CLL cells. Significantly, double transgenic mice died much earlier than did either TRAF2DN or Bcl2 single transgenic mice. Furthermore, the extent of splenomegaly and lymphadenopathy was much more severe in the TRAF2DN/Bcl2 double transgenic mouse. Studies of cell proliferation and apoptosis showed that the malignant cells derived from the TRAF2DN/Bcl2 double transgenic mice were largely resistant to apoptosis and proliferated only very slowly. This model is thought to explain the role of over expressed TRAF1 and Bcl-2 in human CLL cells, particularly with respect to the resistance of these cells to apoptosis (Zapata*, et al* 2004).

A third transgenic model of CLL was generated by over expressing the TNF-related factor **A** **P**rolife**R**ation-**I**nducing **L**igand (APRIL, TNFSF13) under the control of the T cell specific Lck promoter. Over expression of APRIL under these conditions acts to stimulate expansion of the CD5+ B1 cell population, and eventually results in development of a CLL-like disease later in the life of the mouse (Planelles*, et al* 2004). The phenotype of this mouse is much milder than that of either the Tcl1 transgenic or the TRAF2DN/Bcl2 double transgenic mouse (Oppezzo 2012). In the APRIL transgenic mouse model the NF-κB signaling pathway is constitutively active, possibly resembling the constitutive activation of this pathway in human CLL cells (Endo*, et al* 2007). It is believed that the APRIL transgenic model sets up the conditions whereby B cell oncogenic transformation is prompted, but whether this event happens likely requires a “second hit “such as over expression of Bcl-2 or Tcl1 (Michie*, et al* 2007).

Another CLL transgenic mouse model that will be mentioned in this section is the miR-29 transgenic mouse. The rationale for creating this transgenic mouse is based on findings that over-expression of miR-29a is associated with indolent CLL in humans (Calin*, et al* 2004). In this mouse miR-29 is transgenically highly expressed in B cells, and the resulting phenotype is an expansion of the $CD5^+$ B cell population and eventual

development of an indolent “CLL-like” leukaemia later on. An important target gene of miR-29 is TCL1, a gene that is crucial in the pathogenesis of aggressive CLL. This suggests that miR-29 is associated with the pathogenesis of indolent CLL in humans (Santanam*, et al* 2010).

The final mouse model of CLL that I will speak about here results from deletion of a gene cluster on chromosome 13 at position q14. This gene cluster, known as the minimal deleted region (MDR), consists of the genes coding DLEU-2 and miR-15a/16-1 (Calin*, et al* 2008, Klein and Dalla-Favera 2010). This deletion causes the expansion of $CD5^+$ CLL like B cells leading to an indolent form of CLL. That this model represents indolent CLL is consistent with human disease because patients with only 13q14 deletions have better prognosis than patients with other chromosomal abnormalities. Also, low levels of miR15a/16-1 are observed in human CLL cells. The reduction in miR-15a/16-1 levels resulting from the gene deletion seems to stimulate B cell proliferation by regulating the expression of Bcl-2. Thus, Bcl-2 becomes more highly expressed in these cells, leading to increased survival of potentially malignant cells (Klein*, et al* 2010). However, the increase in Bcl-2 expression observed in the B cells of MDR mice does not explain why B-1 cells are selected for expansion. In Bcl2-transgenic mice the development of lymphoid malignancies occurs in all B cell populations, not just B-1 cells. This argues that other genes are also important in B-1 cell differentiation regulated by miR15a/16. Further work needed to identify these genes and their potential impact on CLL pathogenesis (Klein*, et al* 2010, Lichter 2010).

Different CLL mouse models have brought new insight into CLL pathogenesis by emphasizing a particular mechanism that is important in this process. Although the current CLL mouse models do not genuinely represent human disease, combining the different models has given a wider and more comprehensive picture of CLL. One important observation from these mouse models of CLL is that the disease is the result of an expansion of $CD5^+$ B cells. This observation suggests that malignant cells in human CLL originate from an analogous subset of B cells.

1.5 PKC structure and function

PKCs are a family of serine/threonine kinases that have extensive structural homology between the different isoforms. In spite of having similar structures, PKC isoforms mediate different cellular functions such as proliferation, differentiation, apoptosis and cell survival in a wide range of cell types (Dempsey*, et al* 2000, Saito*, et al* 2002). PKCs are divided into three subfamilies based on the structure of their regulatory domains; a structure which determines what co-factors induce activation of PKC. Classical PKCs (PKCα, βI, βII, and γ) require the presence of diacyl-glycerol (DAG) and calcium for activation, while novel PKCs (PKCδ, ε, θ and η) require only the presence of DAG. In contrast, atypical PKCs (PKCζ, ι/λ) are both calcium and DAG independent. The basic structure of all members of the PKC family proteins is illustrated in Figure 1-4 (Tan and Parker 2003).

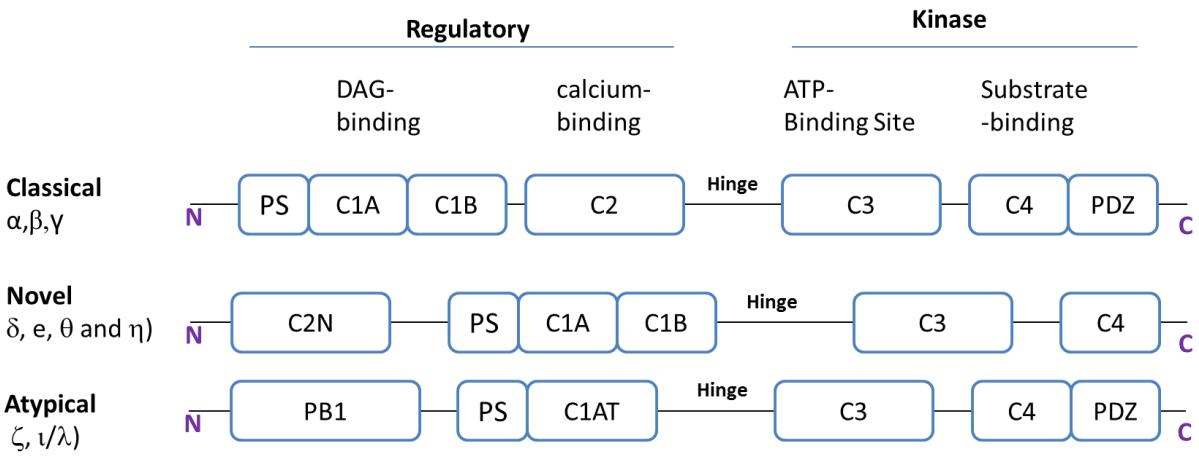

Figure 1-4. Schematic representation of PKC isoforms structure. Pseudo-substrate (PS) sequence is located at PKC' N-terminus and binds to the substrate-binding site within the catalytic domain to hold PKC in an inactive state. C1A and C1B are the regions responsible for DAG binding. C2 is the calcium-binding domain. C3 is the ATP-binding domain. C4 is the substrate-binding domain. PDZ and PB1 mediate protein-protein interactions following kinase activation.

The regulatory domain of PKC has sites for membrane association and activation of the kinase. Within the C1 domain, there are motifs for binding DAG/Phorbol esters and a pseudo-substrate (PS) sequence at its N-terminus. The latter binds to the substrate-binding site within the catalytic domain to hold PKC in an inactive state. Atypical PKCs have a unique C1 region (C1 AT) as well as a Phox and Bem1 (PB1) region which are likely responsible for protein interaction resulting in kinase activation. The C2 domain is responsible for regulation of Ca^{2+}-mediated phospholipid binding to the classical PKC isoforms. Novel PKCs have a C2-like domain that does not bind Ca^{2+} (C2 N). The catalytic domain of all PKCs is conserved and contains the regions necessary for ATP-binding (the C3 domain) and for binding to substrate (the C4 domain). The motif called PDZ exists in some PKC isoforms and mediates protein-protein interactions following kinase activation.

All PKC isoforms have a homologous kinase domain located at the C-terminus of the protein. The structure of the kinase domain is highly conserved and bears homology with the AGC super family of serine/threonine protein kinases (Bononi*, et al* 2011). Within the kinase domain there are the ATP- and substrate-binding sites, as well as a phosphorylation-dependent docking site for regulatory molecules that interact with PKC (Newton 2010).

The kinase domain of PKC is connected by a flexible hinge segment to the N-terminal regulatory domain. This flexible hinge region is crucial for PKC function as it allows the close apposition of the regulatory and catalytic domains when PKC is inactive. Once PKC becomes activated, the hinge region allows the protein to unfold and allow interaction of the catalytic domain with substrates and regulatory proteins(Newton 2010).

1.6 **PKC** regulation

The maturation of PKC isoforms requires a series of ordered, consecutive phosphorylations on serine and/or threonine residues within the catalytic domain (Newton 2003). These phosphorylations are summarized in Figure 1-5. The presence of

these phosphorylations is needed for the stability and catalytic capability of PKCs. The first step of maturation begins when newly synthesized PKC binds the chaperone protein heat shock protein 90 (HSP90) (Gould*, et al* 2009). This occurs via a molecular clamp within the kinase domain of PKC, and is followed by three ordered phosphorylation events within this region. These phosphorylation sites are located in: 1) the activation loop, 2) the turn motif, and 3) the hydrophobic motif (Keranen*, et al* 1995).

Initial phosphorylation of the activation loop within newly synthesized PKC is catalyzed by 3-phosphoinositide-dependent kinase-1(PDK-1) (Chou*, et al* 1998). This is an important site of phosphorylation in conventional and novel PKC isoforms because mutation of this site or disturbance of PDK-1 function disallows maturation of PKC and leads to its degradation (Chou*, et al* 1998, Newton 2010). Phosphorylation within the turn motif of the kinase domain is catalyzed by the mTORC2 complex (Ikenoue*, et al* 2008), and leads to further stabilization of the structure of PKC (Guertin*, et al* 2006). The final phosphorylation within the hydrophobic motif leads to the generation of a fully-mature and catalytically competent PKC enzyme. However, it is not clear whether this phosphorylation is the result of auto-phosphorylation, or whether this site is a second phosphorylation site for the mTORC2 complex (Newton 2010).

Mature PKC enzyme localizes to the cytosol of the cell where it interacts with regulatory proteins. This interaction facilitates binding of the N-terminal PS domain to the substrate-binding site within the catalytic domain, thereby holding PKC in an inactive conformation (Schechtman and Mochly-Rosen 2001). PKC activation occurs when its N-terminus is no longer in close proximity to its C-terminus. In general, classical isoforms of PKC are activated following the induction of PIP2 hydrolysis within certain pathways of intracellular signaling. This produces free Ca^{2+} and DAG, two second messengers that are important for the activation of classical PKCs. Ca^{2+} binds to the C2 domain of classical PKC, and facilitates interaction with phospholipids such as 6-pyruvoyltetrahydropterin synthase (PtS), and Phosphatidylinositol 4,5-bisphosphate (PIP2) that are located in the plasma membrane. DAG is also membrane-bound, and interacts with PKC via the C1 domain (Giorgione*, et al* 2006). In classical PKC isoforms the engagement of both C1 and C2 domains leads to the release of the PS from the

substrate-binding site of the catalytic domain, and frees membrane-bound PKC to catalyze the phosphorylation of downstream substrates. The nature of these substrates and resultant cellular response is largely dependent upon the inciting stimulus and cell type (Gallegos*, et al* 2006, Newton 2010).

1.6.1 Down regulation and degradation

Classical PKC isoform activity is principally down regulated by the removal of Ca^{2+}, through sequestration, and DAG, by diacylglycerol kinases (Hansra, Garcia-Paramio et al. 1999) (Figure 1-5). In this way classical PKC isoforms can shuttle between the cytosol (inactive state) and membrane (active state), thereby PKCs have a long half-life. However, under conditions of long-term stimulation, such as that generated by the presence of Phorbol esters PKCs can be rapidly degraded. This is possibly because when PKC is active for a long period of time, its open conformation makes it more prone to de-phosphorylation, and then protein degradation (Dutil*, et al* 1994, Hansra*, et al* 1999). PH domain leucine-rich repeat protein phosphatases (PHLPP) 1 and 2 are phosphatases that dephosphorylate the hydrophobic motif of novel and classical PKC isoforms that are in open membrane-bound conformation (Brognard and Newton 2008). One model has shown that PHLPP binds and dephosphorylates the hydrophobic motif of activated PKCβII, and this re-localises this PKC isoform into a detergent-insoluble fraction of the cell where it can be further de-phosphorylated at the turn motif by an okadaic acid-sensitive phosphatase such as PP2A. Once PKC is fully dephosphorylated, it is then degraded by the proteasome (Gao*, et al* 2008). However, HSP90 can rescue dephosphorylated PKC from destruction; as in the case with de-novo synthesis of PKCs, HSP90 in this context allows re-phosphorylation of the PKC to take place and generate a catalytically competent enzyme (Gould*, et al* 2009).

The importance of PHLPP in initiating PKC degradation is underlined by studies showing that these phosphatases have crucial role in colon cancer. In this study, reduced PHLPP expression in colon cancer cell lines leads to a threefold increase in the

expression of PKCβII, an isoform of PKC that is highly expressed by primary colon cancer cells (Gao, *et al* 2008).

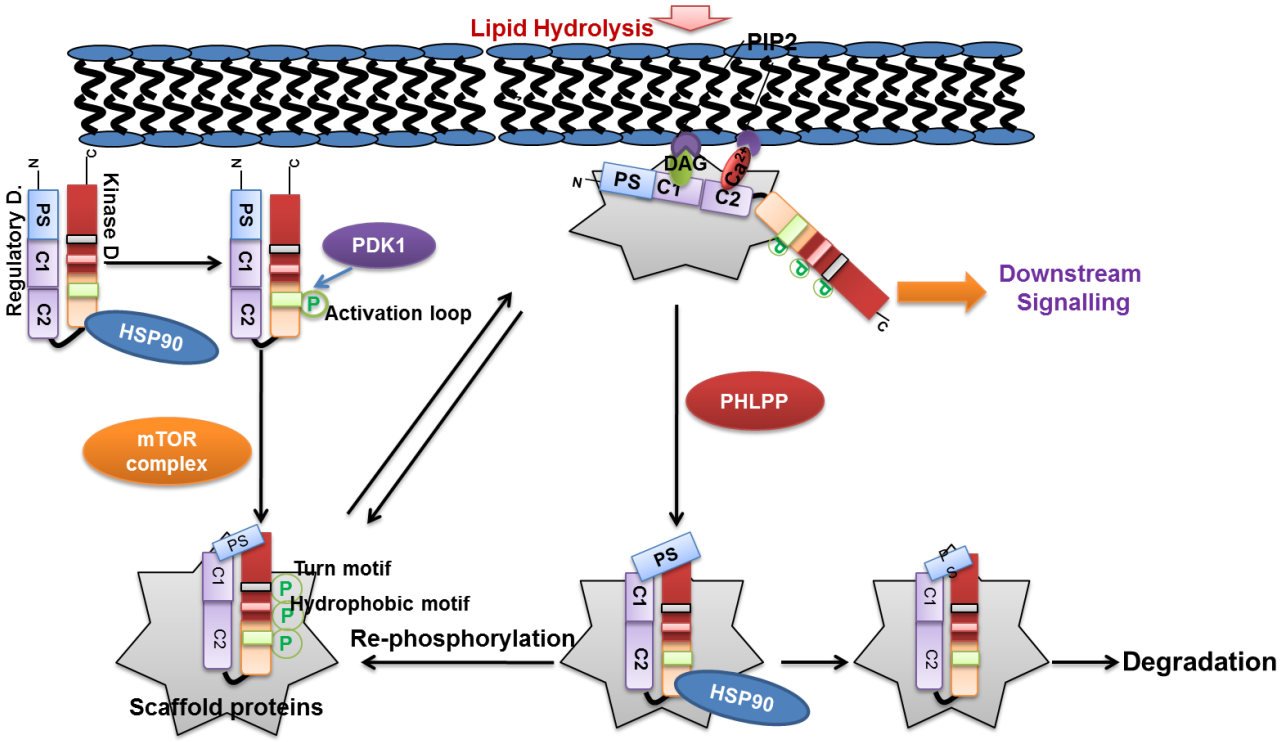

Figure 1-5. Regulation of PKC activation and degradation. (**Adapted from Newton, et al.,2010**) Active PKC is generated by ordered consecutive phosphorylations of serine and threonine residues located in the catalytic domain. However, PKC is not able to phosphorylate its substrates because the regulatory domain holds PKC in a closed state. Interaction with the plasma membrane results in unfolding of PKC allowing interaction with substrates. Deactivation can either be achieved by removal of Ca^{2+}/DAG, or by dephosphorylation by PHLPP. In the latter case PKC can be either recycled or is further dephosphorylated and destroyed in the proteosome.

1.7 PKC in CLL

It is well known that DAG analogues such as bryostatin and phorbol esters induce differentiation of B cells. Therapeutically this property could be useful in the treatment of CLL because the malignant cells of this disease are characteristically resistant to

differentiation. Indeed, one study has demonstrated that bryostatin induces differentiation of CLL cells when it is administered to patients (al-Katib*, et al* 1993, Totterman*, et al* 1980). However, these studies have not been well followed up, possibly because of subsequent studies showing that treatment of CLL cells with bryostatin provided these cells with protection to the cytotoxic effects of glucocorticoids and Fludarabine through up-regulation of XIAP and Mcl-1 expression (Bellosillo*, et al* 1997, Kitada*, et al* 1999, Thomas*, et al* 2004). PKC inhibitors have also been used to understand the role of PKC in CLL cell survival. Compounds such as UCN01 (Byrd*, et al* 2001), PKC412 (Ganeshaguru*, et al* 2002), LY379196 (Abrams*, et al* 2007) and Bisindolymaleimide (Barragan*, et al* 2002) induce apoptosis of CLL cells *in vitro*. Interestingly, the expression of Induced myeloid leukemia cell differentiation protein (Mcl-1) and X-linked inhibitor of apoptosis protein (XIAP) decreases when CLL cells are treated with UCN01 or Bisindolymaleimide, making these cells more susceptible to apoptosis (Kitada*, et al* 2000, Snowden*, et al* 2003). All these observations suggest that activation of PKC is an important mediator of CLL cell survival signals (Oppezzo 2012).

1.7.1 Expression profile

Work in this Department showed that CLL cells express PKCβI, βII, α, δ, ε, ζ, and PKC ι/λ (Abrams*, et al* 2007, Alkan*, et al* 2005). Furthermore, a comparison of the expression levels of these isoforms to those in normal B cells shows that CLL cells express less PKCβI and PKCα, and more PKCδ. However, what clearly distinguishes CLL cells from normal B cells and other B-lymphoid malignancies is an over expression of PKCβII; equating to 0.53 ± 0.25% of total cellular protein(Abrams*, et al* 2007). The focus of this thesis is PKCβII, however, to gain a full understanding of PKC functioning in CLL cells I will first relate the established roles of PKCα, δ and other important PKC isozymes in this disease.

PKCα

PKCα has been shown to have both tumour promoting and tumour suppressing roles. Up-regulation of PKCα is observed in breast, prostate, gastric and brain cancers (Griner and Kazanietz 2007, Michie and Nakagawa 2005). In contrast, down regulated expression of PKCα is found in epithelium, pancreas and colon cancer cells, as well as in CLL cells (Abrams*, et al* 2007, Alvaro*, et al* 1997, Detjen*, et al* 2000, Neill*, et al* 2003). It is thought that over expressed PKCα promotes cancerous cell survival through an ability to phosphorylate Bcl-2 at the mitochondrial membrane. This leads to an increase in the ability of Bcl-2 to sequester the apoptosis-inducing protein Bim, which also acts at the mitochondrial membrane to promote depolarisation (Jiffar*, et al* 2004). With respect to the tumour suppressor effects of PKCα, it has been demonstrated that PKCα knockout mice spontaneously develop intestinal lesions with greater frequency than do wild type mice. Moreover, the mitotic index of malignant cells from PKCα knockout mice is greater than that of malignant cells from wild type mice (Oster and Leitges 2006).

In CLL cells PKCα may also have tumour suppressive effects. Nakagawa et al have shown that expression of a kinase-dead mutant of PKCα (PKCα-KR) within foetal liver-derived hematopoietic progenitor cells (HPCs) that have been stimulated to undergo B cell differentiation induces the development of malignant cells carrying a CLL cell phenotype ($CD19^{hi}$, $CD23^{+}$, $CD5^{+}$, $sIgMl^{o}$). It is not clear how PKCα-KR produces this phenotype. However, this particular model of malignant cell development in CLL is appealing because it allows for genetic manipulation to take place (Nakagawa*, et al* 2006, Oppezzo 2012).

PKCδ

Although PKCδ is implicated in CLL cell pathophysiology, its exact role is unclear (Mecklenbrauker*, et al* 2004). PKCδ plays an important role in the BAFF signaling pathway as demonstrated by work showing that BAFF binding to B cells prevents nuclear localization of this PKC isoform. When B-cell activating factor (BAFF) is absent, PKCδ localizes to the cell nucleus where it contributes to phosphorylation of histone H2B at serine 14. This, in turn, promotes apoptosis by allowing chromosomal de-

condensation and cleavage. In CLL, BAFF plays a key pro-survival role, possibly by promoting PKCδ localisation to the cytosol of the malignant cells. Here, PKCδ may have some additional pro-survival effects that have not yet been characterised (Mecklenbrauker*, et al* 2004, Oppezzo 2012). Ringshausen et al have shown that inhibition of PKCδ leads to the induction of CLL cell apoptosis through down regulation of XIAP and Mcl-1 expression (Ringshausen*, et al* 2006, Ringshausen*, et al* 2002). Subsequent work in this Department agrees with these observations and has shown that PKCδ can have important pro-survival effects in CLL cells by phosphorylating STAT3 on serine 727. Such phosphorylation allows for an increase in Mcl-1 gene expression. This may have therapeutic importance as high expression of Mcl1 is associated with aggressive disease in CLL by protecting the malignant cells against chemotherapy (Allen*, et al* 2011, Pepper*, et al* 2008).

Other PKC isoforms in CLL

With the exception of PKCβII, the roles of other PKC isoforms expressed in CLL cells are less understood. PKCε may play an anti-apoptotic role. This PKC isozyme has been shown to phosphorylate Akt and Signal transducer and activator of transcription 3 (STAT3) in other cell types, and this may be important in CLL because of the established role these proteins play in the pathophysiology of the malignant cells (Aziz*, et al* 2010, Matsumoto*, et al* 2001). Knockout mouse models have shown that atypical PKCζ regulates B-cell survival and proliferation through an ability to participate in Extracellular signal-regulated kinases (ERK) and nuclear factor kappa-light-chain-enhancer of activated B cells signaling pathways (NF-κB). Signaling through these pathways is also patho-physiologically important in maintaining the survival and proliferation of CLL cells (Martin*, et al* 2002). Future studies, not related to this thesis, are needed to pave the way for better understanding of the roles of this group of kinases in CLL pathogenesis.

PKCβII

PKCβII is the most highly expressed PKC isoform in CLL cells. High expression of PKCβII in these cells distinguishes this malignancy from other B cell malignancies such as mantle cell lymphoma, diffuse large B cell lymphoma and follicular lymphoma. High PKCβII protein expression is the result of high expression of the gene coding for this protein, *PRKCB*. This gene is located on chromosome 16 at position p11.2. Two polypeptides, PKCβI and PKCβII, are encoded by this gene, and result from alternative splicing of the transcribed mRNA within the C-terminal exons of the gene. Thus, PKCβI and PKCβII proteins differ within the C-terminal 50 and 52 amino acids, respectively (Ono*, et al* 1986); The mechanism controlling PKCβ mRNA splicing has been partially worked out and it has been shown that insulin facilitates splicing in favour of PKCβII mRNA in cardiac myocytes through a mechanism that involves Akt2. The resulting increased protein level of PKCβII in these cells significantly affects the ability of insulin to induce glucose transport (Blobe*, et al* 1993, Patel*, et al* 2005). In CLL cells approximately 90% of the total PKCβ mRNA that can be extracted codes for PKCβII, and this is reflected in the protein over-expression of PKCβII and under-expression of PKCβI (Abrams*, et al* 2007). The importance of PKCβI versus PKCβII in B lymphocyte development is unclear because gene knockout studies have only considered the function of the entire gene (Leitges*, et al* 1996).

A crucial role for PKCβ in CLL pathogenesis was recently shown in an in-vivo study using a CLL mouse model where the TCL1 oncogene is specifically over expressed by B cells. This mouse model, termed the TCL-1 mouse, develops a disease phenotype that is similar to the aggressive form of CLL in humans, and the malignant cells in this model bear many of the hallmarks of the malignant cells in human CLL (Yan*, et al* 2006). Interestingly, when TCL-1 mice were crossed with mice having disrupted expression of PKCβ, development of the CLL-like disease is inhibited (Figure 1-6). Thus, TCL-1 mice homozygous for disruption of PKCβ gene expression did not develop a CLL like disease over the course of the study. In same study, TCL1-mice heterozygous for disruption of PKCβ gene expression did develop a CLL-like disease, but did so with a much slower kinetic than did TCL-1 mice which were in a wild type configuration for

PKCβ gene expression. These data strongly suggest that the level of expression of PKCβ is a key factor in CLL pathogenesis. An explanation for this observation is that the PKCβ-knockout mouse is deficient in B-1 cells, the population of B cells that expands within TCL-1 mice to eventually develop into a CLL-like disease (Holler*, et al* 2009). Another explanation was recently provided in a paper published by Lutzny et al. Here it was demonstrated that CLL cells induce PKCβII expression in stromal cells, and that expression and activation of PKCβII in these stromal cells supported CLL cell survival. Thus, CLL-like disease would not develop in TCL-1 mice where PKCβ gene expression has been disrupted because the stromal environment would not be able to support disease development (Lutzny G 2013). Taken together, these notions suggest that targeted over-expression of PKCβ in B cells will lead to expansion of the B-1 cell population, and, when crossed with the TCL1 mouse, will result in accelerated development of the CLL-like disease.

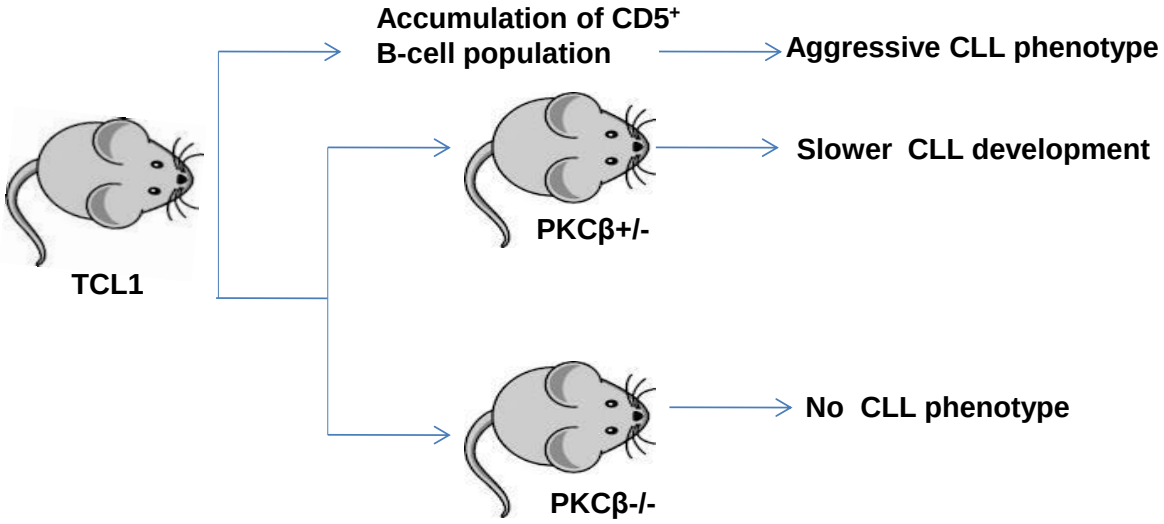

Figure 1-6. PKCβ is essential for the development of TCL1 transgenic mouse model of CLL.

What is the patho-genetic role of PKCβ in the generation of CLL? PKCβ does not have a direct role in the maintenance of CLL cell survival, because inhibition of this enzyme with specific inhibitors only results in the death of a minor proportion of the

malignant cells in CLL (Abrams*, et al* 2007). However, PKCβII known to function within the context of BCR signaling, and BCR signaling is known to contribute to CLL pathogenesis (Kang*, et al* 2001, Stevenson and Caligaris-Cappio 2004).

Role of PKCβ in B cell signalling Pathways

PKCβ functions to activate the NF-κB pathway during BCR engagement, but also functions to down regulate BCR signals. With respect to the former, PKCβ transmits BCR signals to the NF-κB pathway by phosphorylating CARD-containing MAGUK protein 1 (CARMA1), which, together with MALT1 (Mucosa-associated lymphoid tissue lymphoma translocation protein 1), B-cell lymphoma/leukemia 10 (Bcl10) and TAK1 (TGF-beta activated kinase 1) act to stimulate IκB-kinase activity (IKK), which then phosphorylates IκBα to stimulate its dissociation from RelA (v-rel avian reticuloendotheliosis viral oncogene homolog A). Phosphorylated IκBα is then degraded within the proteasome, and RelA translocates to the nucleus where it activates gene transcription (Shinohara*, et al* 2007, Shinohara*, et al* 2005). This pathway of NF-κB activation is illustrated in Figure 1-7A. This may by pathologically important in CLL as constitutive activation of the NF-κB pathway is a characteristic of the malignant cells in this disease (Hewamana*, et al* 2008). The evidence supporting this idea comes from the studies of diffuse large B cell lymphoma (DLBL). Those patients bearing the activated B cell phenotype also have high levels of NF-κB pathway activation caused by over-expressed active PKCβ-mediated phosphorylation of the CARMA1/MALT1/Bcl10 complex. Interestingly, some patients with activated B cell type DLBL benefit from treatment with PKCβ inhibitors (Naylor*, et al* 2011).

With respect to PKCβ-mediated down regulation of BCR signalling, this occurs through an ability of PKCβ to phosphorylate Bruton's tyrosine kinase (Btk) on serine 180. Such phosphorylation of Btk promotes its dissociation from the plasma membrane, and impedes its function by limiting its ability to phosphorylate and activate PLCγ-2 (Phospholipase C-γ2) (Figure 1-7B). Regarding CLL, there is inverse correlation between PKCβII activation and CLL cell response to BCR engagement. Thus, BCR signalling is less efficient in CLL cells bearing highly active PKCβII. It is proposed that

high expression and high activity of PKCβ in CLL cells is patho-genetically important because it suppresses pro-apoptotic BCR signalling (Abrams*, et al* 2010, Abrams*, et al* 2007).

Further work by zum Büschenfeld et al have advanced the role of PKCβII in anti-apoptotic BCR signaling. They have shown that ZAP-70 in CLL cells acts as a platform to recruit downstream signaling proteins, including PKCβII, into lipid rafts. This stimulates the translocation of PKCβII to mitochondrial membranes, where it is able to phosphorylate anti-apoptotic Bcl-2 and pro-apoptotic BimEL. Phosphorylated Bcl2 is able to sequester BimEL and promote cell survival, whereas phosphorylation of BimEL results in its proteasomal degradation (Barragan*, et al* 2006, zum Buschenfelde*, et al* 2010) (Figure 1-7C).

Finally, PKCβII may act to mediate signaling by the receptor for B cell-activating factor (BAFF). In this context BAFF stimulation of B cells results in PKCβ-mediated phosphorylation of Akt on S^{473}, to promote its activation. Active Akt is an important regulator of anti-apoptotic and pro-survival signals in cells (Patke*, et al* 2006)(Figure 1-7D). Therefore, over-expressed PKCβII in CLL cells may additionally protect against apoptosis by activating Akt as has been suggested by Barragán et al (Barragan*, et al* 2006).

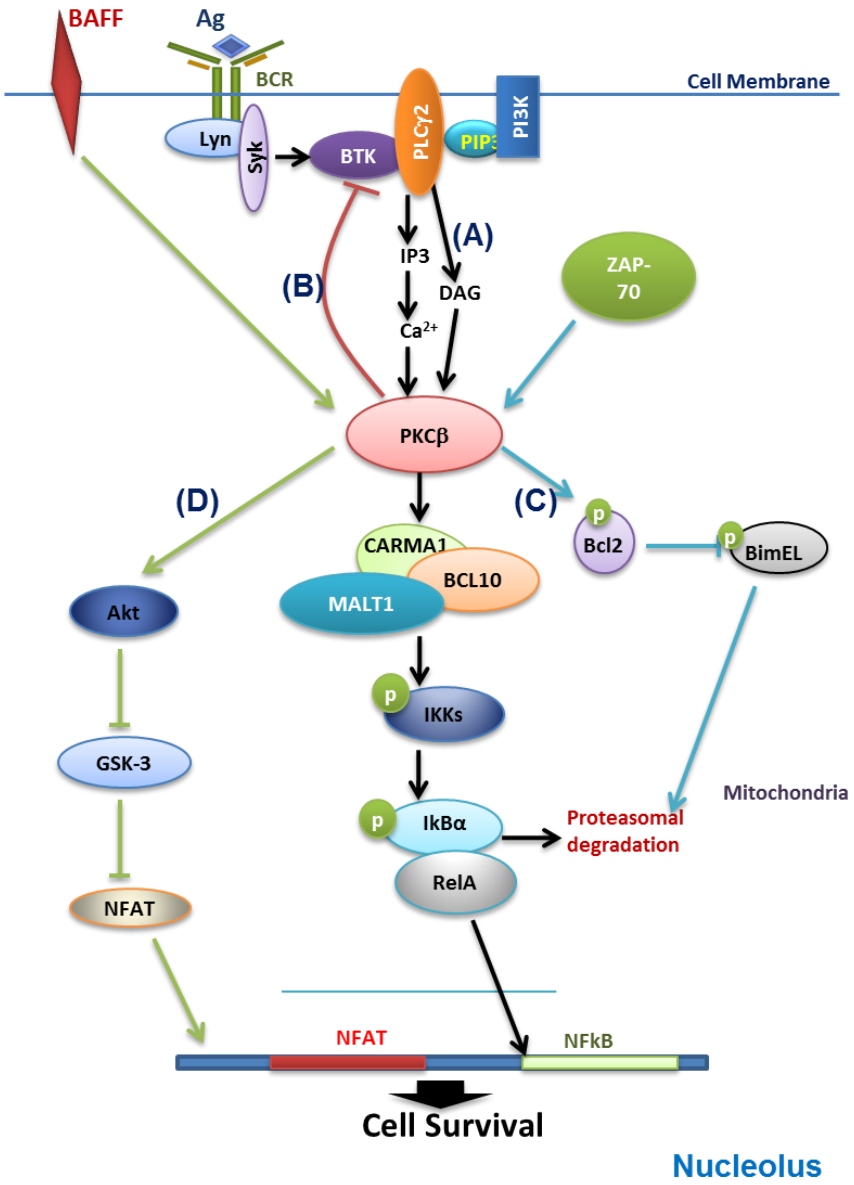

Figure 1-7. Role of PKCβ in B cell signaling pathways. PKCβ is shown to have role in B cell signaling downstream of the BCR by activating the NF-κB pathway **(A)** or down-regulating BCR signaling by phosphorylating Btk on serine 180 and impeding its function of regulating PLCγ2 activation **(B)**. PKCβ also mediates phosphorylation of anti-apoptotic Bcl-2 and pro-apoptotic BimEL, promoting cell survival **(C)** or interacting with BAFF and consequently phosphorylating Akt on S^{473}. Active Akt can then phosphorylate GSK3β to deactivate its kinase activity, and this leads to increased transcription of NFAT in the nucleus due to activation of the APC/β-catenin pathway **(D)**.

In a wider context PKCβII over-expression is important in other cancers. A PKCβII transgenic mouse has been generated to study the role of this protein in oncogenesis of colon cancer. In this model, high expression of PKCβII in intestinal epithelial cells leads to an increased proliferation of these cells, and an increased susceptibility to pre-neoplastic lesions. Also, this work demonstrated that PKCβII mediates the inactivation of glycogen synthase kinase 3β (GSK3β) in these cells. This leads to the activation of the Wnt/adenomatous coli (APC)/β-catenin pathway and increased cell survival (Murray*, et al* 1999). Interestingly, in CLL cells Wnt signals also contribute to cell survival (Lu*, et al* 2004).

In conclusion, the above studies strongly suggest that PKCβII plays a crucial role in maintaining CLL cell survival.

1.8 Hypothesis and Plan

1.8.1 Hypothesis

Although there is controversy about the origin of CLL, in-vivo studies strongly suggest that CLL cells are derived from $CD5^+$ B-1 cells (Hamano*, et al* 1998, Holler*, et al* 2009, Oppezzo 2012). There is a lot of similarity between B-1 and CLL cells: both cell types express CD5, both require antigen binding for further development, and the antigen-binding region of expressed Ig chains use a restricted set of variable region genes (Joshi 2010). B-1 cell development is unclear. If the lineage model of B cell development is used, both B-1 and B-2 cells originate from the same progenitor in the bone marrow. Differentiation into B-1 or B-2 cells is determined at the transitional stage when these cells enter the spleen. This process relies on antigen engagement; B-2 cells develop from cells where BCR is strongly engaged, whereas differentiation into MZ and potentially B-1 cells results from weaker challenge of the BCR (Hardy 2006). Expression of PKCβ is known to play a role in this differentiation process; the absence of PKCβ

results in inhibition of B-1 cell development. This may be because PKCβ controls the strength of antigen receptor signaling. In the TCL1 mouse model of CLL, the absence of PKCβ expression inhibits development of disease (Holler*, et al* 2009). This may be because the B-1 cell population, from which the CLL-like disease develops in this model, is no longer present, and/or because PKCβ plays a central role in CLL pathogenesis.

The main purpose of this project is to generate transgenic mice that over-express PKCβII within their B cells. We hypothesize that such over-expression of PKCβ in B cells will lead to a lymphocytosis of transitional B cells and expand IgM^+ B cells (the B-1 and MZ B cell populations). Furthermore, we also hypothesize that this expansion of the B-1 and MZ B cell population will lead to the development of a CLL-like disease in the transgenic animals (Figure1-8). This study will add further insight into the role of PKCβII in B cell differentiation and in human CLL pathogenesis. Potentially, if this animal is mated with another CLL mouse model (such as the TCL-1 or MDR-KD transgenic mouse), disease development should be accelerated.

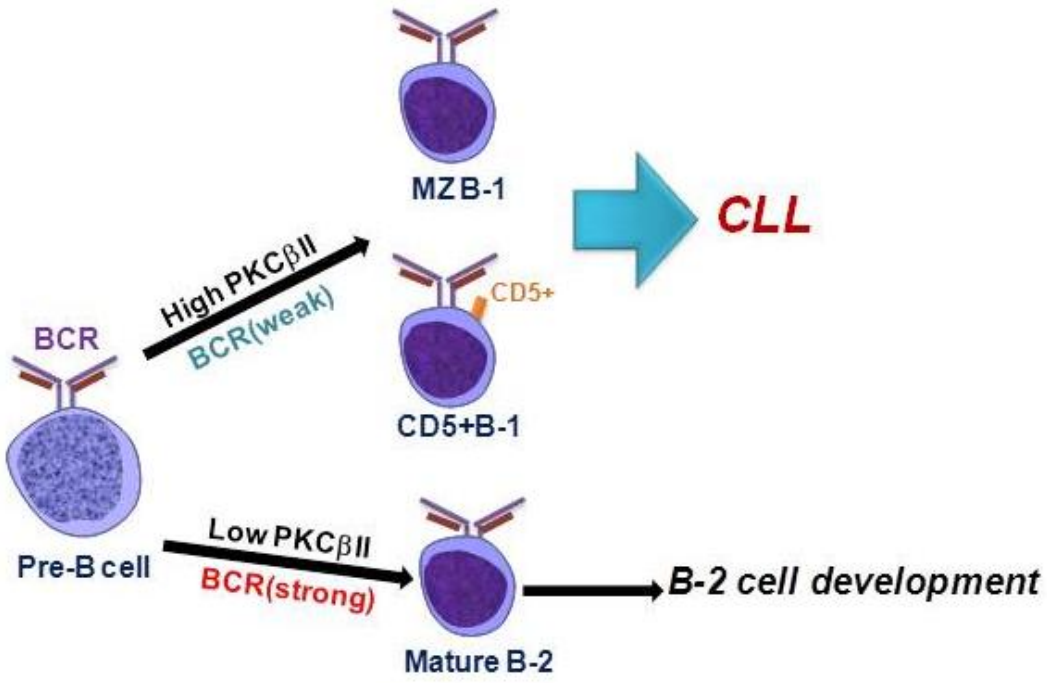

Figure 1-8. The schematic of the hypothesis.

1.8.2 Plan

This project principally consists of creation and characterisation of a transgenic mouse that highly expresses PKCβII within their B cells. This transgenic mouse will be referred to as a Eμ-PKCβII tg mouse for reasons that will become apparent in Chapter 5. Subsequent to this introduction, this thesis consists of 5 additional chapters containing the following information:

Chapter 2

- **Material and methods**

Chapter 3

- Construction of a plasmid to highly express PKCβII specifically in B cells

- Place PKCβ coding sequence into a plasmid where expression is under the control of the promoter for immunoglobulin (Eμ plasmid). This will direct PKCβII expression to B cells within the transgenic mouse.
- Tag PKCβ coding sequence with HA so that transgenic enzyme can be distinguished from endogenous enzyme. The tag also gives the possibility of immuno-precipitating transgenic PKCβII from mouse B cells.
- Add a mCherry gene for tracking transgenic B cells using imaging.
- Ensure plasmid integrity by expression analysis (Western Blotting and confocal microscopy) in a mouse B cell line (A20 cells).

Chapter 4

-Generation of Eμ-PKCβII tg mice

- Create transgenic mouse (injection into fertilised eggs and transfer into recipient mouse to generate founder mice)
- Identification of founder mice by genetic screening for the insertion of the gene.

- Creation of Eμ-PKCβII tg mice by backcrossing founder mice with wt animals, and by inter-crossing identified heterozygous Eμ-PKCβII tg mice. This includes screening for identification.
- Confirmation of creation of homozygous Eμ-PKCβII tg mice by crossing with wt mice.

Chapter 5

-Characterization of Eμ-PKCβII transgenic mice

- Confirmation of protein expression driven by genes encoded by the plasmid in Eμ-PKCβII tg mice.
- Analysis of CLL-like disease development in Eμ-PKCβII tg mice.
- Characterisation of phenotype of Eμ-PKCβII tg mice, examining specifically the B cell populations in periphery, spleen, peritoneum and bone marrow
- Immunohistochemistry(IHC) and histopathological analysis of the spleen of Eμ-PKCβII tg mice
- Perform functional assay to assess PKCβII activity in Eμ-PKCβII tg mice
- Compare PKCβ expression between malignant cells derived from MDR mice and Eμ-PKCβII tg and wild-type mice

Chapter 6

- General discussion

2 Chapter II: Methodology

2.1 Techniques involved in generation of the Eμ-PKCβIItg mice

2.1.1 Bacteria

2.1.1.1 Strains used and basic maintenance

In general, two different kinds of competent bacterial cells were used in this project: Shot® TOP10 Competent Cells (Invitrogen) and dam^-/dcm^- Competent *E. coli* (C2925I)(NEB). TOP10 bacteria were used for general cloning, whereas the dam^-/dcm^- *E. coli* were used when unmethylated DNA was required for digestion by a dam-sensitive restriction enzyme such as Cla-1(see Section 3.2.4).

All bacterial procedures were performed under aseptic conditions. Competent cells were grown in sterile Luria Broth (Sigma-Aldrich) liquid media, consisting of 25g/L of Luria Broth (Formulation 10g/L tryptone, 5g/L yeast extract and 10g/L $NaCl_2$) dissolved in deionised distilled water, followed by autoclaving at 122ºC. Once the solution was cooled, a relevant antibiotic was added to its recommended working concentration (Table 2-1). To prepare solid media, I followed the same recipe but added 15g/L of agar (derived from seaweed).

Antibiotic	Source	Dissolved in	Stock Solution	Concentration
Ampicillin	Sigma Aldrich	H_2O	X 1000	100μg/μl
Kanamycin	Sigma Aldrich	H_2O	X 250	50μg/μl*

Table 2-1.Antibiotics used for DNA cloning. (*:30μg/μl in C2925 strain)

To expand *E.coli* populations carrying a plasmid of interest, cells were initially grown in a starter culture. For this purpose, an individual bacterial colony carrying the plasmid of interest was picked from an LB-agar plate and inoculated into a 14 ml sterile Falcon 2059 tubes containing 5ml LB liquid media (with appropriate antibiotic). This was then incubated overnight at 37ºC with vigorous shaking (~ 230 rpm). For larger scale *E.coli* propagation, a conical flask was used, in which the volume of the flask should be

at least five times the size of the culture volume in order to have enough aeration. The flask containing the media was grown overnight at 37ºC in a shaking incubator with an approximate speed of 230 rpm.

Preparation of transformed *E.coli* for long term storage was done by growing the bacteria overnight so that they reached saturation. The cells were then mixed with 50% glycerol at a ratio of 1:1 and subsequently frozen and maintained at -80ºC. Viability was validated a few weeks later by scraping frozen *E.coli* from the top of frozen glycerol stocks with an inoculation loop (this should be performed promptly to avoid thawing the glycerol stock), and then inoculating an LB-agar plate. The plate was then incubated over night at 37ºC, and if visible clones appeared on the plate the following day, the glycerol stock was accepted.

2.1.1.2 Transformation of plasmid DNA into competent bacteria

The aim of transformation is to introduce foreign DNA (in this case plasmid) into bacteria. For this purpose, heat shock-based chemical transformation was used. Thus, 50 µl of competent bacteria (Top10) were slowly thawed in the 2ml screw cap tube in which they are provided. In the next step, 1 pg-100 ng of plasmid DNA is added, mixed gently and placed on ice for 30 minutes. This was followed by heat shock at 42ºC for 30 seconds (without shaking) and immediate incubation on ice for 5 minutes. 250 µl of Super Optimal broth with Catabolite repression (SOC) medium (Invitrogen) pre-warmed to room temperature was added. The transformation reaction was then incubated at 37ºC for an hour for recovery in shaking incubator with a speed of 250 rpm. Following this the transformation reaction was spread on to pre-warmed LB-agar plates containing the relevant antibiotics, and this was incubated overnight at 37ºC to allow the transformants to grow. In general, for each tube, a 10% and 90% aliquot of the total volume of the transformation reaction was spread on to the LB-agar plates. Transformation efficiency was assessed using 10 pg of control plasmid such as pUC19 (provided by Manufacturer).

2.1.2 DNA extraction methods

2.1.2.1 Basic small scale isolation of plasmid DNA employing alkaline lysis and phenol/chloroform/isoamyl alcohol (PCI)

This technique was used for purifying DNA from recombinant bacterial clones because this allowed a large number of colonies to be screened in a short period of time. Table 2-2 shows the list of the reagents used for this technique. Initially, recombinant bacterial clones were chosen from culture plates and inoculated in 4 ml LB broth containing an appropriate antibiotic. These cultures were grown overnight and then 2ml was transferred into a 2 ml micro-centrifuge tube. This was centrifuged in an Eppendorf centrifuge 5415 at 6800 x g for 5 minutes at RT. The pellet was re-suspended in 200µl of GTE solution (see Table 2-2) by vortexing, and then 200µl of NaOH/SDS lysis solution was added and mixed by gentle pipetting. This was followed by successive adding, and gentle mixing by inversion, of 200µl of K^+Ac^- solution to neutralize NaOH from the previous lysis step, and then 500µl PCI to extract proteins from DNA. The tubes were then centrifuged at maximum speed (12K – 14K xg) for 10 minutes precipitate protein. The supernatant was immediately transferred into a fresh 1.5 ml tube containing 500µl of isopropanol (VWR), mixed and incubated at RT for 5 minutes. To pellet precipitated DNA, the sample was centrifuged at maximum speed for 10 minutes, and the DNA pellet was washed by adding 1 ml of 70% ethanol. The samples were centrifuged briefly (14000xg) and the supernatant was gently decanted, and the residual ethanol allowed to evaporate. The now dry pellet was re-suspended and dissolved in 20µl of 0.1% TE buffer with RNAase (10 µg/ml), then incubated in a 37ºC water-bath for 30-60 minutes. In the end, 2 µl of a 1:10 diluted DNA solution in water was used for measuring the DNA concentration (see section 3.2.3.1).

Solution	Components	Source
GTE(re-suspension buffer)	50mM Glucose 25mM TRIS(pH 7.4) 1mM EDTA (pH 8.0)	AnalaR Calbiochem Sigma-Aldrich
Lysis buffer	1% SDS(w/v) 200mM NaOH	VWR VWR
K^+Ac^- solution(neutralisation buffer)	3M K Ac 11.5% Glacial acetic acid(v/v)	BDH Biochemical MERCK
PCI(24:25:1)	24:Phenol 25:Chloroform 1:Isoamylalcohol	VWR VWR VWR
TE buffer+RNase A	10Mm Tris.Cl(pH 8.0), 1mM EDTA 10µg/ml RNAase A	Qiagen Sigma

Table 2-2. The recipes for the buffers/regents used for small scale isolation of plasmid DNA employing alkaline lysis and PCI.

2.1.2.2 Small scale preparation of high quality plasmid DNA

This technique also relies on alkaline lysis of bacteria, but DNA is purified by binding to a silica membrane under high salt conditions and produces small quantities (5 to 20 µg) of high quality DNA that can be used for downstream applications such as DNA ligation and DNA sequencing. For this purpose, the QIAprep spin Mini-prep kit (QIAGEN) was used. Table 2-3 shows a list of the reagents/buffers provided by all QIAGEN plasmid DNA preparation kits used in this project.

Solution	Components
Buffer P1 (re-suspension buffer)	50mM Tris.Cl (pH 8.0), 10mM EDTA (pH 8.0), 100µg/ml RNase A
Buffer P2 (lysis buffer)	1% SDS(w/v), 200mM NaOH
Buffer P3(neutralisation buffer)	3 M potassium acetate (pH 5.5)
Buffer N3(neutralisation buffer)	Confidential-proprietary component of kit
Buffer PB (binding buffer)	Confidential-proprietary component of kit
Buffer PE (wash buffer)	Confidential-proprietary component of kit
Buffer ER(endotoxin removal buffer)	Confidential-proprietary component of kit
Buffer QC (wash buffer)	Confidential-proprietary component of kit
Buffer QF (elution buffer)	1.25 M NaCl, 50mM Tris.Cl (pH 8.5), 15% isopropanol (v/v)
Buffer QN (elution buffer)	1.6 M NaCl, 50mM MOPS (pH 7.0), 15% isopropanol (v/v)
TE buffer	10 Mm Tris.Cl(pH 8.0), 1mM EDTA

Table 2-3. The recipes of the buffers used in QIAGEN Plasmid DNA preparation kits.

Briefly, the overnight bacteria culture was transferred into 2ml micro-centrifuge tubes and bacteria were pelleted by centrifugation at 6800 x g for 5 minutes at RT. The bacterial pellet was then re-suspended in 250µl of buffer P1, followed by adding 250µl buffer P2 and mixing thoroughly by inverting the tube several times to lyse the bacterial cells. To neutralise the reaction, 350µl of buffer N3 was added, and each sample was centrifuged for 10 minutes at 14000xg at RT. The supernatant was then transferred into a QIAprep spin column and centrifuged for 30-60 seconds at high speed. The flow-through was discarded, and 500µl of buffer PB was added to the column to wash it from endonuclease activity following centrifugation for 30-60 seconds. This flow-through was again discarded and the column further washed by adding 750µl of buffer PE (to remove the salts) following centrifugation for 30-60 seconds. The flow-through was discarded, and the column was centrifuged again for 1 minute to ensure that there was no residual wash buffer left. The QIAprep spin column was then placed into a fresh 1.5 ml micro-centrifuge tube and DNA was eluted by adding 30-50 µl of milliQ H_2O, or X 0.1 TE buffer

(DNA eluted because of the creation of low-salt conditions). The column was allowed to stand on the bench for 1-5 minutes, and then centrifuged for 1 minute. The flow-through was saved, and the DNA concentration was determined using a spectrophotometer equipped with a UV lamp (see section 2.1.3.1).

2.1.2.3 Medium scale preparation of high quality plasmid DNA

A Midi-plasmid prep kit (Qiagen) was used to purify larger quantities (75-100 µg) of high quality DNA. The buffers/ regents used in this technique are listed in table 2-3. Thus, bacteria were grown in 25 ml culture overnight, and then harvested by centrifugation at 4500xg for 60 minutes at 4°C. The bacterial pellet was re-suspended in 4 ml of buffer P1, and then lysed by the addition of 4 ml of buffer P2 and mixing by inverting the reaction tube 4-6 times. The lysis reaction was allowed to sit at room temperature for 5 minutes, and then it was neutralised with 4 ml of chilled buffer P3 and mixed promptly by inverting the sealed tube 4-6 times. This was further incubated on ice for 15 minutes. The lysate suspension was then centrifuged at 20,000xg for 30 minutes at 4°C, the supernatant was removed and transferred into a fresh centrifuge tube and the centrifugation step was repeated.

A QIAGEN-tip 100 anion-exchange resin column was prepared by equilibrating it with 4ml of buffer QBT, and to this column the bacterial extract supernatant was then transferred, allowing it to go through the resin by gravity flow. The resin column was washed twice with 10 ml of buffer QC. After the wash steps, the DNA was eluted with 5 ml of buffer QF, and then precipitated by adding 3.5 ml of RT isopropanol. The sample was centrifuged at 14,000 x g for 30 minutes at 4°C and the DNA pellet was washed with 70% ethanol. Then sample was centrifuged at 14,000 x g for 10 minutes at 4°C and the ethanol was carefully removed from the DNA pellet. In the final stage, the DNA pellet was air dried for 5-10 minutes and then re-suspended in 50-75 µl of TE buffer. DNA concentration was determined spectroscopically.

2.1.2.4 Isolation of genomic DNA from animal tissues

The method for isolation of genomic DNA from mouse tails was adapted from the protocol described in “Molecular Cloning: laboratory Manual” by Sambrook (Sambrook 2000). Typically, each mouse tail (~ 0.5 cm) was chopped into smaller pieces with a scalpel and transferred into a 2ml screw-cap tube. Then, 500 µl of lysis buffer (50 mM Tris (pH 8.0), 100 Mm EDTA and 0.5% SDS (w/v)) with 250 µg proteinase K (final concentration 5µg/µl) (Sigma-Aldrich) was added to the tube and incubated overnight at 55°C in a water bath. The following day, 500 µl of phenol was added to each sample and incubated for 1 hour at RT with gentle shaking using nutator. Then, the sample was centrifuged at 14,000xg for 5 minutes and the supernatant was transferred into a fresh tube. 500 µl of PCI was added and the tube, mixed for 5 minutes by inversion (no vortexing), followed by centrifugation at 14,000xg for 5 min. The supernatant was transferred into a fresh tube and the 50µl 3M sodium acetate (pH 6.0) and 500µl of 100% ethanol were added to precipitate DNA. The tube was well mixed by inversion for 1 minute, and then centrifuged for 10 minutes at 14,000xg to pellet the DNA. The pelleted DNA was washed with 70% ethanol and re-suspended in TE buffer + RNase A.

2.1.2.5 Extraction of DNA from agarose gels

DNA extraction from agarose gels was performed using a GENECLEAN Turbo Kit (Q.Biogene) according to the manufacturer’s guidelines. Typically, the DNA band of interest was excised from the agarose gel using a scalpel blade. The gel slice was placed into a 1.5 ml eppendorf tube, and weighted. To each 100µg of gel slice 100µl of Gene clean turbo salt solution was added, and the sample was incubated in a water bath set to 55°C for approximately 10 minutes, or until the agarose gel was melted completely. Each sample was applied on to a cartridge with glass milk membrane placed inside a second carrier tube which was used to collect the flow-though (called a catch-tube). The DNA/gel/salt solution was then centrifuged for 10 seconds, the liquid in the catch tube was discarded and the membrane was washed twice by adding 500 µl of GENECLEAN turbo wash solution over the column and then centrifuged for 10 seconds. After the second wash, the Gene clean turbo cartridge was spun into an empty tube for

2 minutes at 14,000xg to ensure that the membrane was completely dried and no trace of ethanol was left (ethanol has an inhibitory effect on downstream applications (Loffert 1997)). In the last step, the column was placed into a fresh 1.5 ml micro-centrifuge tube with a detachable lid (provided in the kit) and the DNA was eluted by adding 30 µl of GENE clean turbo elution solution directly on to the cartridge. Each cartridge was incubated for 5 minutes at RT, and then centrifuged for 1 minute at 14000xg to transfer the eluted DNA into the freshly provided tube. To estimate DNA yield, 10% of the eluted sample was run on an agarose gel (see Section 3.2.3).

Also, this technique was particularly used when a segment of DNA needed to be digested by two restriction endonucleases that had incompatible buffers. In this case, a liquid version of the GENECLEAN reaction was used, which is very similar to the GENE CLEAN protocol described above. The only difference is that X5 (v/v) GENECLEAN turbo salt solution was added into the tube containing DNA that was cut by the first restriction enzyme. This was followed by loading the mixture on to a GENECLEAN column and purifying as described. The resulting purified DNA could then be digested with the second restriction enzyme.

2.1.3 DNA analysis

2.1.3.1 Determination of the purity and concentration of DNA by UV spectroscopy

The purity and concentration of DNA were determined using a UV spectrophotometer (BioPhotometer, Eppendorf). 1 µl of extracted DNA was diluted 1:100 with a relevant re-suspension buffer (usually water or TE buffer), mixed well and transferred into an UV cuvette (Eppendorf). The re-suspension buffer without any DNA was used as a blank control. The samples were measured in the BioPhotometer and the concentration of DNA was calculated using the equation described below:

Concentration (µg/ml) = (A_{260} reading - A_{320} reading) x dilution factor x 50µg/ml

Based on this equation, absorbance measured at a wavelength of 260nm (A_{260}) indicates concentration of DNA and this is corrected for the turbidity by subtracting light

absorbance measured at 320nm (A_{320}). The adjusted A_{260} was then multiplied by the dilution factor and 50 (this latter comes from using a relationship in which a 50 µg/ml concentration of DNA has an absorbance of 1 at A_{260}). Total yield of purified DNA was calculated as DNA yield (µg) x total volume (µl). The DNA purity was assessed based the A_{260}/ A_{280} ratio in which pure DNA has value of 1.8, however values between 1.7 and 2 are considered as high quality DNA. A value of less than 1.8 is an indication of protein contamination, whereas a value greater than 2.0 is an indication of RNA contamination.

2.1.3.2 Agarose gel electrophoresis

Agarose gel electrophoresis was used to separate a mixed population of DNA fragments, and also used for estimation of DNA yield after extraction from the agarose gel. In general, Gensieve LE agarose (Flowgen) was used for gel electrophoresis. However, when a DNA fragment was to be used for molecular cloning procedures SeaKem®GTG® agarose (Lonza) was preferred. The agarose solution was melted in a standard microwave oven on full power for 2-4 minutes, and then cooled to approximately 50°C. Then, ethidium bromide (Roche) (0.5 µg/ml) was added to the solution, and this was followed by pouring the solution into a sealed gel cast with comb (to form wells) and allowing the gel to set. Once the gel set comb and sealing tape were carefully removed, and the cast containing the gel was placed in the gel tank containing 1 x TAE buffer (40mM Tris-Base, 1mM EDTA (pH 8.0), and 1.142% glacial acetic acid). There should be a minimum of 1mm of TAE buffer covering the surface of the gel. Samples were prepared by the addition of 10% (v/v) of orange G loading buffer (50% glycerol with adequate amount of orange G dye (BDH) to give clearly visible orange colour), and they were loaded in the wells. At least one well of the gel was loaded with a DNA marker (either the 100bp DNA ladder (NEB) or the 1kb DNA ladder (Invitrogen)) in order to estimate the size of DNA within the loaded samples.

Gels were made up using different percentages of agarose (typically 0.5, 0.7, 1.0, 1.3 and 2% (w/v) agarose) in order to obtain best resolution depending on the size of the DNA. The gel (Scie-Plas) unit was run in horizontal fashion by applying a voltage of 1-10 V/cm. The gel was run until the DNA bands were satisfactorily separated. As a result of

intercalation of ethidium bromide present in the agarose gel into the DNA structure, DNA could be visualised using a High Performance UV trans-illuminator (UVP). A Kodak EDAS 290 digital camera was used to obtain images of the gel, Adobe Photoshop was used to edit pictures into a desirable format. DNA yield was estimated from the agarose gel and is described in Section3.2.3.

2.1.3.3 Southern blotting

In this project Southern blotting was used for detecting the transgene in genomic DNA extracted from the tail of potential Eμ-PKCβII tg mice. The protocol used in this project was adapted from the book, Molecular Cloning: A Laboratory Manual (Sambrook 2000). Thus, 10μg of genomic DNA extracted from the tail of the mice was digested with a relevant restriction enzyme (See section 4.6.1), and then the fragments were separated by electrophoresis on a 0.7% agarose gel. Alongside these samples a 1kb DNA ladder, DNA extracted and similarly prepared from wild-type control and transgene plasmid added at equivalent amounts corresponding to 0.1, 1, 10 and 20 copy numbers of the transgene (used as a positive control (see Section 4.6.1)). Following sufficient electrophoresis the gel was placed on UV trans-illuminator and a ruler was placed beside the gel. A digital photograph was taken to record the ethidium bromide staining pattern, and this was a very important indicator of complete digestion of the genomic DNA samples (see Section 4.6.1).

In the next stage the agarose gel was washed several times in denaturation, depurination and neutralisation solutions (Table 2-4). Initially, the gel was subjected to 3 x 15 min washes in denaturing buffer and using agitation. This was followed by a 5 minute wash in 0.2 N HCL, again with agitation and a quick rinse in ultrapure (>18Mohm) water. Preparation of the gel for transfer was completed by 3 x 15 min washes in neutralisation buffer using agitation. In the meantime, an appropriately sized piece of nitrocellulose membrane (HyClone), Whatman filter papers and paper towels were prepared. The nitrocellulose membrane was soaked in water for 20 minutes, followed by soaking in 10 X Saline-sodium citrate (SSC). Before transfer, the gel was placed into 10 X SSC, and the transfer apparatus was assembled; the layout of the

apparatus is described in Figure 2-1. When the apparatus was set up it was wrapped in cling-film to avoid excessive evaporation. The transfer was performed for 16-24 hours. Table 2.4 shows a list of buffers used for the Southern blotting.

Buffer	Components	Source
Denaturing buffer	1.5 M NaCl 0.5 N NaOH	VWR VWR
Neutralisation buffer	1 M Tris (pH 7.4) 1.5 M NaCl	Calibiochem VWR
20 x SSC (pH 7.0)	3 M NaCl 0.3 M Sodium citrate	VWR Sigma-Aldrich
Pre hybridisation mixture	1 M NaCl 10% Dextran sulphate 1% SDS	VWR PKChemicals VWR

Table 2-4. The recipes of the buffers used in Southern blotting.

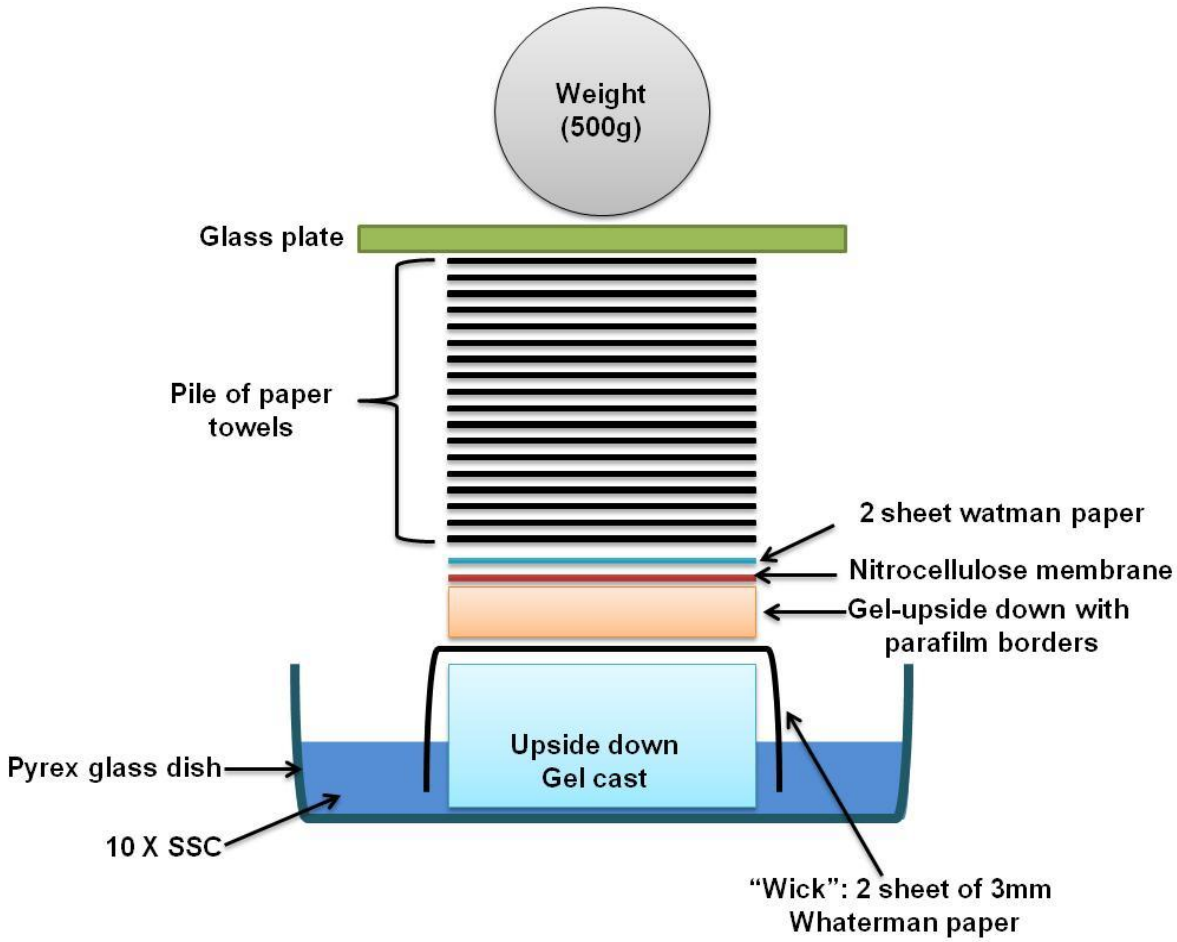

Figure 2-1.Southern blotting transfer apparatus.

After completion of the transfer, the apparatus was disassembled and the back of the nitrocellulose membrane was labelled to identify the position of the first well. To check the transfer efficiency the post-transfer agarose gel was re-stained with a 0.5 µg/ml solution of ethidium bromide for 30 minutes with agitation, followed by visualisation when exposed to UV light. The nitrocellulose membrane was placed on a clean sheet of Whatman paper and air-dried for 10-15 minutes. The bound DNA was immobilised on to the nitrocellulose membrane by exposure to UV irradiation using a UV cross-linker using a set programme for this purpose. The membrane was then soaked in 1 M NaCl for approximately 30 minutes, ensuring that the membrane was thoroughly wet. Meanwhile, the pre-hybridisation mixture (pre-hybe mix) and hybridisation bottles were heated at 65°C in hybridisation oven. In the next step, 25 ml of pre-heated pre-

hybe mix was transferred into the hybridisation bottle. In the case where more than one membrane was used, two membranes could be placed into one hybridisation bottle with a special mesh screen between them. The membrane was then incubated in pre-hybe mix at 65°C with circular moving for approximately 3 hours. If there is no time limitation, the incubation can be performed overnight.

The construction of the probe is described in section 4.6.1. In order to radioactively label the probe, an Amersham Megaprime DNA Labelling System (RPN1604) was employed. Based on this system, 50 ng of probe DNA was added to 5 µl of primer mix in a 0.2 ml PCR tube. A final volume of 26 µl was achieved by adding H_2O. This was followed by heating the mixture in a PCR machine set to 98°C for 5 minutes, and allowing it to cool to RT. A brief centrifugation concentrated the liquid in the bottom of the tube. In the next step, 4µl of dATP (Deoxyadenosine triphosphate), 4µL of dTTP (Thymidine triphosphate), 4µl of dGTP (Guanosine triphosphate) and 5 µl of reaction buffer were added. Then, 5µl of ^{32}P labeled dCTP (Cytidine triphosphate)(Easy Tides Deoxycytidine 5'-triohosphate, [α-^{32}P] 250µCi (9.25 mBq) in 25µl from Perkin Elmer) was added into the mixture (this was done behind a Perspex radiation screen in order to reduce personal exposure to radioactivity), following by addition of 2µl of Klenow DNA polymerase. The reaction was mixed by pipetting and incubated at 37°C for 45 minutes. Meanwhile, a G-50 sephadex separation column was prepared consisting of a glass Pasteur pipette blocked with a small quantity of siliconised glass wool (Sigma-Aldrich) and filled with swollen G-50 sephadex beads (50% G-50 sephadex w/v in water). Once the incubation of the radioactively labelled probe was completed, it was placed on ice for approximately 2 minutes before running it through the column.

To prepare the probe to run through the column, it was first mixed with 20µl of Orange G and 20µl of dextran blue. Then, the mixture was loaded on to the column in a drop-wise fashion, and eluted fractions liquid were collected in a 1.5 ml micro-centrifuge tube. Once all the reaction was loaded, water was added in a drop-wise fashion. Within the column the blue dextran co-migrates with DNA whereas Orange G co-migrates with unincorporated nucleotides. Therefore, the blue droplets are expected to contain the probe (approximately 400µl) and were collected in an allocated screw cap top tube.

For measuring radioactivity, a 2µl aliquot of the probe measured in a scintillation counter (PACKARD, 1500 TRI-CARB). The radioactivity of the probe was represented as dpm/µg, and used to calculate the volume needed to achieve a desired 1 x 10^6 dpm/ml within 25ml of the hybridization buffer. To reduce non-specific binding of the hybridization probe to the surface of the membrane Salmon sperm DNA (Sigma-Aldrich) was used as a blocking regent at a final concentration of 100 µg/ml. This was added into the probe and the mixture was then boiled for 10 minutes and then immediately incubated on ice for 5 minutes before adding it to the pre-heated pre-hybe mix. The hybridisation reaction was performed in a hybridisation bottle at 65°C overnight in the hybridisation oven where the bottle was gently rotated.

The following morning, the membrane was taken out from the hybridisation bottle, briefly washed twice in 2 X SSC buffer on a rocker at RT, and then twice more for 15 min. This was followed by 2 x 15 min washes in 2 X SSC + 0.1 % SDS buffer preheated to 65°C, and this was performed using a sealed Tupperware box in a shaking (60 rpm) water-bath at 65°C. The last wash was in 0.1 X SSC at RT for 5 minutes on the rocker. To visualise the signal the membrane was wrapped in cling-film, placed on to X-ray film (Kodak Biomax MS Film, sourced from Sigma-Aldrich) in a cassette containing an intensifying screen. This was incubated at -80°C for 1-3 days, after which the film was developed. It should be added that all the reagents used for radio-labelling the probe were from Amersham, unless stated otherwise.

2.1.4 Enzyme based DNA manipulation

2.1.4.1 Digestion with restriction endonucleases

Most of the restriction endonucleases used in this project were purchased from New England Biolabs (NEB), and were used for digesting plasmid DNA during the cloning process (i.e. for ligation reactions). Typically, in this process 0.5-1 µg of plasmid DNA, 5-10 units of restriction enzyme, relevant buffer and BSA (final concentration of 100µg/ml if necessary) were mixed in a total volume of 20 µl (Table 2-5). The digestion reaction was incubated for approximately 2 hours at 37°C. The total volume was

determined based on the fact that the enzyme content is not allowed to exceed 10% of the total volume of the digestion reaction (v/v) in order to prevent non-specific cutting, which is called star activity. To ensure that the DNA was completely digested a 10X excess of enzyme (10 U/µg) is used to cut the DNA. The digested DNA fragments can then be separated by electrophoresis on a GTG® (genetic technology grade) agarose gel. In the case that DNA needed to be digested with two restriction endonuclease enzymes, a compatible buffer was chosen that ensured a minimal activity of 75% for both enzymes and this was done following NEB (New England Biolabs)'s guidelines. If the two chosen enzymes did not have a compatible buffer, a sequential digestion was performed by purifying the DNA using the liquid GENECLEAN protocol following the first digestion in order to allow the second restriction digestion to proceed unfettered (see Section 2.1.2.5).

Digestion reaction	**Concentration**
Plasmid DNA	Approx. 0.5-10 µg
NEBuffer	10 X
BSA	(100 µg/ml)
Restriction endonulease	Approx. 10 U/µg
Water	Up to final volume

Table 2-5.Components of a typical digestion reaction.

2.1.4.2 De-phosphorylation of Vector DNA (Antarctic phosphatase reaction)

To prevent vector self-ligation, Antarctic phosphatase (NEB) was used to remove the 5' phosphate group. Thus, following restriction enzyme digestion of backbone vector DNA (1-5 µg) further enzymatic activity was inactivated by incubation at 65°C. In the next step the reaction was mixed with a $1/10^{th}$ volume of provided 10X Antarctic phosphatase buffer and 1µl of Antarctic phosphatase (5 units). This was mixed by vortexing for 2-3 seconds, and the reaction was briefly centrifuged and then incubated at 37°C for 15 minutes for 5' extensions or 60 minutes for 3' extensions. The reaction was

then stopped by heating to 65°C for 5 minutes, or alternatively by adding 1/10 volume of orange G dye.

2.1.4.3 Blunting DNA ends using DNA polymerase I, large (Klenow) fragment

During DNA cloning, DNA blunting is used when no compatible end restriction sites are available, or if the sticky end created by a restriction enzyme is required to be removed for a particular downstream cloning purpose (see Section 3.4). DNA polymerase I, known as the large (klenow) fragment (NEB) is used to create blunt ends on digested DNA fragments by either filling in 5' overhangs or by removing 3' overhangs. To do this plasmid digests where the restriction enzyme reaction (Total volume of 100µl) was heat inactivated at 65°C for 15 minutes were mixed with 1 unit of Klenow/1µg of DNA and 33 µM of each dNTP (Deoxyribonucleotide triphosphate)according to the manufacturer's protocol. This reaction was then incubated at 25°C for 15 minutes. The reaction was stopped by heat inactivation at 75°C for 10 minutes, and then let to cool down slowly. To ensure that the blunting reaction was stopped, EDTA (Ethylenediaminetetraacetic acid)was added to the final concentration of 10mM before adding x 10 orange-G loading buffer and running the samples on a GTG® agarose gel.

2.1.4.4 Ligation of DNA fragments

T4 DNA ligase (Fermentus) was used for DNA ligation, and the procedure was performed according to the manufacturer's instructions; the components of the ligation reaction were mixed together in a 0.2 ml PCR tube (table 2-6) to a final volume of 10µl, well mixed by vortexing for 2-3 seconds, centrifuged briefly and incubated at 14°C for a minimum of 18 hours. Then, 1-5 µl of the reaction was added to competent cells within the transformation reaction (see Section 2.1.1.2). Two control reactions were also routinely used, consisting of the vector DNA with and without DNA ligase in the appropriate buffer. The presence of bacterial clones on the control plate with ligase would suggest that the de-phosphorylation reaction has not been successful, whereas the presence of the clones in the control without ligase means that the digestion of the

DNA was incomplete and the ligation reaction might have been contaminated with uncut plasmid DNA.

Compounds	Amount
Vector	50 ng
Insert (DNA)	At least 1:1 molar ratio of vector: insert, but aimed for much higher insert concentration up to 1:10
10 x T4 buffer	1 µl
T4 DNA ligase (1 unit)	1 µl
Water	Make up volume 10 µl

Table 2-6.Components of a typical ligation reaction.

2.1.4.5 Using intermediate vector (TA-cloning)

The details of the TA cloning strategy I employed in this project are described in section 3.2.3. Firstly, I had to ensure that there was no trace of Phusion DNA polymerase because this enzyme has 3' to 5' exonuclease activity which could result in the removal of the desired poly A-tail. Inactivation of Phusion DNA polymerase was achieved by heat-treating the reaction at 98°C for 20 minutes promptly after completion of the PCR. Then, the reaction was allowed to cool slowly, and once cool 1µl of 10mM dATPs and 1 µl of Taq DNA polymerase (10 units) were added into the old PCR reaction (50 µl), mixed well ,and centrifuged briefly. This was followed by incubation at 72°C for 20 minutes. Finally, the reaction was run on a GTG® agarose gel and DNA was extracted for downstream cloning.

2.1.5 Amplification of DNA by polymerase chain reaction (PCR)

2.1.5.1 Standard Procedures and optimization

Polymerase chain reaction (PCR) was used to amplify the DNA of interest using appropriate forward/reverse primers, and was mediated by a thermo-stable DNA polymerase such as Taq or Phusion. In general, the total volume of the PCR reaction

was 20-25 µl and contained a polymerase enzyme supplemented with its buffer, 800 µM dNTPs (GE Healthcare), 0.05 µg of each primer and an adequate amount of the template DNA which required PCR optimisation and was typically 10 ng of DNA (see Section 3.2.2) (see table 2-7). The reaction was then topped-up with distilled water to achieve a total volume of 25µl. Finally, the PCR tube containing the reaction mixture was placed in a thermal cycler (P X2 Thermal Cycler, Thermo.Electron Corporation). The appropriate number of cycles as determined by PCR optimisation was applied for the specific DNA of interest (see Section 3.2.2). Amplified DNA was separated on an agarose gel by electrophoresis and then visualized by UV light after staining with ethidium bromide.

Taq DNA polymerase (NEB) was used to amplify DNA fragments destined for DNA cloning, and for screening of bacterial colonies. Phusion (Hot Start) High-Fidelity DNA polymerase (Finnzymes) and JumpStart Taq DNA polymerase (Sigma-Aldrich) were used for screening of genomic DNA extracted from mouse tails. The PCR conditions for these DNA polymerases are listed in table 2-8.

To design primers for PCR, Primer3 (http://simgene.com/Primer3) and primer BLAST (http://www.ncbi.nlm.nih.gov/tools/primer-blast) programmes were used. The length of primers was typically 18-25 nucleotides with a 40-70% GC content and a melting temperature (Tm) of approximately 60°C. The designed oligonucleotides were synthesised by Eurofin (http://www.eurofinsgenomics.eu/) MWG Operon and reconstituted in water before using. Primers used in this project are listed in Appendix A.

Compounds	25µl
Buffer	X2 or X5
Forward Primer	0.05µg
Reverse Primer	0.05µg
dNTPs	200µM
DNA polymerase	0.4-1 units
DNA template	250 ng-1µg of genomic DNA 5-10 ng of plasmid DNA
Water	q.s. to 25µl

Table 2-7. Typical components of a PCR reaction.

	Phusion High-Fidelity DNA Polymerase			***Taq DNA Polymerase(NEB)***			***JumpStart Taq DNA polymerase***		
	Temp.	**Time**	**cycles**	**Temp.**	**Time**	**cycles**	**Temp.**	**Time**	**cycles**
Initial denaturation	98°C	30 s	1	95°C	30 s	1	94°C	2 m	1
Denaturation **Annealing** **Extension**	98°C 50-65°C 72 °C	10 s 30 s 30 s/kb	15-35	95°C 50-65°C 68 °C	30 s 30 s 60 s/kb	15-35	94°C 55-68°C 72 °C	30 s 30 s 2 m	15-35
Final Extension	72°C	5-10m	1	68°C	5 m	1	72°C	5 m	1
Hold	4°C			4°C			4°C		

Table 2-8. Standard cycle condition for the DNA polymerases used in this project.

2.1.5.2 Specialized PCR methods

2.1.5.2.1 DNA Sequencing (Eurofins MWG Operon/GATC)

In order to sequence the DNA, high quality DNA was prepared using a QIAGEN mini-prep kit (see Section 2.1.2.2). In this project, the DNA samples were sent to either Eurofins MWG Operon or GATC Biotech for sequencing. The DNA samples were

prepared for sequencing according to manufacturer's instructions, which are summarized in table 2-9.

	Eurofins MWG Operon	**GATC Biotech**
High quality plasmid DNA	50-100 ng/µl in 15µl per reaction	30-100 ng/µl in 20µl (enough for 8 reactions)
Primers	15 pmol, sent pre-mixed with template DNA	10 pmol/µl in 20 µl (enough for 8 reactions)

Table 2-9. Standard high quality DNA preparation for sequencing at Eurofins MWG Operon and GATC Biotech.

2.1.5.3 Phire Animal Tissue Direct PCR kit

Phire® Animal Tissue Direct PCR Kit (Finnzyme) was used to DNA isolated directly from tissues without the need for high quality purification. This method was used for the propagation of the MDR-KO mice used in Chapter 5 of this thesis. Tissue samples from these mice were typically ear-notches of 2-3 mm in diameter, and these had been stored at -20°C until used. To extract DNA, the tissue was placed into 20µl of Dilution Buffer and 0.5µl of DNA Release Additive was added. The solution was mixed by vortexing, centrifuged briefly and then incubated for 2-5 minutes at RT. The reaction was then placed into pre-heated block (98°C) for 2 minutes, supernatant transferred into a fresh tube and stored at -20°C if not used immediately. The PCR was performed using Phire ® Hot Start II DNA Polymerase, provided with the kit. This polymerase has a high resistance to many PCR inhibitors residing in animal tissues. PCR was performed on 1-2 µl of isolated DNA using conditions shown in table 2-10.

A

	Phire ® Animal Tissue Direct PCR Kit		
	Temp.	**Time**	**cycles**
Initial denaturation	98°C	5min	1
Denaturation **Annealing** **Extension**	98°C 65°C 72 °C	10 s 30 s 1 m	30-35
Final Extension	72°C	1 m	1
Hold	4°C		

B

	20 µl
Buffer	**X 2**
Forward Primer	**0.5µM**
Reverse Primer	**0.5µM**
dNTPs	**200µM**
Phire ® Hot Start II DNA Polymerase	**0.4 µl**
DNA	**1-2 µl**
Water	**q.s. to 20µl**

Table 2-10.Standard cycle condition(A) and reaction (B) for PCR using Real time PCR Phire ® Animal Tissue Direct PCR Kit.

2.1.6 Quantitative Real Time PCR

Quantitative Real-Time PCR (RT-PCR) was used to quantify mCherry as part of the transgene integrated into the genomic DNA of the transgenic mice I created. This was important in order to distinguish heterozygous from homozygous Eμ-PKCβII tg mice. To do this I used the 5 x HOT FIREPol® EvaGreen® qPCR Mix plus (ROX) (Solis Bio Dyne). This kit is an optimised ready-to-use solution for real-time quantitative PCR assays and consists of: HOT FIREPol® DNA polymerase, ultrapure dNTPs, $MgCl_2$ and EvaGreen® dye. The EvaGreen® is a DNA-binding dye which has a similar spectrum to SYBER® Green, but is more stable dye and inhibits PCR less. The PCR reaction was prepared according to a slightly modified version of the manufacture's instruction described in table 2-11. Firstly, extracted genomic DNA was placed in the bottom of flat-bottomed 96 plate and the master mix was added. The reaction plate was sealed with a provided adhesive sticker using a plate sealer tool, centrifuged briefly and placed into a

real-time thermal cycler, Mx3005P Q-PCR system (Agilent Technologies). The quantification of the transgene by q-PCR is extensively discussed in section 4.7.

A

	HOT FIREPol® EvaGreen® qPCR Mix Plus		
	Temp.	**Time**	**cycles**
Initial denaturation	95°C	10 min	1
Denaturation **Annealing** **Extension**	95°C 70°C 72 °C	30 s 30 s 1 m	35

B

Components	**20 µl**
HOT FIREPol® EvaGreen® qPCR Mix Plus	4 µl
Forward Primer	80-250 nM
Reverse Primer	80-250 nM
DNA template	50-250 µg
Water	q.s. to 20µl

Table 2-11.Real Time PCR cycles (A) and reaction mix (B) used for quantification of the transgene in E-PKCβII transgenic mice.

2.2 Techniques involved in phenotypic analysis of the Eμ-PKCβII tg mice

2.2.1 Cell lines used and cell culture

Two cell lines were used in this project, A20 and MEC-1 cells. The A20 cell line is a BALB/c-derived B cell lymphoma line purchased from the American Type Culture Collection (ATCC). MEC-1 is the cell line originating from the peripheral blood (PB) of a patient with B-CLL who was undergoing pro-lymphcytic transformation. MEC-1 cells were purchased from the Deutsche Sammlung von Mikroorganismen und Zellkulturen (DSMZ). These cell lines were grown according the manufactures' instructions. The recommended media for growing A-20 cells was **R**oswell **P**ark **M**emorial **I**nstitute **1641** (**RPMI 1641**) supplemented with 10% Fetal bovine serum (FBS), and for MEC-1 was

90% **D**ulbecco's **M**odified **E**agle's **M**edium (**DMEM**) supplemented with 10% FBS(see Section 3.4.2).

2.2.2 Introducing DNA plasmid into mammalian cells using Nucleofection

Nucleofection was used as a transfection method to introduce plasmid DNA into mammalian cells. This method employs an electroporation cell and special buffers that are included within a Nucleofection kit (Lonza Biologics plc, Tewkesbury UK). Briefly, 2 x 10^6 cells were transfected using the Amaxa solution V transfection kit according to the manufacturer's protocol. The cell suspension was mixed with 2 µg of DNA, transferred into the provided cuvette, placed in Nucleofector® device and electroporated with the appropriate programme (U-013 for A20 cell line and X-001 for MEC-1 cell line). Following transfection the cells were transferred into the relevant pre-heated media, and incubated in a humidified incubator at 37°C for an appropriate period of time (24 hours for A20 and 48 hours for MEC-1 cell lines). A plasmid encoding maxGFP (Lonza), a green fluorescent protein, was used to aid analysis of the transfection efficiency.

2.2.3 Tissue isolation and preparation of single cell suspensions

2.2.3.1 Tissue isolation

The tissues I isolated from mice were spleen, peritoneum, bone marrow and peripheral blood. Single cell suspensions were prepared from each of these tissues for FACS analysis. In the following sections I describe isolation for each individual tissue mentioned above:

2.2.3.1.1 Peripheral Blood

Blood collection was performed immediately after sacrificing the mice with CO_2 by performing a cardiac puncture in which the needle (19 g) was inserted at a 20-30 degree angle from the horizontal axis of the sternum into the heart of the dead animal.

Approximately 500-1000 µl of peripheral blood was collected, and this was enough to perform FACS analysis.

2.2.3.1.2 Peritoneum

Following blood collection the mouse was laid down on its right side, the outer skin was swabbed with 70% Ethanol and an incision was made with scissors so that the outer skin could be pulled back using forceps to expose the inner skin covering the peritoneal cavity. In the next step, 10 ml of ice cold modified Phosphate buffered saline (PBC) (1% BSA + 0.1% Sodium Azide, pH 7.2) was injected gently into the peritoneum cavity using a 27g needle and then the peritoneal cavity was gently massaged. This was followed by insertion of the needle back into the cavity and the fluid was collected carefully avoiding clogging the needle with fat tissue or other organs. To collect as much peritoneal fluid as possible, an incision was then made in the inner skin of the peritoneum and the skin held up with forceps so that a plastic Pasteur pipette could be used to collect the remaining peritoneal fluid from the cavity (Figure 2-2).

Figure 2-2. Isolation of Peritoneal cells in mouse. This figure shows how cells are isolated from peritoneum following lavage with modified PBS. A plastic Pasteur pipette is used in the final stage of collection.

2.2.3.1.3 Spleen

The spleen is located on the left side of the abdominal cavity, above the kidney and below the heart. Thus, after opening the abdominal cavity the spleen was found. In the next step the spleen was lifted by holding the surrounding fat pads with forceps and then isolating the spleen from these surrounding fat pads and placing it in a petri dish containing 5 ml of medium (RPMI). The isolated spleen was divided into three pieces: one piece was snap frozen in liquid nitrogen for protein extraction (see Section 2.2.4), one piece was formalin fixed and then paraffin embedded for histochemistry analysis (see Section 2.2.6) and the final piece was used to prepared a single cell suspension for FACS analysis. The single cell suspension was prepared by physically dissociating (titrating) the spleen with a Pasteur pipette in the petri dish containing 5 ml medium. The titration was continued until there was homogenous suspension of splenic tissue, then the connective tissue of the spleen was manually removed and red blood cells were lysed (Figure 2-3).

Figure 2-3. Isolation of spleen from body cavity in mouse. This figure shows dissection of the mouse with the purpose of obtaining the spleen. The spleen in this figure is held by the forceps.

2.2.3.1.4 Bone Marrow

To isolate bone marrow cells the skin surrounding the lower part of the mouse body, including the legs, was removed completely. Then, the femur was dissected from the tibia and hip by scissors (Figure 2-4A) and separated from the body. The remaining tissues were removed from dissected femora bone to avoid contamination of bone marrow cells with other cell types (Figure 2-4B). A 5 cc syringe with a 25g needle

containing 5 ml of modified PBS was inserted into the broken end of the femora (Figure 2-4AC) and cavity gently flushed the modified PBS. The PBS containing bone marrow cells was transferred into a fresh 15 ml tube. The bone marrow cell suspension was topped with modified PBS up to 15 ml, and well mixed by pipetting up and down to ensure that I have a homogenous suspension of bone marrow cells.

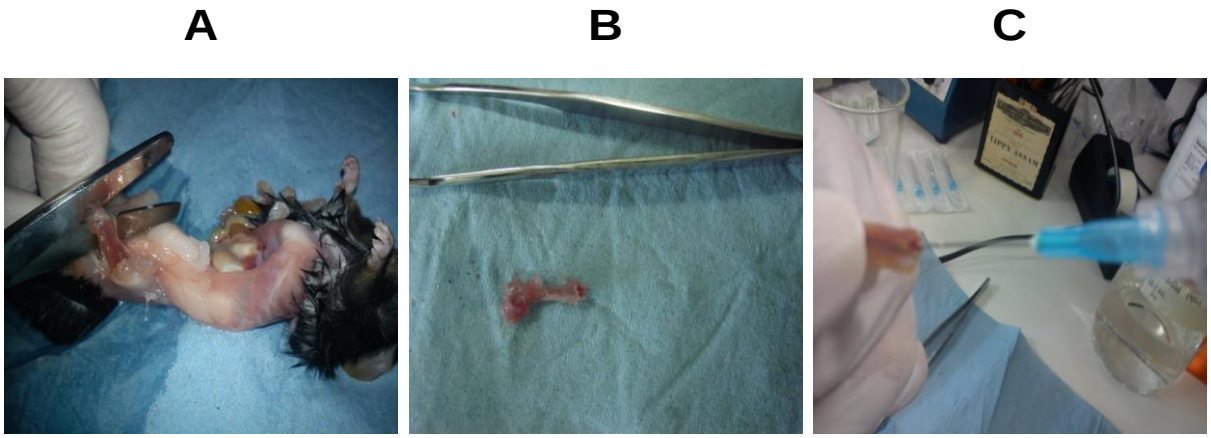

Figure 2-4. Isolation of Bone Marrow cells from Femora in mouse. This figure shows dissection of the femur from the mouse (**A**), removal of surrounding muscle and connective tissue (**B**) and isolation of marrow using a syringe (**C**).

2.2.3.2 Single cell suspension

After the cells were isolated from peripheral blood, peritoneum, spleen and bone marrow they were transferred into 15 ml tubes and topped-up with 15 ml of the RPMI medium. The cell suspensions were mixed well with a pasteur pipette to achieve a homogenous population of the cells. Then, the cell suspension was centrifuged at 1500 rpm (150xg) for 3-5 minutes, the supernatant was decanted, then 1-2 ml 0.83% Ammonium chloride (in water) was added and the pellet re-suspended and incubated at RT for 2-5 minutes to lyse red blood cells. Then, the samples were topped-up with RPMI medium to 5ml and then centrifuged at 1500 rpm for 5 minutes and re-suspended into fresh media containing 90% RPMI and 10% FCS. In the end, the cell suspension was counted and incubated on ice overnight and the FACS experiment was performed the following morning.

2.2.4 Protein extraction from cells

Protein extraction from tissue

To extract the protein from tissues (Spleen, Kidney, Heart and Liver) of mice I took snap-frozen tissue samples and powdered them with a mortar and pestle under liquid N_2. It was important to prevent warming the tissues, therefore I constantly topped-up the liquid N_2 level until the tissues were completely powdered. In next step the powdered tissues were re-suspended in 3x packed volume of Buffer C (see table 2.2-1) and were subjected to 3 cycles of freezing with liquid N_2 and subsequent thawing on ice in order to homogenize the tissues. This was followed by centrifugation at maximum speed for 10 minutes at 4°C, and the supernatant was transferred into a fresh 1.5 ml tube. Protein determination was performed using a Bradford assay.

Solutions	Component
Lysis Buffer C used for protein extraction from tissue	20mM HEPES, 25%Glycerol, 0.42 M NaCl, 1.5mM $MaCl_2$, 0.2mM EDTA, 1mM DTT, 1mM PMSF ,Protein Inhibitors
Protein Inhibitors	Aprotinin (A)(X1000), Leupeptin (L)(X1000), Pepstatin(P)(X1000), Phenylmethylsulphonyl fluoride (PMSF)(X100), Soybean Trypsin (STI)(X1000)
Protein sample buffer	0.25 M Tris (pH 6.8), 8% Sodium dodecyl sulphate (SDS), 40% glycerol, 4mg/ml bromophenol blue, 1% β-mercaptoethanol
PBS	0.065M Na_2HPO_4, 0.015 M $NaH_2PO_4xH_2O$, 0.075 M NaCl

Table 2-12. Recipes for the buffers used for protein extraction from the tissue.

Protein sample preparation and quantification (Bradford assay)

To perform a protein determination using the Bradford Assay a series of protein standards were prepared consisting of 20, 10, 5, 2.5, 1.25, 0.625 and 0.3125 mg/ml of bovine serum albumin (BSA) dissolved in buffer lysate C. Then 2µl of supernatant containing the protein extracted from the tissue or 2µl of protein standard at each concentration were added to 1 ml of Bradford reagent (BioRad-diluted in 1 in 5 water). This was vortexed for a short time. The presence of protein was detected in the Bradford

reagent with a change in spectral properties of Coomassie Brilliant Blue G-250 that can be measured by light absorbance at 595 nm. Protein concentration of the sample is determined from a graph constructed from the absorbance readings of the protein standards. The samples were then prepared to a concentration of 25-50 µg/20µl in sample buffer, incubated at 95°C for 5 min, and then stored at -80°C.

Protein extraction from cell lines

To extract protein from cell lines 2 x 10^6 cells were pelleted, then washed in PBS and lysed with 200µl of lysis buffer (125mM Tris pH 6.8 + 5 mM EDTA +1% SDS). The cell lysates were then sonicated and incubated for 5-10 minutes at 95°C. This was followed by centrifugation of the cell lysate at 12,000 rpm for 5 minutes, then the supernatant was transferred in a fresh micro tube and protein determination was performed. The protein lysate was kept at -20°C.

2.2.5 SDS-PAGE and Western blotting

In this project Western blotting was used for detection of transgene at the protein level, and also for the quantification of PKCβII in both Eµ-PKCβII tg and wt mice. Thus, sodium dodecyl sulphate-polyacrylamide gel electrophoresis (SDS-PAGE) was used to separate the proteins of splenic tissue (25-50 µg) based on their molecular weight. The recipes for the solutions used in for Western blotting are described in table 2-13. To prepare the gel, resolving gel mixture was poured into a glass cassette sandwich at an appropriate percentage of acrylamide (usually 10-12%), and topped-up with water to avoid drying the gel. The gel was allowed to polymerize for approximately 30 minutes. Then the water was poured off, and stacking gel mixture was loaded on top of the lower resolving gel. This was followed immediately by gentle insertion of a comb into the stacking gel that allowed for the formation of sample wells. Then the gel was allowed to set for 5-10 minutes. Once the gel was completely polymerised, the comb was carefully removed, and the gel cassette was placed in the electrophoresis tank in a vertical position. In the meantime, an appropriate amount of protein sample was defrosted on

ice, boiled at 100°C for 5 minutes, then vortexed and centrifuged at 16,000 x g for 4 minutes at 4°C. Then, the protein lysate was loaded on to the gel, the tank filled with running buffer and protein was separated in the gel when current at 30mA/gel was applied for approximately 60 minutes.

The next step was to transfer separated proteins from the lysate on to Immobilon^{TM} Transfer Membrane (Millipore, Fisher Scientific UK Ltd, Loughborough, UK), a polyvinyldifluoride polymer (PVDF) membrane. Blotting cassettes were assembled together and consisted of -ve electrode-fibre pad-whatman paper-gel-PVDF membrane-whatman paper-fibre pad-+ve electrode, all pre-soaked in transfer buffer. The cassette was then placed in a gel tank containing transfer buffer and an ice block, and transfer was facilitated by application of an electric current of 400mA for 60 minutes. The sandwich was disassembled once the transfer was completed, and, at this point, the membrane was stained with Ponceau S solution (0.1% (w/v) in 5% acetic acid – Sigma-Aldrich) in order to visualize the pattern of protein distribution and ensure equal protein loading and that transfer was even.

The membrane was then blocked with in a solution of 5% non-fat dry milk (Marvel) dissolved in wash buffer for an hour at RT on an orbital shaker. After blocking, the membrane was incubated with primary antibody (at a dilution of 1:1000) prepared in 5% milk solution for an hour at RT or overnight at 4°C on an orbital shaker. This was followed by washing the membrane with TBS-T (Tris-Buffered Saline and Tween 20) buffer using a protocol of 2 x 30 sec, 2 x 5 min and 1 x 15 min washes. Then, the membrane was probed with horse radish peroxidase (HRP)-conjugated secondary antibody (1/5000) dissolved in milk solution for 1 hour at R/T with shaking. This was followed by a wash cycle similar to that performed after primary antibody incubation. Finally, the membrane was developed with ECL-advance (Electrochemiluminescence) Western Blotting Detection reagents. Chemiluminescence was read using a Fujifilm LAS-1000 Image Analyser. Equal protein loading was assessed by probing the membrane with anti β-Actin antibodies used at 1/10000 dilution (see Sections 3.4.2 and 5.2.1). The list of all the antibodies used in this project is summarized in Appendix C.

Gel/buffer used for Western Blotting	Component\
SDS-PAGE running buffer	Tris 25mM, Glycine 192mM, SDS 0.1%(w/v)
Resolving gel buffer (4x):	Tris (pH 8.8) 1.5M, SDS 0.4%(w/v) [Purchased from National diagnostics, Hessle Hull, England]
Resolving gel:	Acrylamide Varied (usually 10%), 4x Running gel buffer 25% , TEMED 0.01% Ammonium persulphate 0.04%(w/v), Made up to 100% with ddH2O
Stacking gel buffer	Tris (pH 6.8) 0.5M, SDS 0.4%(w/v) [Purchased from National diagnostics, Hessle Hull, England
Stacking gel (5%)	Acrylamide 5%, Stacking gel buffer 25%, TEMED 0.1%,Ammonium persulphate 0.08%(w/v), Made up to 100% with ddH2O.
Transfer buffer (10X)	Tris (pH 6.8) 0.25M , Glycine 1.92M [Purchased from National diagnostics, Hessle Hull, England]
TBS-T	Tris(pH 7.4) 10mM, Sodium chloride 150mM, Tween-20 0.1%

Table 2-13. Recipes for gel/buffers used for Western Blotting.

2.2.6 Immunohistochemistry (IHC)

Immunohistochemistry (IHC) was used to detect the transgene in splenic tissue of Eμ-PKCβII tg mice. Formalin fixed and paraffin embedded splenic tissues were sectioned to a thickness of 4 μm using a microtome, and applied to a glass microscope slide. To remove the paraffin, rehydrate the tissue slice and retrieve the epitope a PT Link device (DAKO) was used. The procedures used followed the manufacturer's instructions. Thus, a rack of slides containing the tissue slices were placed in a 65°C pre-heated PT Link tank within the DAKO target retrieval solution (TRS). A preparation programme that takes approximately 1 hour was initiated and here the temperature increased up to 96°C and then decreased to 65°C. Following this preparation step, samples were placed into room temperature TBS wash buffer for 5 minutes to cool down. To stain the sections, the DAKO Auto-stainer was used which is an automated slide processing system designed to perform IHC staining automatically. To stain the section a EnVision™ FLEX/HRP (DAKO, K8012) kit was used which consisted of Peroxidase-Blocking Reagent(DM821), secondary rabbit antibodies (also called rabbit LINKER, K8019), EnVision™ FLEX DAB+ Chromogen (which contains, a concentrated diaminobenzidine (DAB) solution(DM827) and EnVision™ FLEX Substrate Buffer

(DM823)) and Wash Buffer (20x) (DM831). Thus, the rack containing my glass slides were placed in the autostainer and an appropriate programme was applied.

Once staining of the section was completed, the sections were counter stained with Haematoxylin solution and then rinsed with tap water until it ran clear. This was followed by dipping the sections in acid alcohol, and rinsing again with tap water. Finally, the sections were dipped in ammonia water for 30 seconds, rinsed with tap water and returned to a bath of dH_2O. The slides were then dehydrated through five changes of Industrial Methylated Spirit (IMS), cleared in two changes of Xylene before mounting the slides in DPX (Sigma-Aldrich). IHC results are discussed in section 5.3.

2.2.7 Haematoxylin and eosin (H&E) Staining

Haematoxylin and Eosin (H&E) staining was used to morphologically assess the spleen of Eμ-PKCβII tg mice compared with wild type mice. In H&E staining Haematoxylin colours basophilic structures such as the cell nucleus blue-purple. On the other hand, Eosin colours eosinophilic structures such as cytoplasm of the spleen bright pink. This allows high-resolution study of the morphology of tissues. Thus, the slides containing tissue slices were placed in a rack and placed in a bath containing xylene for 5 minutes to eliminate paraffin. Slides were agitating for 30 seconds and transferred into 2 subsequent xylene chambers in order to fully remove all trace of paraffin. Then the sections were subjected 3 X 30 second washes using different 100% IMS chambers. This was followed by another wash in a 70% IMS chamber, and finally a rinse with tap water. The sections were placed in Haematoxylin for 5 minutes, and then rinsed with running tap water until the water ran clear. The slide was agitated for 30 seconds in acid water, rinsed again with running tap water, and then agitated in 100% IMS for 30 seconds before placing in eosin for 2 minutes. To remove excess eosin the sections were washed in the following manner; 2x30s washes with 100% IMS, then 2x30s washes with xylene. In the end, the sections were mounted with DPX (see Section 5.3.1).

2.2.8 Flow cytometry analysis

The multi-colour flow cytometric analysis used to characterize B cell subsets in Eμ-PKCβII transgenic mice is comprehensively discussed in Section 5.4. The technical procedure used for staining and preparation for flow cytometry is as follows. In general, approximately 2-5 x 10^6 cells were suspended in 200μl of modified PBS (supplemented with 1% BSA and 0.1% sodium azide, pH7.2), then an appropriate concentration of antibody (see Appendix C) was added and the cell suspension was incubated in a FACS tube on ice for 20-30 minutes in the dark. Following this the cell suspension was topped-up to 500 μl with modified PBS, and then centrifuged at 2000 rpm at 4°C for 2 minutes. The supernatant was decanted and the pellet was re-suspended in 100-200μl of fresh modified PBS and 100μl FACS flow (BD biosciences). Now the cell suspension was ready to run in the flow cytometer. The list of all the antibodies used for flow cytometry is summarized in Appendix C.

2.3 BIOINFORMATICS

2.3.1 Basic Local Alignment Search Tool (BLAST)

The Basic Local Alignment Search Tool or BLAST is an algorithm that compares primary biological sequences and aligns them with known nucleotide or protein sequences. In this project, BLAST searches were used for two main purposes: 1. To align data from DNA sequencing against a database, mainly the mouse genome. 2. To compare the query sequence with my own input material such as vector sequences.

Website: http://blast.ncbi.nlm.nih.gov/

2.3.2 Translation tool (ExPASy)

To translate nucleotide sequences into their associated amino acid code, I used the ExPASy Translation tool. This tool was specifically used to check if my

recombinant/amplified DNA sequences were in frame, and also to check if any un-wanted DNA mutations were introduced during cloning that resulted in an altered protein sequence.

Website: http://web.expasy.org/translate/

2.3.3 Reverse complement

To design reverse primers I used the following tool that calculated the reverse complementary sequence of DNA. This tool was practically useful prior to ordering reverse primers.

Website: http://www.bioinformatics.org/sms/rev_comp.html

2.3.4 Restriction site mapping (NEBcutter)

To choose an appropriate restriction enzyme for DNA cloning the NEBcutter tool was used. This online tool maps the restriction sites within a query DNA sequence, and is useful for applications such as cloning, and for finding an appropriate restriction enzyme to fragment genomic DNA for Southern blotting applications.

Website: http://rna.lundberg.gu.se/cutter2/

2.3.5 Chromatogram analysis (Sequence Scanner)

To open the chromatogram files containing sequencing data for the samples sent to GATC Biotech, Sequence Scanner Software version 1.0 (Applied Bio systems) was used. The sequencing data files are represented with the suffix of .ab1. Inspection of the sequence was performed in two ways; the sequence data from my samples were compared to known standard sequences using the BLAST tool. If a mutation in this query sequence was found, I inspected the relevant chromatogram to confirm that this mutation was genuine rather than being a base miscall. If this mutation was real, then the query sequence was translated to its polypeptide sequence using the ExPASy translation tool to see if this change resulted in a change in an amino acid.

2.3.6 Statistical analysis

The statistical significance was calculated using either a Student's t-test or a Mann-Whitney U-test as indicated in the Figure legends. This analysis was performed using SPSS™ ver20 software.

3 Chapter III: Construction of a plasmid highly expressing PKCβII with specific promoter for B cells:

3.1 Cloning Strategy

To generate PKCβII transgenic mice, the first step was to design a plasmid that highly expresses PKCβII specifically in mouse B cells. This construct was injected into pro-nuclei of fertilized ova isolated from pregnant mice. The injected ova were then transferred to recipient mice in order to generate potential founder mice. I used the pBSVE6BK plasmid designed by Frederick Alt (Shaw*, et al* 1999) which exploits the VH promoter and the IgH-enhancer to specifically direct expression of target genes in B cells. This vector is commonly referred to as the pEμ vector and is based on a pBluescript® backbone that also includes a poly (A) site of the human β-globin gene (Appendix B).

Before sub-cloning the PKCβII gene into pEμ, I tagged the gene with Human influenza hemagglutinin (HA). The HA sequence codes for a short polypeptide sequence that has no bioactivity and allows for detection and isolation of the gene of interest (in this case human PKCβII) within transgenic cells that express this protein. The HA sequence was introduced at the 3′ end of the sequence coding for human PKCβII, and was planned to yield a protein that would express the tag as an addition to the C-terminus and therefore it would not potentially interfere with pseudo-substrate binding to the active pocket when the PKC enzyme was at rest.

I also added a gene coding for the fluorescent protein mCherry to this construct. This was done to create a visualization tool to identify transgenic B cells in live animals by imaging. For this purpose, mCherry was a good candidate because its excitation and emission profiles allow for deep tissue visualisation that allowed internal structures such as the spleen and lymph nodes to be observed without having to sacrifice the animal. In order to ensure equal expression of PKCβII and mCherry from my pEμ plasmid, I inserted an IRES (internal ribosome entry site) sequence between the PKCβII and mCherry genes. An IRES sequence allows for multiple gene expression from a single promoter and was therefore a useful tool for ensuring expression of multiple transgenes from a single promoter(Pelletier and Sonenberg 1988).

The cloning of the ultimate construct for the generation of Eμ-PKCβII transgenic mice consists of three steps (Figure3.1):

I. Sub-cloning PKCβII into Eμ vector

II. Sub-cloning of IRES sequence into pm-Cherry vector

III. Sub-cloning of IRES/mCherry into Eμ: PKCβII HA

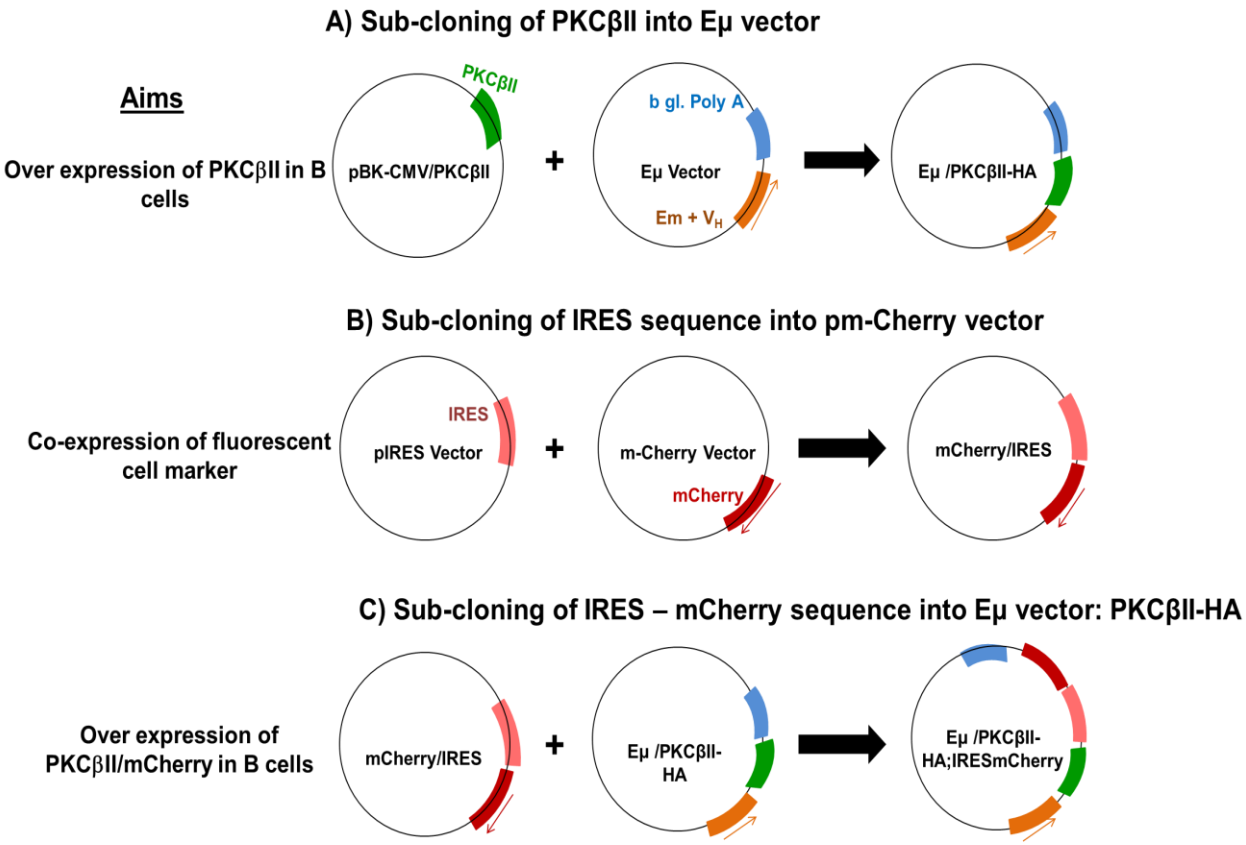

Figure 3-1. Cloning strategy for generation of plasmid construct for generation of Eμ-PKCβII tg mice. (A) Sub-cloning strategy to introduce PKCβII into the Eμ vector **(B)** Sub-cloning strategy to introduce IRES sequence into pm-Cherry vector **(C)** Sub-cloning strategy to introduce IRES/mCherry into the Eμ:PKCβII HA plasmid.

Thus, the final plasmid construct for generation of PKCβII obtains five important components: the Eμ promoter, PKCβIIHA, IRES, pm-Cherry and β-globin (haemoglobin subunit beta). In this section the results will be brought in chronological order.

3.2 Sub-cloning of PKCβII into the Eμ vector

3.2.1 Sequencing

The starting material for this study was human PKCβII tagged with EGFP (Enhanced Green Fluorescent Protein) that was encoded within the Phagemid vector pBK-CMV (See Appendix B). This plasmid was sent for sequencing to ensure there was no significant change within the PKCβII coding sequence. BLAST software (see Section 2.3.1) was used for pair sequencing with the standard human PKCβII sequence (PRKCB1). Figure 3-2 shows this comparison, and illustrates two conservative changes within the nucleotide sequence; T1191C and G1726A (Table 3-1). The nucleotide sequence was then translated into the peptide sequence (see Section 2.3.2) and again submitted for comparison with the standard human PKCβII peptide sequence using BLAST software. Figure 3-3 shows that the two nucleotide changes detected do not change the amino acid sequence encoded by the starting plasmid. Thus, although there were some mutations in rhw coding sequence of wild type PKCβII, they were all silent mutations and it was determined that this sequence could be used in subsequent cloning steps.

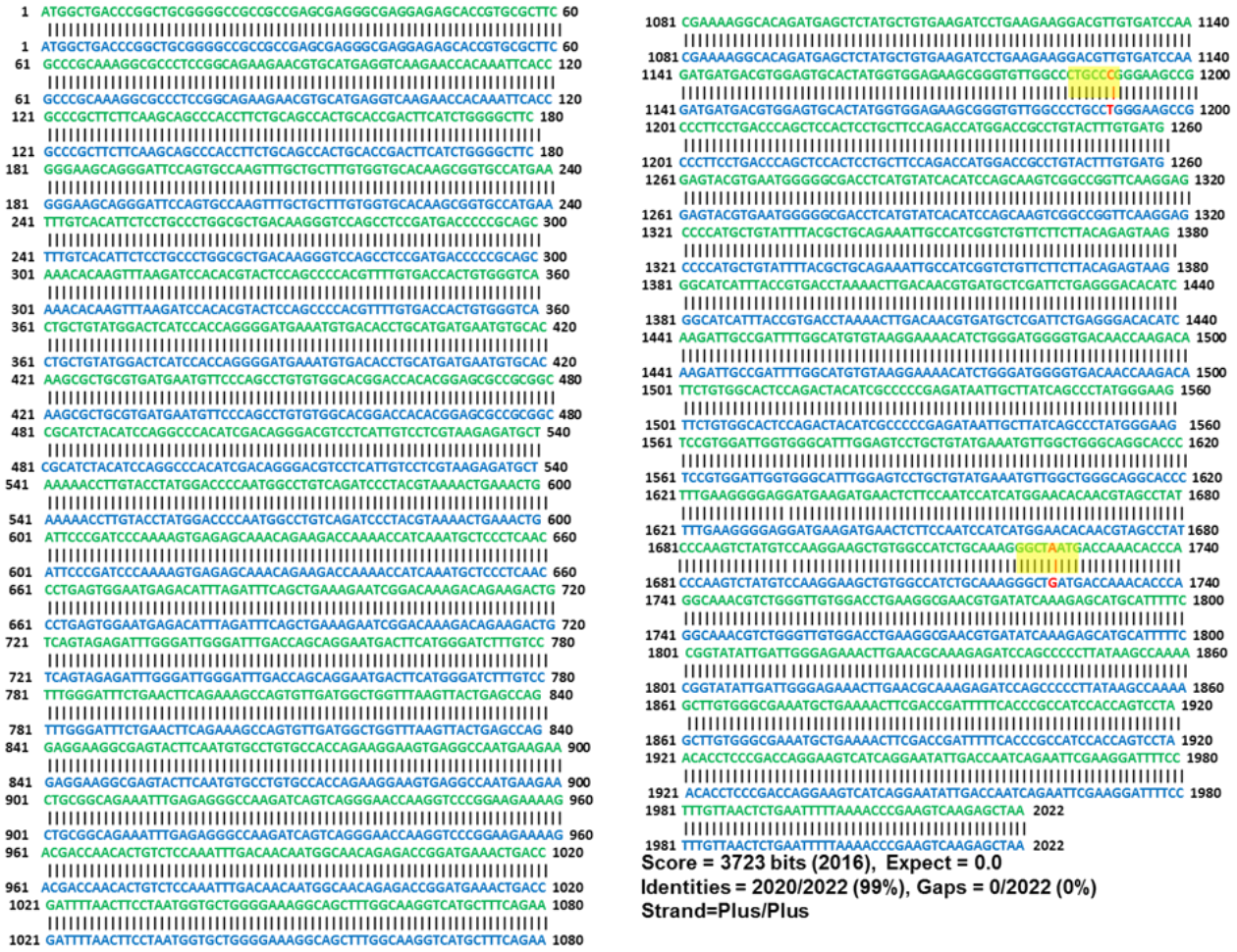

Figure 3-2. Alignments of nucleic acid sequence of PKCβII within the Phagemid vector pBK-CMV (highlighted green) with standard nucleic acid sequence of PKCβII (highlighted with blue) using the BLAST software (Zhang, *et al* 2000). The starting material for DNA cloning in this study was human PKCβII-EGFP encoded within the Phagemid vector pBK-CMV. The probe sequence is highlighted green and compared with the standard nucleotide sequence for human PKCβII (accession number), highlighted blue. BLAST software was used for comparison analysis. The yellow highlights indicate where a mutation was detected in the probe sequence, and the actual nucleotide is marked in red.

Mutation position	1191	1726
Nucleotide	t/C	g/A

Table 3-1 The nucleotides after mutation depict with capital letter.

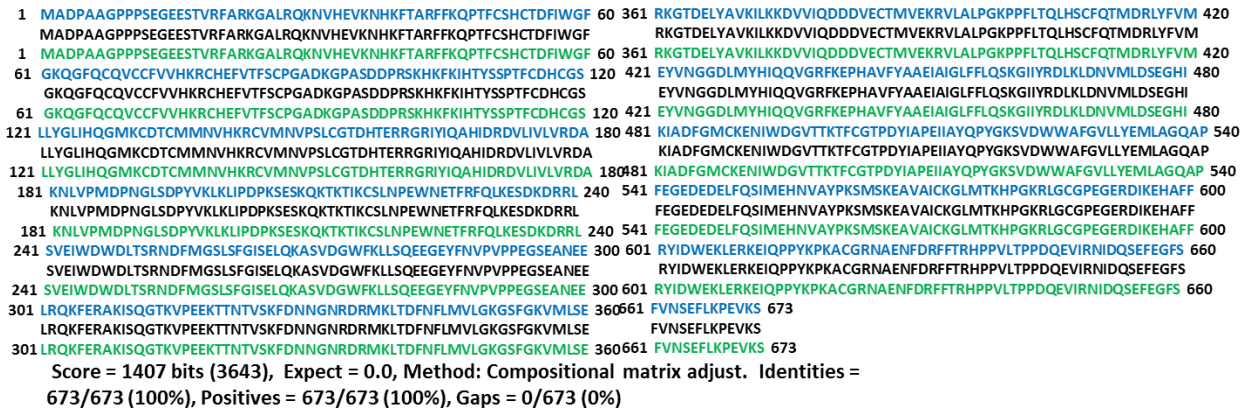

Figure 3-3.Comparison of amino acid sequence of PKCβII within the Phagemid vector pBK-CMV with the standard amino acid sequence for PKCβII using BLAST software (Altschul, *et al* 1997). The nucleotide sequence of PKCβII within the phagmid was translated into the peptide sequence **(highlighted green)**, and then compared with the human standard amino acid sequence for PKCβII using BLAST software **(highlighted with blue)**.

3.2.2 PCR optimisation of PKCβII

In the first step of cloning, the coding sequence for PKCβII was amplified by PCR. Thus, PCR optimisation was performed to increase specificity and reduce the introduction of unwanted random mutations. Optimisation involved establishing the optimal annealing temperature using a temperature gradient, determining the optimal amount of DNA template to use and ascertaining the optimal number of cycles to find the minimum required for PKCβII amplification.

Forward and Reverse primers were designed to introduce restriction sites for Cla-I and Sal-I restriction enzymes to the respective 5′ and 3′ ends of the PKCβII sequence. The reasons for choosing Cla-I and Sal-I were that neither of them cut within the PKCβII coding sequence, and they were within the multiple cloning region of the final Eμ vector.

In designing the primer for the 3′ end, an additional coding sequence for HA tag was also introduced before the Sal-I restriction site. The detail of these primers is listed in Appendix A. These primers were then used in the optimisation experiments described below.

Figure 3-4 shows the effect of an annealing temperature gradient from 52 to 62ºC on the amplification of the PKCβII coding sequence. There was no significant difference in relation to the efficiency of the reaction at the various temperatures of the gradient. Therefore, a temperature of 60.3°C was chosen because this temperature was high enough to prevent primer dimerization.

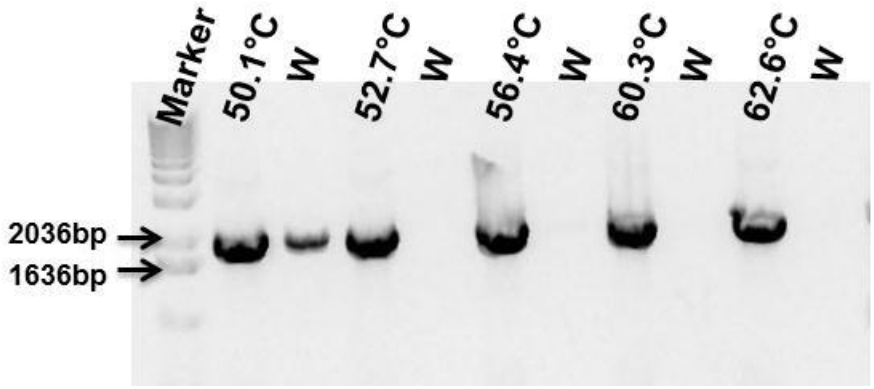

Figure 3-4. Effect of annealing temperature on PCR amplification of the PKCβII coding sequence. Different annealing temperatures (indicated) were used to amplify annealing the PKCβII coding sequence from the vector pBK-CMV. Illustrated is a 0.7% agarose gel separation of the PCR products that were generated. The PKCβII band was approximately 2kB in size. "W" indicates a PCR reaction performed on water as a negative control.

Figure 3-5 shows the effect of different amounts of DNA template and numbers of PCR cycles on the amplification of the PKCβII coding sequence. 0.1,1 and 10ng of DNA template and 5, 15, 20 and 30 PCR cycles were chosen for this reaction. Water was chosen as a control reaction, and showed no amplification, even when 30 PCR cycles was used. I found that optimal amplification was achieved using 10ng of template and 15 PCR cycles.

Thus, to amplify the PKCβII coding sequence from the template DNA, I used the following conditions: 10ng of template, an annealing temperature of 60.3°C, elongation time was 1 min at 72°C followed by denaturation at 95°C for 30s. This cycle was repeated 15 times and at the final cycle an elongation time of 5min was imposed to finish off all reactions. At the termination of the PCR reaction, the temperature was reduced to 4°C.

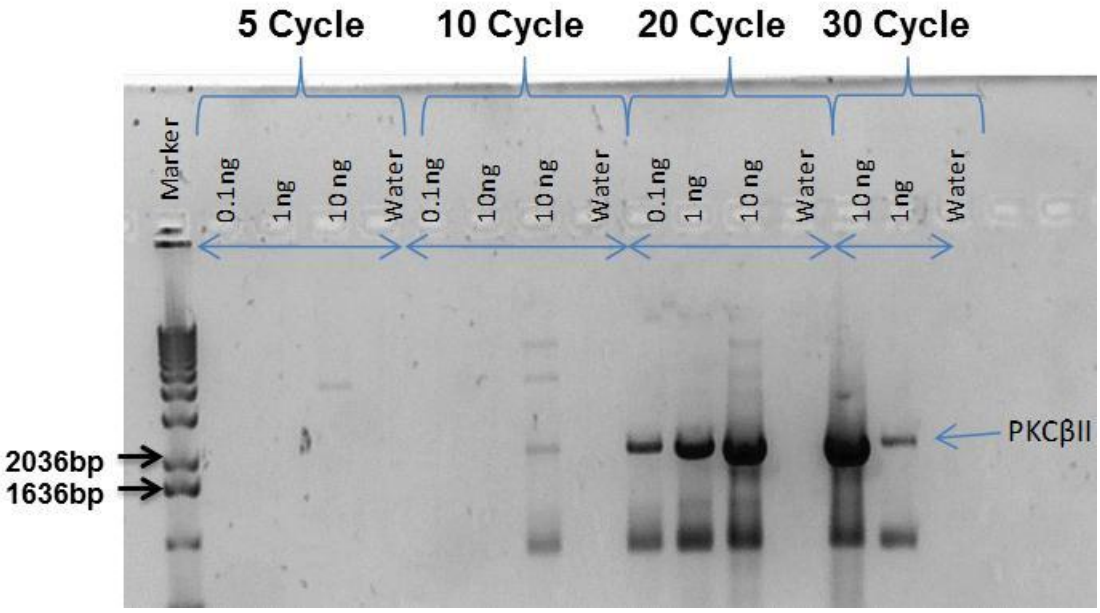

Figure 3-5. PCR optimisation of the PKCβII coding sequence for DNA template and cycle number. The PCR optimisation of PKCβII sequence was performed for DNA template and cycle number. For this purpose, 0.1,1 and 10ng of DNA template and 5, 15, 20 and 30 PCR cycles were chosen. Illustrated is a 0.7% agarose gel separation of the PCR products that were generated. The PKCβII band was approximately 2kB in size.

3.2.3 Insertion of PKCβII coding sequence into PCR2.1

3.2.3.1 Strategy

The initial target plasmid for the amplified PKCβII coding sequence was PCR2.1, a TA vector that allows direct insertion of a PCR amplicon. TA cloning is a “sub-cloning technique” that does not use restriction enzymes. The technique is based on the hybridization/ligation of complementary base pairs of adenine (A) and thymine (T) on

different DNA fragments, which is mediated by ligase. So, firstly, PKCβII was amplified by Taq DNA polymerase, an enzyme that preferentially adds an adenine to the 3' end of the PKCβII coding sequence. This was then added to linearized TA vector that has complementary 3' thymidine overhangs, and ligation proceeds when DNA ligase is added. The use of TA cloning helps to boost ligation efficacy (Figure3-6).

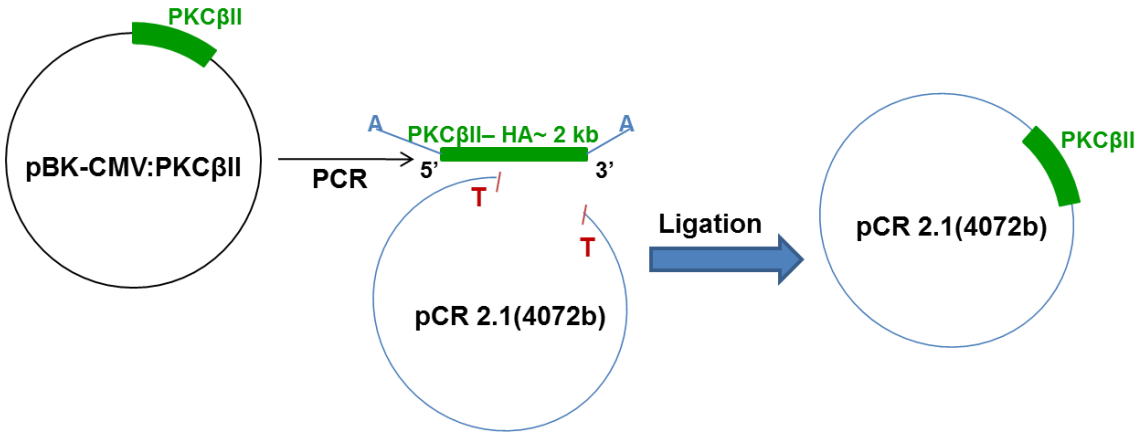

Figure 3-6. Sub-cloning of PKCβII into PCR2.1 by TA cloning. In the TA cloning, PKCβII coding sequence was amplified by Taq DNA polymerase which preferentially adds an adenine to the 3' end of the PKCβII coding sequence. Then, amplified PKCβII was ligated with linearized TA vector that has complementary 3' thymine overhangs and this was mediated by ligase.

This completes the optimisation protocol to ensure efficient amplification of the PKCβII coding sequence for subsequent cloning steps. Thus, after insertion of the PKCβII coding sequence within PCR2.1, and appropriate sequencing to ensure integrity, the pPKCβII-PCR2.1 is then digested with Sal-I and Cla-I to release the coding sequence which would be then inserted into prepared pEμ plasmid (pre-digested with Sal-I and Cla-I) by ligation. Figure 3-7 shows a schematic of how this was done. In this next section I describe the step by step procedures.

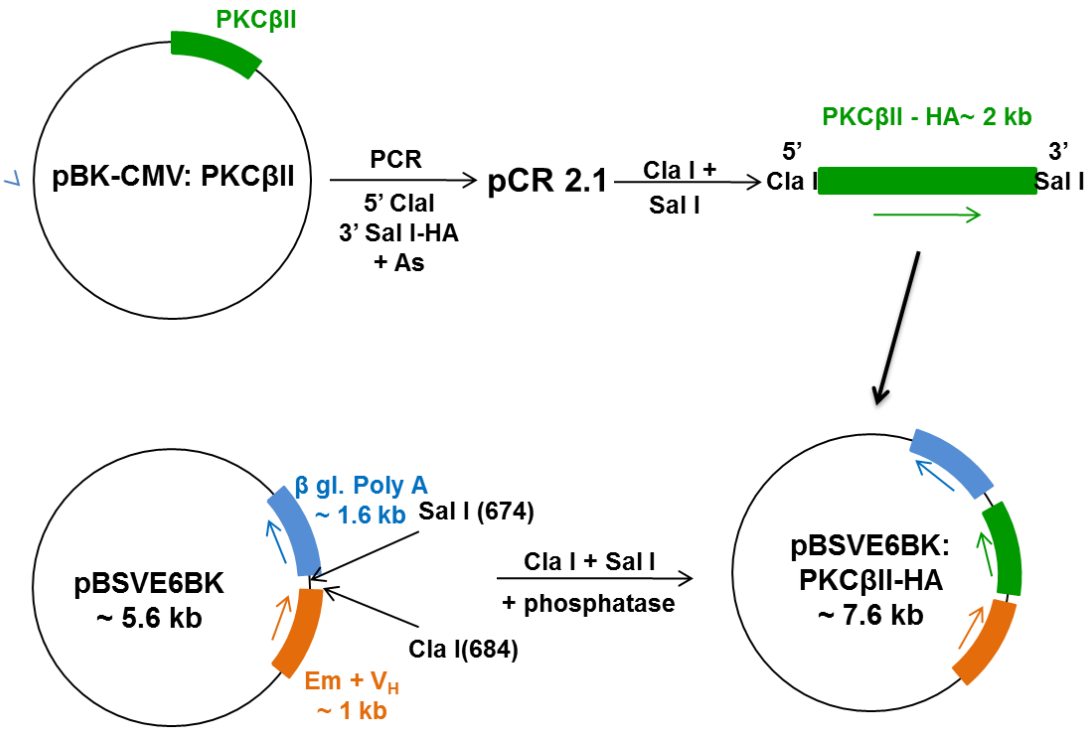

Figure 3-7. Sub-cloning of PKCβIIHA into pBSVR6BK (Eμ) vector. The PKCβII coding sequence was firstly inserted into a PCR2.1 vector by TA cloning. PPKCβIIHA-PCR2.1 is then digested with Sal-I and Cla-I to release the PKCβII coding sequence which is then inserted into a prepared Sal-I and Cla-I pre-digested pEμ plasmid by ligation.

The PKCβIIHA PCR product was amplified from pEGFP-PKCβII using the plasmids, primers and procedure described above. I used a 0.7% high quality agarose gel and isolated the 2kb PKCβIIHA band (product of the correct size) by scalpel. I then extracted the DNA from this gel slice using a GENE CLEAN kit (see Section 2.1.2.5). After gel extraction, the DNA coding sequence for PKCβII was again run in a gel to estimate its concentration. Figure 3-8 shows that the PKCβII PCR product ran as a single band with an approximate 2kb size. Concentration of this product was estimated by comparing the density of the 1636b band in the DNA ladder with that of the DNA for PKCβII. The 1636b band is associated with 100ng of DNA. Thus, I was able to estimate a value of 50ng of PKCβIIHA DNA.

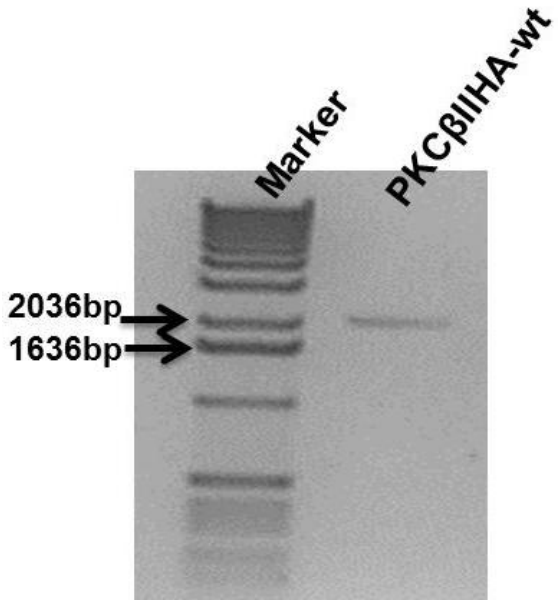

Figure 3-8. Amplified PKCβIIHA for use in subsequent cloning steps is of the correct size and runs as a single band. Agarose gel separation of the PKCβIIHA PCR product extracted from the agarose gel used to purify the PCR products ran as a single band of approximately 2kb size (product of the correct size). Amount of PKCβIIHA PCR product was estimated by comparing the density of the PKCβIIHA band with the MW standard band running at 1636b.

The next step involved ligating the PKCβIIHA PCR product into PCR2.1. This was done by taking 10ng of the PKCβIIHA PCR product and adding this to 25ng of PCR2.1 vector. T4 DNA ligase was then added and the reaction was incubated at 14°C for 8 hrs. (See Section2.1.4.4).The product of the ligation reaction was then transformed into TOP10 competent cells by heat-shock (see Section 2.1.1.2). Bacterial cells containing the PKCβIIHA/PCR2.1 plasmid were selected by culturing the cells on Lysogeny broth (LB) agar plates containing kanamycin. Transformation efficiency was estimated by using pUC vector which was a standard plasmid for determination of transformation efficiency. The transformation efficiency for the ligation of PKCβIIHA/PCR2.1 into TOP10 competent cells was 10^8 colony forming units (cfu)/µg of DNA used for ligation. Ten colonies from the culture plates were randomly picked in order to characterise whether the created plasmids were correct. These colonies were grown in liquid LB broth under kanamycin selection pressure in overnight cultures that were vigorously mixed and maintained at a temperature of 37°C.

The formation of a clone did not necessary mean that ligation of PKCβIIHA into the PCR2.1 vector had been successful. In order to ensure correct insertion, I exploited two EcoRI restriction sites within the MCS of PCR2.1. Within my cloning strategy, these sites come just before and just after the site of insertion for PKCβII, and digestion of PCR2.1 containing PKCβII with EcoRI would result in the generation of two bands; PKCβIIHA (2kb) and PCR2.1 vector backbone (4kb). There was also an additional EcoRI site within the PKCβIIHA coding sequence, at position 1963. This additional site did not have influence on my screening protocol because the end digestion product was slightly less than the expected 2kb product. Figure 3-9 shows the results of this experiment, clone numbers 1,2,3,5,6,7,8 and 10 had 2kb and 4kb bands, indicating the presence of the PKCβIIHA insert and vector backbone, respectively. In contrast, clones number 4 and 9 had only a single 4kb band, indicating presence of only the PCR 2.1 backbone. Thus, clone numbers 1 and 2 (designated pPKCβIIHA-wt-1/PCR2.1 and pPKCβIIHA-wt-2/PCR2.1) were chosen for further cloning purposes.

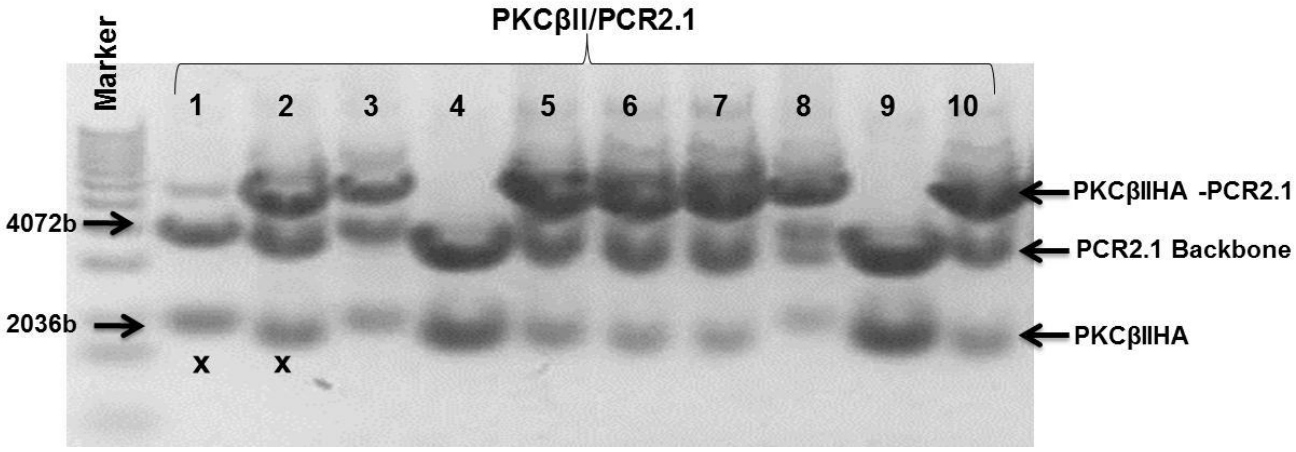

Figure 3-9. Screening the PKCβII/PCR2.1 colonies using EcoRI restriction enzyme. Agarose gel separation of EcoRI digests PKCβIIHA/PCR2.1 plasmids isolated from 10 colonies of the ligation reaction. The generation of two bands; PKCβII (2kb) and PCR2.1 vector backbone (4kb) indicated success of the ligation.

In the next step, the PKCβIIHA coding sequence was sub-cloned into the Eμ vector. This was done by digesting pPKCβIIHA-wt-1/PCR2.1 with Cla-I and Sal-I to release PKCβIIHA-wt-1. The Eμ vector was also digested with Cla-I and Sal-I to prepare

it to receive the PKCβIIHA coding sequence from pPKCβIIHA-wt-1/PCR2.1. Figure 3-10 shows that the digestion of pPKCβIHAI-wt-1/PCR2.1 by Cla-1 and Sal-I was not initially successful and PKCβIIHA was not separated from the PCR2.1 backbone vector. Digestion of pPKCβIIHA-wt-1/PCR2.1 with Cla-I alone revealed that the plasmid was not digested with this restriction enzyme. A possible explanation for the failure of Cla-I to digest pPKCβIIHA-wt-1/PCR2.1 was dam-methylation catalysed by the methylase enzyme encoded by the *dam* gene and is known to inhibit Cla-I DNA digestion (Figure 3-11) (NEB). Methylation of this site may have occurred as a consequence of the cloning strategy used when PKCβIIHA was amplified with the forward PCR primer.

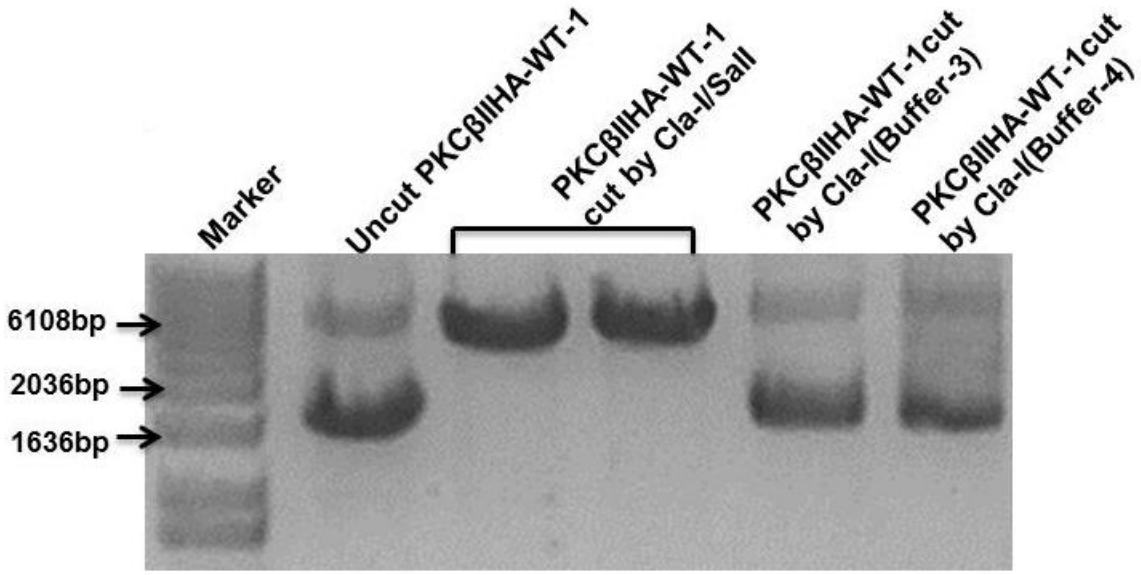

Figure 3-10. Cla-I does not digest PKCβIIHA-wt-1/PCR2.1. Agarose gel analysis of PKCβIIHA-wt-1/PCR2.1 digested with Cla-I / Sal-I or Cla-I alone. Buffer 3 and 4 refer to the optimal buffers used for Cla-I and Sal-I within the protocol supplied by NEB.

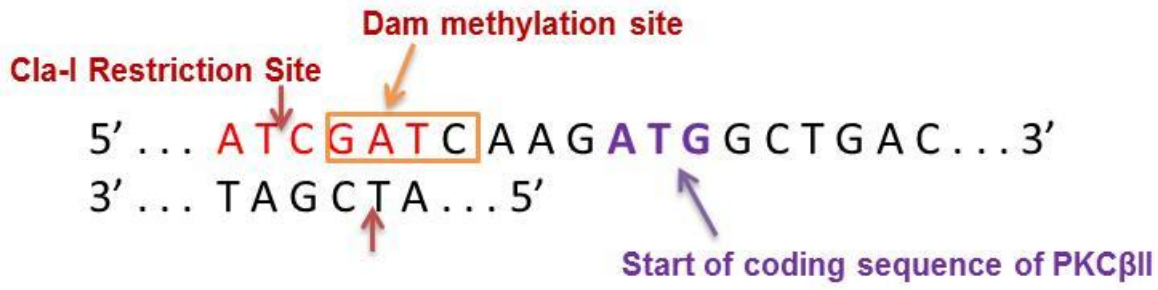

Figure 3-11. Dam-methylation site within Cla-I restriction site potentially affecting digestion of the PCR2.1/PKCβII-wt-1. Dam-methylation is catalysed by a methylase enzyme encoded by the *dam* gene. This methylase transfers a methyl group from S-adenosylmethionine to the adenine residue within a GATC sequence which is a part of the restriction site for Cla-1. Creation of this site may have occurred as a consequence of the cloning strategy used, and created a situation where the plasmid could not be digested with Cla-I.

3.2.4 Using dam$^-$dcm$^-$ competent cells for transformation pPKCβII-wt/PCR2.1

To prevent the occurrence of methylation, pPKCβIIHA-wt-1/PCR2.1 was transformed into *dam*$^-$*dcm*$^-$ E. coli (C2925, NEB) which are competent cells that are used to grow plasmids which are free of dam/dcm methylation. Figure 3-12A shows that pPKCβIIHA-wt-1/PCR2.1 could be successfully digested by Cla-I and Sal-I following isolation of this plasmid from transformed dam$^-$/dcm$^-$ competent bacteria. This figure was photographed without the PKCβIIHA and Eμ plasmid bands that resulted from digestion in order to reduce possible UV light-induced mutation caused by the system we used for visualisation. Figure 3-12B shows a sampling of the purified band products (using a GENECLEAN kit) isolated from the bands in Figure 3-12A The PKCβIIHA coding sequence is represented by the 2kb band whereas the prepared pEμ (plasmid) is represented by the approximate 6kb band.

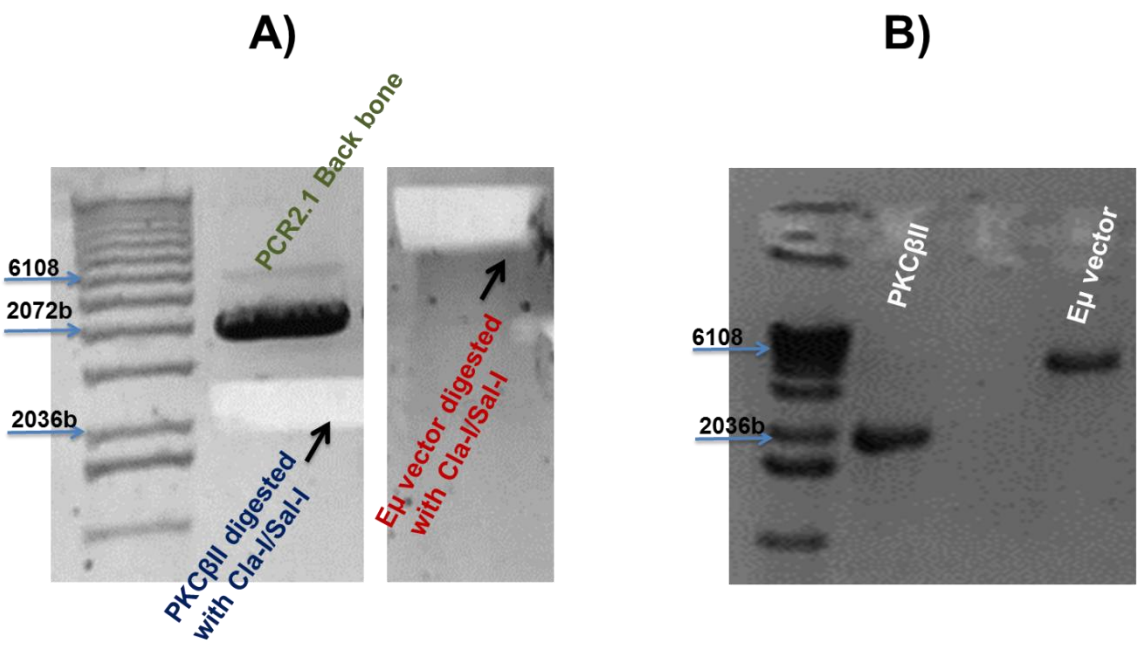

Figure 3-12. Cla-I / Sal-I completely digest PKCβIIHA-wt-1/PCR2.1 extracted from *dam*$^-$ */dcm*$^-$ competent cells. Agarose gel analysis of PKCβIIHA-wt-1/PCR2.1 plasmid digested with Cla-I / Sal-I. The PKCβII-wt-1/PCR2.1 plasmid was extracted from *dam*$^-$/*dcm*$^-$ competent cells. **(A)** Bands corresponding to PKCβIIHA and pEμ were excised by scalpel and explains the missing band images **(B)** PKCβIIHA and pEμ bands were of the correct size following GENECLEAN purification from the gel slices taken in part A.

The digested Eμ plasmid was prepared for ligation by treating with Antarctic phosphatase to remove 5′ phosphate residues (see Section 2.1.4.2), and then it was ligated with the PKCβII coding sequence. The product of this ligation was transformed into dam$^-$/dcm$^-$ competent E coli, and then grown in LB-Agar plates overnight. 30 colonies were taken for screening using Cla-I/Sal-I to digest the plasmid that was purified from cultures of these isolates. Figure 3-13 partially illustrates this procedure, and shows that the PKCβIIHA coding sequence was successfully ligated into the pEμ plasmid in clones 27, 28 and 29. Cla-I/Sal-I digests of the isolated plasmids from these clones showed three bands; partially digested pEμ-PKCβIIHA and fully digested pEμ vector and PKCβII coding sequence. These clones were taken and stored for later use. Clone number 29 (PKCβIIHA-wt-1/Eμ-29) was selected for sequencing to ensure

integrity of the cloning procedure. The results of this sequencing showed that the PKCβIIHA-wt coding sequence was successfully cloned into the pEμ vector in the correct orientation and had the same sequence as the PKCβII-HA starting material.

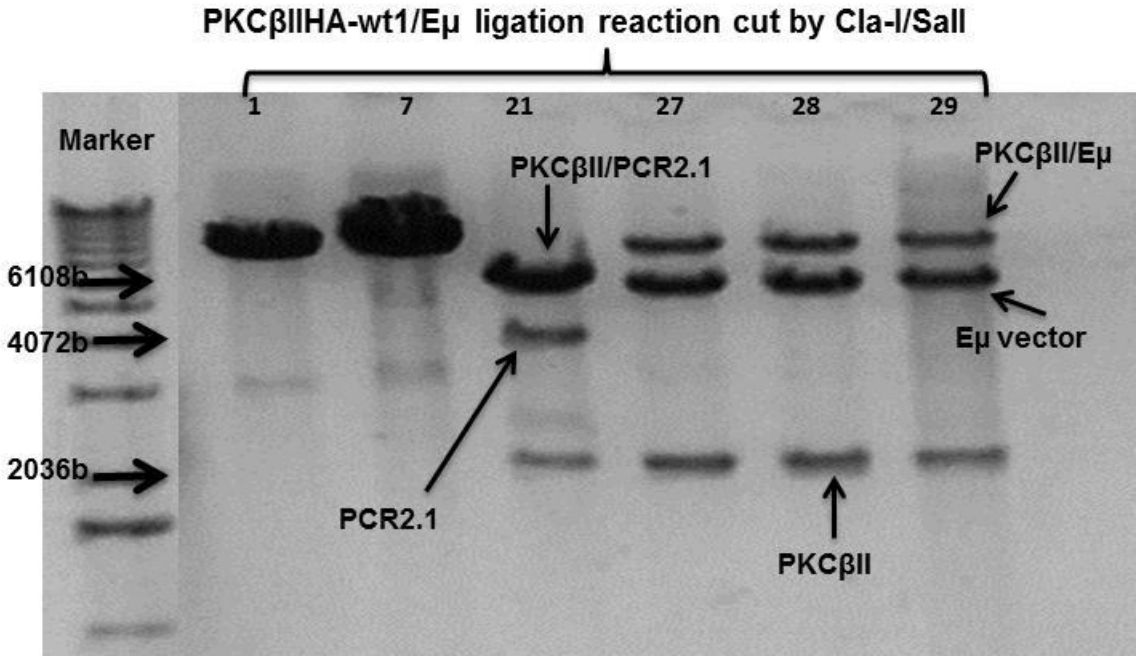

Figure 3-13. Integration of PKCβIIHA into pEμ. Agarose gel analysis of the PKCβIIHA-pEμ ligation product digested with Cla-I and Sal-I. The PKCβIIHA-pEμ ligation product was grown in dam^-/dcm^- bacteria to ensure successful digestion with Cla-I. Clones numbered 27, 28 and 29 showed the correct digestion products for PKCβIIHA (2kB) and pEμ (6kB)**.**

3.3 Sub-cloning of an IRES sequence into pmCherry

The aim of this step was to sub-clone an Intra Ribosomal Entry Site (IRES) coding sequence that would allow dual expression of PKCβII and mCherry from the Eμ promoter. Thus, the goal of these preparative procedures was to sub-clone the IRES sequence into the vicinity of the coding sequence for mCherry (Figure 3-14), with the eventual goal of placing the IRES/mCherry construct into the PKCβII/Eμ vector.

The steps involved are shown in Figure 3-14 and consisted of PCR amplification of the IRES sequence, sub-cloning into the PCR2.1 intermediate vector and final

insertion of the IRES sequence into a plasmid containing mCherry (see Appendix B). The PCR amplification step also involved the addition of Sal-I and BamHI restriction sites into the IRES coding sequence to ease the process of sub-cloning. Thus, the forward PCR primer also contained an additional Sal-I restriction site added to its 5′ sequence, while the reverse PCR primer contained a BamHI restriction site added to its 3′ sequence (detail of the primers is in Appendix A). Sal-I and Bam-HI were chosen because these restriction enzymes do not cut the IRES coding sequence, and also allow for efficient sub-cloning into the final pEμ-PKCβIIwt-HA plasmid construct.

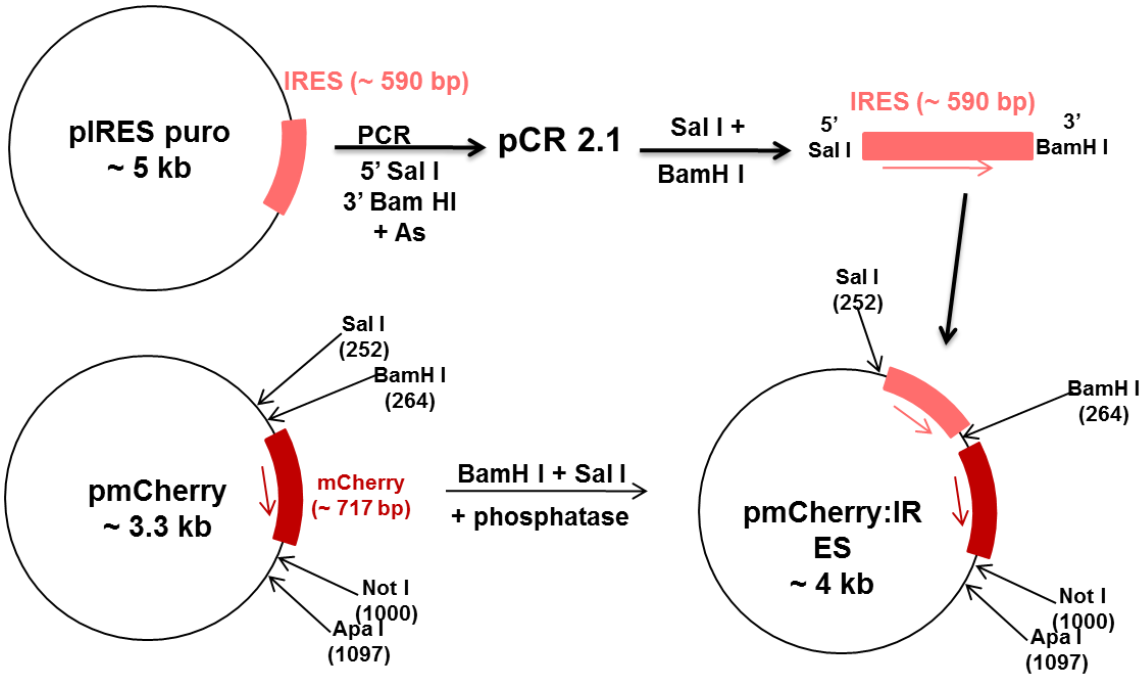

Figure 3-14. Schematic showing the sub-cloning of the IRES sequence into the m-Cherry vector. The IRES coding sequence was first inserted into the PCR2.1 vector. The IRES-PCR2.1 was digested with Sal-I and BamHI to release the IRES coding sequence. The IRES sequence was then inserted into Sal-I and BamHI pre-digested pmCherry plasmid by ligation.

3.3.1 PCR optimisation of IRES

In the first step of cloning, the coding sequence for IRES was amplified by PCR. Figure 3-15 shows that optimal amplification of the IRES coding sequence was achieved

using 30ng of template and 20 PCR cycles using the following conditions: an annealing temperature of 62°C, an elongation time of 1 min at 72°C being followed by a denaturation step at 95°C for 30s. The last PCR cycle included a final elongation time of 5 min to finish off all reactions. At the termination of the PCR reaction, the temperature was reduced to 4°C.

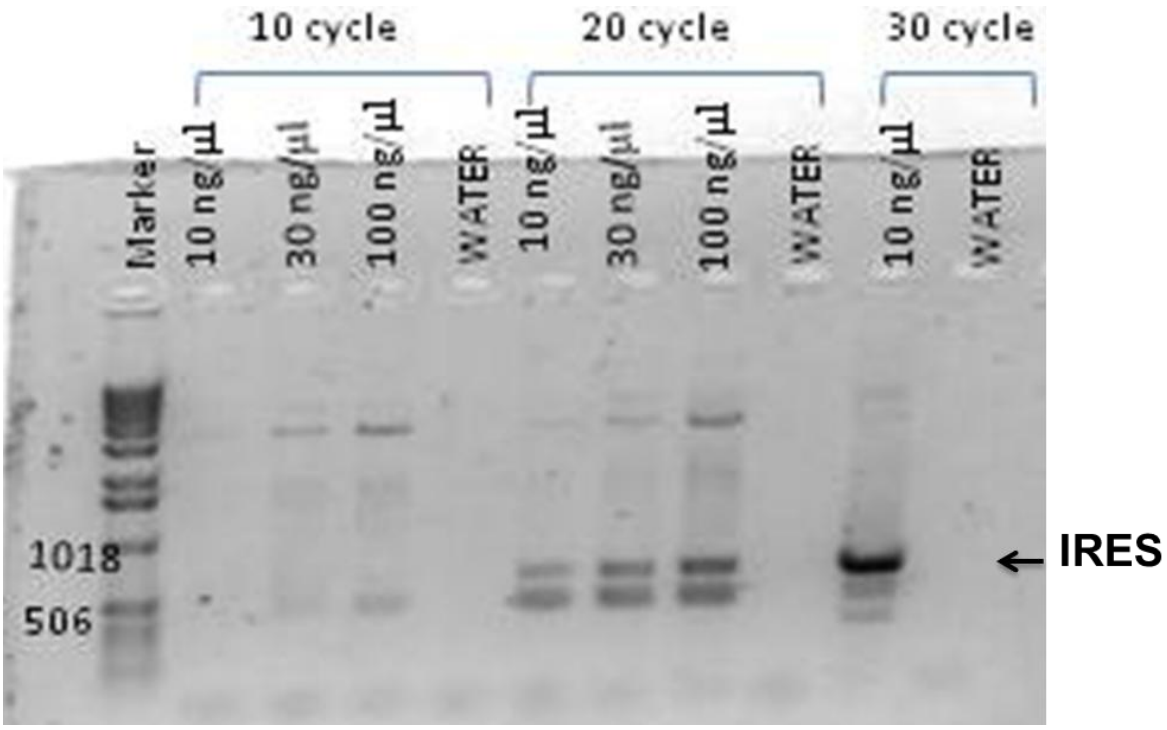

Figure 3-15. PCR optimization for DNA template and cycle number for amplification of the IRES coding sequence. PCR optimisation of the IRES sequence was performed for DNA template and cycle number. For this purpose 10, 30 and 100ng of DNA template and 10, 20 and 30 PCR cycles were chosen. Illustrated is a 1.5% agarose gel separation of the PCR products that were generated. The IRES band is 590b in size.

3.3.2 Sub cloning of IRES into pCR2.1 and pmCherry

The amplified IRES coding sequence was ligated into a linearized TA vector using the same conditions that were used for the cloning of PKCβII (see Section 3.2.3). The IRES/PCR2.1 ligation reaction was transformed into TOP10 competent cells, the

cells cultured on Kanamycin selection plates overnight, and ten colonies were randomly chosen for plasmid purification. DNA extracted from these clones was then digested by EcoRI, and then separated by electrophoresis using a 1.5% agarose gel to see which clones contained the IRES sequence. Figure 3-16 shows that all the clones contained the IRES coding sequence. Clones #4, 7 and 9 were selected for glycerol storage as the digestion patterns were the cleanest. Clone #9 was selected for future cloning steps (designated IRES-9) and was sent for sequencing to ensure sequence integrity. Results from this sequencing showed that my cloning operations did not introduce any mutations into the IRES coding sequence (data not shown).

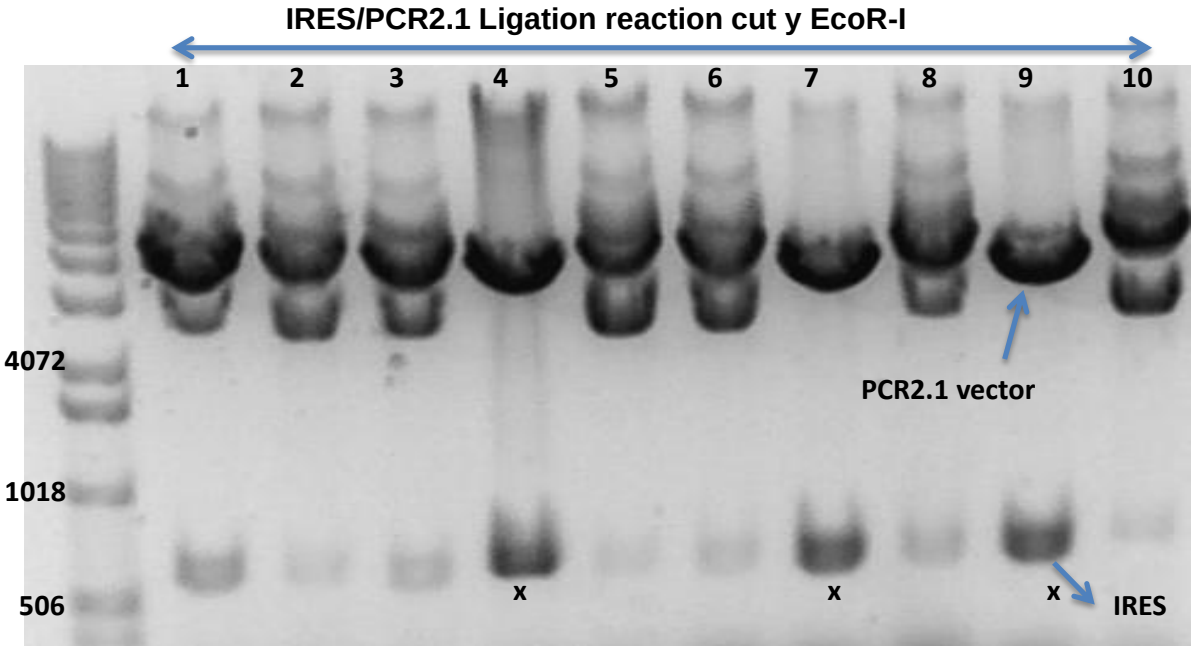

Figure 3-16. Screening the IRES/pCR2 colonies using EcoRI restriction enzyme. Agarose gel separation of EcoRI digests of IRES/PCR2.1 plasmids isolated from 10 colonies of the ligation reaction. The generation of two bands; IRES (590b) and PCR2.1 vector backbone (4kb) indicated success of the ligation.

The IRES coding sequence was then sub-cloned from pCR2.1 into the pmCherry vector by first releasing the IRES sequence from PCR2.1 and preparing the pmCherry plasmid by digestion of both with Bam HI /Sal-I. Figure 3-17 show the results of these digestions, the IRES coding sequence ran as a 590 bp band and pmCherry ran as a

3344 bp band in an agarose gel. The IRES coding sequence was then ligated into the linearized pmCherry (see Section 2.1.4.4).

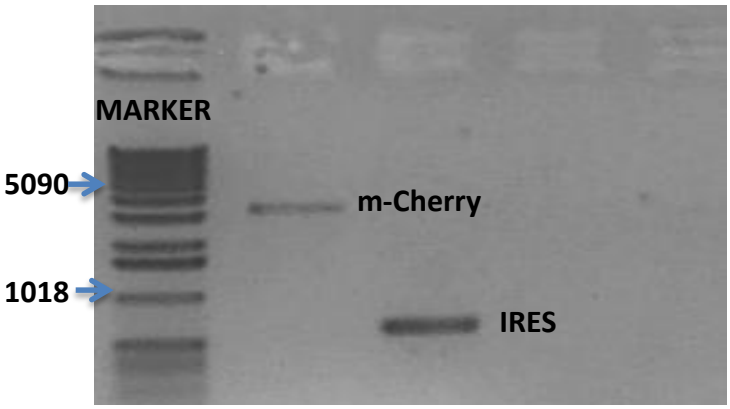

Figure 3-17. Digestion of IRES and pm-Cherry with Bam-HI and SalI before ligation. To ligate IRES into pmCherry vector, the IRES was released from PCR2.1 vector backbone by BamHI/SalI digestion. The pmCherry was prepared by digestion of BamHI/SalI restriction enzymes. Bands corresponding to IRES and mCherry were excised by scalpel and purified from agarose gel. This figure is the agarose gel analysis of 2µl digested IRES and mCherry that extracted from the gel, and illustrates that IRES (590bp) and mCherry (3344bp) were of the correct size following GENECLEAN purification from the gel slices.

The ligation reaction was allowed to proceed overnight and then it was transformed into TOP10 competent cells which were grown on ampicillin selection plates. The reason ampicillin was used for selection was the mCherry plasmid contains the gene resistant to ampicillin. The transformation efficacy was 5 x 10^8 cfu/µg and 13 colonies were selected for analysis. DNA extracted from these clones were then digested by BamH-I and Sal-I to see which clones contained the IRES/mCherry sequence, and I found that clones #2, 6 and 7 contained this sequence (Data not shown). The DNA from these colonies was further test digested to ensure the presence of the insert (Figure 3-18). Single digestion with either BamHI or Sal-I resulted in a single band with an expected size of approximately 4 kb. Digestion with the combination of BamH1 and Sal-I resulted in the generation of a 590bp band associated with the IRES coding sequence and a 3344bp band associated with the mCherry plasmid. Digestion with SalI and Not-I released the IRES-mCherry coding sequence from the

plasmid, designated by the appearance of a 1.5 kb band. Taken together, these observations demonstrate that ligation of IRES into the mCherry vector was successful. Clone number 6 (IRES9/mCherry-6) was selected for the ligation into PKCβIIwtHA-1/Eμ-29 in the next step of cloning.

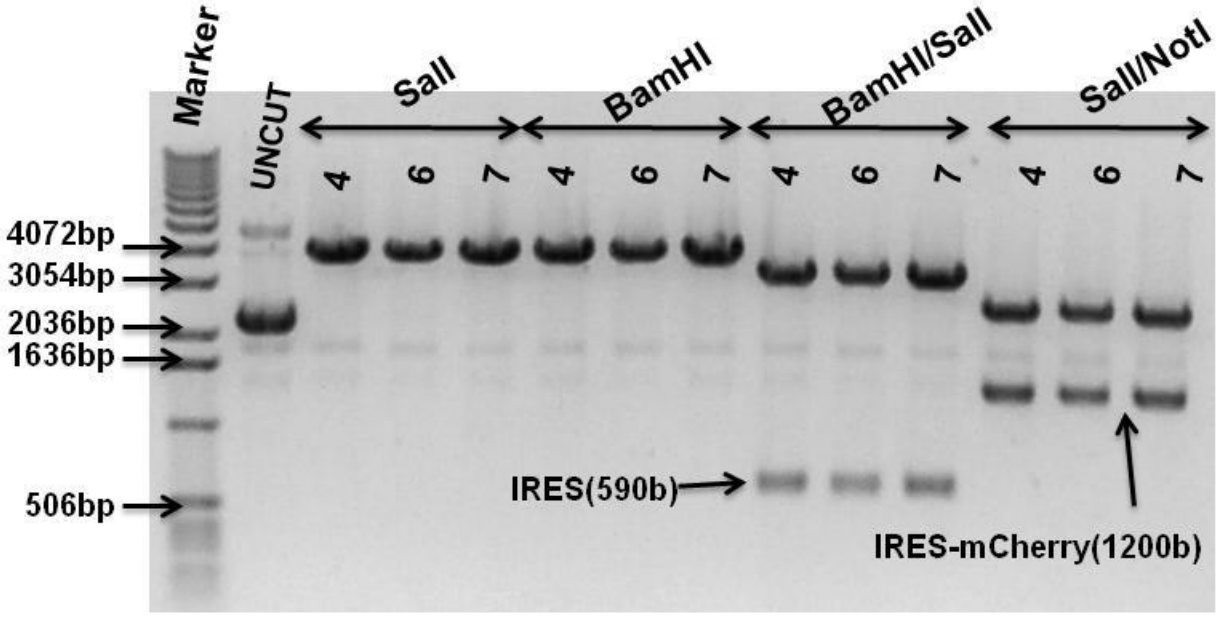

Figure 3-18. Integration of IRES into pmCherry. Agarose gel analysis of clones 4, 6 and 7 containing the IRES-pmCherry ligation product. DNA was digested with SalI, BamHI, BamHI/Sal-I and Sal-I/NotI restriction enzymes to ensure IRES was successfully integrated within the pmCherry vector.

3.4 Sub-cloning of IRES/mCherry into Eμ: PKCβIIHA

The final stage of cloning involved taking the IRES9-mCherry coding sequence and placing it in a 5'→3' unilateral fashion between the PKCβIIHA and β-poly-globin coding sequences within the Eμ vector (Figure 3-19). The methodology involved an initial digestion of pIRES9-mCherry with Not-I followed by blunting of the 3'-end with Klenow, which is a 3'-5' exonuclease (see Section 2.1.4.3). The next step involved preparing the pEμ-PKCβIIwt-HA vector to receive the IRES9-mCherry coding sequence. This was done by first digesting with Apa-I, which cut between the β-poly-globin and

PKCβIIHA coding sequences. The digested plasmid was then blunted by Klenow, and this was followed by digestion with Sal-I to create the acceptor sites for the IRES9-mCherry coding sequence. Final ligation and transformation created the pEμ-PKCβIIwt-HA-IRES-mCherry plasmid.

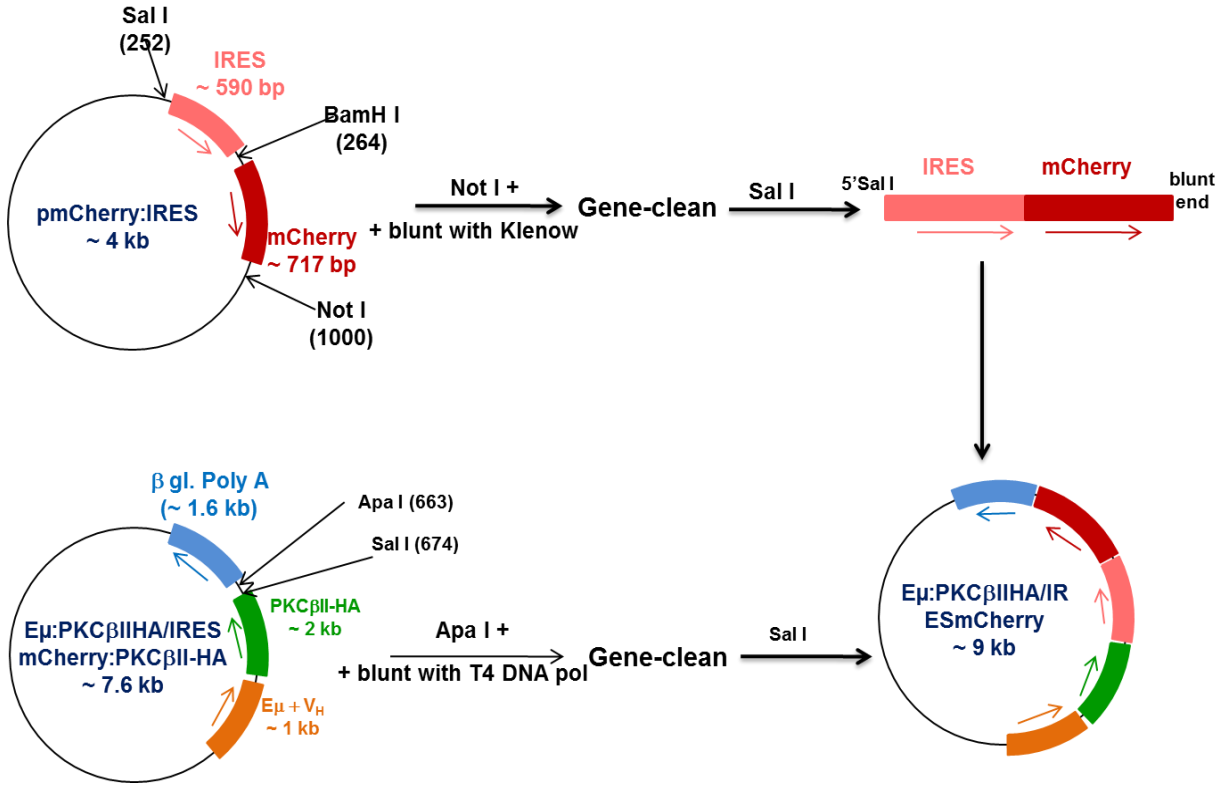

Figure 3-19. Schematic showing sub-cloning of IRES-9/mCherry-6 into PKCβIIHA-wt1/Eμ-29. The IRES9-mCherry coding sequence was first digested with NotI followed by blunting of the 3'-end with Klenow. On the other hand, the pEμ-PKCβII-HA-wt1 vector was digested with Apa-I, and also blunted by Klenow. Both IRES9-mCherry and pEμ-PKCβII-HA-wt1 were then digested with SalI to to release IRES-mCherry from the former plasmid, and create the complementary sites for receiving IRES9-mCherry in the latter plasmid. Finally, the IRES-mCherry coding sequence was ligated into the prepared pEμ-PKCβIIHA-wt1 vector.

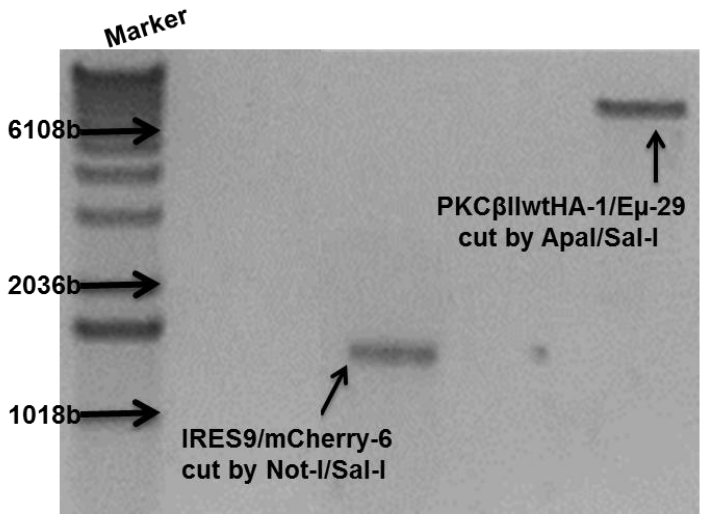

Figure 3-20. Preparation of PKCβIIwtHA-1/Eμ-29 and IRES9/mCherry-6 for the ligation. This figure is an agarose gel analysis of the preparation of PKCβIIwtHA-1/Eμ-29 and IRES9/mCherry-6 as described in Figure 3-19. This illustrates that PKCβIIwtHA-1/Eμ-29 (~7.6kb) and the IRES-mCherry coding sequence (1.2kb) were of the correct size following GENECLEAN purification from the gel slices.

Figure 3-20 shows the digestion products of the reaction described above after GEANCLEAN. The IRES-mCherry coding sequence ran as a 1.2kb band and the pEμ-PKCβIIHA backbone ran as a ~7.6kb band. Thus, after extraction from the gel the IRES-mCherry coding sequence was ligated into PKCβIIwtHA-1/Eμ-29 in the presence of DNA Ligase (see Section 2.1.4.4). The transformation efficiency was $1x10^7$ cfu/μg. Twenty clones were selected for screening, plasmid DNA was isolated and subjected to test digestions with either EcoRV (single nuclease digestion) or with Not-I/Sal-I (double nuclease digestion). Figure 3-21 shows a cartoon representation of the correct digestion pattern using this test digest approach. With EcoRV, correct insertion of the IRES/mCherry coding sequence would produce bands of 1.8kb and 7.2 kb. With the Not-I/Sal-I, double digestions correct insertion of the IRES/mCherry coding sequence would produce bands of 1.5kb and 6kb. The apparent 1.5kb loss in plasmid size using this approach was because Not-I cuts the pEμ-PKCβIIHA plasmid within the PKCβIIHA coding sequence as well as just before the Eμpromoter to yield a 1.5kb band.

Figure 3-22 shows the results of these test digests on the plasmid DNA purified from clones 11 – 19. Clones #13, #14, #17, #18 and #19 showed correct insertion of the IRES-mCherry coding sequence into the pEμ-PKCβIIHA plasmid because of the appearance of bands with the correct sizes following digestion with EcoRV, or with Not-I/Sal-I (Figure 3-21 C). However, clones #11, #15 and #16 showed that the IRES-mCherry coding sequence was not inserted into the pEμ-PKCβIIHA plasmid because the incorrect size of the plasmid backbone (5.8kb for EcoRV and 4.6kb for NotI/Sal-I). Clone number 18 was taken as my desired plasmid, pEμ-PKCβIIHA-IRES-mCherry, and this were sent for sequencing.

A

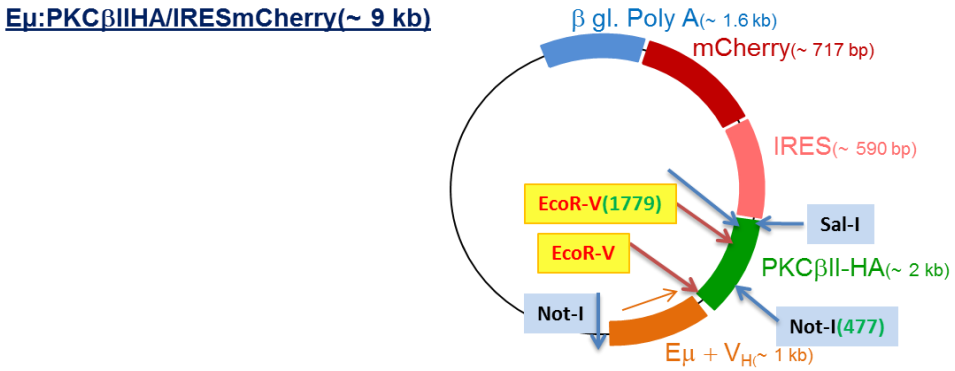

B

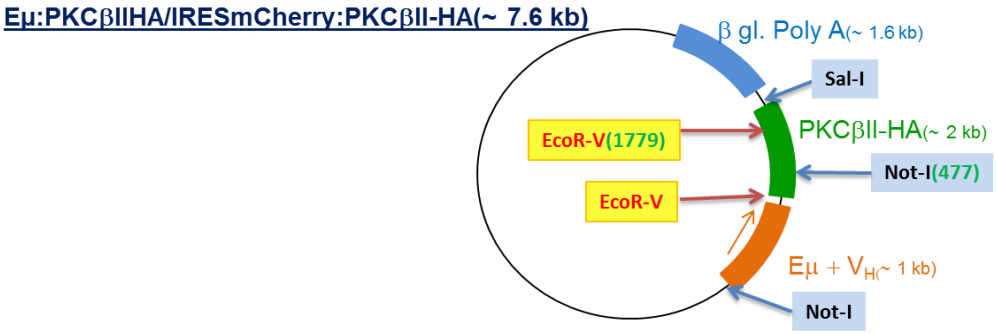

C

	EcoR-V	Not-I/SalI
Eμ/PKCβIIwt;IRES/mCherry	1.8Kb+7.2Kb	1.5Kb+1.5Kb+6Kb
Eμ/PKCβIIwt	1.8Kb+5.8Kb	1.5Kb+1.5Kb+4.6Kb

Figure 3-21. Strategies used for designing the test digestions for detecting colonies containing pEμ-PKCβIIHA-IRES-mCherry. In order to detect those colonies in which IRES-mCherry was successfully integrated into the Eμ/PKCβIIHA vector, the DNA is digested with either EcoRV or Not-I/SalI. **(A)** The schematic map of the restriction sites for EcoRV and for Not-I/SalI in a plasmid in which ligation of IRES-mCherry into the Eμ/PKCβIIHA vector was successful. **(B)** The schematic map of restriction sites for EcoRV or Not-I/SalI in a plasmid that only contains Eμ/PKCβIIHA. **(C)** This table lists the size of bands produced as a result of digestion of the plasmid in both scenarios.

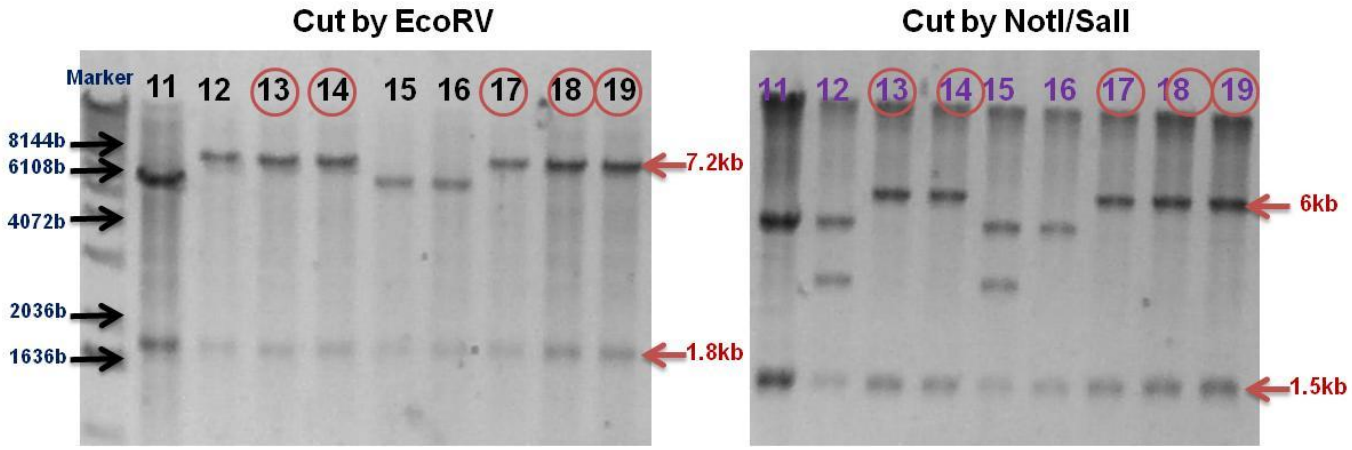

Figure 3-22. Integration of IRES-mCherry into the Eμ/PKCβIIHAwt1-29 vector. Agarose gel analysis of ten clones numbered 11 to 20 containing the pEμ-PKCβIIHA-IRES-mCherry ligation product. This DNA was digested with either EcoRV or with NotI/SalI.

3.4.1 Sequencing the pEμ-PKCβIIHA-IRES-mCherry plasmid

The pEμ-PKCβIIHA-IRES-mCherry plasmid was sent for sequencing to ensure that all the components of the transgene were present: the Eμ promoter, PKCβIIHA, IRES, mCherry and β-globin poly-A coding sequences. The vector backbone for the final plasmid was pBluescript in which there are recognition sites for the universal primers T3 and T7 just before and just after the multiple cloning sites (MSC). I used these primers to sequence the Eμ promoter (T3) and the β-globin poly-A (T7). In addition, I used PKCP5B and PKCP4 primers (see Appendix A) to respectively sequence the 5' and 3' ends of PKCβII (Figure 3-23). The sequencing data produced by using the above primers was subjected to a BLAST search of both human (for PKCβII) and mouse (for the Eμ promoter and β-globin) genomes (see Section 2.3.1).

Figure 3-24 shows the results of this sequencing and analysis. BLAST analysis of the sequences produced by the T3 and T7 primers showed that the Eμ promoter (Figure 3-24 B, C) and HbA-Sen50 beta globin (HBB) coding sequences (Figure 3-24 D) were present and intact within the pEμ-PKCβIIHA-IRES-mCherry plasmid. Sequences produced by the PKCP5B primer demonstrated that the PKCβII coding sequence was

contiguous with the Eμ promoter region (Figure 3-24 A, B). The sequence produced by the PKCP4 primer demonstrated that the PKCβII coding sequence was contiguous with the full sequence of IRES and mCherry (Figure 3-24 E, F, G). In conclusion, the digestion test and sequencing results demonstrated that the pEμ-PKCβIIHA-IRES-mCherry plasmid was complete and ready for expression analysis with the final goal of creating the transgenic mouse.

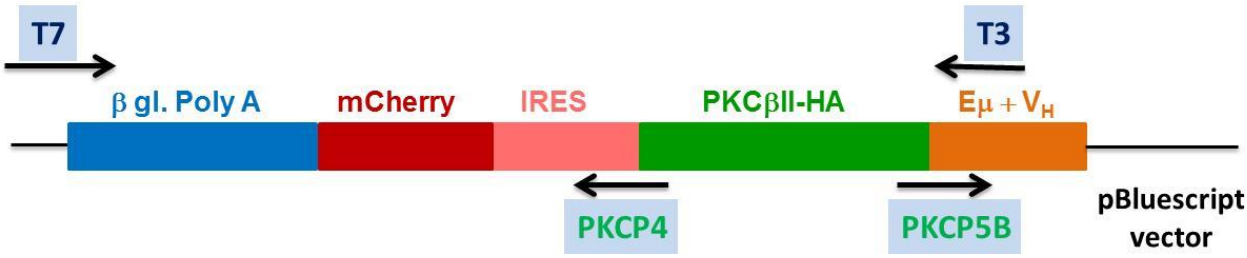

Figure 3-23. Primers used for sequencing the pEμ-PKCβIIHA-IRES-mCherry plasmid. The pEμ-PKCβIIHA-IRES-mCherry plasmid has five components: Eμ promoter, PKCβIIHA, IRES, mCherry and β-globin poly-A coding sequences. The T3 and T7 primers were used to sequence the Eμ promoter and the β-globin poly-A respectively. PKCP5B and PKCP4 primers were used sequence the 5' and 3' ends of PKCβII respectively.

A)BLAST analysis of sequence produced by Primer PKCP5B in human genome

-PRKCB:Homo sapiens PRKCB gene for protein kinase C, beta

-Score:558bits ,Identities:307/310(99%)

B) BLAST analysis of sequence produced by Primer PKCP5B in Mouse genome

-IgH:Mus musculus immunoglobulin heavy chain complex on chromosome 12

-Score:621bits ,Identities:338/339(99%)

C) BLAST analysis of sequence produced by primer T3 in mouse genome

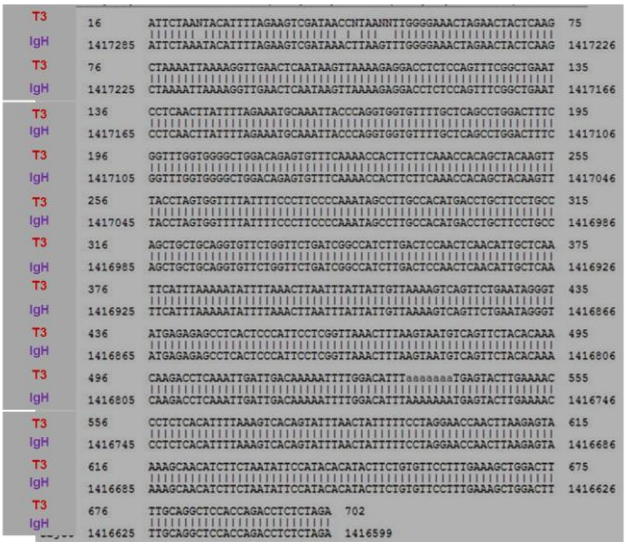

-IgH:Mus musculus immunoglobulin heavy chain complex

-Score:1249bits ,Identities:682/687(99%)

D) BLAST analysis of sequence produced by primer T7 in mouse genome

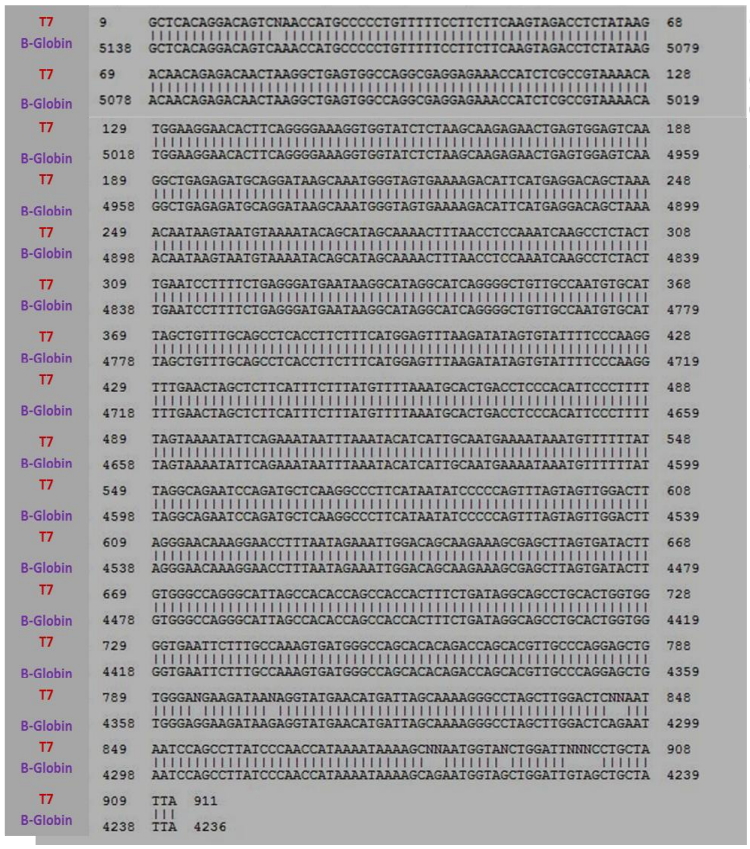

-β-globin: Homo sapiens isolate HbA-Sen50 beta globin(HBB) gene, complete coding sequence

-Score:1622bits ,Identities:891/903(99%)

E) BLAST analysis of sequence produced by primer PKCP4 and IRES coding sequence

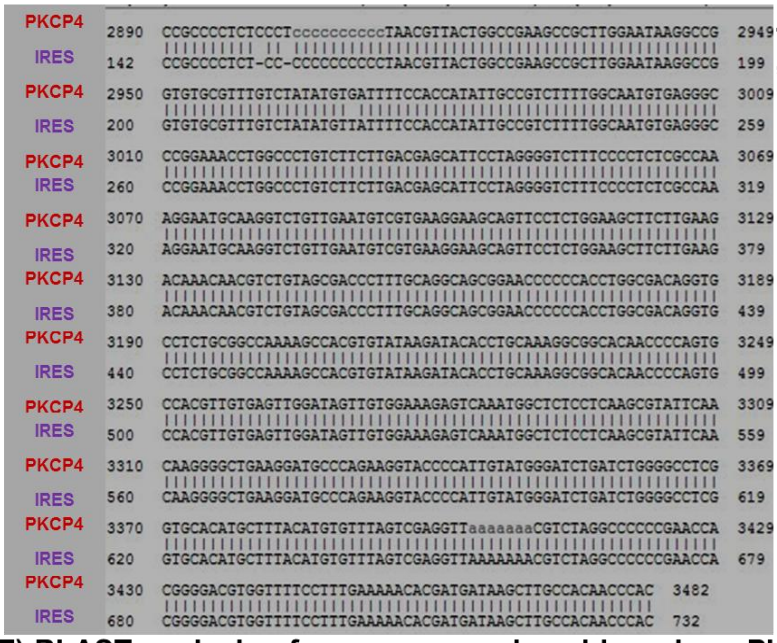

-Score:1077bits ,Identities:590/593(99%)

F) BLAST analysis of sequence produced by primer PKCP4 and mCherry coding sequence

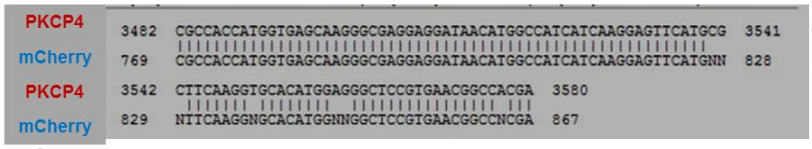

-Score:158bits ,Identities:92/99(93%)

G) BLAST analysis of sequence produced by primer PKCP4 and PRKCB

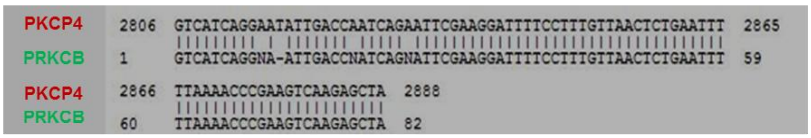

-Score:135bits ,Identities:79/83(95%)

Figure 3-24. Sequencing the pEμ-PKCβIIHA-IRES-mCherry plasmid. Four primers were used to sequence the pEμ-PKCβIIHA-IRES-mCherry plasmid. The sequencing data produced by using these primers were subjected to a BLAST search of both human (for PKCβII) and mouse (for the Eμ promoter and βglobin) genomes. **A)** Sequence comparison of the PKCP5B sequence product with the human genome. **B)** Sequence comparison of the PKCP5B sequence product with the mouse genome. **C)** Sequence comparison of the T3 sequence product with the mouse genome. **D)** Sequence comparison of the T7 sequence product with the mouse genome. **E)** Sequence comparison of the PKCP4 sequence product and the IRES coding sequence, **F)** Sequence comparison of the PKCP4 sequence product and the mCherry coding sequence, **G)** Sequence comparison of the PKCP4 sequence product and the sequence produced by PRKCB

3.4.2 Analysis of transgene expression in a mouse B cell line using transient transfection

To ensure that the pEμ-PKCβIIwtHA-IRES-mCherry plasmid was functional prior to the making of a transgenic mouse, I tested whether expression of this gene could be observed in a mouse cell line of B cell origin. The mouse cell line I used was A20 cells (see Appendix B), which are a B lymphoma cell line derived from a spontaneously occurring reticulum cell neoplasm(Kim*, et al* 1979) that have been used in many studies of mouse B cell biology. To transfect A20 cells, I used Nucleofection™ which is an electroporation methodology that combines different DNA encapsulating agents with different electric pulses to achieve optimal cell transfection (see Section 2.2.2). Transfected A20 cells were then analysed by Western blot to detect expression of the PKCβII transgene, and by confocal microscopy to detect the expression of mCherry. The pathway of this investigation is illustrated Figure 3-25.

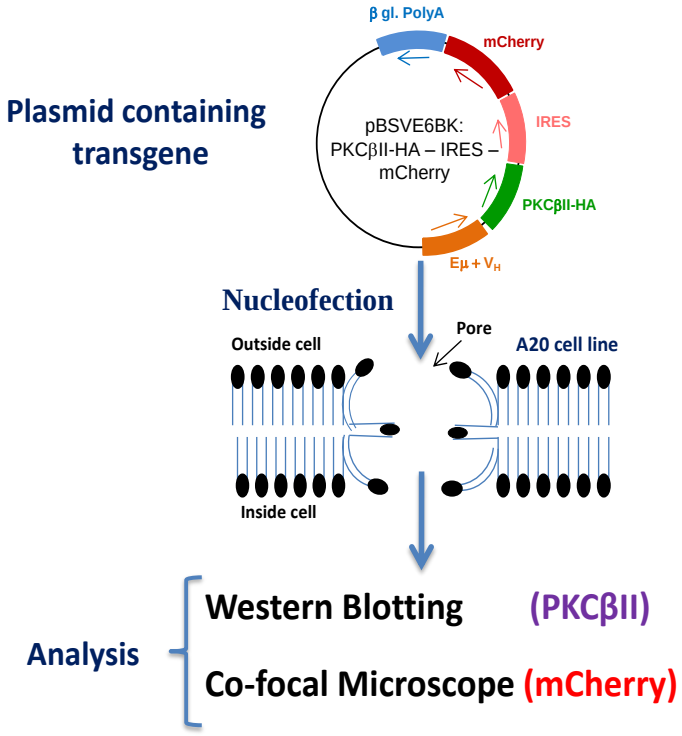

Figure 3-25. Testing transgene expression. The A20 cells are transfected with pEμ-PKCβIIHA-IRES-mCherry plasmid by Nucleofection, then the cell lysate is prepared for Western blotting to detect expression of PKCβIIHA. Also, live transfected A20 cells were imaged by confocal microscopy to detect mCherry expressing A20 cells.

I used the recommended protocol for performing Nucleofection in A20 cells, this involved solution V and programme U-15. I initially tested the efficiency of this transfection protocol with a plasmid containing a GFP gene under the control of a CMV promoter. Figure 3-26 shows flow cytometry traces of GFP expression in un-transfected and transfected cells, and indicated that I could achieve 70% transfection of A20 cells.

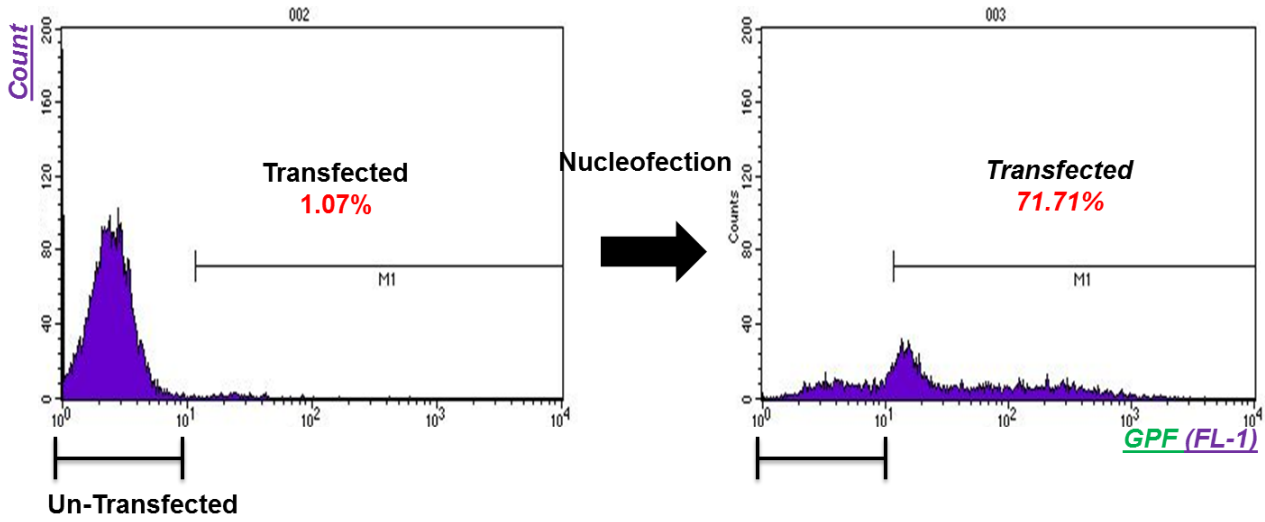

Figure 3-26. Determination of transfection efficiency in A20 cells by using flow cytometry. Flow cytometry analysis of GFP in untransfected A20 cells and A20 cells transfected with pEGFP.

I next tested the pEμ-PKCβIIHA-IRES-mCherry plasmid. $2x10^6$ A20 cells were transfected with 2μg of this plasmid using the U-15 nucleofection protocol. Following 24h incubation the cells were harvested and analysed for expression of the genes coded for by pEμ-PKCβIIHA-IRES-mCherry. Figure 3-27 shows Western blot analysis of HA expression in lysates of A20 cells transfected with pEμ-PKCβIIHA-IRES-mCherry plasmid and compared to cells transfected with either pCEP4-PKCβIIHA or pPKCβII-GFP. The PKCβIIHA gene codes for a protein of approximately 80kD and only A20 cells transfected with pEμ-PKCβIIHA-IRES-mCherry or with pCEP4-PKCβIIHA show a band at this molecular weight that is reactive with the HA antibody. The band associated with the A20 cells transfected with pCEP4-PKCβIIwtHA was more intense than in A20 cells transfected with pEμ-PKCβIIHA-IRES-mCherry. This is possibly because the pCEP4

vector uses a CMV promoter to drive expression of inserted genes (see Appendix B). The relative strength of the CMV and Eμ promoters was therefore likely reflected in the relative amounts of PKCβIIHA that was expressed. Nevertheless, this experiment shows that PKCβIIHA protein expression could be driven from the pEμ-PKCβIIHA-IRES-mCherry plasmid I prepared.

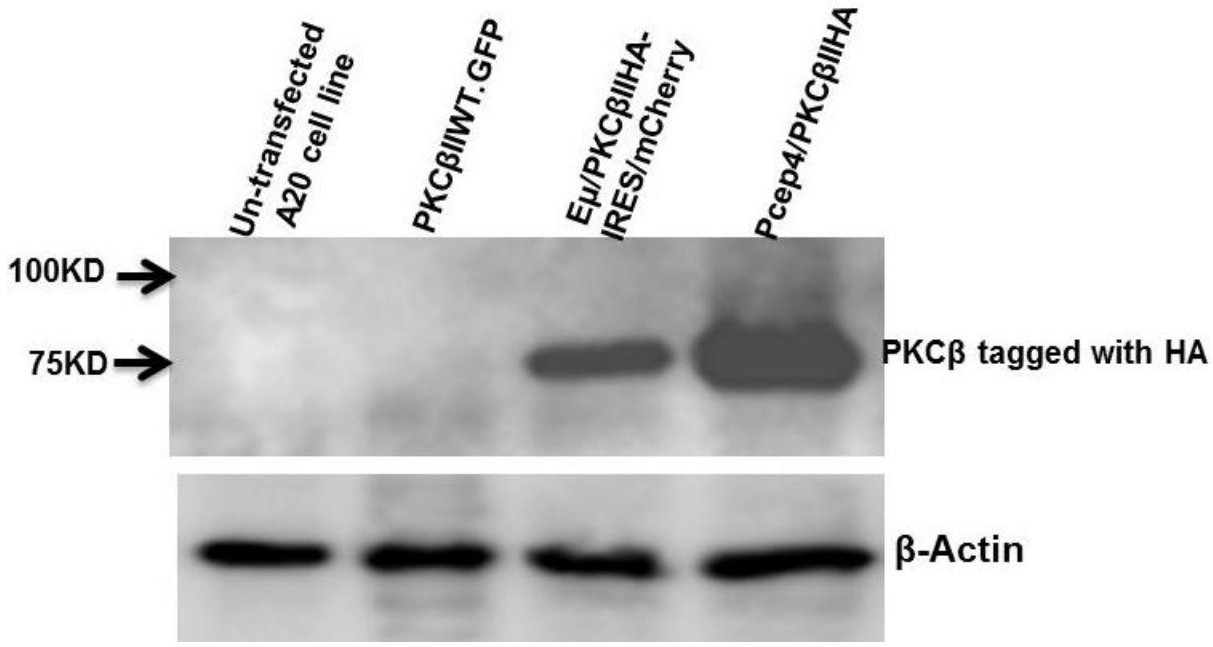

Figure 3-27. Detection of HA protein in transfected A20 cells with pEμ-PKCβIIHA-IRES-mCherry by Western blot. Western blot analysis of A20 cell lyates transfected in the indicated manner. 10μg of protein was analysed in each case. β-actin is used as a loading control.

I next analysed transfected A20 cells for expression of the mCherry gene. I performed this using confocal microscopy equipped with a 561nm laser to excite the fluorphore. Figure 3-28 shows that a large number of A20 cells transfected with pEμ-PKCβIIHA-IRES-mCherry expressed mCherry. These data, taken together with the experiments showing expression of PKCβIIHA, indicate that the pEμ-PKCβIIHA-IRES-mCherry plasmid is functional and ready to be used to make a transgenic mouse.

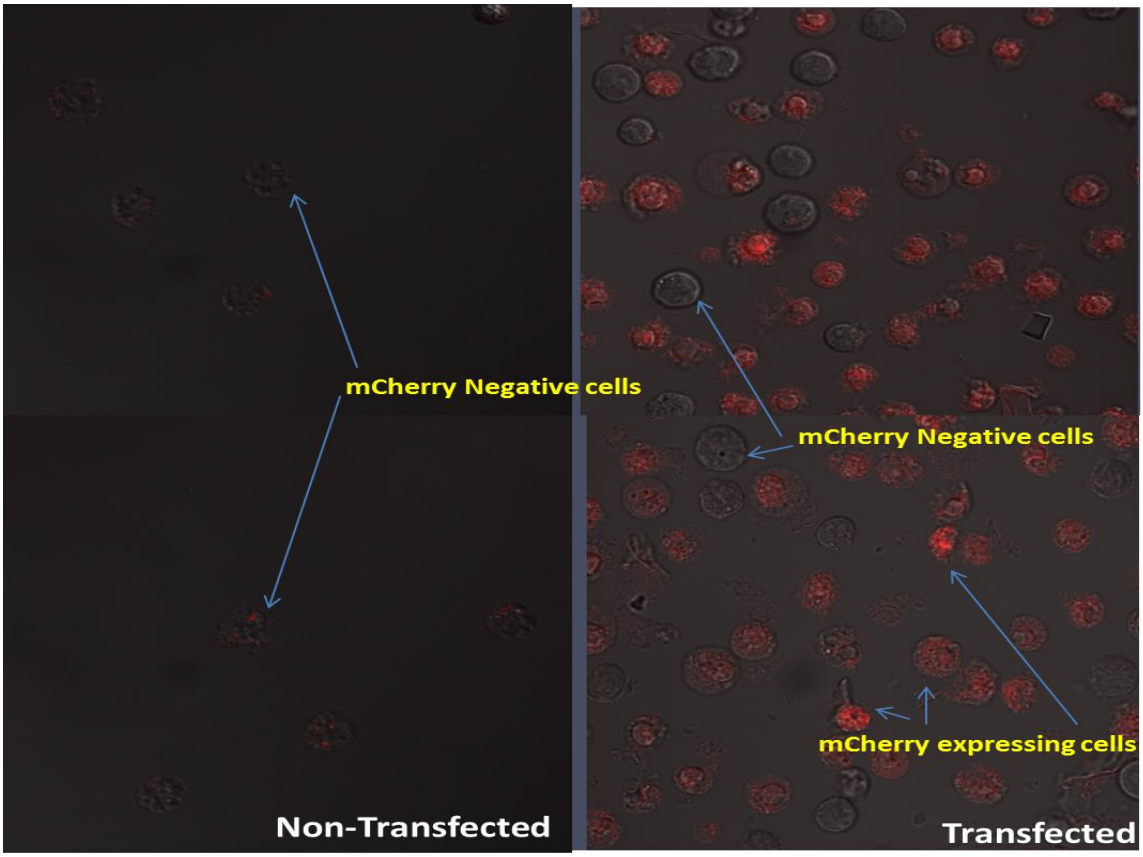

Figure 3-28. Detection of mCherry protein in A20 cells transfected with pEμ-PKCβIIHA-IRES-mCherry using a confocal microscope. The untransfected A20 cells and A20 cells transfected with pEμ-PKCβIIHA-IRES-mCherry were imaged by confocal microscopy using a 560nm laser to excite mCherry and detecting fluorescence at 610nm..

4 CHAPTER IV: Generation of Eμ-PKCβII tg mice

4.1 Preface

The first step of making a transgenic mouse was injection of the *pEμ*-PKCβIIHA-IRES-mCherry transgene into the pro-nuclei of fertilized eggs. This was followed by transferring the injected eggs into the oviducts of pseudo-pregnant mice where they would develop. The litters born from these foster mother mice were then screened in order to identify which of the animals carries the transgene. The mice that carried the transgene were known as founder mice. These founder mice were then backcrossed with wild type mice to establish the transgenic line. This chapter is concerned with describing the generation of a mouse that was transgenic for PKCβII expression specifically in B cells using the pEμ-PKCβIIHA-IRES-mCherry plasmid made in Chapter 3.

4.2 Gel-Based DNA purification of the pEμ-PKCβIIHA-IRES-mCherry transgene

In Chapter 2, I show that transfection of the pEμ-PKCβIIHA-IRES-mCherry plasmid into a mouse B cell line (A20 cells) results in expression of both PKCβIIHA and mCherry in these cells. This demonstrates that the quality of the plasmid was high. To prepare the Eμ-PKCβIIHA-IRES-mCherry coding sequence for injection, it must first be digested from the host plasmid (pBluescript II SK). This is because long stretches of DNA, such as the non-coding vector sequence, are toxic to mouse zygotes and this could lead to death of the embryo and/or poor efficiency in generating transgenic mice.

To isolate the Eμ-PKCβIIHA-IRES-mCherry transgene from its vector backbone, I used Pvu-I and Spe-I in a double digestion of the pEμ-PKCβIIHA-IRES-mCherry plasmid. Figure 4-1A shows the map of the intended results of this digestion; the Eμ-PKCβIIHA-IRES-mCherry coding sequence will have an approximate 6kb band size, whereas the vector backbone will run as two bands of 1.7 and 1.1kb. Figure 4-1B shows that this was indeed the case in the actual digestion of pEμ-PKCβIIHA-IRES-mCherry. Thus, the 6kb Eμ-PKCβIIHA-IRES-mCherry band was excised from the agarose gel

(Figure 4-1C), and the concentration of the isolated DNA was estimated from a 6108bp band (containing 100ng DNA) that was within the DNA ladder that was also run concomitantly with the purified Eμ-PKCβIIHA-IRES-mCherry DNA (Figure 4.2-1D). Thus, 2μl of the Eμ-PKCβIIHA-IRES-mCherry coding sequence preparation contained 100ng or 50ng/μl DNA.

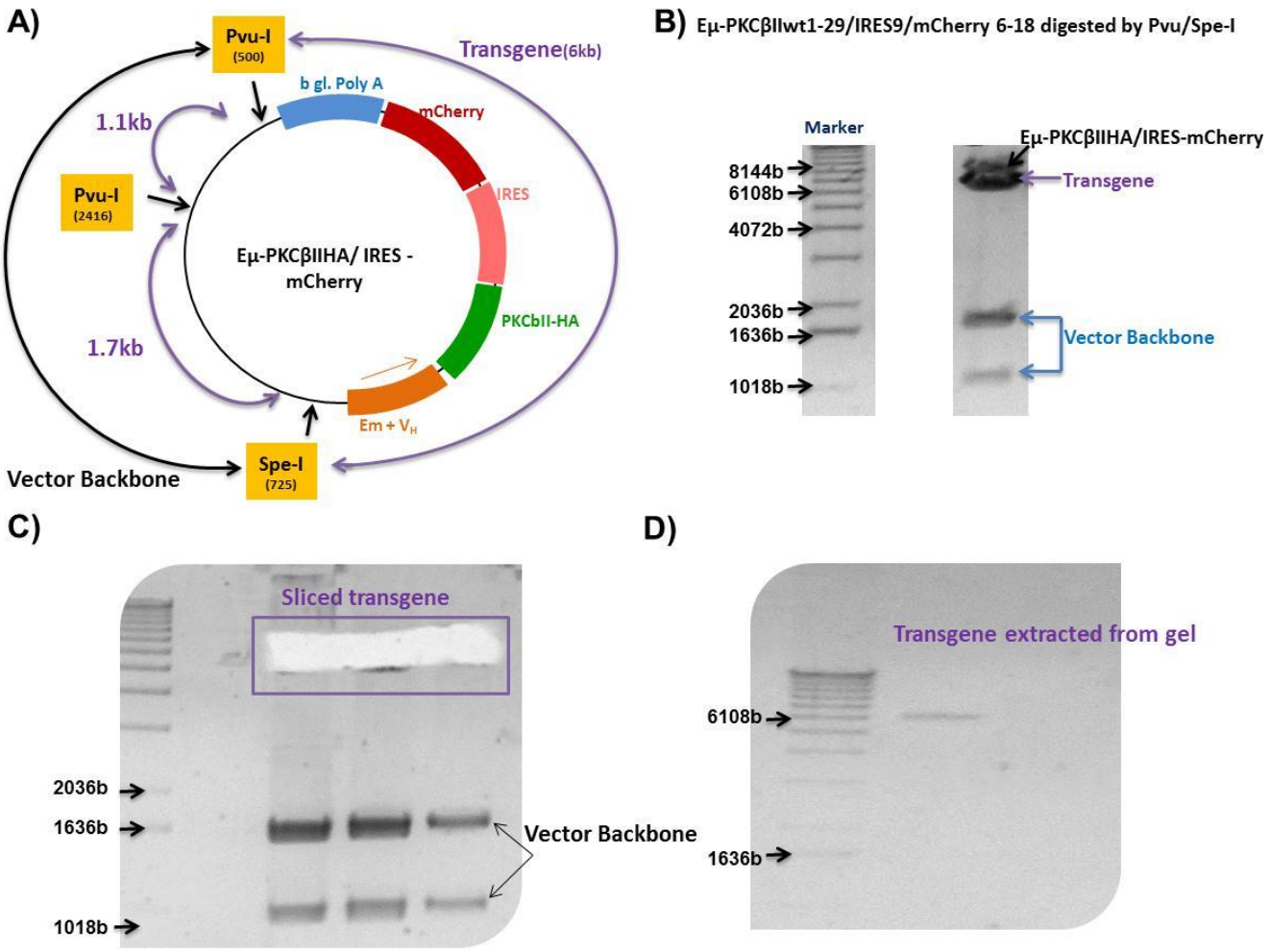

Figure 4-1. Preparation of transgene for pro-nuclei injection. Before injection into fertilized eggs, the Eμ-PKCβIIHA-IRES-mCherry transgene was isolated from its vector backbone by digestion with Pvu-I and Spe-I restriction enzymes. **A)** The schematic showing the map of the intended results of Eμ-PKCβIIHA-IRES-mCherry plasmid digestion with Pvu-I/Spe-I. **B)** Actual digestion of pEμ-PKCβIIHA-IRES-mCherry with Pvu-I and Spe-I. **C)** To prepare the transgene for Pro-nuclei injection, the 6kb Eμ-PKCβIIHA-IRES-mCherry band was excised from the agarose gel, **D) E**xtracted DNA from the gel was purified using GENECLEAN, and then 2μl the Eμ-PKCβIIHA-IRES-mCherry coding sequence was run on the gel to estimate DNA concentration from a 6108bp band (containing 100ng DNA) that was within the DNA ladder.

4.3 Preparation of Fertilized Eggs for Microinjection

Immediately following fertilization the nuclei containing chromosomes derived from the male (sperm) and female (egg) partners, called pro-nuclei, eventually fuse at the centre of the egg cell to form a single nucleus (Figure 4-2). Microinjection of transgenic DNA is best accomplished at this pro-nuclei stage. This is a very narrow window of opportunity, and needs to be precisely timed in order to ensure efficient isolation of early fertilized egg cells.

In order to prepare the fertilized eggs, female mice were injected with Pregnant Mare's Serum Gonadotropin (PMSG) and human chorionic gonadotropin (HCG, Intervet) intra-peritoneally. These two hormones cause super ovulation of eggs in the mouse ovary, and after approximately 24h this female was mated with a stud male mouse. Mating success was observed by the appearance of a "plug" where the vulva of the female mouse became distended following intercourse.

Mice having this plugged appearance were sacrificed, and the entire ovary and oviduct were dissected from the body cavity by cutting them from the upper part of the uterus. The ovary and oviduct was then transferred into medium containing hyaluronidase, and zygotic egg cells were released by gently squeezing the ampulla using micro-dissection forceps. Zygotic cells were isolated from cumulus cells by appearance; healthy cells were selected and transferred to another petridish, whereas cells with an abnormal appearance were excluded.

In the first attempt to generate PKCβII transgenic mice, 167 zygotes were harvested from 5 super-ovulated female mice, and of these zygotes 130 were healthy enough for transgene injection. Table 4-1 summarizes the total number of the isolated fertilized eggs as well as the numbers of healthy eggs used for the generation of transgenic mice.

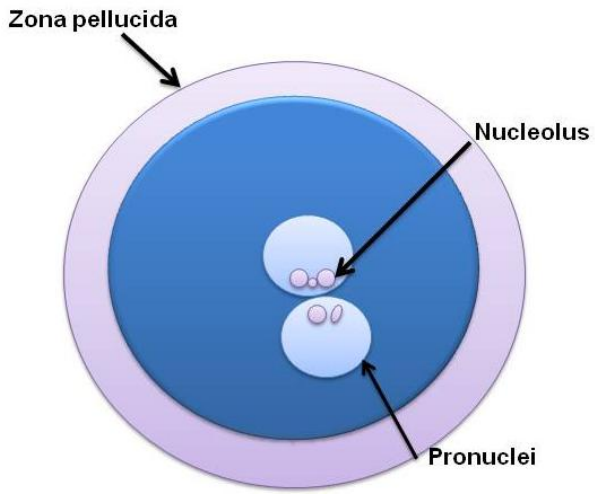

Figure 4-2. Pro-nuclei stage in fertilization. In the first stage of fertilisation which is called the pro-nuclei stage, the nuclei containing chromosomes derived from the male (sperm) fuse to female (egg) partners at the centre of the egg cell to form a single nucleus. Each of these pro-nuclei contains nucleolus. In this stage, the zygotic cell is surrounded by a membrane called the zona pellucida.

4.4 Pro-nuclei microinjection of the transgene into mouse zygotes

There are several parameters that are important for transgene integration into the mouse genome. The optimal concentration of injected transgene is one of them; too high a concentration could lead to lysis of the zygotes, whereas too low a concentration may result in lack of integration into the host genome. I used a DNA concentration of 2 ng/µl for microinjection as it is known that this concentration gives the most efficient integration of transgene into a genome. In addition, injection performance is another important factor in transgene integration and should be performed in a gentle and prompt way to minimize the possibility of damage to the zygotes. Last but not least, the timing of the microinjection should be precisely followed because the optimal window for transgene integration into the mouse genome is narrow, and can be easily missed. An

injection window of 11 to 13hrs was used following insemination of donor female mice. And this is the time that pro-nuclei are visible and the transgene can be injected into them.

The microinjection procedure was performed using a specialised microscope unit consisting of an inverted microscope equipped with micromanipulators, injectors and other peripheral equipment. The procedure begins by fixing egg cells into position with a holding pipette. The injection needle, containing the DNA transgene (at a concentration of 2ng/µl) was then pushed through the plasma membrane of the egg cell into the vicinity of the pronuclei membrane, and preferably the male pronuclei because of its bigger size compared to its female counterpart. It was important to avoid touching visible nucleoli, and it is common that the injection needles stick to nucleosomes and need to be replaced before moving on. The microinjection procedure was stopped after observation of a slight swelling of the pronucleus (Fiqure 4-3). After injection, the fertilized eggs were incubated at 37°C for 24 hrs to let the cells undergo a first round of cell division. This was done to ensure that the injected fertilized eggs were healthy and able to replicate.

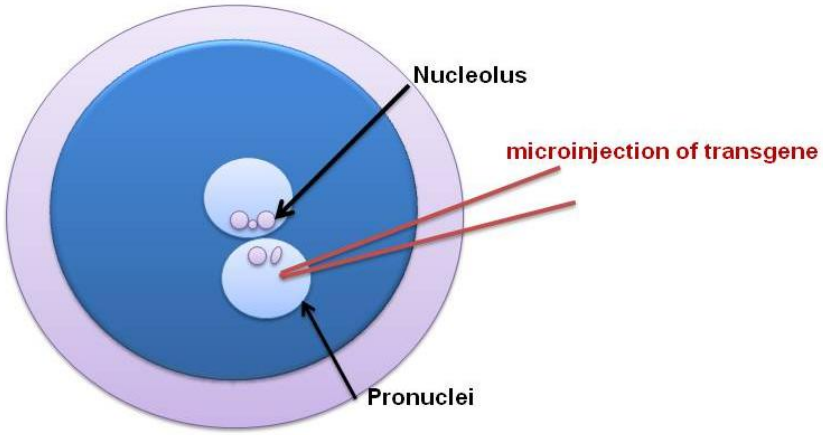

Figure 4-3. Schematic for microinjection of transgene into the pro-nucleus of fertilised egg.

4.5 Oviduct transfer

The injected fertilized eggs as healthy embryos are then surgically transferred into the oviducts of recipient female mice (foster mice). Thus, intended recipient female mice were anesthetized and placed on an operation platform. A small incision was made in the skin of the mouse dorso-laterally just below the rib cage. The skin was opened with scissors to make an opening of approximately 6 – 8 mm. The body wall was lifted with forceps and opened with a second incision that was made in the same direction as the first and avoiding obvious blood vessels. The upper lip of the body wall was held open with a suture, and the exposed ovary, oviduct and uterus could be pulled out by lifting up the fat pad attached to the ovary. The uterus was located beneath the ovary and the infundibulum “a funnel-like end of the mammalian oviduct” was visible just above the uterus. At this stage, the mouse was transferred to a dissecting microscope and the procedure was performed under 15-20 X magnification. The prepared embryos were placed into the infundibulum using a transfer pipette that was prepared in such a way that successful deposition of the embryos could be ensured. After completion of the transfer, the pipet was removed, and the mouse was placed back on to the operation platform. The uterus, oviduct and ovary were repositioned back into the body cavity which was then sutured, the skin incision was closed using a wound clip. Depending on the number of embryos to be injected, this procedure was performed either unilaterally or bilaterally.

Table 4-1 summarizes the details of four consecutive attempts to inject prepared embryos for the generation of transgenic animals. In general, eighteen recipient female mice were subjected to oviduct transfer, using up to 130 prepared embryos. Following oviduct transfer, the foster mice were allowed to complete normal gestation of the embryos.

	Number Donor Female mice	Total Eggs	Normal/Fertilised Eggs	Embryo Transfer	Injected eggs
11/02/11	5	167	130	FT-1	24(Two Sides)
				FT-2	24(Two Sides)
				FT-3	24(Two Sides)
17/02/11	4	83	50	FT-4	20(Two Sides)
				FT-5	20(Two Sides)
24/02/11	5	81	20	FT-6	10(One Side)
				FT-7	10(One Side)
01/03/11	4	127	48	FT-8	14(One Side)
				FT-9	15(One Side)

Table 4-1. Details of four consecutive attempts to inject prepared embryos into oviduct of recipient mice for generation of the Eμ-PKCβII transgenic mice.

4.6 Genotyping transgenic founder mice

The pups born from foster mice were weaned at three weeks of age. Tissue samples were taken from these animals by clipping either the tail or the ear, and were used for subsequent genotypic screening.

Screening for presence of the transgene and identification of founder mice involved both PCR and Southern blot methods as described below. Both these methods were used because PCR screening quickly gives information about the presence of the transgene, whereas Southern blotting also gives information about the copy number of the transgene inserted into the genome. Importantly, both methods are complementary and can be used to validate each other. For example, there is a risk of obtaining false positive or false negative results when animals are screened only by PCR. In my approach, I initially used Southern blotting to identify founder animals. In subsequent screening assays, I sometimes used both methods to validate each other.

4.6.1 Southern blot strategy for detecting founder mice

The technique developed by Southern (Southern 1975), known as Southern blotting, consists of DNA isolation from tissues, fragmentation of this DNA by restriction endonuclease digestion, separation of the DNA fragments by electrophoresis, transfer of separated DNA fragments to a nylon membrane and hybridization with a probe oligonucleotide whose sequence is complementary to the gene of interest (see Section 2.1.3.3). In the present study, my probe was developed using a sequence that was found only in the transgene and not in the genome of wild type mice. Thus, I used the mCherry coding sequence contained within my transgene for this purpose. PCR was used to prepare the mCherry probe, and primers were designed that would amplify a 717bp sequence from the transgene template I constructed previously (Figure 4-4A). After amplifying this product, it was labelled with ^{32}P-dCTP using Klenow DNA polymerase. This labelled probe was then used for hybridization with DNA isolated from mouse tissues (see Section 2.1.3.3).

I used EcoRI to fragment the DNA isolated from the transgenic mice I generated. This is because this restriction enzyme cuts twice within the transgene sequence of the Eμ-PKCβIIHA-IRES-mCherry construct, but does not cut into the coding sequence of mCherry. Using this strategy, it is now possible to isolate a 2.1kb band containing mCherry following fragment separation of genomic DNA by electrophoresis (Figure 4-4B, C).

The next consideration is the copy number of the incorporated transgene. In the majority of cases micro-injected transgenes integrate into host DNA in a head-to-tail concatemer fashion. Therefore, anywhere from one copy of the gene, to multiple copies of the gene may be present. This can be estimated following the hybridization reaction by using the intensity of the detected band because this depends on the number of copies of transgene present. Importantly, band intensity can be used to discriminate between animals that are heterozygous or homozygous for the transgene, but also band intensity can be used at the founder stage to estimate the number of copies of

transgene that integrated into the genome. Thus, in my experiments digestion with EcoRI of genomic DNA from a founder mouse containing the Eμ-PKCβIIHA-IRES-mCherry transgene would result in the generation of a 2.1kb band, the intensity of which could be used to determine the copy number of integrated transgenic DNA (Figure 4-4D, E).

.

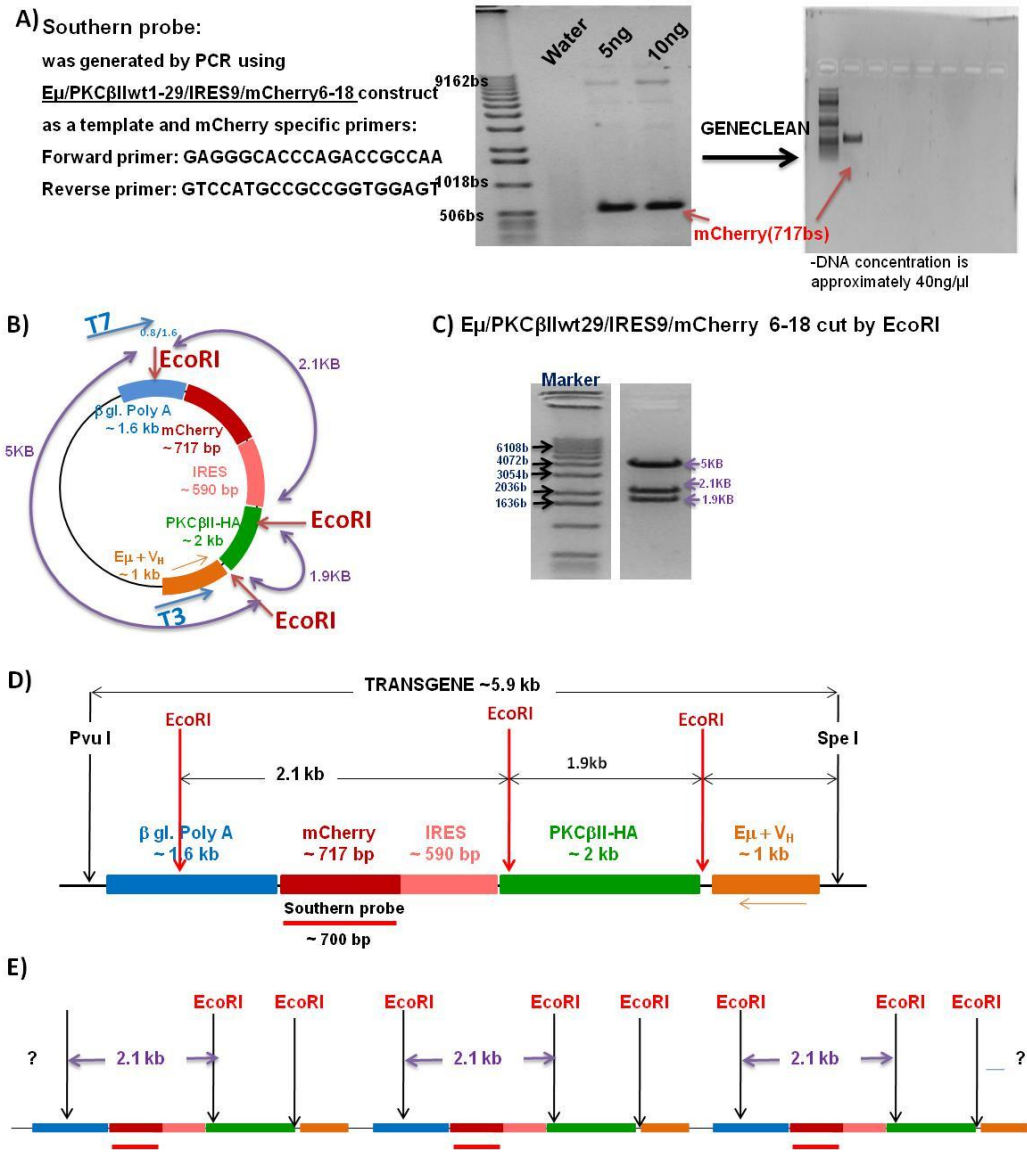

Figure 4-4. Southern blotting strategy used for detecting potential founder mice. A) Agarose gel analysis of the PCR product derived from primers that were designed to amplify the mCherry (717bp) sequence from the Eμ-PKCβIIHA-IRES-mCherry plasmid. This product was to be used as a probe for Southern blotting. **B**) A schematic of the EcoRI digestion of the the Eμ-PKCβIIHA-IRES-mCherry plasmid showing that the mCherry coding sequence is intact. **C)** Agarose gel analysis of a EcoRI digestion of pEμ-PKCβIIHA-IRES-mCherry. **D)** Schematic showing where the mCherry PCR probe would bind transgenic DNA. **E)** Schematic showing potential transgene integration within the genomic DNA in concatemer fashion. Here, the intensity of the 2.1kb band would determine the copy number of transgene.

4.6.2 Calculation of transgene copy numbers

To estimate the number of copies of transgene integrated into the host genome, the formula illustrated in Figure 4-5 was used. The calculation of the formula is based on the fact that the potential founder mice are hemizygous, meaning that the transgene integrates randomly into the DNA of one chromosome of any chromosome pair. Calculation of copy number must take into account the haploid size of the mouse genome. Thus, Mass of transgene DNA is a function of the size of the transgene (in bp) X the amount of genomic DNA used (μg) in the reaction divided by the haploid size of the mouse genome (which is 3×10^9 base pairs). From this formula I calculated that 19pg of transgenic / 10μg of genomic DNA is equivalent to 1 copy of the transgene present in the genome. To estimate copy number following the hybridization reaction, I used 1.9, 19, 190, 360 and 720 pg amounts of the Eμ-PKCβIIwtHA-IRES-mCherry coding sequence on the same electrophoresis gel to act as a standard curve. These amounts of standard DNA correspond to 0.1, 1, 10, 20 and 40 copies of transgene per genome. (Figure 4-5) In order to accurately estimate single integration of the transgene, the standard curve must accommodate a corresponding value that is less than 1 but greater than zero.

$$\frac{\text{Mass of transgene DNA}}{\text{N mg genomic DNA}} = \frac{\text{N bp transgene DNA}}{3 \times 10^9 \text{ bp genomic DNA}}$$

$$\frac{\text{Mass of transgene DNA}}{1\mu\text{g of genomic DNA}} = \frac{\text{5900bp transgene DNA}}{3 \times 10^9 \text{ bp genomic DNA}} \quad \text{or}$$

$$\text{Mass of transgene DNA} = \frac{(\text{5900bp transgene DNA}) \times (10\mu\text{g of genomic DNA})}{3 \times 10^9 \text{ bp genomic DNA}} \quad \text{or}$$

Mass of transgene DNA = 19 picoograms per 10 µg genomic DNA

-Thus, 19 pg transgene should be added to 10 µg of genomic DNA

Thus:

0.1copy	1.9 pg
1 copy	19 pg
10 copy	190 pg
20 copy	380 pg
40 copy	760 pg

Figure 4-5. Example of calculation for transgene copy number

4.6.2.1 Detection of the founder mouse

In total, 31 potential founder mice were born from foster mice following nine oviduct transfers of injected fertilized eggs containing the transgene. As indicated above, genomic DNA was isolated either from tail or ear tissue clips taken from the pups. This extracted DNA was then digested by EcoRI. At this stage it was important to ensure complete digestion of the genomic DNA to ensure that false negative results were avoided. Complete digestion of DNA was judged based on the appearance of a smear. Undigested or partially digested DNA clumps at the top of the gel, whereas DNA that is degraded prior to digestion lacks either of these attributes. Figure 4-6A shows the results of EcoRI digestion of genomic DNA isolated from the 31 potential transgenic animals. DNA from mouse 47-2, 49-1 and 49-4 appeared either degraded or partially digested and these animals were excluded from further study. The DNA from the rest of the animals showed an appropriate smear, indicating complete digestion.

Figure 4-6B shows the Southern blot of the DNA isolated from the 31 potential transgenic animals. The Southern blot was prepared by hybridizing the DNA transferred to nylon membranes with the mCherry probe I prepared. The expected 2.1kb band corresponding to the transgene containing mCherry was only observed in mouse number 45-2, a female mouse. It is noteworthy that there were two additional bands sized 4 and 6 kb also detected in the DNA of this mouse. The presence of these two bands likely represents the junction between integrated transgene concatemer and flanking chromosome DNA. Thus, mouse 45-2 was considered as a founder mouse. Estimation of the copy number of transgene integrated into the genome of mouse 45-2 suggested that there were less than 10 copies, but more than 1. For comparative purposes, genomic DNA from a known wild type mouse (wt) was chosen as a negative control.

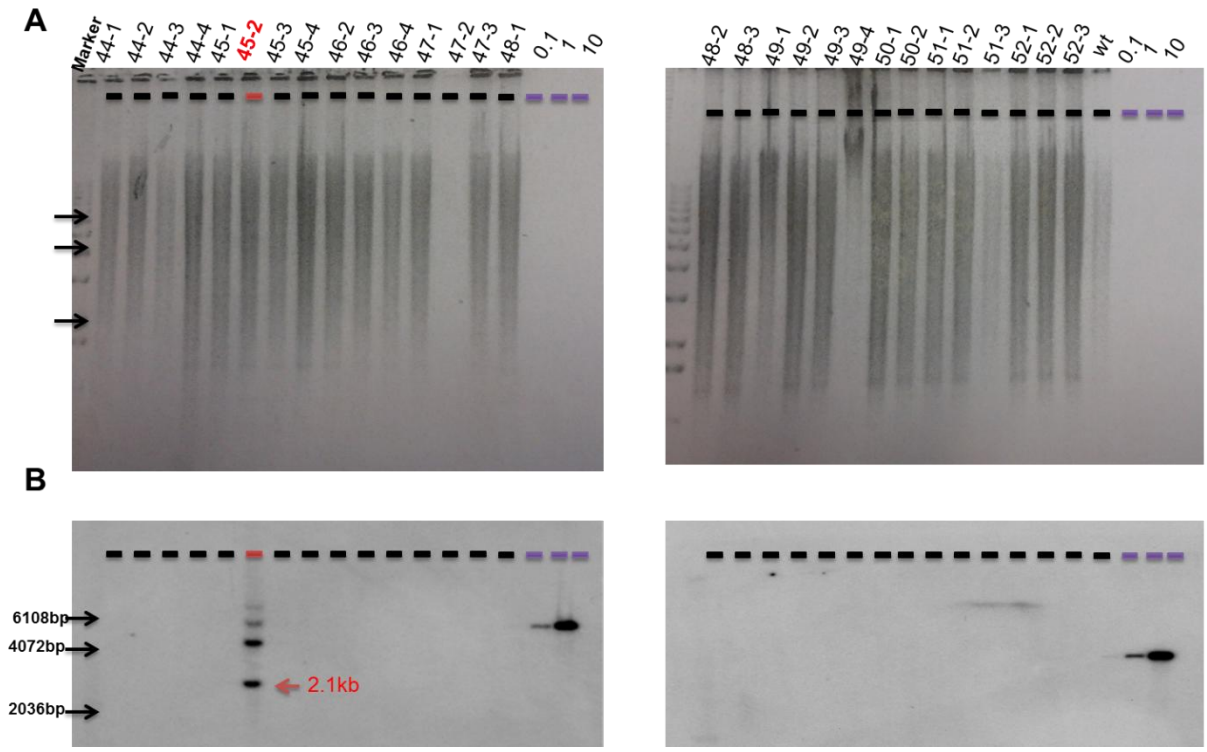

Figure 4-6. Detection of the trasngene in the mouse pups born from foster mice by Southern blot. 31 potential founder mice were born from foster mice following nine oviduct transfers of injected fertilized eggs in the foster mice. The genomic DNA was extracted from tail of these mice and Southern blotting was performed on these samples to detect the 2.1kb band carrying mCherry. **A)** Agarose gel representation of EcoRI digestion of genomic DNA isolated from the mouse pups. **B)** The EcoRI fragmented genomic DNA was probed for the presence of mCherry using Southern blotting.

4.6.3 Establishing the PKCβII transgenic mouse line

After establishing that mouse 45-2 was a founder mouse for the Eμ-PKCβII transgenic line, the next step was to back cross this animal with C57BL/6 wild type mice to generate Eμ-PKCβII homozygous mice. Figure 4-7 shows a schematic relating to the establishment of first-generation Eμ-PKCβII heterozygous mice. In this schematic, I show the attempts at generating the transgenic founder mouse, followed by the results

of the multiple matings needed for the heterozygous mice. What follows is a description of the procedures and results I received from the screening of these matings.

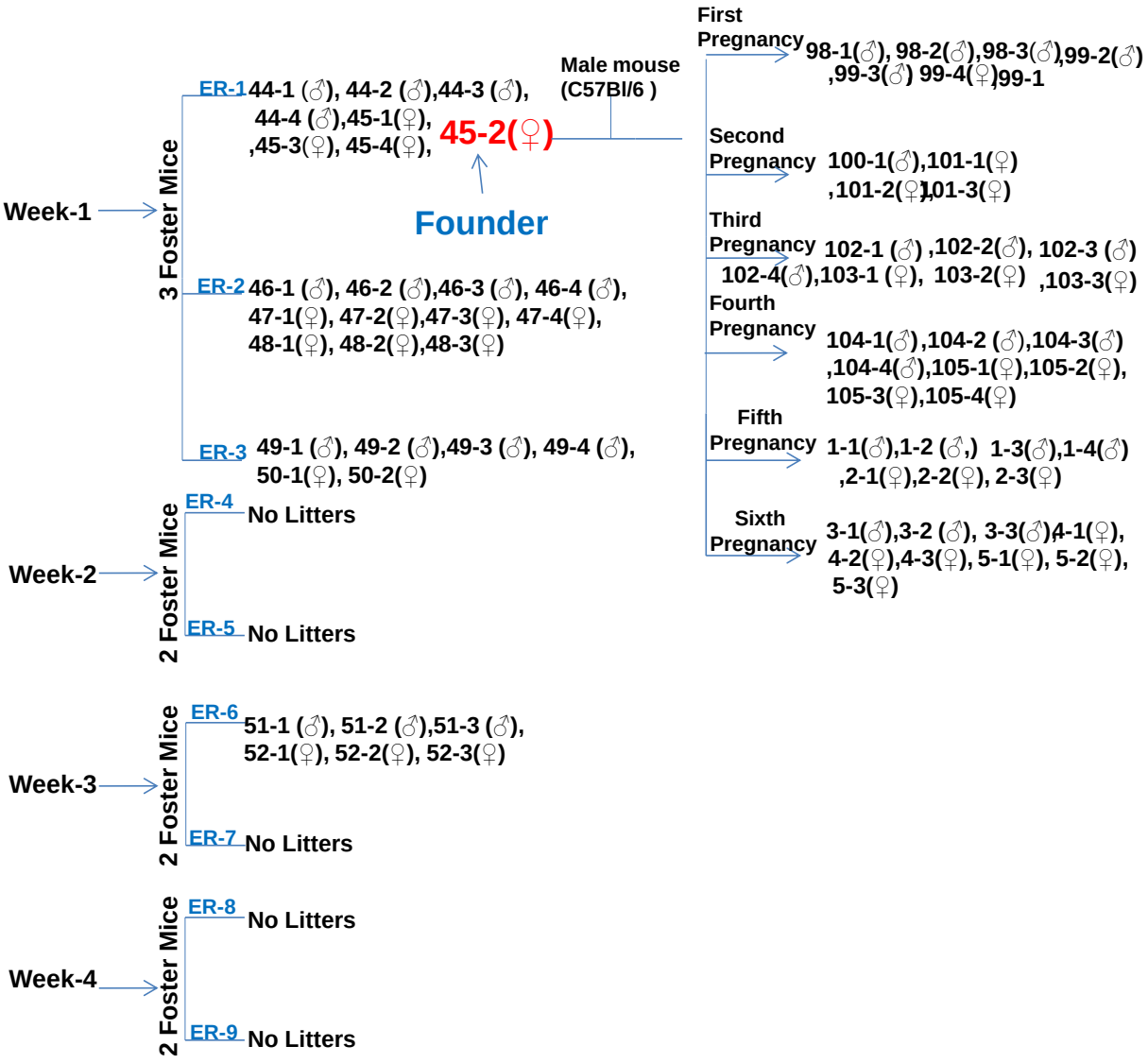

Figure 4-7. The time table for generation of Eμ-PKCβII transgenic mice.

The mice born from the first generation litters were screened for the presence of the Eμ-PKCβII transgene by both Southern blot and PCR. For PCR screening, I recycled the cloning primers I used in Chapter 3 (also see Appendix A) to clone IRES and

mCherry. Thus, I used the IRES forward primer and mCherry reverse primer in this reaction to amplify an IRES-mCherry coding sequence of 1.2kb in length from genomic DNA isolated from first generation transgenic animals. For Southern blot screening of these animals, and as described above, I searched for the presence of a 2.1kb band. These methods were complementary and fairly easy to carry out because Southern blot analysis requires approximately 10μg of DNA whereas the PCR method requires less than 1μg.

Figure 4-8 illustrates the results of my initial attempts to analyse for the presence of the Eμ-PKCβII transgene in the founder mouse and first two litters from this mouse using the PCR method I developed. As a positive control for the PCR reaction, I used the pEμ-PKCβIIHA-IRES-mCherry plasmid and was able to show successful amplification of a 1.2kb IRES-mCherry band. I next analysed DNA isolated from the founder mouse (45-2) and 2 mice negative for the presence of the transgene (analysed by Southern blot, see Figure 4-6). As expected, I was able to amplify the 1.2kb IRES-mCherry band from mouse 45-2 but not from mice 44-1 nor 45-4. Analysis of DNA isolated from the progeny in the first and second litters from mouse 45-2 shows amplification of the IRES-mCherry band in mice numbered 98-1, 98-3, 99-4 and 101-3. Unfortunately, I was not able to perform Southern blot analysis for these animals because I did not have enough DNA. Nevertheless, based on the results I received from my positive and negative controls in this experiment, I could be fairly confident that this assay method gives accurate results.

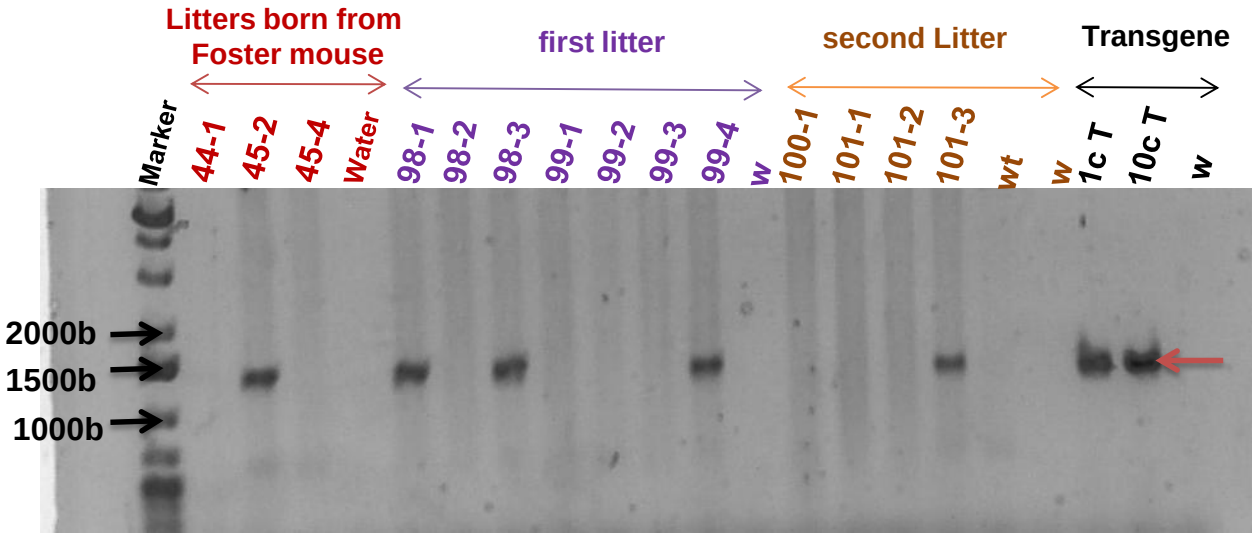

Figure 4-8. Detection of the transgene in 45-2 founder mouse and its progeny using PCR. IRES forward and mCherry reverse primers were used to amplify an IRES-mCherry coding sequence of 1.2kb in length (arrowed red) from genomic DNA isolated from transgenic animals. This figure is an agarose gel analysis screening the founder mouse 45-2 and its first two litters for detection of the transgene (IRES-mCherry) using PCR. As a positive control 1 and 10 copies of pEμ-PKCβIIHA-IRES-mCherry were amplified.

I used the PCR method to screen the progeny of the third and fourth litters that were born from the founder mouse (45-2). Figure 4-9A shows that mice numbered 102-1,102-3,102-4,103-1,103-3 and 104-1 appeared to carry the Eμ-PKCβII transgene, and Figure 4-9B shows that these results are confirmed using the Southern blot method. Importantly, mouse 102-2 was classified as undefined because the DNA isolated from this animal was degraded (Figure 4-9B).

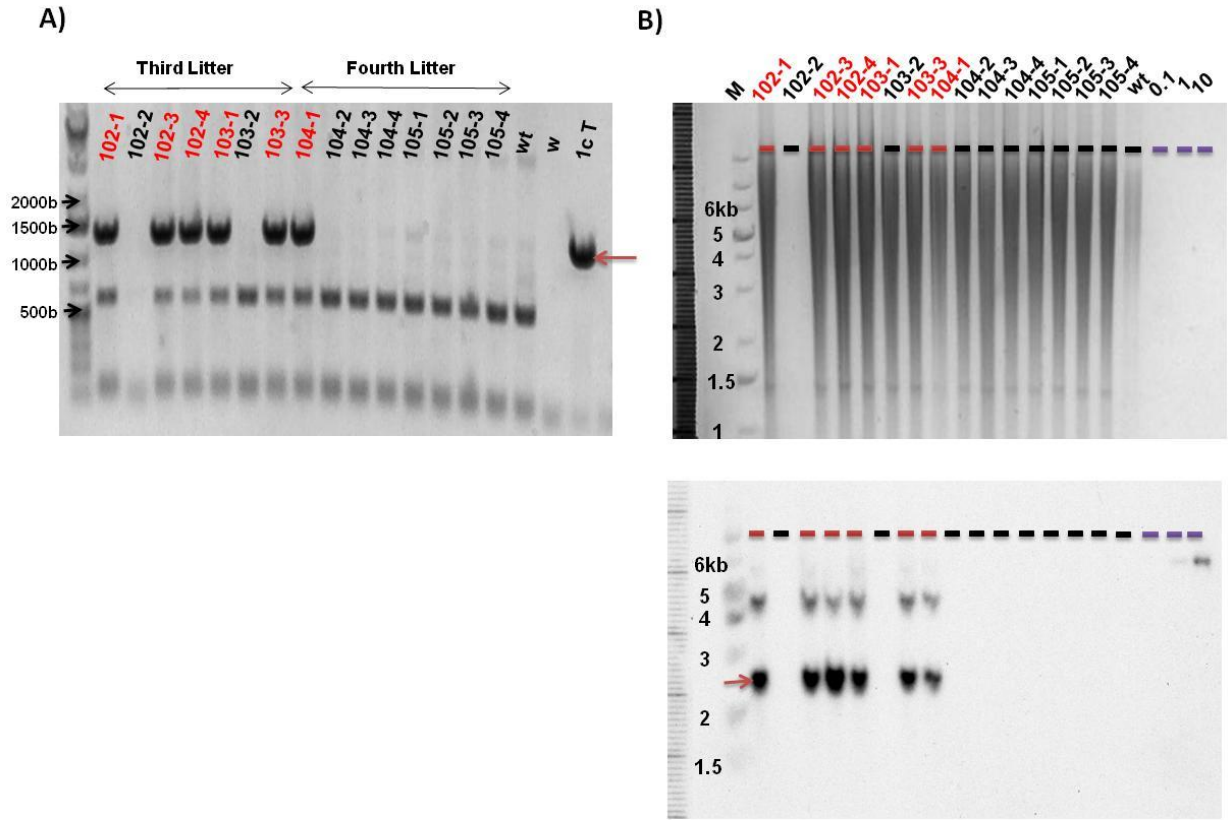

Figure 4-9. Detection of transgene in the third and fourth litters born from 45-2 founder mouse. The mouse pups born in the third and fourth litters of founder mouse 45-2 were screened for the presence of IRES-mCherry using PCR, and for the presence of mCherry using Southern blotting. **A) G**enomic DNA isolated from these mice was subjected to PCR to detect IRES-mCherry. **B)** Genomic DNA isolated from these animals was fragmented with EcoRI (*upper figure*), and then probed for the presence of mCherry using Southern blotting (*lower figure*).

4.6.3.1 Genomic DNA digestion with EcoRI versus Sph-I

Screening of the fifth litter revealed a technical problem with respect to partial digestion of isolated genomic DNA. This was a surprising problem to arise because EcoRI was a robust restriction enzyme that is relatively insensitive to DNA quality. As I had a limited source of genomic DNA for each sample, I decided a second strategy using a different restriction enzyme for DNA digestion was required for southern blotting.

For this purpose, I chose Sph-I because this restriction enzyme cuts once within the transgene sequence. A comparison of DNA digestion using EcoRI and Sph-I showed that Sph-I was more effective at complete digestion of the genomic DNA (Figure 4-10). Thus, I decided to replace EcoRI with Sph-I for digesting genomic DNA isolated from the animals of the fifth litter. Because Sph-I cuts differently than EcoRI, I needed to determine the size of the band carrying the transgene. Sph-I cuts the Eμ-PKCβIIHA-IRES-mCherry plasmid at a single site which was in the 3' end of the PKCβII coding sequence, producing a single band sized 9kb. This 9kb band contains the transgene (6kb) and the Eμ vector backbone (3kb) (Figure 4-11 A and B). With respect to the Southern blot, I again probed with the mCherry probe and expected a band sized approximately 6kb band containing entire sequence of the transgene because of the way Sph-I cut within the concatemer transgene integrated into genomic DNA (Figure 4-11 C and D). In this way, I was able to detect the presence and number of copies of transgene in the genomic DNA of the transgenic animals. Importantly, EcoRI remained the restriction enzyme of choice, and Sph-I was used only in cases where EcoRI could not digest genomic DNA.

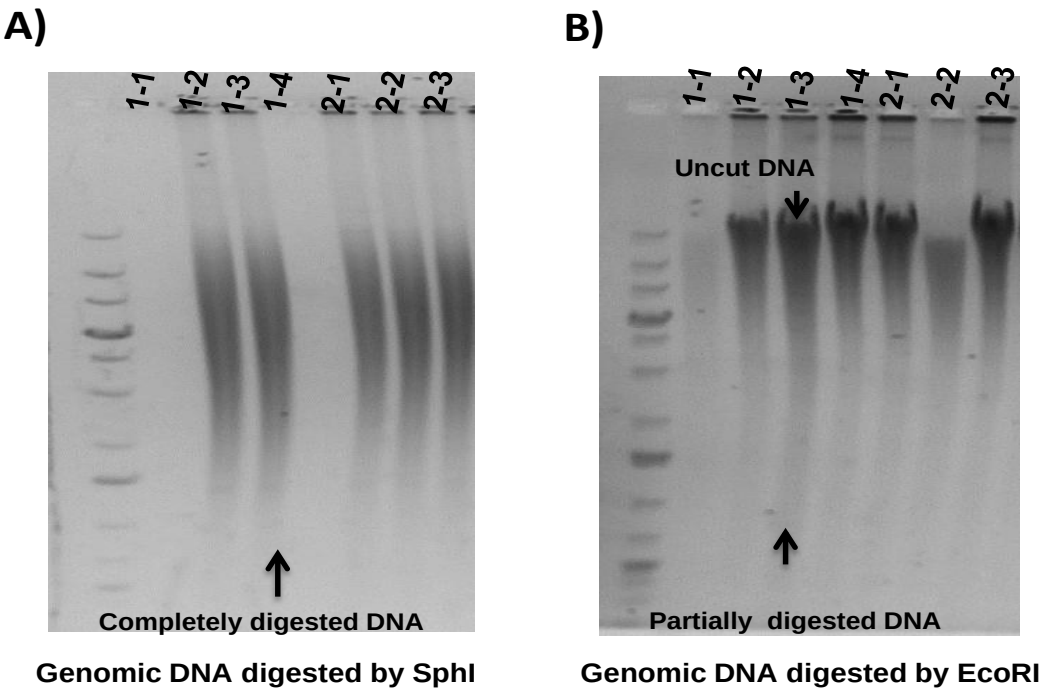

Figure 4-10. Comparison of EcoRI and SphI restriction enzymes in their ability in digesting mouse genomic DNA. 1µg of genomic DNA of the mice # 1-1, 1-2, 1-3, 1-4, 2-1, 2-2 and 2-3 were digested with EcoRI and Sph-I restriction enzymes. **A)** Agarose gel analysis of the genomic DNA of these mice digested by Sph-I, **B)** and EcoR-I.

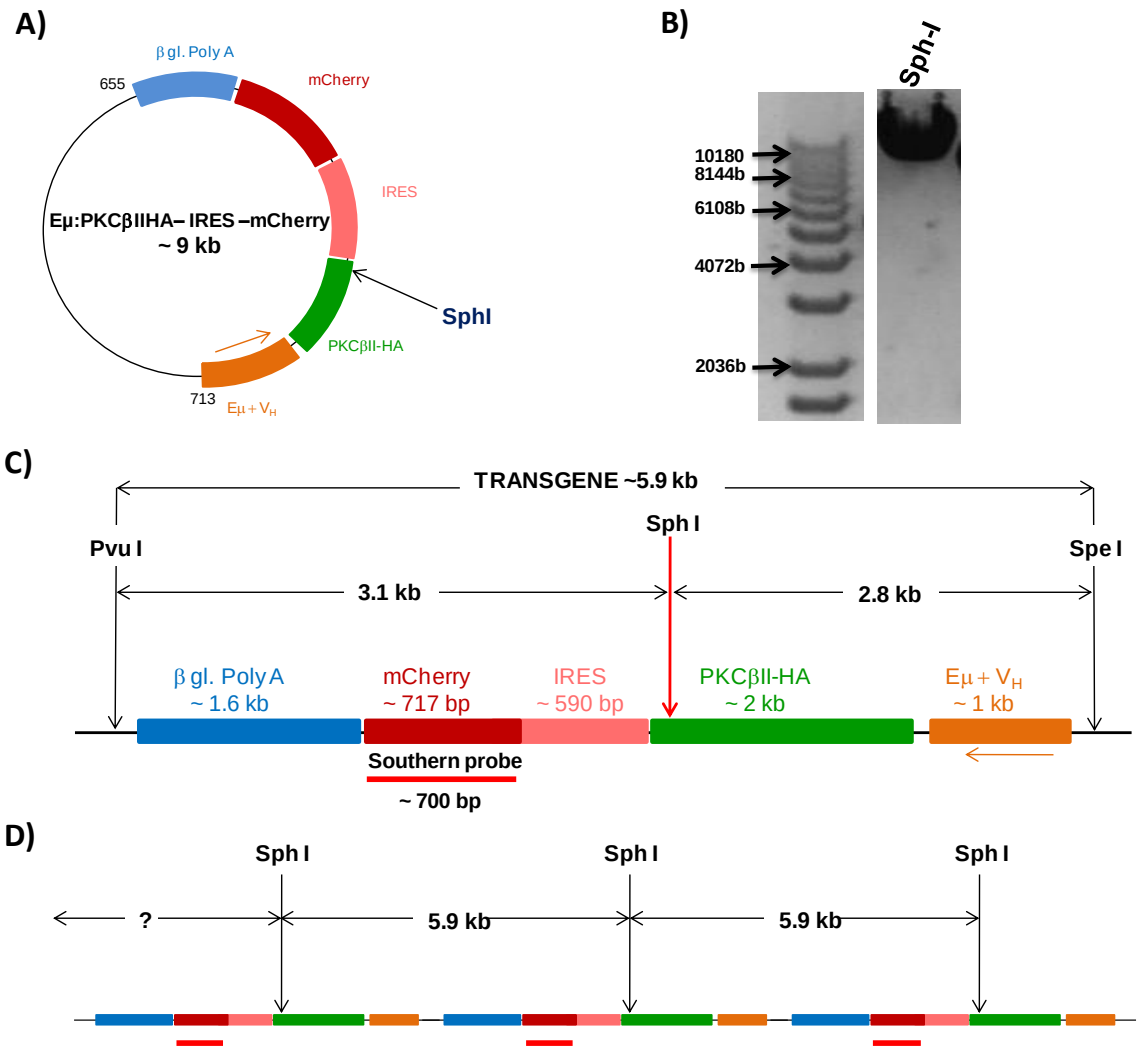

Figure 4-11. Developing a secondary Southern blotting strategy for detecting transgene (mCherry). **A)** Schematic map showing the single Sph-I site within the Eμ-PKCβIIHA-IRES-mCherry plasmid, **B)** **A**ctual digestion of pEμ-PKCβIIHA-IRES-mCherry with Sph-I. **C)** Schematic showing the Sph-I cutting site with the Eμ-PKCβIIHA-IRES-mCherry transgene., **D)** Schematic showing the Sph-I cutting sites and expected fragment size in the case where transgene is integrated within genomic DNA in concatemer fashion.

Screening of the fifth and sixth litters was conducted using this new strategy. Figure 4-12 A and B shows the PCR and Southern blot analysis for litter 5. PCR analysis identified animals 1-1, 1-2, 1-3, 1-4 and 2-2 as carrying the transgene within this litter. Southern blot analysis using Sph-I to digest the genomic DNA confirmed that animals 1-1, 1-2 and 2-3 carried the transgene in sufficient copy number (which was

greater than 1 but less than 10).Thus, the Southern blot result for 2-3 was not correlated with the PCR result. Animals 1-3 and 1-4 from this litter were excluded from further analysis because of failure within the Southern blot. Figure 4-12 C and D shows the PCR and Southern blot analysis for litter 6. Here animals 4-1, 4-2 and 4-3 showed presence of the transgene within the PCR analysis, and the presence of the transgene in animals 4-1 and 4-2 was confirmed in the Southern blot. With respect to this latter analysis I was able to use EcoRI to digest the genomic DNA.

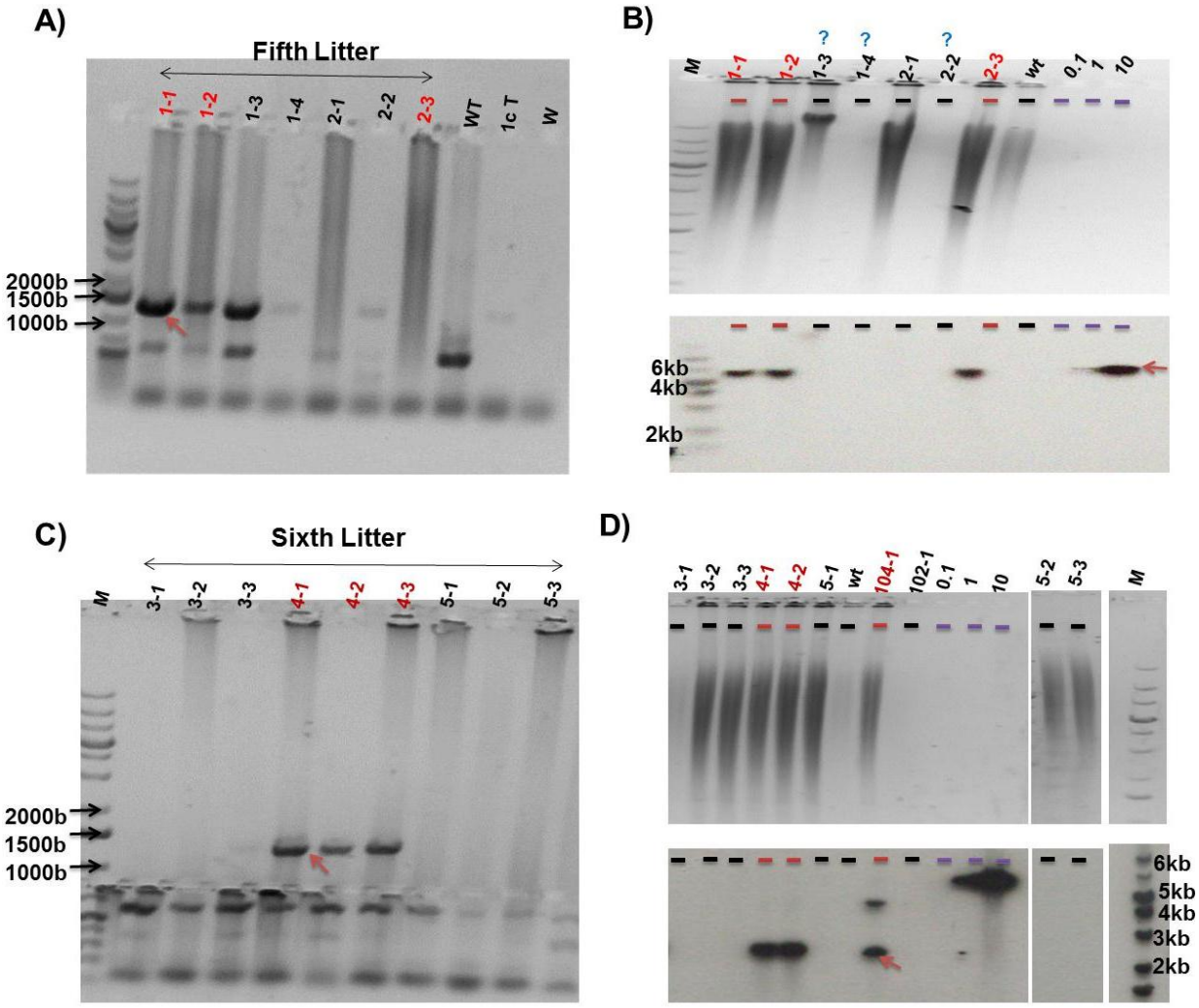

Figure 4-12. Detection of transgene in fifth and sixth litters born from founder mouse 45-2. The mouse pups born in the fifth and sixth litters of founder mouse 45-2 were screened for the presence of the transgene using PCR and Southern blotting. For performing the Southern blotting on DNA isolated from animals of the fifth litter, genomic DNA was fragmented by Sph-I, whereas EcoRI was used for digestion of genomic DNA isolated from animals of the sixth litter. **A)** Agrose gel separation for PCR screening the genomic DNA isolated from fifth litter for detecting the transgene by PCR. **B)** The genomic DNA isolated from the mouse pups born in the fifth litter was fragmented with Sph-I, and then probed for the presence of mCherry using Southern blotting. **C)** Agarose gel separation for PCR screening the genomic DNA isolated from the mouse pups born in the from sixth litter for detecting the transgene using PCR. **D)** The genomic DNA isolated from the mouse pups born in the of fifth litter was fragmented with EcoRI, and then probed for the presence of mCherry using Southern blotting.

4.6.4 Inter-crossing PKCβII heterozygous transgenic animals to generate homozygous animals

The results from my experiments described above show that I have generated a PKCβII transgenic founder mouse, and that the transgene is transferred to F1 progeny. The next step was to generate animals which were homozygous for the *Eμ*-PKCβIIwtHA-IRES-mCherry transgene. Figure 4-13 shows the mating strategy I employed: heterozygous animals were paired (het x het) and, based on Mandelian rules, one quarter of the animals born from such inter-crossings are predicted to be homozygous for the PKCβII transgene. Half of the progeny would be heterozygous, and the final quarter of these animals would have a wildtype genotype. The generation of wildtype animlas was important because they would be used as littermate controls during chracterization of the trangenic animals. For the inter-crossing I set up four pairs of PKCβII transgenic animals which were: **98-1(♂)x 99-4(♀)**, **98-3(♂)x 101-3(♀)**, **102-3(♂)x 103-3(♀)** and **102-1(♂)x 103-1(♀).**

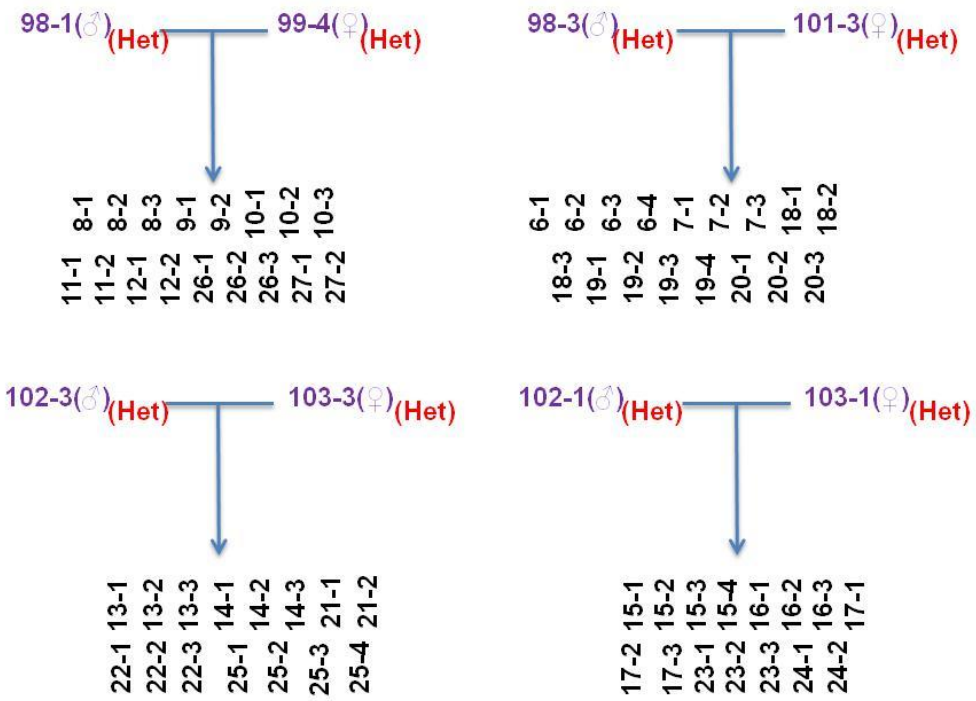

Figure 4-13. Inter-crossing heterozygous Eμ-PKCβII transgenic mice to generate homozygous Eμ-PKCβII transgenic mice. This figure illustrates a schematic of expected results based on Mendalian rules.

The result of inter-crossing resulted in the birth of 64 pups. Initially, I screened these animals by PCR (analysing for IRES-mCherry) in order to detect the presence of the PKCβII transgene. Figure 4-14 shows the results of this screening on 60 of these pups. To ensure experimental validity I used wt animals (to ensure specificity) and ran these samples at various places within my analysis. I also ran a water sample (designated w) to ensure sensitivity, and two amounts of the transgene corresponding to 1 copy [**T (1c)**] and 10 copies **[T (10c)**]. The transgene was detected in the animals whose designation number is marked in red in the figure 4-14. In total there were 12 animals without the transgene likely bearing a wild type genotype, and 48 animals which contained the transgene. This means that approximately 1/5 of the animals reverted to the wild type genotype representing an acceptable ratio according to simple Mendelian genetics.

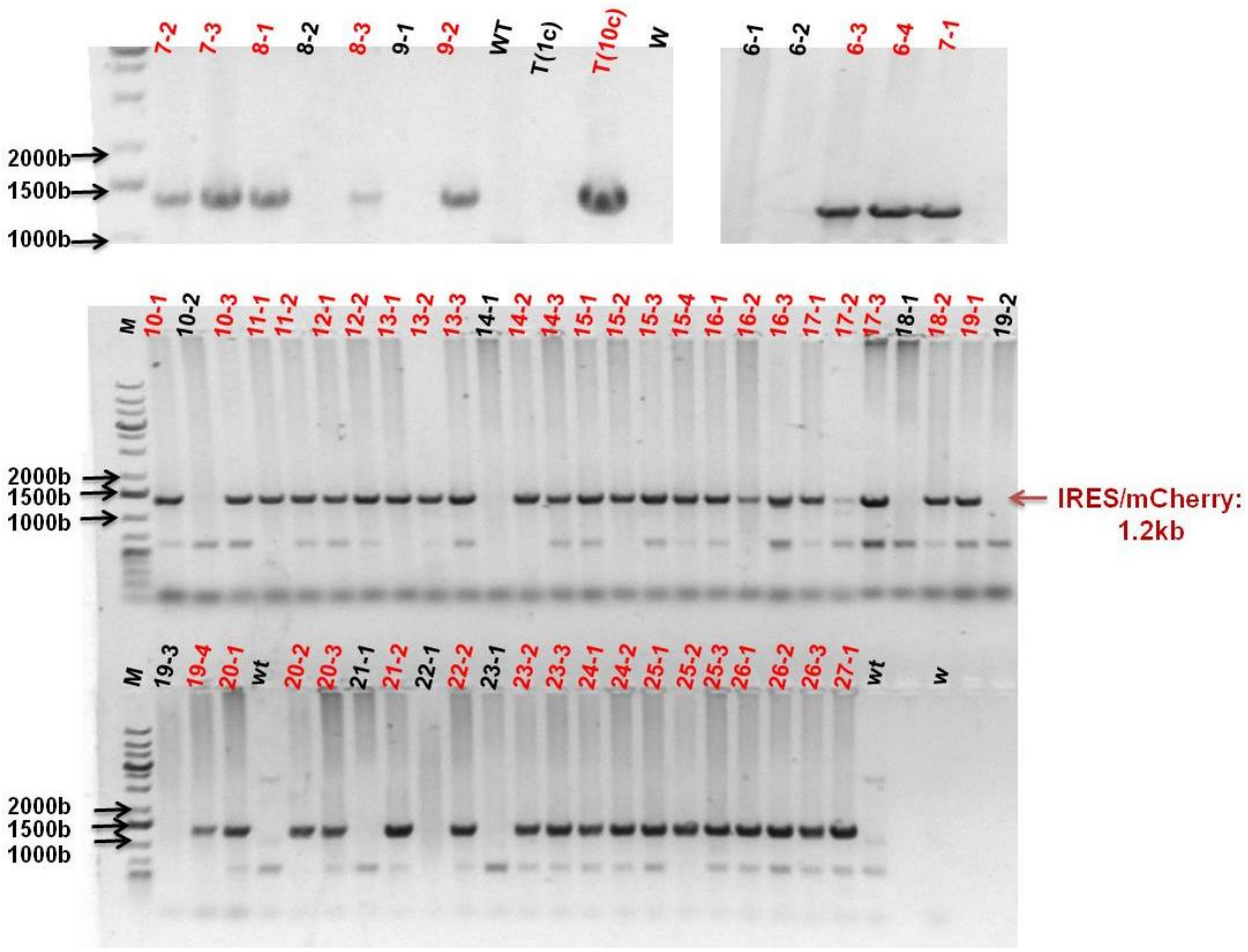

Figure 4-14. PCR-based detection of the transgene (IRES-mCherry) in mice born from inter-crossing heterozygous Eμ-PKCβII transgenic mice. 60 mouse pups were born from the inter-crossing of heterozygous Eμ-PKCβII transgenic mice. Genomic DNA isolated from these mouse pups was screened for the presence of the IRES-mCherry transgene using PCR. **T (1c)** and **T (10c)** refer to control amounts of pEμ-PKCβIIHA-IRES-mCherry which correspond, respectively to 1 copy and 10 copies. **wt** refers to a known wild type control, and **w** refers to a water control. The case numbers highlighted in **red** carry the transgene.

I also screened the animals using Southern blot because I wanted to confirm the PCR results, and also estimate the zygosity status of these animals (Figure 4-15). Zygosity status was determined based on the intensity of the 2.1kb band carrying the Eμ-PKCβIIHA (wt)-IRES-mCherry transgene, and animals were categorized as potential

homozygous, heterozygous and littermate control (wt animals). Therefore, potential homozygous animals contained approximately two fold more transgene than potential heterozygous animals, and wt animals contained no detectable transgene. Screening using Southern blot largely confirmed my results with PCR; nearly all the animals showing the presence of a PCR product in Figure 4-15 showed the presence of a 2.1kb band carrying the transgene. There was a discrepancy between Southern blot and PCR result in animal 19-3, in which the transgene was detected by Southern blot whereas no transgene was observed by PCR. It should be noted that the DNA isolated for animals 6-1, 6-4, 7-3, 10-2, 17-2, 18-2 and 25-1 were degraded, thus I was not able to confirm the PCR result by Southern blot, and these animals were excluded from the further analysis.

In my Southern blot, I detected seven animals that did not carry the transgene; the identity of these animals is marked in green in Figure 4-15. Where the transgene was present, a comparison of band intensities suggested that 22 of the mice were potential homozygous (marked in red) and 25 of the animals were potential heterozygous (marked in purple). As a positive control I used DNA isolated from mice numbered 4-2, 102-4, 101-3 and 104-1 (marked in brown), as these animals were definitely heterozygous because they are F1 progeny of the founder mouse. To confirm homozygous and heterozygous presence of the transgene I next used quantitative PCR.

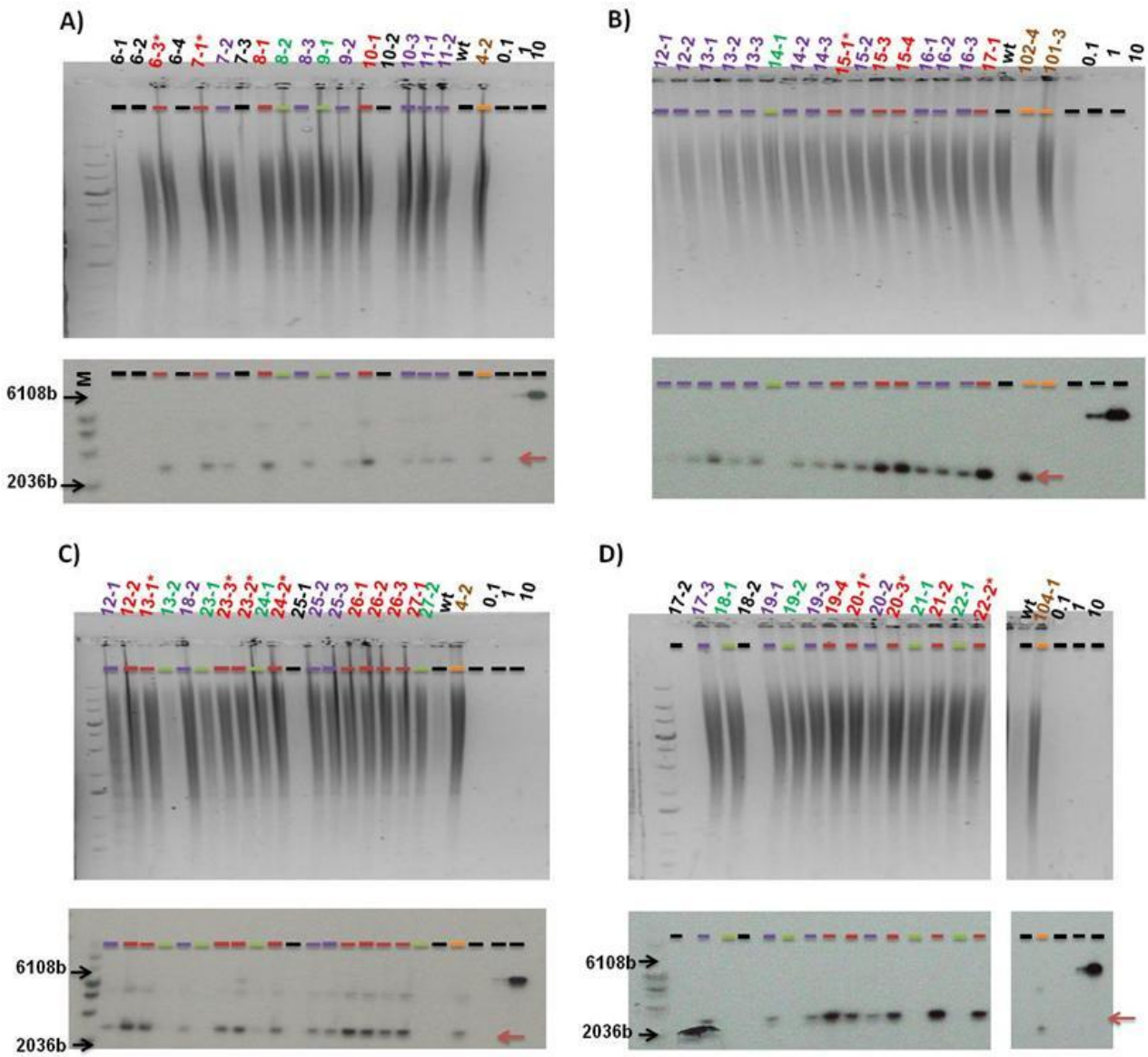

Figure 4-15. Detection of the transgene in mice born from the inter-crossing of heterozygous Eμ-PKCβII transgenic mice by Southern blotting. A, **B**, **C** and **D** represent agarose gel electrophoresis of EcoRI-digested genomic DNA isolated from the mice born from the inter-crossing of heterozygous Eμ-PKCβII transgenic mice (upper figure). Screening for the presence of transgene (a 2.1kb band containing mCherry) using Southern blot is represented in the lower figure of **A**, **B**, **C** and **D**. Mice that did not carry the transgene are marked in **green**; mice which are potentially homozygous Eμ-PKCβII tg mice are marked in **red**; potentially heterozygous Eμ-PKCβII tg mice are marked in **purple** and mice that were used as positive controls are marked in **brown**.

4.7 Quantification of the Eμ-PKCβIIHA (wt)-IRES-mCherry transgene by quantitative real time PCR

Quantitative real time PCR (qrtPCR) is a more reliable method for distinguishing between homozygous and heterozygous transgenic animals. This method is based on the detection of a fluorescent dye (SYBER green) that specifically binds to the double–stranded PCR product that is amplified by DNA polymerase during the PCR reaction. Binding and detection of this dye is proportional to the amount of dsDNA present, and can therefore be used for quantification (see section 2.1.6). This quantification is done by the PCR instrument which measures the Ct value, which is the number of cycles required for the detected fluorescence signal to cross a threshold and exceed background levels. To quantify the transgene I used the same primers I used for cloning mCherry in Chapter 3. These primers produced a PCR product that was sized approximately 500bp. The PCR amplification of the mCherry transgene was normalized to a reference gene, *gapdh*, a house keeping gene expected to have homozygous representation in the mouse genome. The amount of mCherry transgene can then be determined by calculating the ΔC_T value which is:

$$\Delta C_T = C_{T,\ mCherry}\ (mouse\ A) - C_{T,\ gapdh}\ (mouse\ A)$$

To distinguish between homozygous and heterozygous animals I calculated a $\Delta\Delta C_T$ value which compares the ΔC_T value from a known heterozygous animal (mouse B) with that of my unknown transgenic (mouse A). Because each cycle of the PCR reaction creates twice as much dsDNA as the previous cycle, the fold difference in transgene between two animals can be determined using the power function $2^{-\Delta\Delta C}{}_{T.}$ The equations I used are listed below using the example of a comparison between a heterozygous and homozygous animal.

$$\Delta\Delta C_{T=} \Delta C_{T\,(A)} - \Delta C_{T\,(B)} (C_{T,\,mCherry\,(A)} - C_{T,\,GAPDH\,(A)}) - (C_{T,\,mCherry\,(B)} - C_{T,\,GAPDH\,(B)})$$

or

$$\Delta\Delta C_{T=} (C_{T,\,mCherry\,(HOM)} - C_{T,\,GAPDH\,(HOM)}) - (C_{T,\,mCherry\,(HET)} - C_{T,\,GAPDH\,(HET)}) = -1$$

$$\textbf{Fold difference} = 2^{-\Delta\Delta C}{}_T = 2^1 = 2$$

Example: 4-2: *known heterozygous* ***15-4:*** *Unknown*

$$\Delta\Delta C_{T=} \Delta C_T\,(15\text{-}4) - \Delta CT\,(4\text{-}2) = (23.78\text{-}18.44)\text{-}(25.64\text{-}18.85) = 5.34 - 6.79 = -1.45$$

$$\textbf{Fold difference} = 2^{-\Delta\Delta C}{}_T = 2^{(-)\text{-}1.45} = 2.7$$

Thus, using the method I have described the $\Delta\Delta C_T$ value of homozygous transgenic animals should approximate -1, whereas heterozygous animals should have a value close to zero. In the example I present I compare mouse 4-2 (which is a known heterozygous animal because it is an F1 progeny) with mouse 15-4 (F2 progeny that contains the transgene and is suggested to be homozygous from the Southern blot result). The calculated $\Delta\Delta C_T$ value equals -1.45, which when substituted into the $2^{-\Delta\Delta C}{}_T$ equation yields a value of 2.7. This means that mouse 15-4 contains 2.7 fold more transgene than mouse 4-2, and that mouse 15-4 is likely to be homozygous. Figure 4-16 shows the result of a typical PCR run using this method, indicating both the specificity and sensitivity of the primers used, as well as the dissociation curves to ensure that primer hybrids are well distinguished from the mCherry and *gapdh* amplicons.

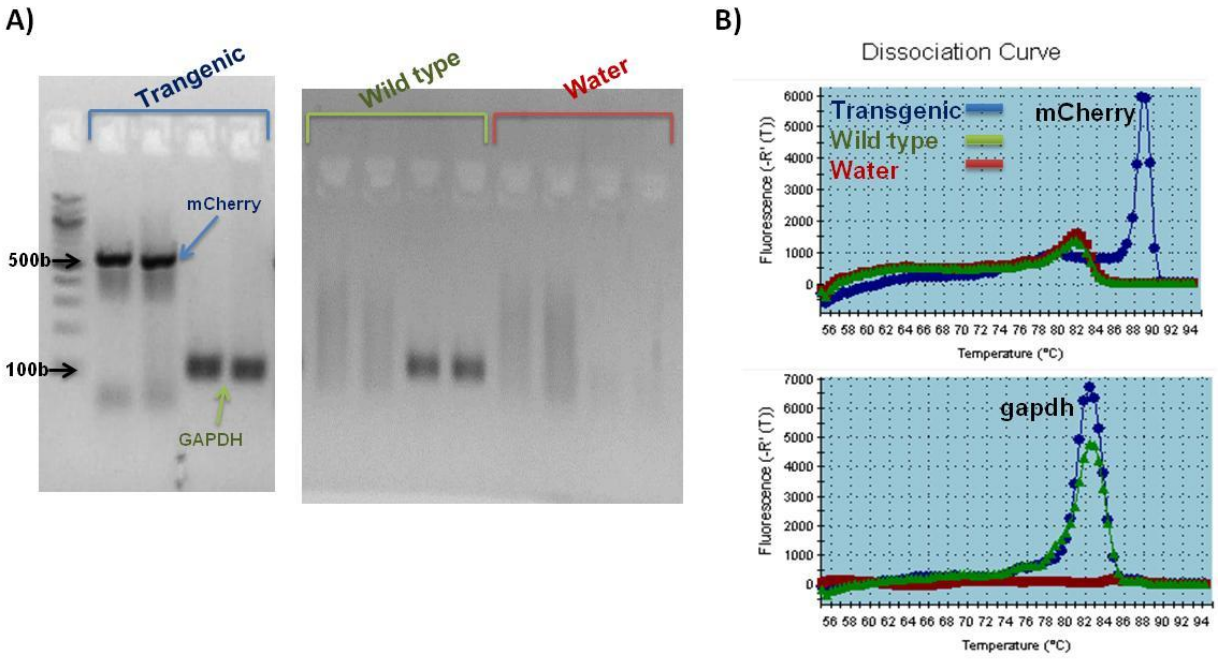

Figure 4-16. Amplification of mCherry and *gapdh* by using qrtPCR. **A)** Agarose gel separation for a typical qrtPCR performed for amplification of mCherry and gapdh in Eμ-PKCβII tg and wild type mice**. B)** Dissociation curve for mCherry and *gapdh* amplifications.

Figure 4-17A summarizes the quantification of transgene in the F2 progeny that were generated. The results are all relative to a known heterozygous control animal, mouse 4-2. Using this method 18 of the animals were determined to be homozygous, and are indicated as purple bars in the presented histogram. Moreover, 25 of the mice were determined to be heterozygous for the transgene, and are indicated as blue bars in the presented histogram. Figure 4-17B shows the distribution of $2^{-\Delta\Delta C}{}_T$ values obtained for homozygous and heterozygous animals. This illustration is important because it shows that transgene content was approximately 2-fold greater in homozygous compared with heterozygous animals. Table 4-2 compares the Southern blot and qrtPCR methods for distinguishing between homozygous and heterozygous animals. Both methods largely confirmed each other with the exception of animals numbered 6-3, 7-1, 14-2, 14-3, 15-1, 16-2, 17-2, 19-3, 20-1, 20-2, 20-3 and 26-3. These animals were excluded from further study.

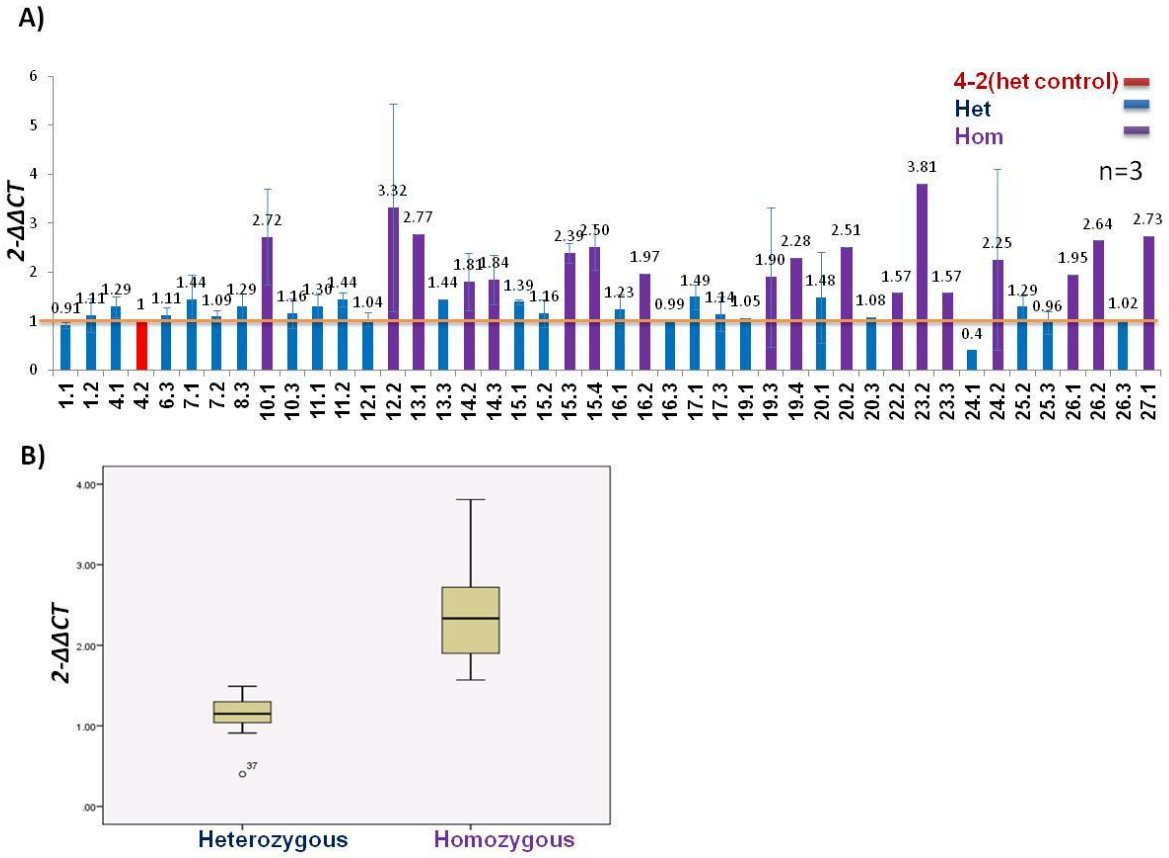

Figure 4-17. The quantification of transgene (mCherry) in the F2 progeny of Eμ-PKCβII tg mice using qrtPCR. A) The graphical representation for transgene quantification in the F2 progeny of Eμ-PKCβII transgenic mice by qrtPCR. This quantification was relative to a known heterozygous control animal, mouse 4-2 (highlighted in red). The potential homozygous Eμ-PKCβII tg mice are highlighted in purple, and the potential heterozygous Eμ-PKCβII tg mice are highlighted in blue. **B)** Box plot representation of the distribution of $2^{-\Delta\Delta C}{}_{T}$ values obtained for homozygous and heterozygous mice.

As a final assurance that the homozygous animals we generated were indeed homozygous we backcrossed these animals with wild type mice. I selected seven animals where Southern blot and qrtPCR results were confirmatory. These animals were 13-1, 15-3, 15-4, 17-1, 19-4, 21-2 and 22-2. Figure 4-18 illustrates PCR analysis of IRES-mCherry presence in the progeny of the backcross of these animals with wt mice. The transgene was detected in all the pups that were born from mice numbered 13-1, 15-3, 17-1 and 21-2 demonstrating that these animals are homozygous for the

transgene. However, mice numbered 15-4, 19-4 and 22-2 delivered progeny that did not consistently carry the transgene. This result could be due to technical reasons or because the animals are heterozygous, in any event they were excluded from further study.

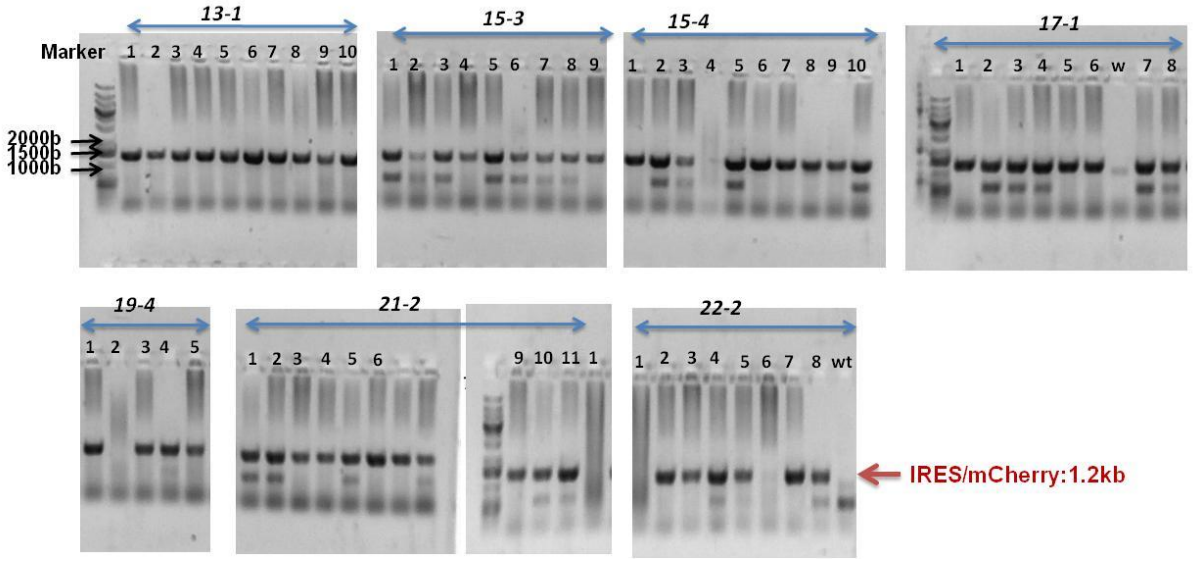

Figure 4-18. Detection of the transgene (IRES-mCherry) in the mouse pups born from the backcrossing the potential homozygous Eμ-PKCβII tg mice with wild type mice using PCR. To confirm homozygosity of potential homozygous Eμ-PKCβII tg mice, these mice were back-crossed with wild type mice, and then the genomic DNA extracted from the tail of the mouse pups born from this back-crossing were screened for the presence of the transgene (IRES-mCherry) by using PCR.

Table 4-2 presents a summary of all the screening methods used for generating the transgene animals in this study. Based on this table I could safely conclude that mice numbered 13-1(male) and 17-1(female) are homozygous for the Eμ-PKCβIIHA (wt)-IRES-mCherry transgene, and that the progeny generated from crossing these animals would also be homozygous. Crossing these animals generated 47 mice, 20 of these animal were kept and aged for phenotypic analysis (called hom-1 to hom20), while 25 mice were sent for cryopreservation.

At this stage the generation of the Eμ-PKCβIIHA (wt)-IRES-mCherry transgenic mouse is now complete. Figure 4-19 shows a schematic summary of the process

involved in generating this mouse. In the next chapter, I will describe the phenotype that resulted from expression of this transgene.

Animal	southern Blot	PCR	Q-PCR	Back-crossing
45-2	+/-	+		
98-1	-	+		
98-3	-	+		
99-4	-	+		
101-3	-	+		
102-1	+/-	+		
102-3	+/-	+		
102-4	+/-	+		
103-1	+/-	+		
103-3	+/-	+		
104-1	+/-	+		
1.1	(+/-)	+	(+/-)	
1.2	(+/-)	+	(+/-)	
1.3		+		
2.1	-	-		
2.2	-	+		
2.3	+	+		
1.4		-		
3-1		-		
3-2	-	-		
3-3	-	-		
4-1	+/-	+	(+/-)	
4-2	+/-	+	(+/-)	

Animal	southern Blot	PCR	Q-PCR	Back-crossing
4-3				
5-1	-	-		
5-2	-	-		
5-3	-	-		
6-1	-	-		
6-2	-	-		
6-3	+/+?	+	(+/-)	
6-4		+		
7-1	+/+?	+	(+/-)	
7-2	+/-	+	(+/-)	
7-3		+		
10-1	+/+	+	(+/+)	
10-2		-		
10-3	+/-	+	(+/-)	
11-1	+/-	+	(+/-)	
11-2	+/-	+	(+/-)?	
12-1	+/-	+	(+/-)	
12-2	+/+	+	(+/+)	
13-1	+/+?	+	(+/+)	(+/+)
13-2	+/-	+		
13-3	+/-	+	(+/-)	
14-1	-	-		
14-2	+/-	+	(+/+)	

Animal	southern Blot	PCR	Q-PCR	Back-crossing
14-3	+/-	+	(+/+)	
15-1	+/+?	+	(+/-)	(+/-)
15-2	+/-	+	(+/-)	(+/-)
15-3	+/+	+	(+/+)	(+/+)
15-4	+/+	+	(+/+)	(+/+)?
16-1	+/-	+	(+/-)	
16-2	+/-	+	(+/+)	
16-3	+/-	+	(+/-)	
17-1	+/+	+	(+/-)	(+/+)
17-2	-	+		
17-3	+/-	+	(+/-)	
18-1	-	-		
18-2	+/-	+		
19-1	+/-	+	(+/-)	
19-2	-	-		
19-3	+/-	-	(+/+)	
19-4	+/+	+	(+/+)	(+/+)?
20-1	+/+?	+	(+/-)	(+/-)
20-2	+/-	+	(+/+)	
20-3	+/+?	+	(+/-)	
21-1	-	-		

Animal	southern Blot	PCR	Q-PCR	Back-crossing
22-2	+/+?	+	(+/+)	(-/+)
22-3				
23-1	-	-		
23-2	+/+?	+	(+/+)?	
23-3	+/+?	+	(+/+)	
24-1	+/-	+	(+/-)	
24-2	+/+?	+	(+/+)	
25-1		+		
25-2	+/-	+	(+/-)	
25-3	+/-	+	(+/-)	
26-1	+/+	+	(+/+)	
26-2	+/+	+	(+/+)	
26-3	+/+	+	(+/-)	
27-1	+/+	+	(+/+)	
27-2	-	-		

Homozygous: Red
Heterozygous: Purple
Wild: Blue
Conflicted result: Grey

Table 4-2. Summary of all the screening methods used for screening/generating Eμ-PKCβII transgene mice.

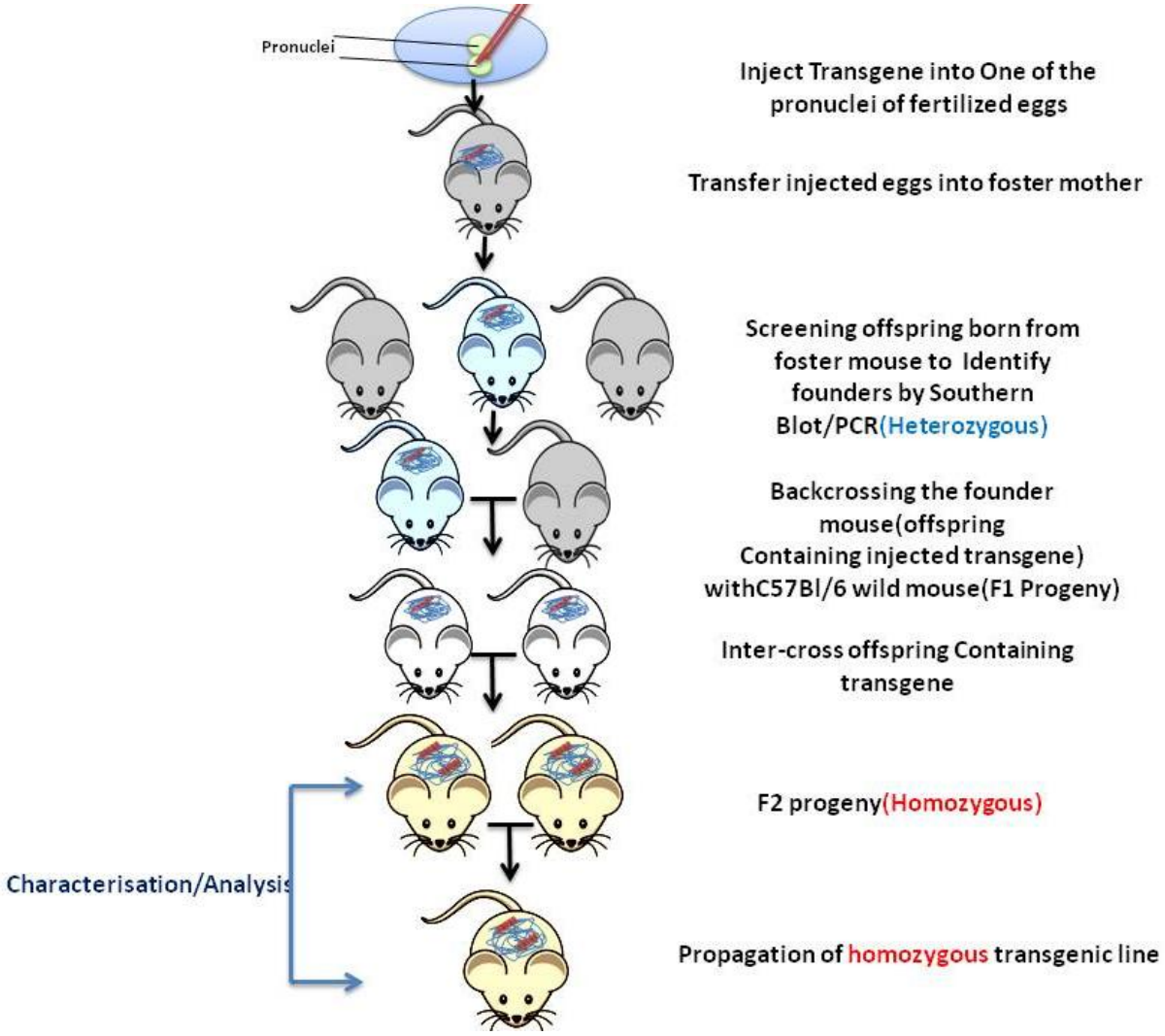

Figure 4-19. The Schematic of the generation of Eμ-PKCβII transgenic line.

5 Chapter V: Characterization of Eμ-PKCβII transgenic mice

5.1 Preface

The ultimate goal of this project was to generate homozygous Eμ-PKCβIIHA (wt)-IRES-mCherry (abbreviated from now on as Eμ-PKCβII) transgenic mice. Thus, I constructed the transgene Eμ-PKCβIIHA(wt)-IRES-mCherry by DNA cloning, tested this construct to ensure that it was functional (see Section 3.4.2), and then generated a homozygous line expressing this transgene by inter-crossing heterozygous F-1 progeny born from the founder mouse mice described in chapter 4. Thus, I used homozygous animals from the F-2 progeny to expand the numbers of Eμ-PKCβII mice I would need for phenotypic characterization. I also selected wild type animals from the F-2 progeny to be used as littermate controls. I aged the Eμ-PKCβII transgenic mice for 6 and 14 months. For the wild type littermate controls there were a limited number of mice generated, these mice were aged for 14 months. For the mice aged only 6 months, non-littermate control animals were used. Therefore, in this section of my thesis, I have made comparisons between the wild type littermate and non-littermate mice in order to establish similarity. All animals were sacrificed at their designated ages, and then characterized.

Characterization of the mice I generated involved first establishing that the transgene was expressed by the transgenic mice, that this expression was B cell-specific, and ascertaining that the homozygous Eμ-PKCβII transgenic mice were healthy and aged normally. The transgenic animals were assessed to see if they developed a CLL-like phenotype in B cell rich organs (spleen, peritoneum, peripheral blood and bone marrow), and B cell subsets were analysed in these organs to note any changes.

The structure of this chapter is arranged in three sections:

1. Detection and quantification of the transgene
2. Pathological/Morphological study of the spleen of the transgenic mice
3. Full characterization of B cell subsets by flow cytometry

5.2 Detection of transgenic PKCβIIHA by Western blot

To establish whether the Eμ-PKCβIIHA (wt)-IRES-mCherry transgene was expressed in the homozygous animals I first used Western blot to ascertain the presence of transgenic PKCβII tagged with HA and mCherry. For this purpose, the spleens of transgenic and wt mice were isolated and protein lysates were prepared. A protein determination was carried out and equal amounts of protein were separated by SDS-PAGE. Finally, the separated proteins were transferred to PVDF membranes and probed for PKCβIIHA and mCherry using specific antibodies.

Figure 5-1 shows a comparison of transgene expression in PKCβII transgenic and wt mice. I used two different mouse monoclonal HA antibodies, clones numbered 6B12 and 12CAS, to detect the HA tag attached to PKCβII in the transgene (Figure 5-1A and B). Thus, transgenically expressed PKCβIIHA was detected as an approximate 80 kDa band only in transgenic mice. This 80kDa band was recognised by both antibodies, but with the 12CAS antibody there were additional faster running bands which were non-specific because they also appeared in the lysate derived from the wt mouse. This 80kDa band was also detected by a PKCβII specific antibody (Figure 5-1C), thus in this representation, PKCβIIHA ran as a slower migrating band to endogenous PKCβII. Interestingly, all three antibodies, the 2 HA-specific and 1 PKCβII-specific antibody, detected an additional band running slightly faster than the 175kDa molecular weight marker in transgenic mice. This suggests that this high molecular weight band is also transgenic PKCβIIHA that is possibly migrating as a dimer because it is approximately double the expected size of PKCβIIHA.

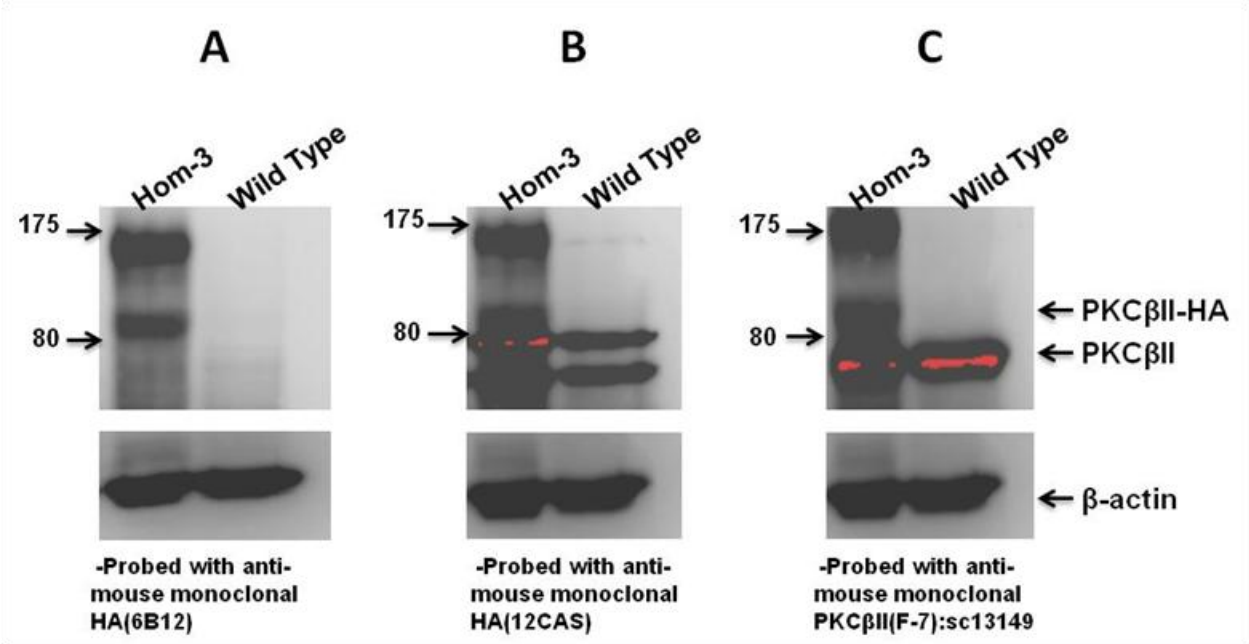

Figure 5-1. Detection of transgenic PKCβIIHA in the spleen of Eμ-PKCβII tg mice. The protein lysates of the spleen of Eμ-PKCβII tg and wild type mice were prepared and probed for the presence of the transgenic PKCβIIHA using Western blotting. **A)** Detection of transgenic PKCβIIHA using anti-HA mAb 6B12. **B)** Detection of transgenic PKCβIIHA using anti-HA mAb 12CAS. **(C)** Detection of endogenous and transgenic PKCβII using the anti-PKCβII mAb F-7 (Hom-3: homozygous number 3).

Figure 5-1 suggested that antibody 6B12 would be optimal for the detection of transgenic PKCβII-HA. Therefore, I used this antibody to investigate expression of PKCβII-HA in lysate of splenic tissue isolated from the founder mouse (#45-2) and some of its progeny where we were sure the transgene was present as detected by Southern blot and PCR (mice numbered 1-1, 1-2, 3-2 and 7-1; See Section 4.6.3)(Figure 5-2). The lanes marked Ct-3 and Ct-4 were samples derived from splenic tissue from two aged matched wild type mice. As positive control I used whole cell lysates of Mec1 cells in which PKCβIIHA was stably expressed. In Figure 5-2, PKCβII-HA was identified as a band running slightly faster than the 100kD molecular weight marker. This faint band was present in the founder mouse as well as progeny. However, there was a strong band running slightly slower than the 100kD molecular weight marker that was present

in all samples with the exception of Mec1 cells. This strong band was likely to be non-specific, and this made it difficult to make strong conclusions regarding the expression of PKCβII-HA using antibody 6B12.

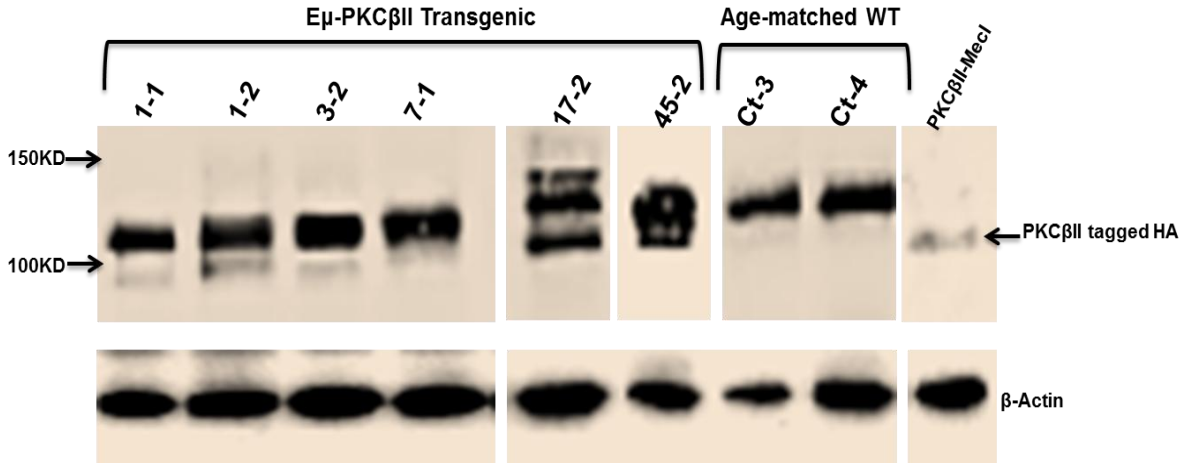

Figure 5-2. Detection of HA protein in splenic tissue of the Eμ-PKCβII tg founder mouse and its F-1 progeny. HA antibody (6B12) was used for detecting transgenic PKCβIIHA in lysates of splenic tissue derived from the founder mouse 45-2 and its progeny: 1-1, 1-2, 3-2 and 7-1. The spleen lysates of wild type mice ct-3 and ct-4 were used as negative controls. The cell lysate of stable PKCβIIHA Mec-I cell line was used as a positive control.

Ultimately, it is very important to be able to analyse tissue lysates for unambiguous expression of the transgene. The mouse monoclonal antibodies suggested that the PKCβII-HA transgene was present, but because of the appearance of non-specific bands that could potentially interfere with interpretation I needed an antibody which had greater specificity. To do this I employed a monoclonal Rabbit anti-HA antibody (C29F4). Figure 5-3 shows a Western blot analysis of tissue lysates derived from spleens isolated from transgenic heterozygous and homozygous mice, and from wild-type littermate controls. As positive control, I used the lysate of A20 cells that had been transiently transfected with pEμ-PKCβIIHA (wt)-IRES-mCherry. A single band migrating with an apparent molecular weight corresponding to PKCβII (approximately 80kD) was detected in the transgenic mice and positive control, but was not present in

the wild-type littermate control animals. Importantly, the higher molecular weight band I suggested is a dimer of PKCβIIHA (Figure 5-1) is not present, suggesting that this higher molecular weight band reflects non-specific reactivity with the second layer (anti-mouse) antibodies I used to process the Western blot. Taken together, the single band reactivity of the rabbit anti-HA antibody indicated that this antibody was specific for the detection of HA-tagged epitopes in my system and could therefore be used in subsequent analyses of tissue-specific expression of the PKCβII-HA transgene.

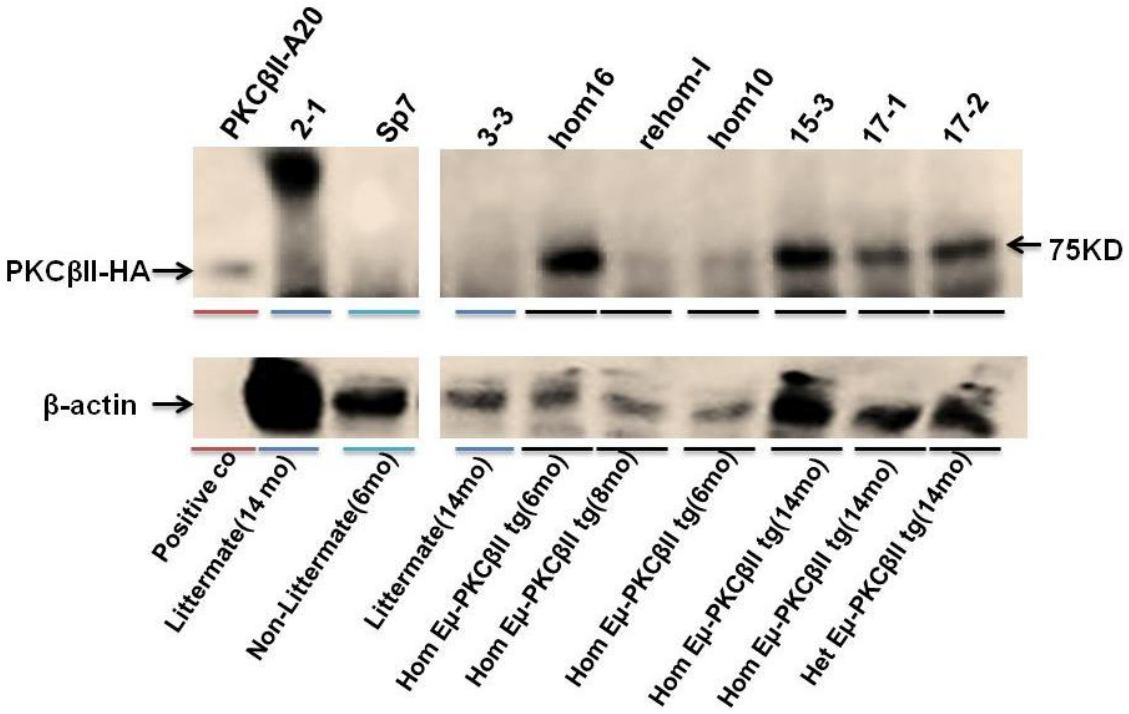

Figure 5-3. **Detection of HA in F-2 progeny of Eμ-PKCβII tg mice.** Western blot was performed on cell lysates of splenic tissue isolated from heterozygous (17-2) and homozygous (15-3, 17-1, hom-10, hom-16 and re-hom-I) Eμ-PKCβII tg mice as well as wild type mice (non-littermate (sp-7) and littermate (2-1 and 3-3)) in order to detect HA protein. The cell lysate of A20 cells transfected with pEμ-PKCβIIHA-IRES-mCherry was used as a positive control.

Because expression of PKCβII-HA is under the control of the Eμ promoter, expression of this protein should be restricted to B cell-rich tissues. To show tissue specificity of the transgene, I probed protein lysates derived from spleen and liver, an organ in which B cells are not normally found. Figure 5-4 shows the results of this

comparison using homozygous transgenic animals 17-1 (14 month aged mouse) and hom-10 (6 month aged mouse). I found that expression of transgenic PKCβII-HA was only present in splenic tissue and not in liver. This suggests that expression of the transgene is likely to be B cell specific.

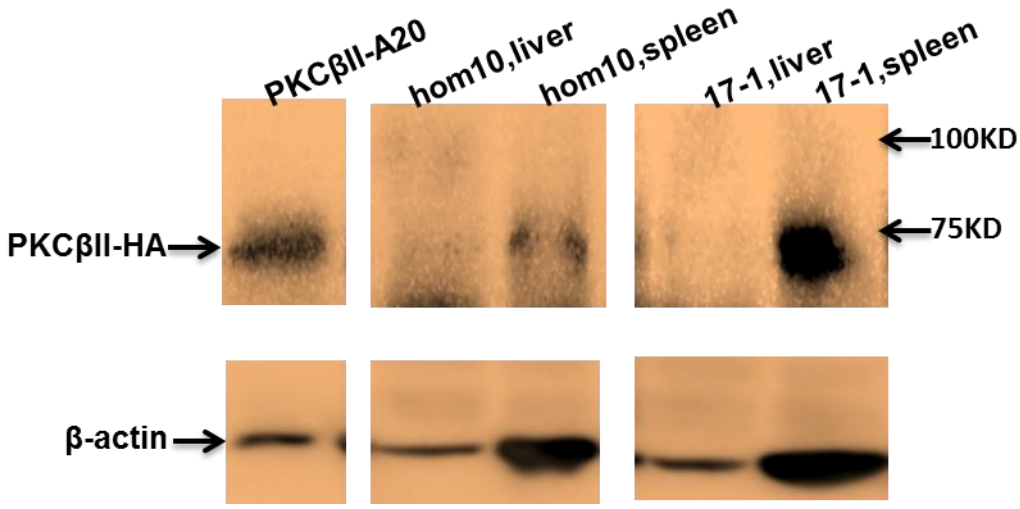

Figure 5-4. Comparison of transgenic PKCβIIHA expression in liver and splenic tissue of the Eμ-PKCβII transgenic mice. Cell lysates from the spleen and liver of homozygous Eμ-PKCβIII tg mice 17-1 (14 month aged mouse) and hom-10 (6 month aged mouse) were probed for the presence of HA using Western blotting.

5.2.1 Quantification of the PKCβII

The rationale for generation of the Eμ-PKCβII transgenic mice was to over-express PKCβII in B cells. Thus, I performed Western blot analysis on whole lysates derived from the splenic tissue of transgenic and wild mice to compare PKCβII expression levels between these animals. For this purpose I used a Rabbit polyclonal PKCβII antibody (C-18: sc-210), and Figure 5-5A and B shows that PKCβII expression in the founder mouse (#45-2) and its progeny (#1-2, 3-2 and 7-1) was significantly ($p=0.03$) higher compared with that in three non-littermate wild type control mice (#ct-1, ct-2 and ct-3). A comparison of PKCβII levels in homozygous Eμ-PKCβII transgenic mice (#15-3, 21-2, hom-16, and re-hom-1 (F-2 progeny)) with that in three wild type control mice (#2-1 and 3-3 are wild type littermate controls and #sp-6 is a wild type non-littermate control) also showed significantly higher ($p=0.03$) expression of PKCβII (Figure 5-5C and D). These results suggest that PKCβII is overexpressed in the transgenic mice. This overexpression is also observed in histo-chemical staining of splenic tissue using the same antibody. This result will be introduced and discussed later in this Chapter.

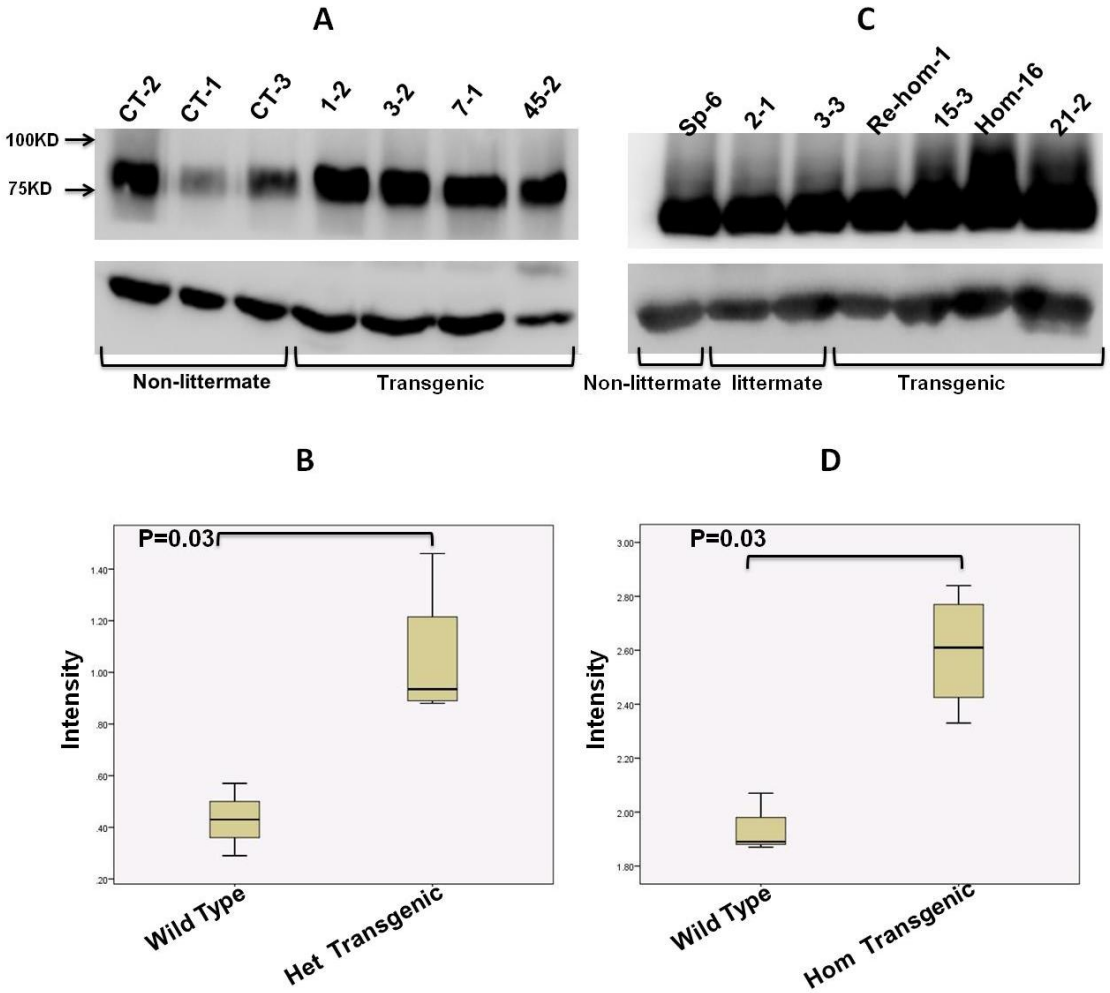

Figure 5-5. Quantification of total expression of PKCβII protein in splenic lysate isolated from Eμ-PKCβII tg and wild type mice. Protein lysates isolated from splenic tissue of Eμ-PKCβII tg and wild type mice were probed with Rabbit polyclonal PKCβII antibody and β-actin antibody (lower blot) in order to quantify total PKCβII protein. **A)** Western blot analysis comparing total PKCβII (upper blot) and β-actin (lower blot) expression in the founder mouse (#45-2) and its progeny (#1-2, 3-2 and 7-1) with non-littermate wild type mice (# ct-1, ct-2 and ct-3). **B)** Box plot representation of part A using the PKCβII/β-actin ratio determined by densitometry. **C)** Western blot comparison of PKCβII levels in homozygous Eμ-PKCβII tg mice (#15-3, 21-2, hom-16, and re-hom-1 (F-2 progeny)) with 3 wild type control mice (#2-1 and 3-3 are wild type littermate controls and #sp-6 is a wild type non-littermate control. **D)** Box plot representation of part C using the PKCβII/β-actin ratio determined by densitometry. Statistical analysis for parts B and D were performed using a Mann-Whitney U-test.

5.2.2 Detection of mCherry

The Eμ-PKCβIIHA (wt)-IRES-mCherry transgene also contains a gene for mCherry that is separated from the PKCβII coding sequence by IRES (intra-ribosomal entry site). This means that a goal for the generation of the Eμ-PKCβII transgenic mice was also the expression of mCherry. MCherry is a monomeric fluorescent protein whose fluorescence emission at 610nm can be stimulated by light at 587nm. These excitation and emission qualities can be measured in a flow cytometer that is equipped with at a 560nm yellow-green laser and appropriate filters for measuring emission at 610nm.

I prepared a single cell suspension of spleen tissue from a homozygous Eμ-PKCβII transgenic mouse and a wild type littermate control. I analysed these cells using a Becton Dickinson LSR-Fortessa analytical flow cytometer equipped with a yellow-green laser and detectors capable of measuring emission at 610nm. As positive control for this experiment I used A20 cells that had been transfected with pEμ-PKCβIIHA (wt)-IRES-mCherry. Figure 5-6A shows that transfected A20 cells expressed mCherry as is demonstrated by the shift in detected fluorescence. However, cells isolated from a PKCβII-transgenic mouse showed similar fluorescence to those isolated from a wild type littermate control mouse (Figure 5-6B). There are two possible explanations for this: either mCherry is not expressed or the expression levels are too low to be detected using FACS analysis. To address these questions I used Western blot to probe lysates of splenic tissue and bone marrow isolated from PKCβII-transgenic and wild type mice with a mCherry monoclonal mouse antibody (Clontech). Figure 5-6C shows that a 27kD band corresponding to mCherry could be detected in bone marrow of a homozygous PKCβII transgenic mouse. This band was at best very weakly present in lysates from splenic tissue from heterozygous PKCβII transgenic mice, and was absent in the wild type mouse. Analysis of splenic tissue from homozygous PKCβII transgenic mice showed that mCherry was weakly expressed (Figure 5-6D). The band corresponding to mCherry was only present in lysates derived from splenic tissue but not in lysates derived from either the liver or kidney. From these experiments I concluded that mCherry is weakly expressed, but that the levels are insufficient for detection using

fluorescence technologies. This is in keeping with recognised weaknesses of dual gene expression within the IRES system, efficient expression of the gene following the IRES sequence is not always guaranteed(Kozak 2005).

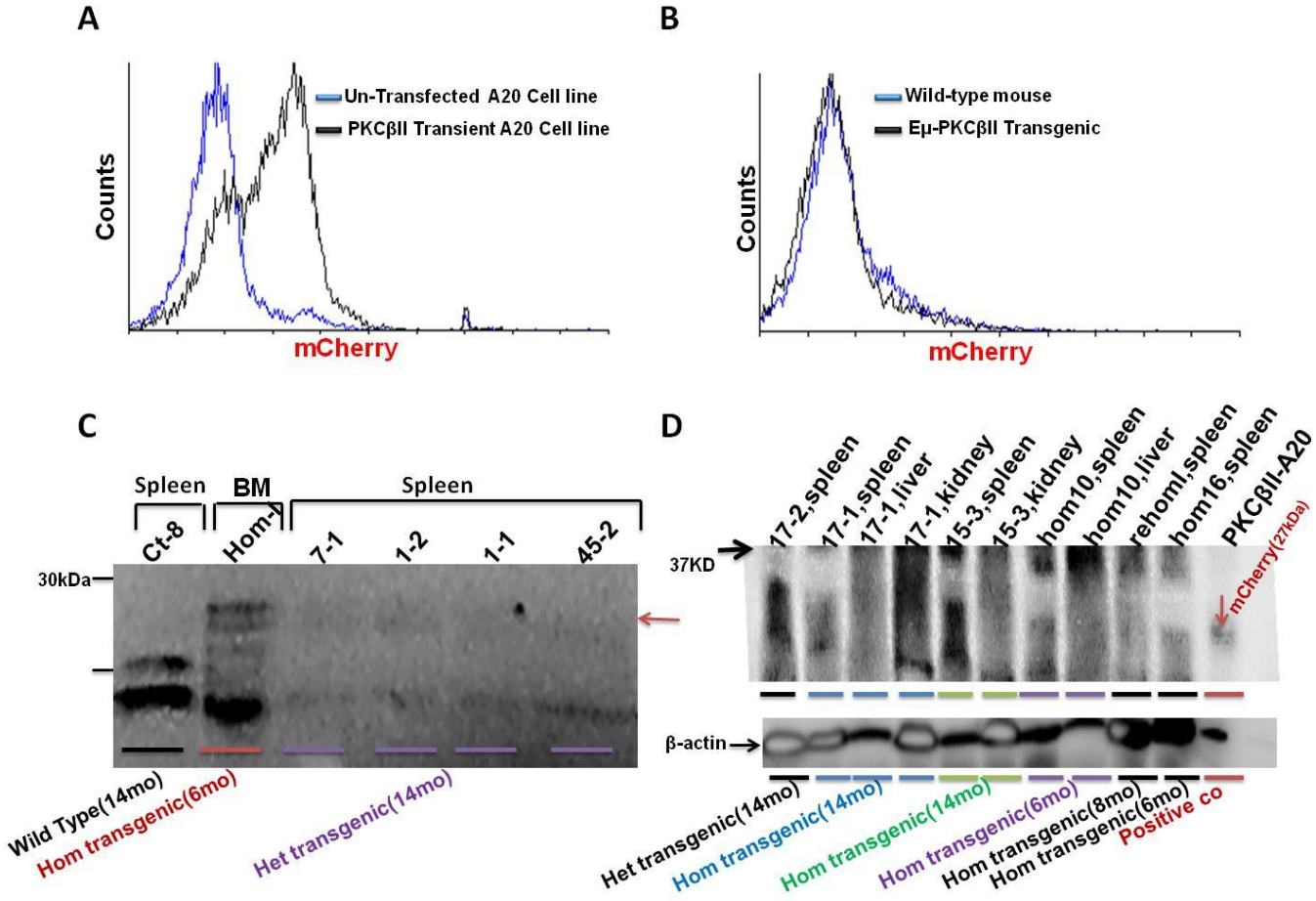

Figure 5-6. Detection of mCherry in Eμ-PKCβII tg mice. A) Flow cytometric analysis of untransfected A20 cells (blue line), and A20 cells transfected with Eμ- PKCβIIHA-IRES-mCherry (black line). **B)** Flow cytometric analysis of single cell suspensions prepared from spleen isolated from a homozygous Eμ-PKCβII tg (black line) and wild type (blue line) mice. **C)** Splenic and bone marrow lysate of Eμ-PKCβII tg (1-1, 1-2 and 7-1) and splenic lystae of wild type mice (ct-8) were probed for the presence of mCherry using Western blotting. **D)** The protein lysate of spleen, kidney and liver of Eμ-PKCβII tg mice (15-3, 17-1, hom-10, hom-16 and re-hom-I) were probed for the presence of mCherry using Western blotting. The cell lysate of A20 cells transfected with pEμ-PKCβIIHA-IRES-mCherry was used as a positive control.

5.3 Detection of transgenic PKCβIIHA by immunohistochemistry (IHC)

Using Western blot analysis I have established that PKCβIIHA is expressed in the spleen of transgenic mice. However, this analysis is disadvantaged because it only detects the presence of the transgene and does not indicate where in the spleen high or low expression may be present. Therefore, in order to confirm the results of my Western blot analysis and show the pattern of transgene expression within splenic tissue I used immunohistochemistry (IHC).

The microscopic structure of spleen consists of two areas, the white and red pulp. The white pulp takes arterial blood and is structured around a “tree” of branched arterial vessels where smaller arterioles are surrounded by lymphoid tissue that is called the peri-arteriolar lymphoid sheath (PALS). The PALS has three regions, a T cell rich area adjacent to the arteriole, a B cell rich area called the follicle and the marginal zone which surrounds the entire white pulp. It is in this area that humoral immunity is generated. In contrast, the red pulp is associated with the venous system and acts as a filter for the blood where antigens, microorganisms and aged/defective blood cells are removed. Figure 5-7 shows a haematoxylin-eosin stain (H&E stain) of splenic tissue from an Eμ-PKCβIIHA transgenic mouse. Part A shows a low power magnification (4X) showing white and red pulp. Part B shows a higher magnification (10X) and illustrates the T cell, B cell and marginal zone of the white pulp. Part C shows this fine structure as a schematic diagram.

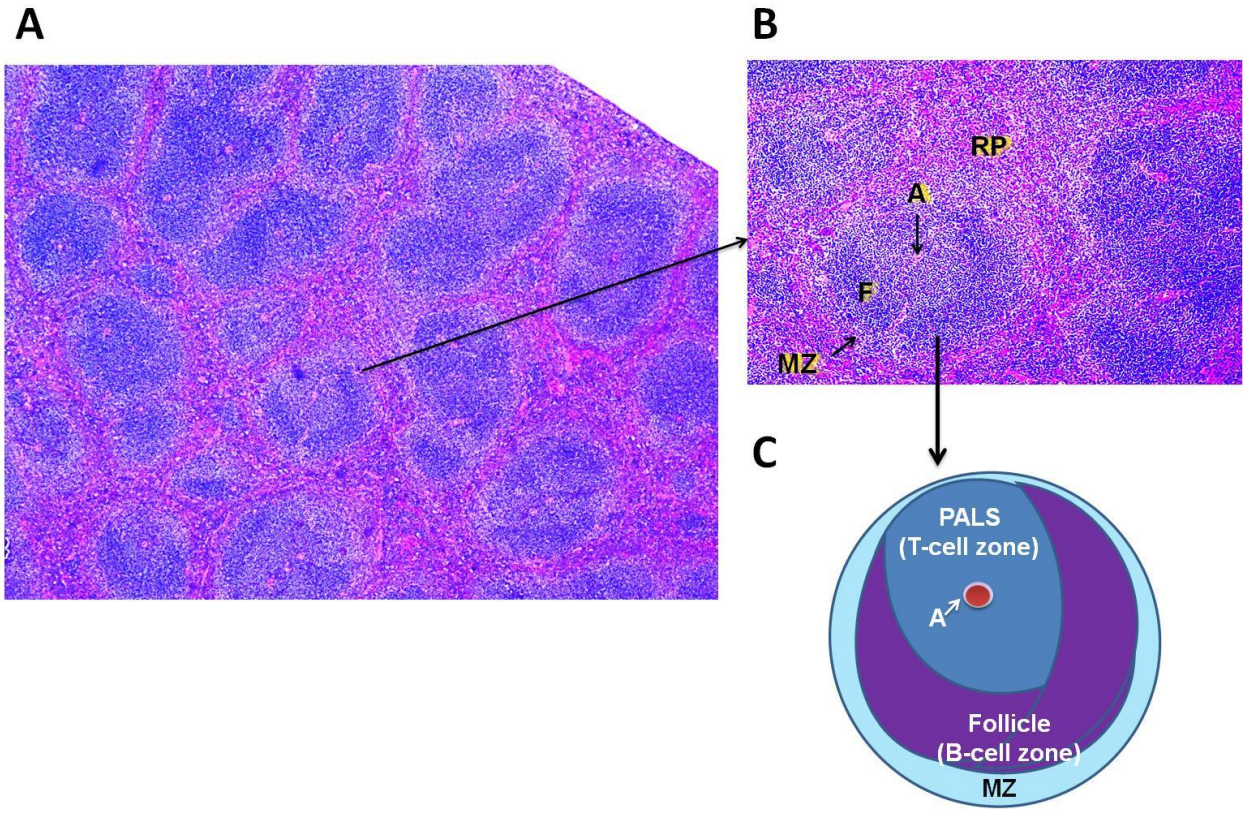

Figure 5-7. Microscopic structure of the spleen. The spleen consists of two areas, the white and red pulps. The white pulp contains the peri-arteriolar lymphoid sheath (PALS) which surrounds the arterioles. There are three regions in the PALS, a T cell rich area adjacent to the arteriole, a B cell rich area called the follicle and the marginal zone which surrounds the entire white pulp. **A)** Low power magnification (4X) showing white and red pulps in splenic tissue of a Eμ-PKCβIIHA transgenic mouse. **B)** a higher magnification (10X) illustrating the arteriole (A), follicle (F) and marginal zone (MZ) of the white pulp, as well as the red pulp (RP). **C)** Schematic diagram of spleen structure. **RP**: red pulp, **MZ**: marginal zone, **F**: follicle, **A**: artery.

I next investigated expression of the PKCβIIHA transgene in splenic tissue of transgenic and wild type control mice. This was done using a monoclonal Rabbit anti-HA antibody (C29F4) and a rabbit anti-PKCβII antibody. Figure 5-8 compares anti-HA antibody reactivity with splenic tissue derived from wild type littermate (#3-3) and non-littermate control (#Ct-8) mice (Parts A and B) with splenic tissue from two homozygous Eμ-PKCβIIHA transgenic mice (#Hom-3 and #Hom-4, Parts C and D respectively).

There is some background staining associated with the red pulp in both wild type and transgenic mice, and this was taken to be non-specific because of the high level of macrophage-associated peroxidase activity that is associated with the red pulp. In contrast, transgenic mice additionally showed a specific pattern of HA antibody reactivity associated with the white pulp. In particular, HA expression (highlighted with the yellow arrow in the higher magnified images) appeared to be associated with the follicle area of the PALS which is a B cell rich area of white pulp. This result confirms the Western blot analysis and shows expression of the PKCβIIHA transgene.

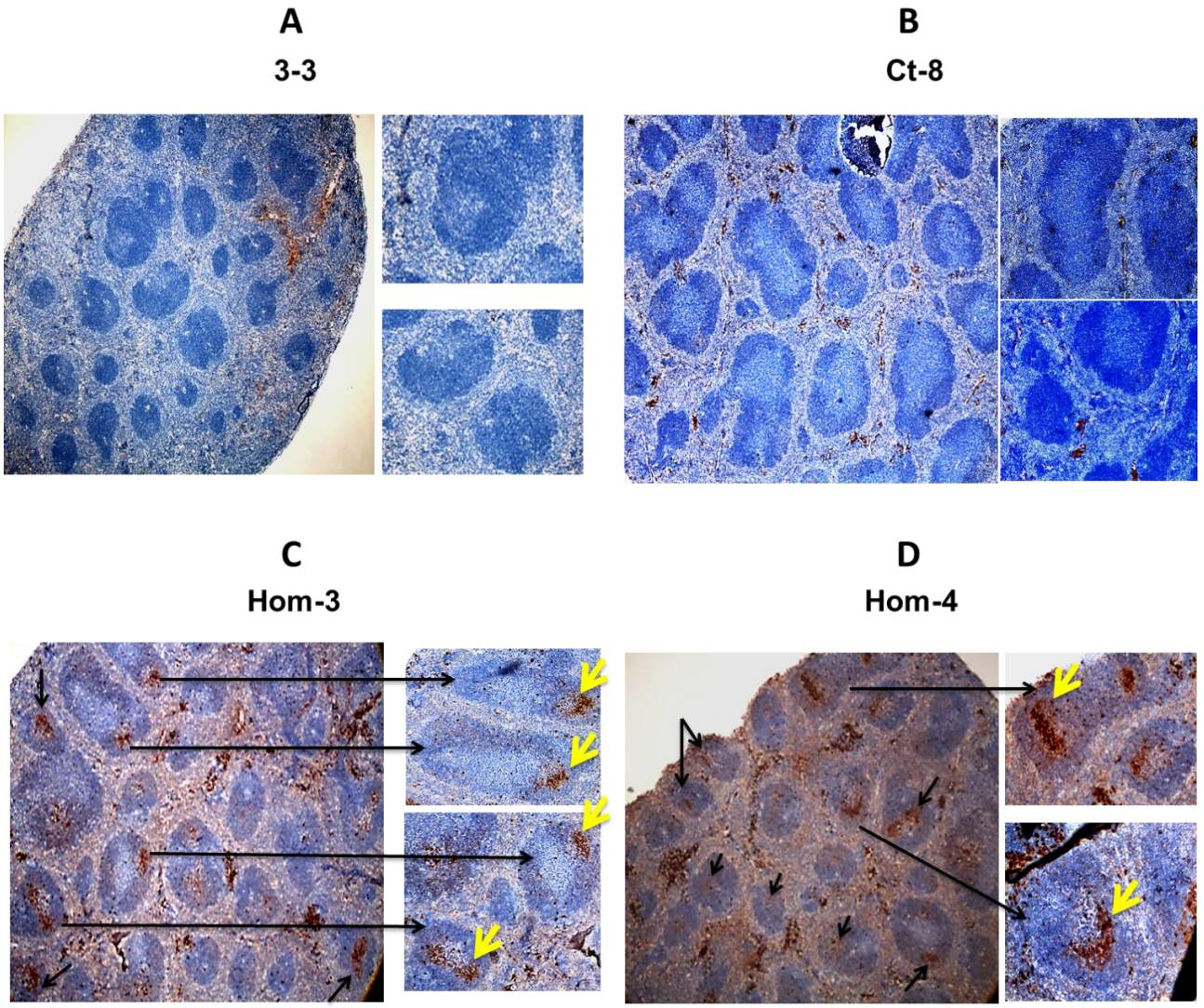

Figure 5-8. Immunohistochemical staining of the spleen from Eμ-PKCβII tg and wild type mice. Sectioned slices of paraffin-imbedded spleen were stained for the presence of HA using rabbit anti-HA antibody (C29F4). **A)** wild type mouse 3-3 (littermate control), **B)** wild type mouse ct-8 (non-litter mate control), **C)** Eμ-PKCβII tg mouse Hom-3 and **D)** Eμ-PKCβII tg mouse Hom-4(Homozygous Eμ-PKCβII transgenic mice).Note:total number of the mice used for this experiment:Non littermate: 7, littermate: 5, and transgenic mice: 15.

I next analysed for PKCβII expression in splenic tissues from wild type and transgenic mice. Figure 5-9 A and B shows the pattern of PKCβII expression in wild type littermate (#3-3) and non-littermate (#Sp-7) control mice. PKCβII expression is easily detectable and shows staining of the marginal zone as well as concentrated staining to

one end of the PALS. We considered that this area of concentrated PKCβII expression was associated with the follicle. PKCβII expression in splenic tissue from Eμ-PKCβIIHA transgenic mice showed a similar pattern of staining (Figure 5-9C and D) to wild type mice, but the intensity of staining was much greater. Importantly, PKCβII antibody reactivity was restricted to the marginal zone surrounding the PALS and to the region we anticipate is the B cell rich follicle.

Considering that the anti-HA and anti-PKCβII antibodies had similar patterns of reactivity with splenic tissue from transgenic mice, I next analysed serial slices of splenic tissue to establish co-reactivity. Figure 5-10 shows in transgenic animals that the areas of white pulp that stained strongly for PKCβII also had reactivity with the anti-HA antibody. In particular, concentrated staining of anti-HA and anti-PKCβII was associated with the follicular area of the white pulp. The follicular region of white pulp can contain germinal centres where B cells undergo rapid proliferation. A second analysis of serial spleen sections to include Ki67 as a marker of proliferating cells showed that anti-HA reactivity in transgenic mice was associated with anti-Ki67 and with strong anti-PKCβII reactivity (Figure 5-11). Taken together, these data show expression of the PKCβIIHA transgene, that expression of PKCβII is higher in transgenic than in wild type mice, and that expression of the transgene is specific to the B cell component of the white pulp of the spleen.

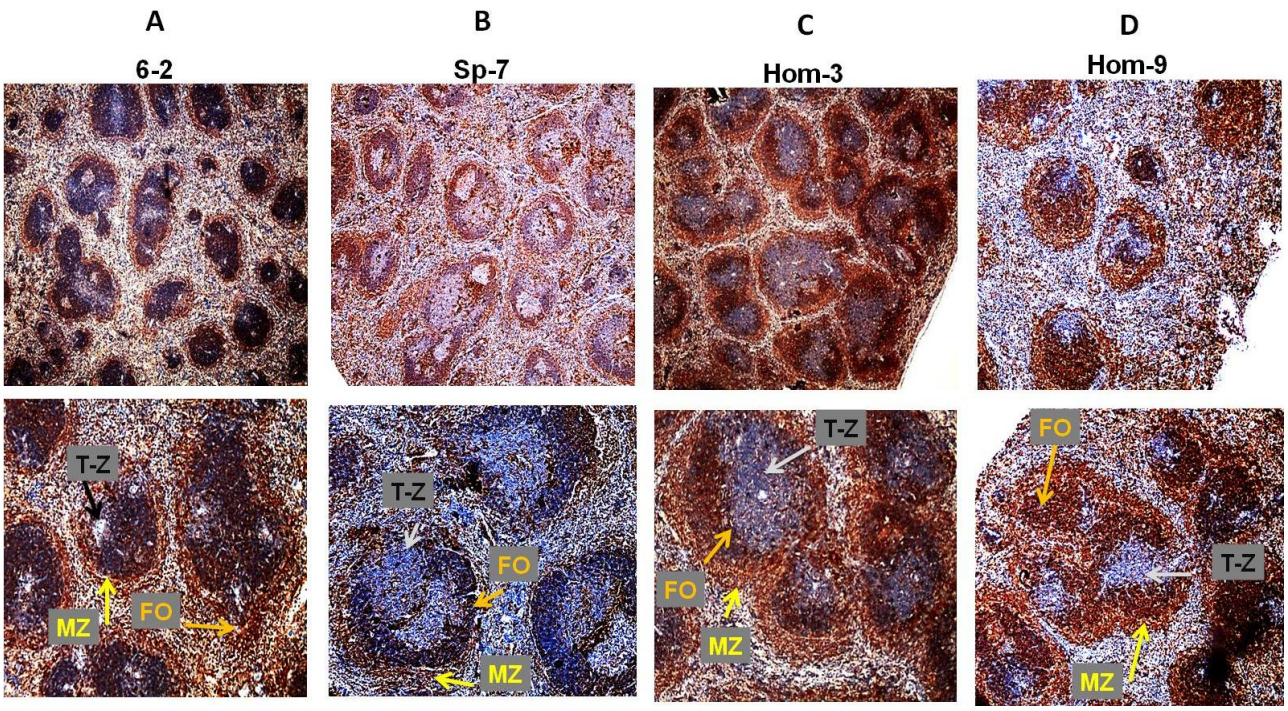

Figure 5-9. Immunohistochemical staining of the spleen of Eμ-PKCβII tg and wild type mice with polyclonal rabbit anti-PKCβII antibody. The sectioned slices of the spleen of **A)** wild type littermate (#6-2), **B)** non-littermate (#Sp-7) control mice, **C)** Homozygous Eμ-PKCβII tg mice Hom-3, and **D)** Hom-9 were stained with polyclonal rabbit anti-PKCβII antibody for the detection of PKCβII protein. The upper images are low magnification (4X) and the lower images are higher magnification (10X). Note:total number of the mice used for this experiment:Non littermate: 7, littermate: 5, and transgenic mice: 15.

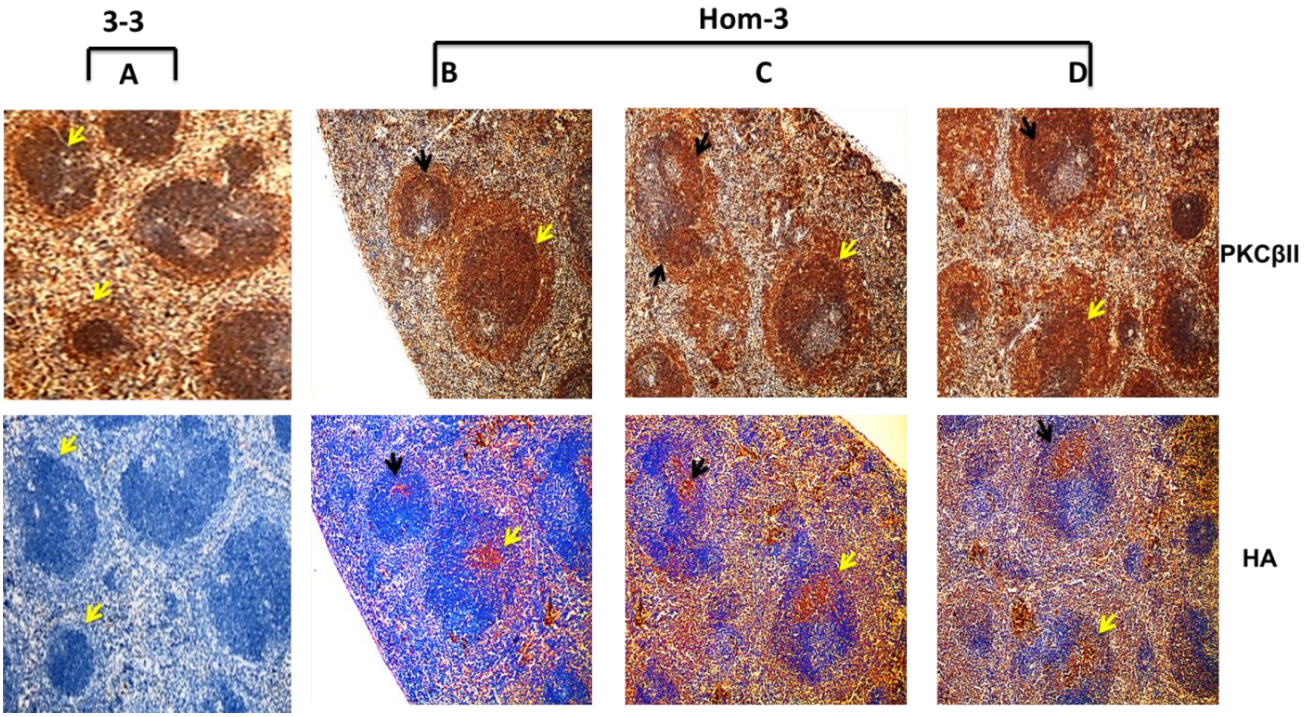

Figure 5-10. Immunohistochemical staining of sequential spleen sections from Eμ-PKCβII tg and wild type mice with anti-HA and anti-PKCβII antibodies. Sequential sectioned slices of spleen from **A)** 3-3 (Littermate control mouse), **B, C, D)** Hom-3 (6 month old homozygous Eμ-PKCβII tg mouse) were stained with rabbit anti-PKCβII antibody (upper images) and rabbit anti-HA antibody (lower images). Corresponding follicles within the white pulp of each section is highlighted with the yellow arrow. The magnification used for these images in 10X. Note:total number of the mice used for this experiment:Non littermate: 7, littermate: 5, and transgenic mice: 15.

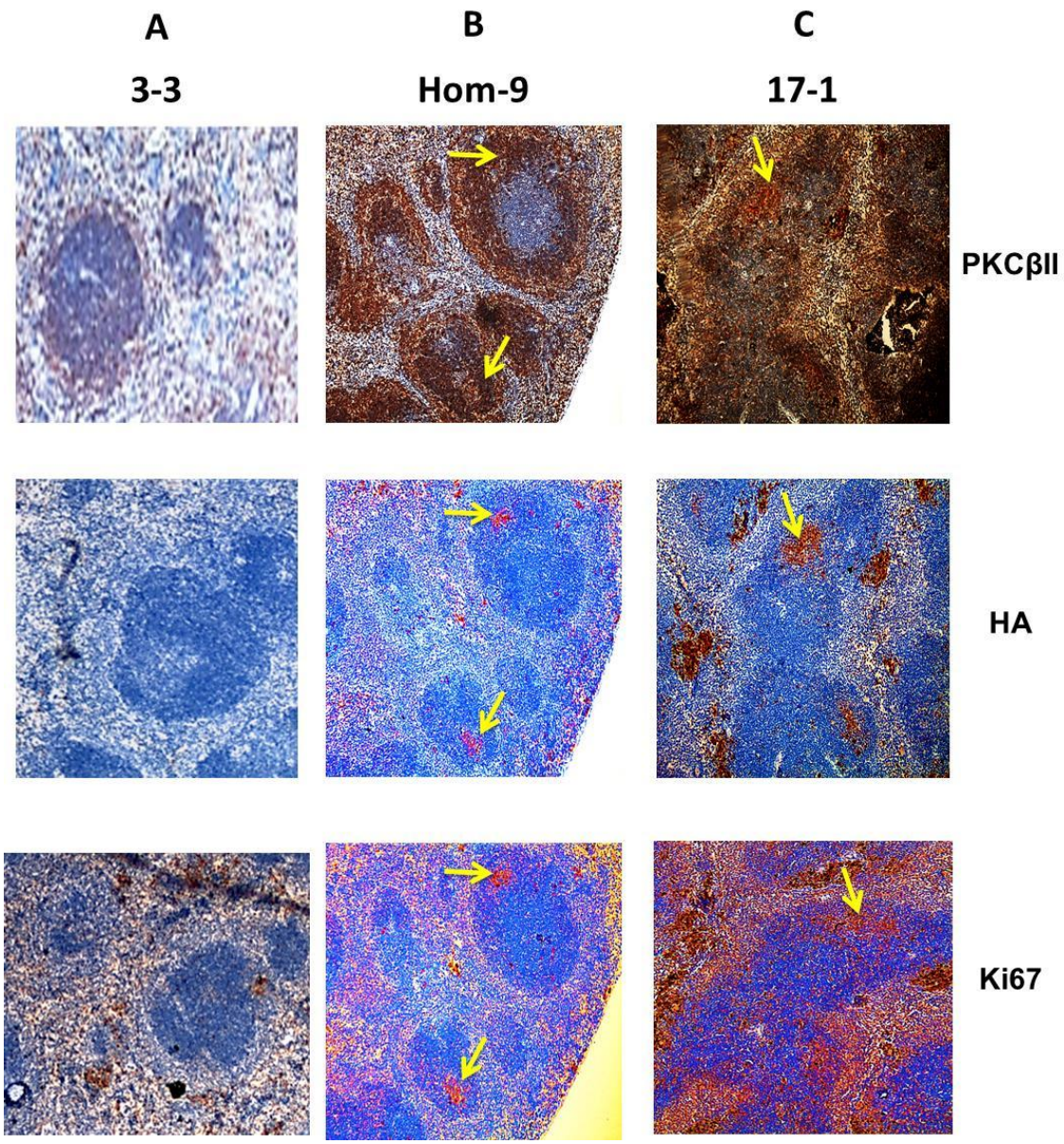

Figure 5-11. Immunohistochemical staining of sequential spleen sections from Eμ-PKCβII tg and wild type mice for PKCβII, HA and Ki-67. Sequential sectioned slices of spleen from **(A)** 3-3 (Littermate control mouse), **(B)** Hom-9 (6 month old homozygous Eμ-PKCβII tg mice) and **(C)** 17-1 (14 month old homozygous Eμ-PKCβII tg mice) were stained with rabbit anti-PKCβII antibody (upper images), rabbit anti-HA antibody (middle images) and Ki67 antibody (lower images). Corresponding follicles within the white pulp of each section is highlighted with the yellow arrow. The magnification used for these images in 10X. Note:total number of the mice used for this experiment:Non littermate: 7, littermate: 5, and transgenic mice: 15.

5.3.1 B cell-specific expression of PKCβII results in a structural change within the white pulp of spleens from transgenic mice

To complete the microscopic analysis of splenic tissue isolated from Eμ-PKCβII transgenic mice I stained tissue slices with haematoxylin and eosin stain (H&E). H&E staining discriminates the different structures of splenic tissue, and white pulp and red pulp are easily identifiable. Moreover, the structure of the follicle becomes more highly defined and structures such as the marginal zone can be easily observed. Figure 5-12 shows a comparison of H&E staining of splenic tissue isolated from a littermate control (6-2), non-littermate control (sp-11) and two Eμ-PKCβII tg transgenic mice (hom-9 and hom-10). A major difference between wild type and transgenic mice is the structure of the marginal zone. The marginal zone seemed much thicker in Eμ-PKCβII tg mice than in wild type mice. This is the same area that stains heavily for PKCβII (Figure 5-13A and B) and confirms the pattern of staining observed in Figures 5-9, 5-10 and 5-11.

Further analysis of this expanded marginal zone in splenic tissue from Eμ-PKCβII tg mice shows that it is positive for IgM, indicating that these cells are likely MZ B cells (Figure 5-13C and D). Thus, these results suggest that overexpression of PKCβII in B cells results in expansion of the MZ B cell population in the spleen.

In conclusion, my results so far demonstrate that transgenic mouse I have generated expresses PKCβII specifically in B cells, and suggests that such expression leads to changes in B cell populations of the spleen.

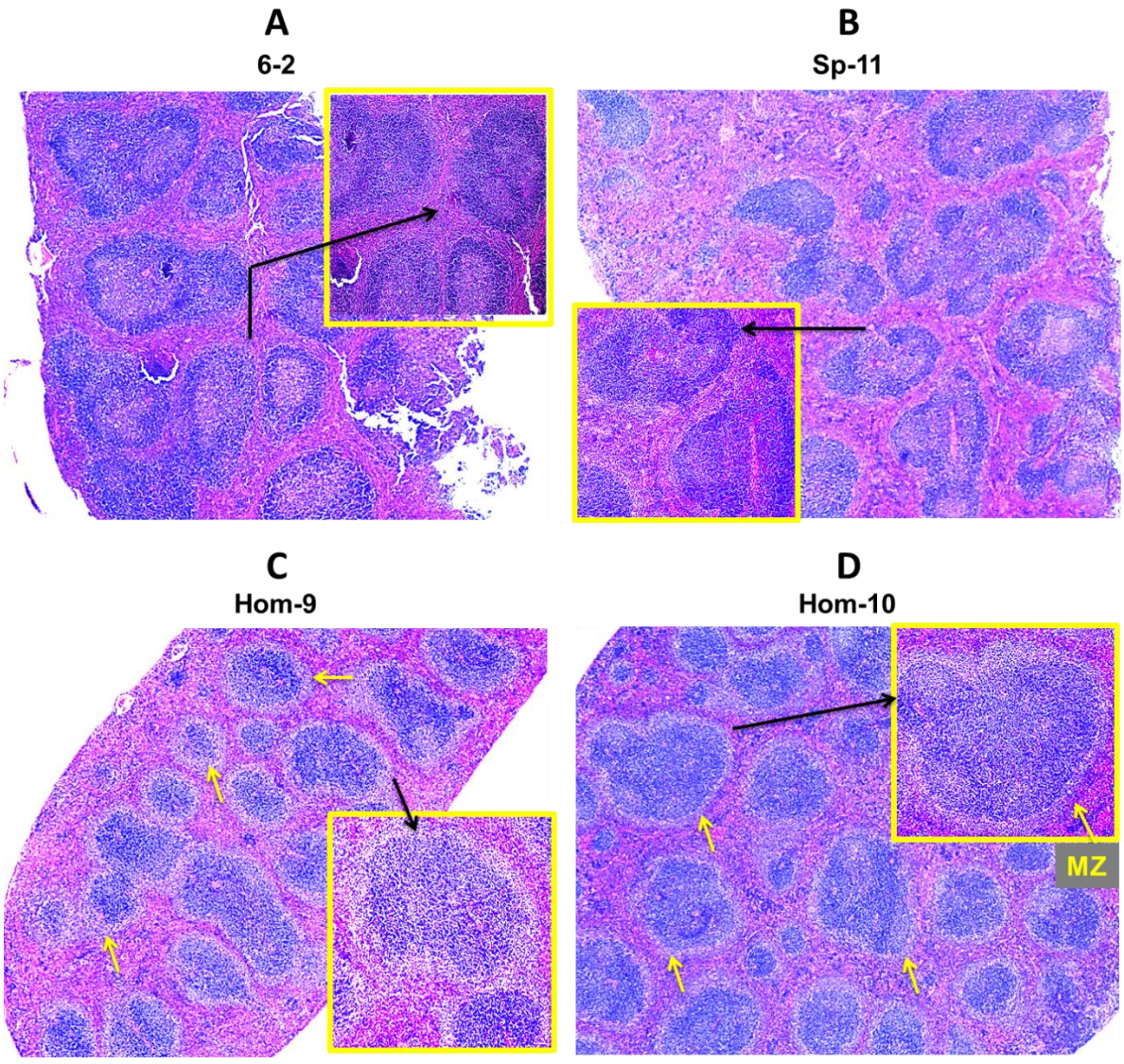

Figure 5-12. H&E staining of splenic tissue from Eμ-PKCβII transgenic and wild type mice. **M**orphological study of the spleen using H&E staining. **A)** Splenic tissue from a littermate control mouse (6-2), **B)** Splenic tissue from a non-littermate control mouse (sp-11), **C and D)** Splenic tissue from Eμ-PKCβII transgenic mice hom-9 and hom-10, respectively. Note:total number of the mice used for this experiment:Non littermate: 7, littermate: 5, and transgenic mice: 15.

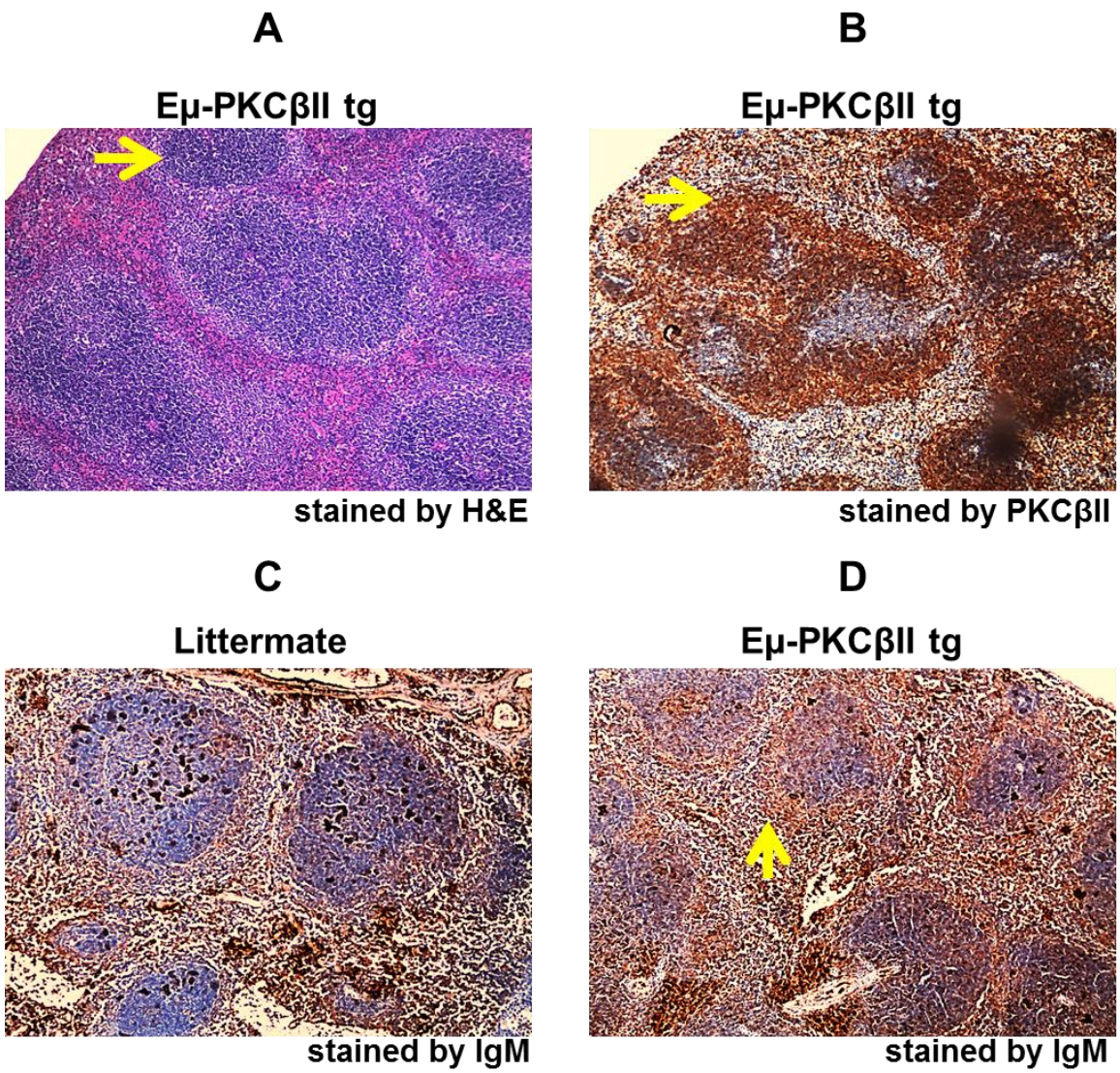

Figure 5-13. Immunohistochemical staining of spleen sections from Eμ-PKCβII tg and wild type mice by H&E, PKCβII and IgM antibodies. Sequential sectioned slices of spleen from a Eμ-PKCβII tg mouse was stained with **A)** H&E, **B)** PKCβII antibody. **C and D)** A comparison of rabbit anti-IgM staining in splenic tissue from a wild type littermate mouse (**C**) and Eμ-PKCβII tg mouse (**D**). The marginal zone of the spleen is highlighted with the yellow arrow.

.

5.4 Flow cytometric characterization of B cell subsets in wild type and Eμ-PKCβII transgenic mice

The peripheral B cell compartment of mice and men comprises several distinct subpopulations. In mice these include B-1a, B-1b, B-2, marginal zone (MZ), transitional/immature and follicular B cells. The B cells within each of these compartments can be differentiated from each other based on a characteristic expression of cell surface markers (Table 5-1). Flow cytometry is an excellent tool that is able to identify cells carrying these markers, and in this section I used a Becton Dickinson LSR-Fortessa analytical flow cytometer for this purpose. This machine, referred to previously in section 3.4.2 is equipped with 5 lasers including a UV laser (355nm), violet laser (405nm), blue laser (488nm), yellow-green laser (561nm) and red laser (640nm). This machine is capable of simultaneously detecting 18 fluorophores plus forward and side scatter making it a very powerful analytical tool for my purposes.

Cell population	Phenotype
Transitional type 1	$B220^{+}$ $CD21^{l-/lo}$ $CD23^{-}$ $CD24^{+}$ IgM^{+} IgD^{-}
Transitional type 2	$B220^{+}$ $CD21^{mid}$ $CD23^{+}$ $CD24^{+}$ IgM^{+} IgD^{-}
Marginal zone precursor	$B220^{+}$ $CD21^{+}$ $CD23^{+}$ IgM^{+} IgD^{+}
Marginal zone	$B220^{+}$ $CD21^{+}$ $CD23^{-}$ $CD24^{+}$ IgM^{+} IgD^{lo}
Follicular type	$B220^{+}$ $CD21^{mid}$ $CD23^{+}$ $CD24^{lo}$ IgM^{low} IgD^{high}
Germinal center	$B220^{+}$ $CD43^{-}$ $CD24^{+}$
B1a	$B220^{+}$ IgM^{+} $CD43^{+}$ $CD5^{+}$
B1b	$B220^{+}$ IgM^{+} $CD43^{+}$ $CD5^{-}$

Table 5-1. B cell subset markers. This table is the list of the surface markers expressing on the different B cell subsets in mouse, consisting of transitional type 1 and 2, marginal zone, follicular, germinal centre and B-1 (a, b) B cells.

I characterised B cell subset composition in the spleen, peritoneum, peripheral blood and bone marrow of both Eμ-PKCβII transgenic and wild-type mice. These cells were isolated from their respective tissues and single cell suspensions were prepared. Isolated cells were incubated with antibodies conjugated with fluorophore for 20min on ice, and then excess antibody was washed away and data were collected during flow cytometric analysis.

In order to perform simultaneous multichannel analysis I had to choose the fluorophores that were conjugated to my antibodies carefully. This is because the emission spectrum for each fluorophore can sometimes leak into the channel of other fluorophores. This spectral overlap fluorescence is proportional to the emission in the primary channel, and can therefore be estimated and subtracted from the overall fluorescence collected in a given channel to allow precise detection and quantitation. The process of subtraction of this overlapped fluorescence is called Fluorescence compensation. Prior to each run the flow cytometer is standardized with beads bearing fluorophores similar to the conjugated antibodies I used in my analysis. I then ran a series of samples that were stained with only one fluorophore, and this is called the compensation sample. FACS data for each compensation sample allowed for stained and non-stained cells to be defined, and based on this definition multichannel analysis could then be performed and this was calculated by the software package (known as Diva version 2.0) that accompanied the LSR-Fortessa. Collected data was analysed using FlowJo software and is represented in each figure as a contour plot with outliers in order to ensure the best possible resolution. Table 5-2 lists the antibody cocktail I used to characterise B cell subsets, and also lists the fluorophore conjugate.

Marker	Conjugated Fluorophore
B220	PE anti-mouse/human CD45R/B220 Antibody
IgD	APC anti-mouse IgD Antibody(
IgM	APC/Cy7 anti-mouse IgM Antibody
CD43	FITC anti-mouse CD43 Antibody
CD5	PE/Cy5 anti-mouse CD5 Antibody
CD21	PE/Cy7 anti-mouse CD21/CD35
CD23	Pacific Blue™ anti-mouse CD23 Antibody
CD24	PerCP/Cy5.5 anti-mouse CD24 Antibody

Table 5-2. Fluorochrome conjugated antibodies used for flow cytometry analysis of B cell subsets in the Eμ-PKCβII tg and wild type mice. This table is a list of the fluorochrome-conjugated antibodies that were used for characterization of B cell subsets in this study.

In designing this panel of antibodies I chose the brightest fluorophore, phycoerytherin (PE) for B220 expression because this is the primary maker for gating B cells. This is important to ensure that I detect all the B220 expressing cells in the tissues I analysed. I also selected bright fluorophores for proteins which were expected to have lower expression. For instance, CD5, CD21 and CD24 are not expressed highly on normal B cells. Detection of IgD is also important and so required a bright fluorophore. For detecting IgM and CD43 I used APC-Cy7 and FITC fluorophores which have moderate stain indexes as I believed that these two markers are expressed highly on B cells and did not need bright fluorophores.

Another important consideration in designing the antibody panel was to avoid using two fluorophores whose fluorescence properties have overlap, especially when the antibodies react with the same B cell subset. For example, the majority of B cell subsets express both IgD and IgM to some degree, so to avoid significant compensation that may influence my interpretation I chose IgD conjugated with APC and IgM conjugated with APC-Cy7 because there is only 2.9% of APC-Cy7 leakage on to the

APC channel, and this is negligible. However, with some antibodies this was not possible because of limited availability of conjugates and compensation was performed. In this section of my thesis I have split the flow cytometric analysis into four subsections: 1) Spleen (SP), 2) Peritoneum (PE), 3) Peripheral Blood (PB),4) Bone Marrow (BM).

5.4.1 Spleen

The main B cell subsets contained by the spleen include Follicular (FO) B cells, immature/transitional (Imm) B cells, marginal zone (MZ) B cells and B-1 B cells. For my analysis I gated on live lymphocytes that were B220 positive (Figure 5-14A). I then used my panel of antibodies to identify the B cell subsets within this population of $B220^{+}$ cells based on a sequential gating strategy illustrated in Figure 5-14B. Thus, FO B cells were differentiated from MZ/Imm/B-1 B cells based on IgD and IgM expression. FO B cells which express high levels of IgD were then further characterised for CD21, CD23 and CD24 expression. IgM positive MZ/Imm B cells were differentiated from B-1 B cells based on CD43 expression and B-1 B cells further differentiated between B-1a and B-1b based on CD5 expression. MZ B cells were differentiated from Imm B cells based on strong expression of CD21 and CD24 which marks mature MZ B cells. Imm B cells were CD21 negative, CD23 weak and CD24 positive. It was not always possible to gain clear results when I analysed for CD43, CD23 and CD5. This is because I experienced difficulties with respect to compensation during multicolour analysis in the early stages of this study. What was reliable was discriminating between FO B cells and IgM+ B cells. Thus, statistical comparisons of B cell populations between wild type and transgenic mice were performed on these two populations and using a Mann-Whitney U-Test to calculate the P value.

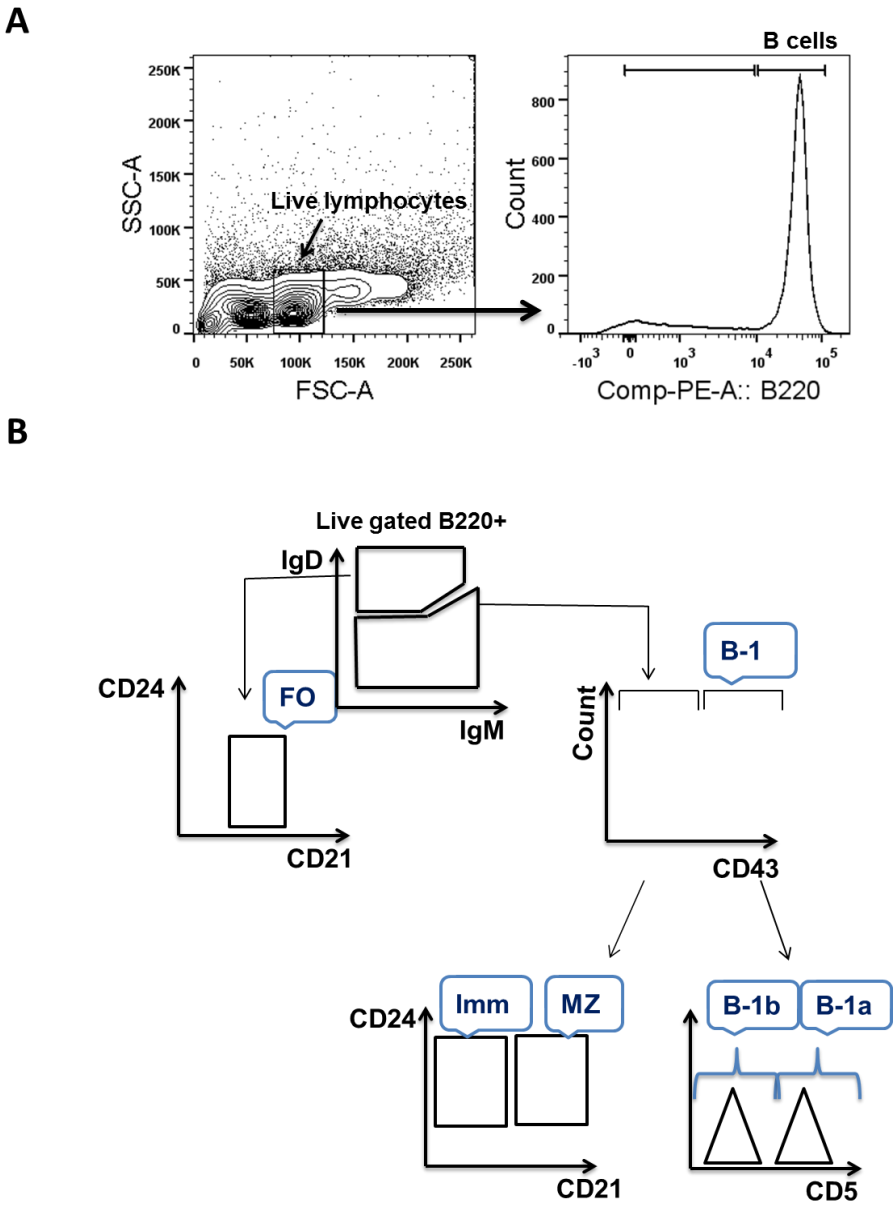

Figure 5-14.Schematic of the FACS gating strategy used for characterization of splenic B cells in Eμ-PKCβII tg and wild type mice. A) In order to characterize the B cell subsets in the spleen of Eμ-PKCβII tg and wild type mice the initial gating focused on live lymphocytes (right hand panel), and this was followed by further gating these cells for B220 expression (left hand panel). **B)** Then, sequential gating was performed on live $B220^{+}$ cells to detect Follicular (**FO**) B cells ($B220^{+}IgM^{low}IgD^{high}CD21^{mid}CD24^{lo}$), immature/transitional (**Imm**) B cells ($B220^{+}IgM^{+}IgD^{-}CD21^{-/+}CD24^{+}$), marginal zone (**MZ**) B cells and **B-1** cells($B220^{+}IgM^{+}IgD^{lo}CD21^{+}CD24^{+}$).

Figure 5-15 shows a typical FACS analysis of splenic tissue according to the protocol illustrated in Figure 5-14 B. The data represented in Figure 5-15A and B were derived from 2 wild type control mice, and in Figure 5-15C and D from 2 homozygous Eμ-PKCβII transgenic mice. Figure 5-15 clearly shows that the staining protocol I used can discriminate and identify each of the B cell subsets of the spleen. Thus, I could identify FO B cells, MZ B cells, Imm B cells and B-1a and B-1b cells. Although this is the optimal analysis I wished to achieve, this was not possible in my early analysis which reliably only discriminated between FO B cells and IgM^+ B cells (which includes all Imm, MZ and B-1 B cells).

With respect to the wild type control mice, one was a littermate control aged for 14 months (mouse #6-2, Figure 5-15A), whereas the second was a non-littermate mouse aged for 6 months (mouse# sp-10, Figure 5-15B). The reason for taking non-littermate animals is because young littermate mice were unavailable, and because I reasoned that if there were no significant differences between littermate and non-littermate animals the data derived from them could be assessed as a single group (Figure 5-16). Thus, a comparison of percentage B cells in the FO and IgM^+ B cell compartments showed that wild type littermate and non-littermate animals were largely similar. Within the wild type littermate mice there was a slight increase in the numbers of FO B cells, but this difference was not significant. This indicates that the data I generated using the non-littermate and littermate wild type mice can be used as a single group of wild type mice for the purposes of this study (Figure 5-16).

With respect to the homozygous Eμ-PKCβII trangenic mice, both these animals were aged for 6 months. The most striking difference between transgenic and wildtype mice is the increased percentage of IgM^+ B cells and decreased percentage of FO B cells observed in the transgenic mice (Figure 5-15). This difference is significant in both comparisons as is illustrated in Figure 5-17 and seems to be proportional suggesting that the increase in IgM^+ cells represents a shift in B cell population rather than lymphocytosis. This increase in IgM^+ B cells using FACS analysis is in agreement with our histochemical data showing that IgM^+ B cells are overrepresented in the spleens of transgenic animals. Taken together, these results suggest that expression of transgenic

PKCβII leads to a shift in B cell subpopulations that favours the development of IgM^{+} B cells.

Interestingly, the optimal analysis represented in Figure 5-15 shows that the percentage of MZ B cells increased in comparison to the wild type mice, and that the majority of B-1 B cells from transgenic mice were of the B-1a (CD5^{+}) phenotype. In contrast, in the wild type animals there was a more or less equal distribution of B-1a and B-1b B cells. Although statistical analysis cannot be performed on these data, they nevertheless provide support for the central hypothesis of my thesis that overexpression of PKCβII would lead to favored development of MZ and B-1 B cells.

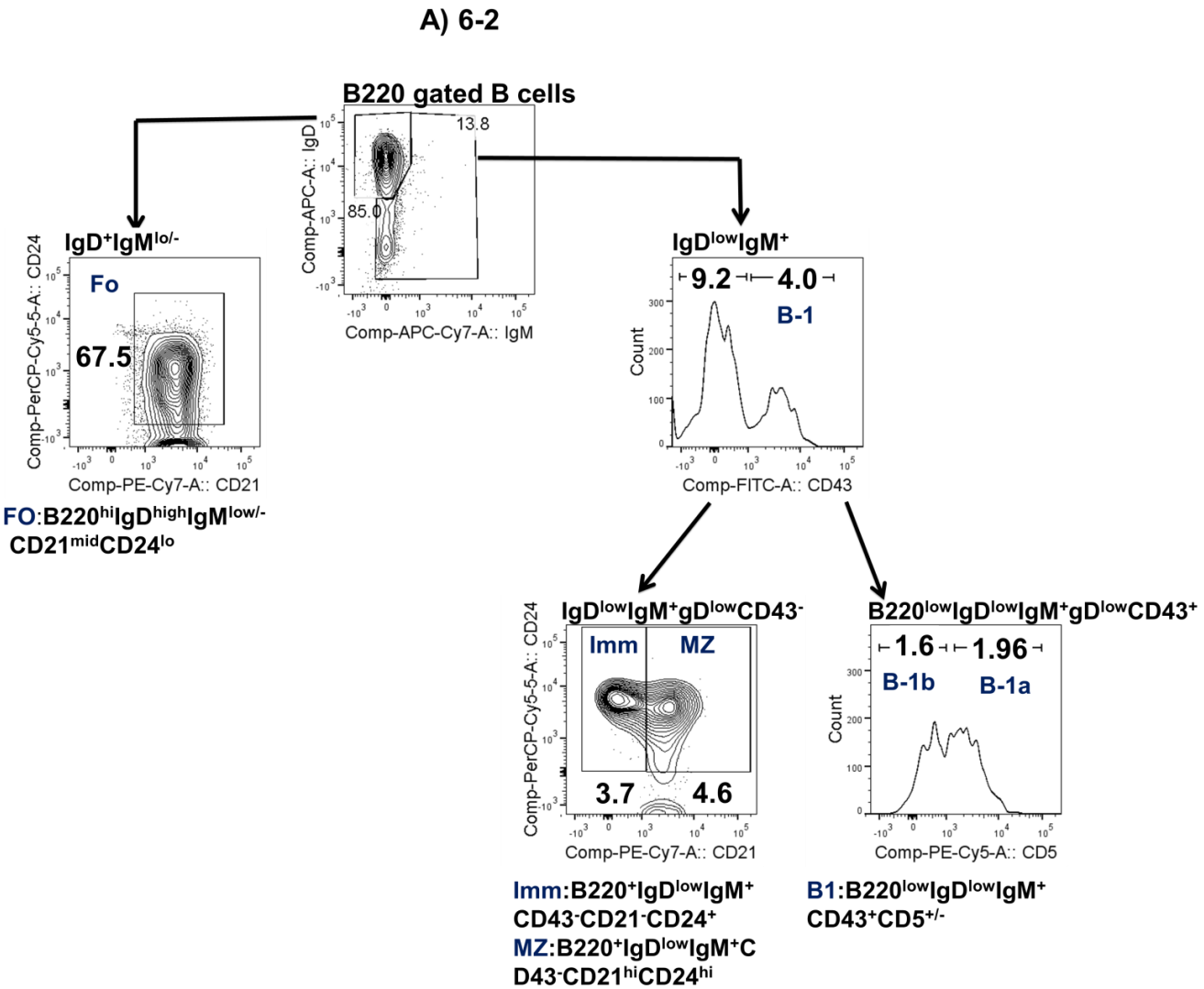

B) Sp-10

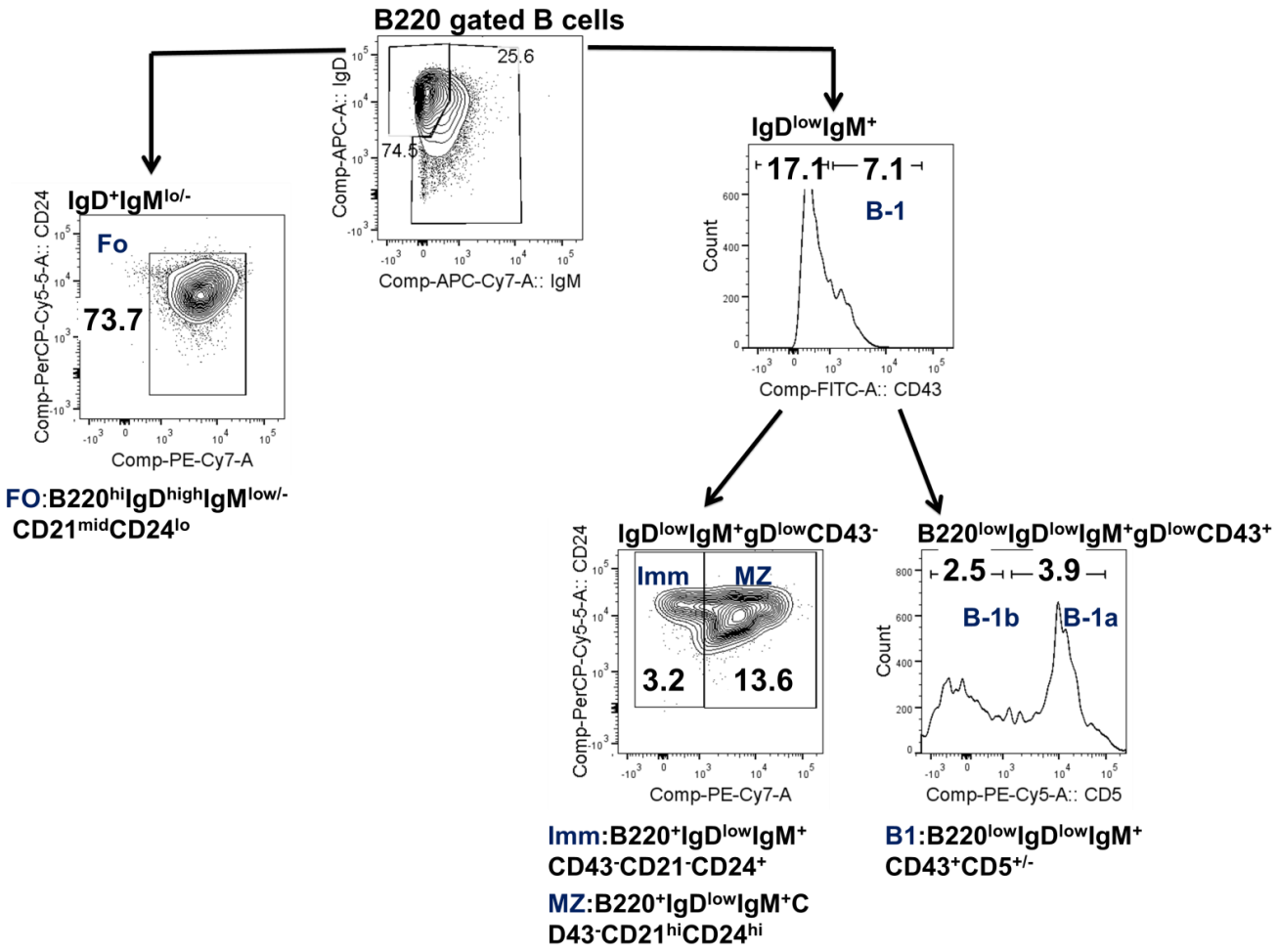

FO:B220^{hi}IgD^{high}IgM$^{low/-}$ CD21^{mid}CD24^{lo}

Imm:B220^{+}IgD^{low}IgM^{+} CD43^{-}CD21^{-}CD24^{+}

MZ:B220^{+}IgD^{low}IgM^{+}C D43^{-}CD21^{hi}CD24^{hi}

B1:B220^{low}IgD^{low}IgM^{+} CD43^{+}CD5$^{+/-}$

C) hom-17

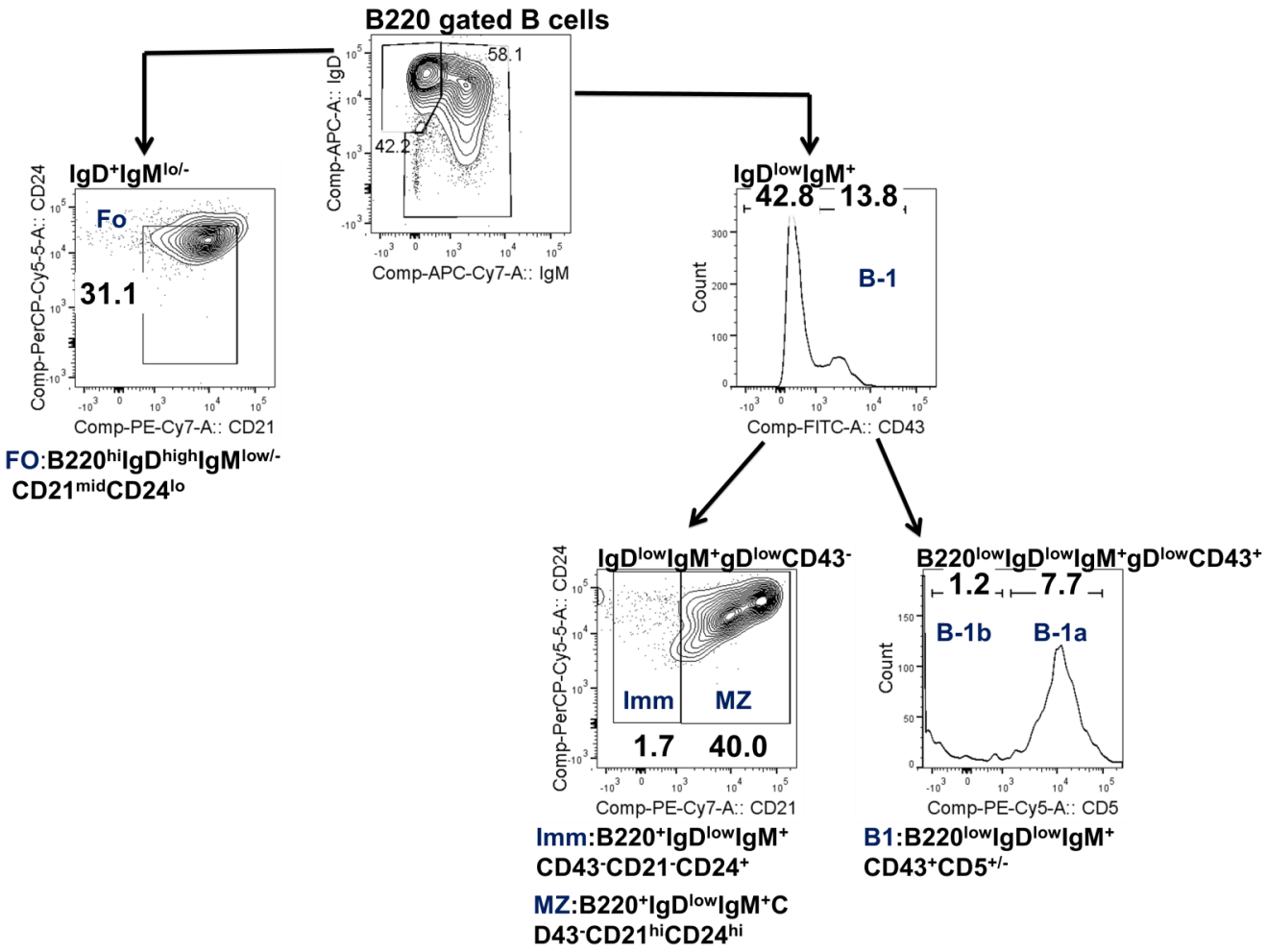
B220 gated B cells
Comp-APC-A:: IgD
Comp-APC-Cy7-A:: IgM
58.1
42.2
IgD+IgM lo/-
Fo
31.1
Comp-PerCP-Cy5-5-A:: CD24
Comp-PE-Cy7-A:: CD21
FO:B220hiIgDhighIgMlow/-
CD21midCD24lo
IgDlowIgM+
42.8
13.8
B-1
Count
Comp-FITC-A:: CD43
IgDlowIgM+gDlowCD43-
Imm
MZ
1.7
40.0
Comp-PerCP-Cy5-5-A:: CD24
Comp-PE-Cy7-A:: CD21
Imm:B220+IgDlowIgM+
CD43-CD21-CD24+
MZ:B220+IgDlowIgM+C
D43-CD21hiCD24hi
B220lowIgDlowIgM+gDlowCD43+
1.2
7.7
B-1b
B-1a
Count
Comp-PE-Cy5-A:: CD5
B1:B220lowIgDlowIgM+
CD43+CD5+/-

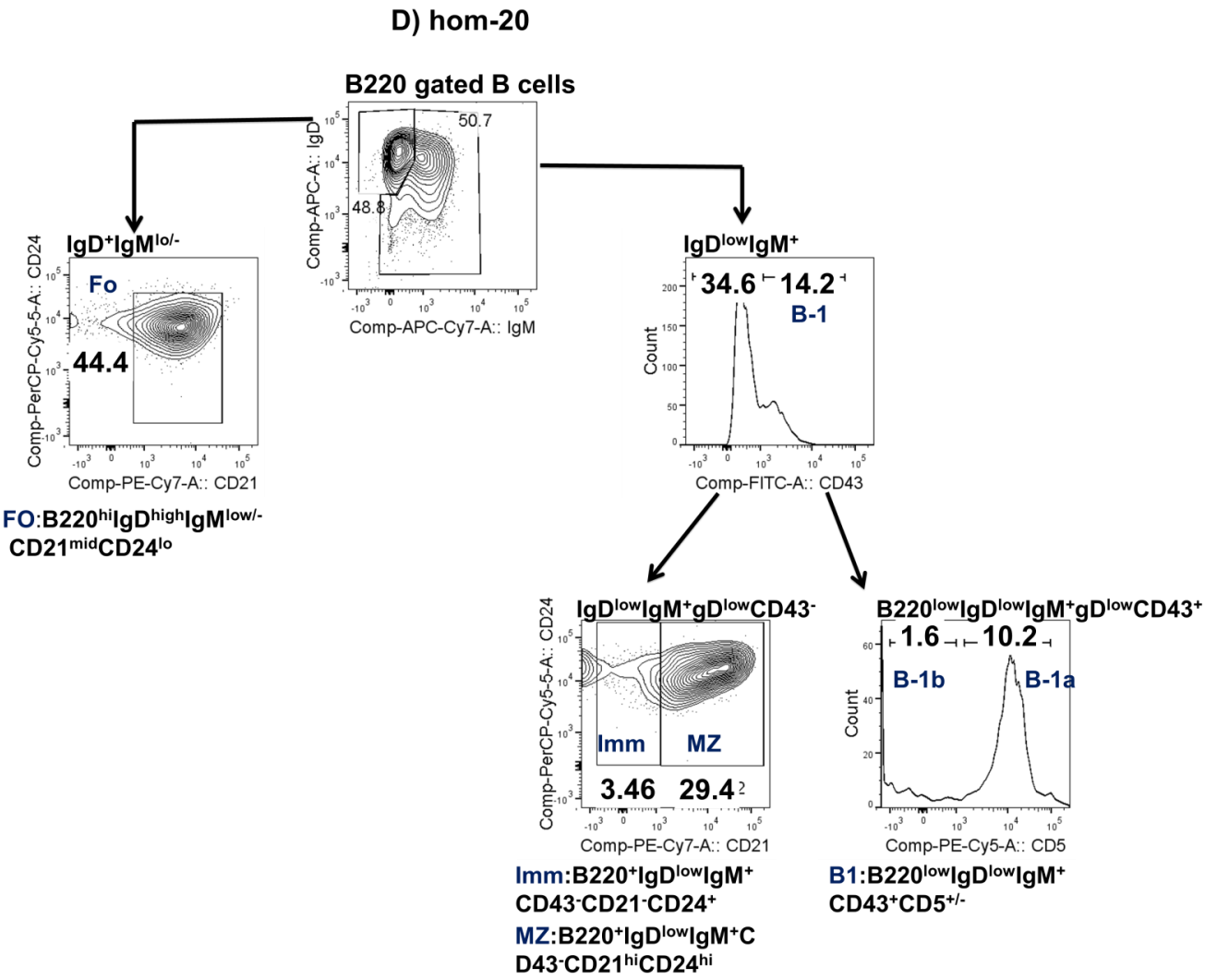

Figure 5-15. FACS analysis of splenic B cells of Eμ-PKCβII tg and wild type mice. Single cell suspensions prepared from spleens isolated from Eμ-PKCβII tg and wild type mice were stained with a cocktail of antibodies described in Figure 5-14B, and then analysed by flow cytometry. **(A)** Spleen cells from a wildtype littermate control mouse (6-2, 14 months old), **(B)** Spleen cells from a wildtype non-littermate control mouse (sp-10, 6 months old). **(C and D)** Spleen cells from homozygous Eμ-PKCβII trangenic mice (hom-17 and hom-20, both aged for 6 months).

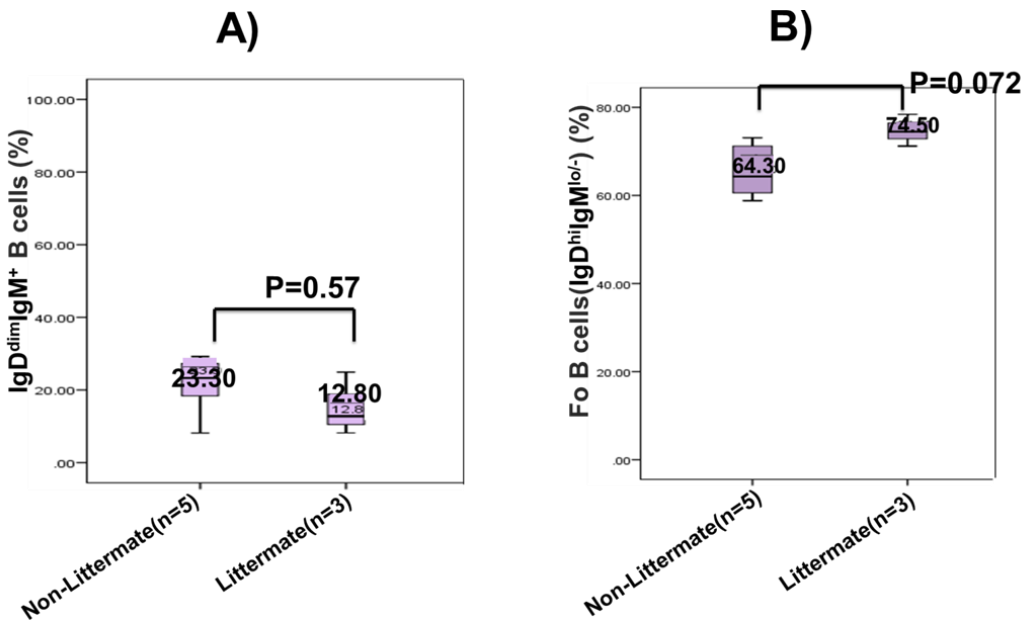

Figure 5-16. Statistical comparison of $IgD^{dim}IgM^{+}$ and Follicular B cells in non-littermate and littermate wild type mice. Box plot representation comparing percentage of **A)** $IgD^{dim}IgM^{+}$ cells, and **B)** $IgD^{hi}IgM^{lo/-}$ (FO B cells) cells in the $B220^{+}$ population of cells isolated from splenic tissue of 5 non-littermate and 3 littermate wild type mice. Statistical significance was assessed using a Mann-Whitney U test.

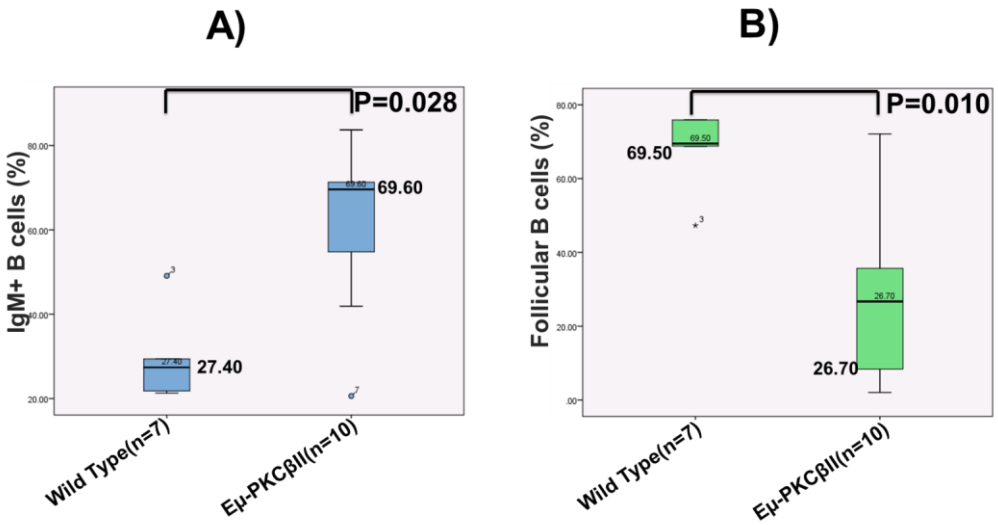

Figure 5-17. Statistical comparison of $IgD^{dim}IgM^{+}$ and Follicular B cells in wild type and Eμ-PKCβII tg mice. Box plot representation comparing percentage of **A)** $IgD^{dim}IgM^{+}$ cells, and **B)** $IgD^{hi}IgM^{lo/-}$ (FO B cells) cells in the $B220^{+}$ population of cells isolated from splenic tissue of 7 wild type and 10 Eμ-PKCβII tg mice. Statistical significance was assessed using a Mann-Whitney U test.

5.4.2 Peritoneum

To analyse the B cell subpopulations in the peritoneum I employed a slightly different gating strategy than what I used for the spleen. This strategy is illustrated in Figure 5-18 and shows how I discriminated between B cells and B-1 B cells, the major subsets within peritoneum. Like with the splenic cells I gated on live lymphocytes and took only cells that were B220+ for further analysis. I then used IgD and IgM to differentiate FO ($B220^{hi}IgD^{high}IgM^{low/-}$) B cells from $IgD^{lo}IgM^{+}$ B cells. FO B cells were then further characterised based on CD21 and CD24 expression. In this analysis I also show B220 expression on FO B cells because this is known to be strong and sharp (Hua Gu 2004). The $IgD^{lo}IgM^{+}$ B cells were further gated for the expression of CD24 and CD43 to separate B-1 B cells ($CD24^{hi}CD43^{+}$) from Imm B cells ($CD24^{+}CD43^{-}$). The population that was $CD24^{hi}CD43^{+}$ was further analysed for CD5 expression, distinguishing B-1a ($CD5^{+}$) from B-1b cells ($CD5^{-}$). B220 expression on the entire population of B-1 B cells is shown to confirm that its expression, as is reported, is weaker than on FO B cells (Hua Gu 2004).

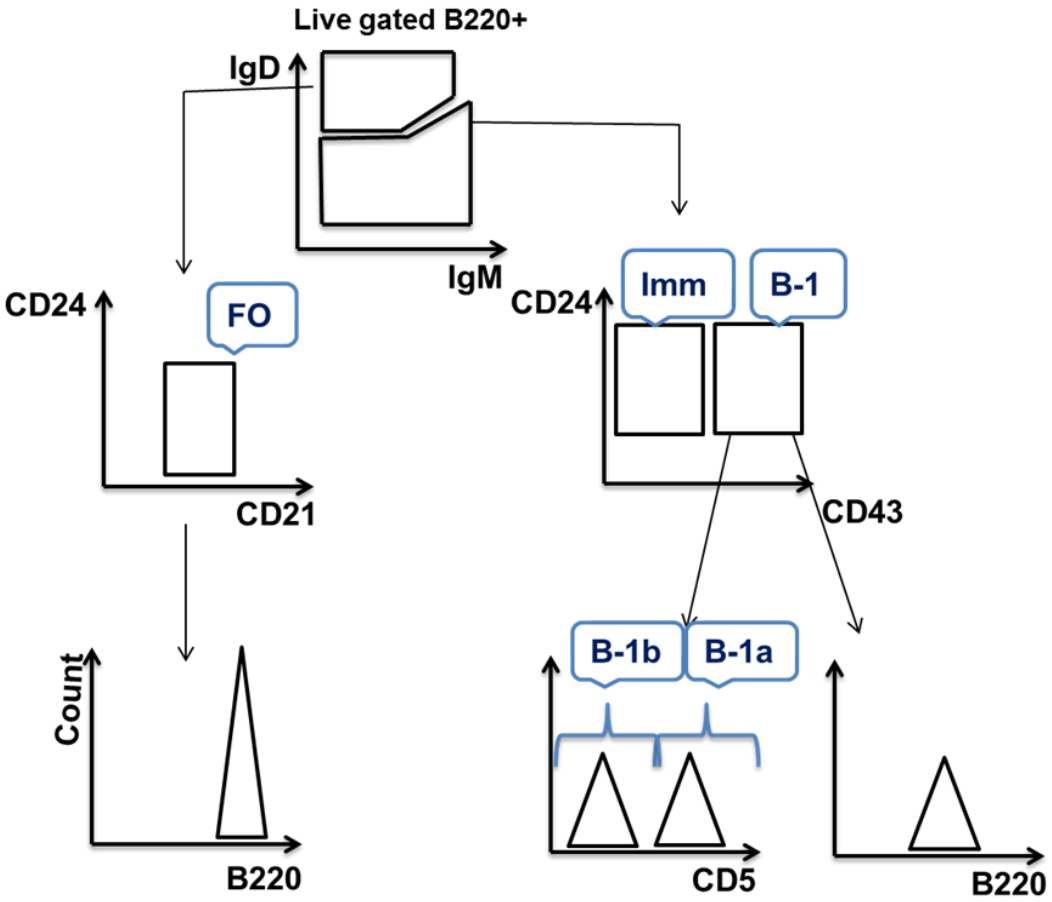

Figure 5-18. The schematic of the FACS gating strategy for characterization of B cells in peritoneum of Eμ-PKCβII tg and wild type mice. To characterize the peritoneal B cells, IgM, IgD, CD5, CD21, CD24, CD43 markers were used. Sequential gating was performed on live cells gated for $B220^{+}$ cells to detect Follicular (**FO**) B cells ($B220^{+}IgM^{low}IgD^{high}CD21^{mid}CD24^{lo}$), immature/transitional (**Imm**) B cells ($B220^{+}IgM^{+}IgD^{-}CD21^{-/+}CD24^{+}$), and **B-1** cells ($B220^{+}IgM^{+}IgD^{lo}CD21^{+}CD24^{+}CD5^{+/-}$) in the Eμ-PKCβII tg and wild type mice.

Figure 5-19 shows a typical FACS analysis of peritoneal cells according to the protocol illustrated in Figure 5-18. The data represented in Figure 5-19A and B, like with my analysis of splenic cells, was derived from 2 wild type control mice; one a 14 month littermate control and the second a 6 month old non-littermate mouse. Figure 5-19C shows analysis of cells derived from of a 6 month old homozygous Eμ-PKCβII transgenic mouse. These analyses clearly show that the staining protocol I used can discriminate and identify each of the major B cell subsets of the peritoneum. Thus, I

could identify FO B cells, Imm B cells and B-1 B cells. A comparison of the littermate and non-littermate wild type mice showed that there is a difference in the FO B cell population, the littermate wild type mice showed a reduction in the percentage of cells within the defined parameters. Also, the pattern of the distribution of the $IgD^{dim}IgM^{+}$ population was different between the littermate and non-littermate wild type mice. In this case the B220+ cells derived from the littermate mouse showed weaker IgM expression than did the B220+ cells from the non-littermate control mouse. However, further gating of these cells with CD24, CD43 and CD5 showed that despite low IgM expression on the cells derived from the littermate mouse, the population percentage of B-1 B cells were largely similar in both littermate and non-littermate mice. Statistical comparison of B cell populations between littermate and non-littermate mice was not possible because data was derived from only two littermate control mice. I reasoned that because the B-1 B cell populations of the littermate and non-littermate control mice were similar in terms of percentages, they could be considered as a single group. Therefore, for comparative study with the transgenic mouse I have excluded the FO B cell compartment and compared only the B-1 B cell populations.

With respect to the homozygous Eμ-PKCβII trangenic mice the most striking difference to wildtype mice is the significant increase in IgM^{+} B cells (Figure 5-20A). Further analysis of this population showed that the majority of IgM^{+} B cells were B-1a cells, and that the increased percentage associated with transgenic mice was also significant (Figure 5-20B). Although I do not perform a statistical comparison of the FO B cell population between transgenic and wildtype mice, there seems to be a much lower percentage of FO B cells observed in Eμ-PKCβII transgenic mice. This is similar to what I observe in the spleen, therefore, I can conclude that this data suggest that expression of transgenic PKCβII leads to favoured expression of B-1a cells in the peritoneum.

A) 6-2

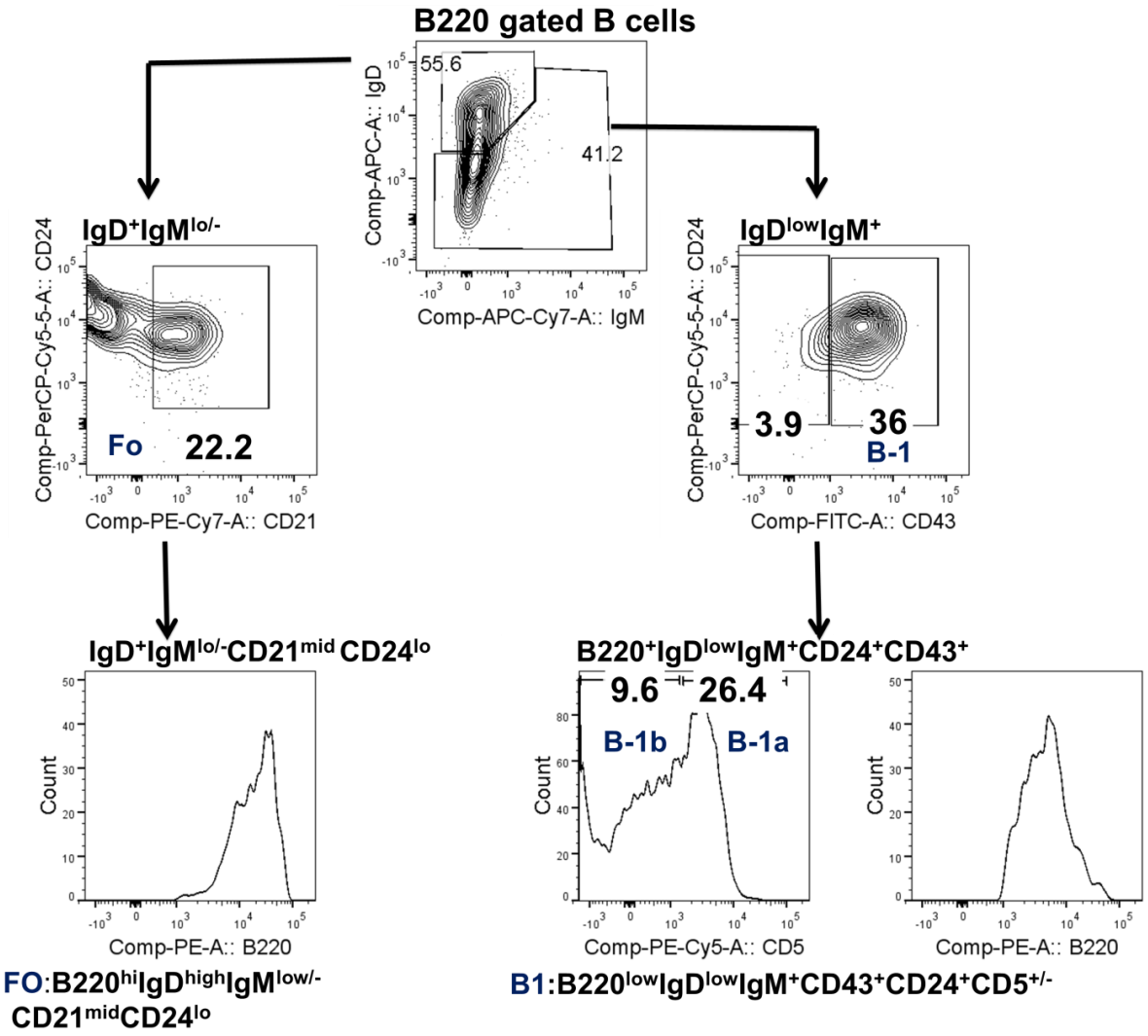
B220 gated B cells
55.6
41.2
Comp-APC-A:: IgD
Comp-APC-Cy7-A:: IgM
IgD+IgMlo/-
Comp-PerCP-Cy5-5-A:: CD24
Fo
22.2
Comp-PE-Cy7-A:: CD21
IgDlowIgM+
3.9
36
B-1
Comp-FITC-A:: CD43
IgD+IgMlo/-CD21mid CD24lo
Count
Comp-PE-A:: B220
B220+IgDlowIgM+CD24+CD43+
9.6
26.4
B-1b
B-1a
Comp-PE-Cy5-A:: CD5
FO:B220hiIgDhighIgMlow/-
CD21midCD24lo
B1:B220lowIgDlowIgM+CD43+CD24+CD5+/-

B) SP-5

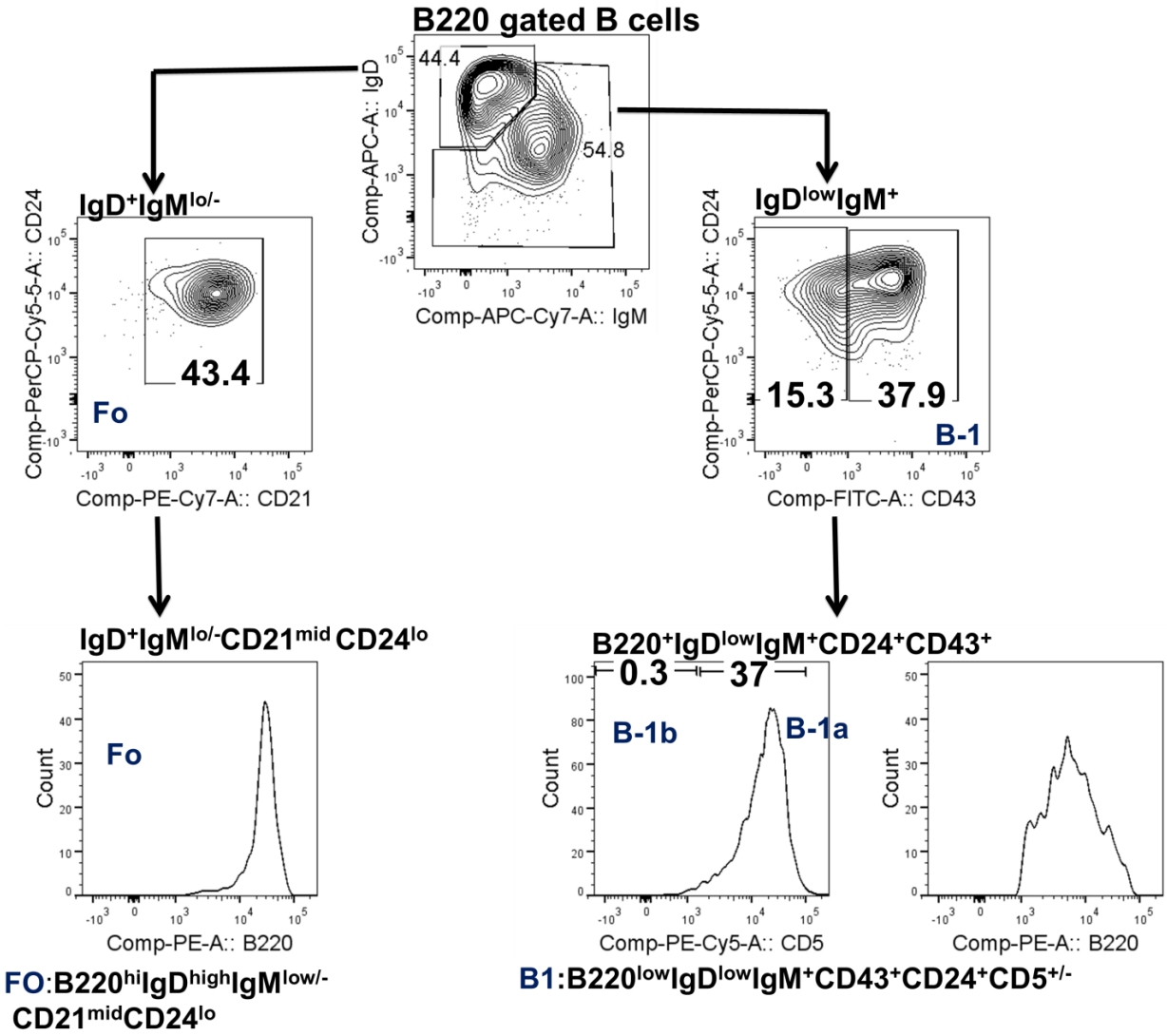

FO:B220^{hi}IgD^{high}IgM$^{low/-}$ CD21^{mid}CD24^{lo}

B1:B220^{low}IgD^{low}IgM^{+}CD43^{+}CD24^{+}CD5$^{+/-}$

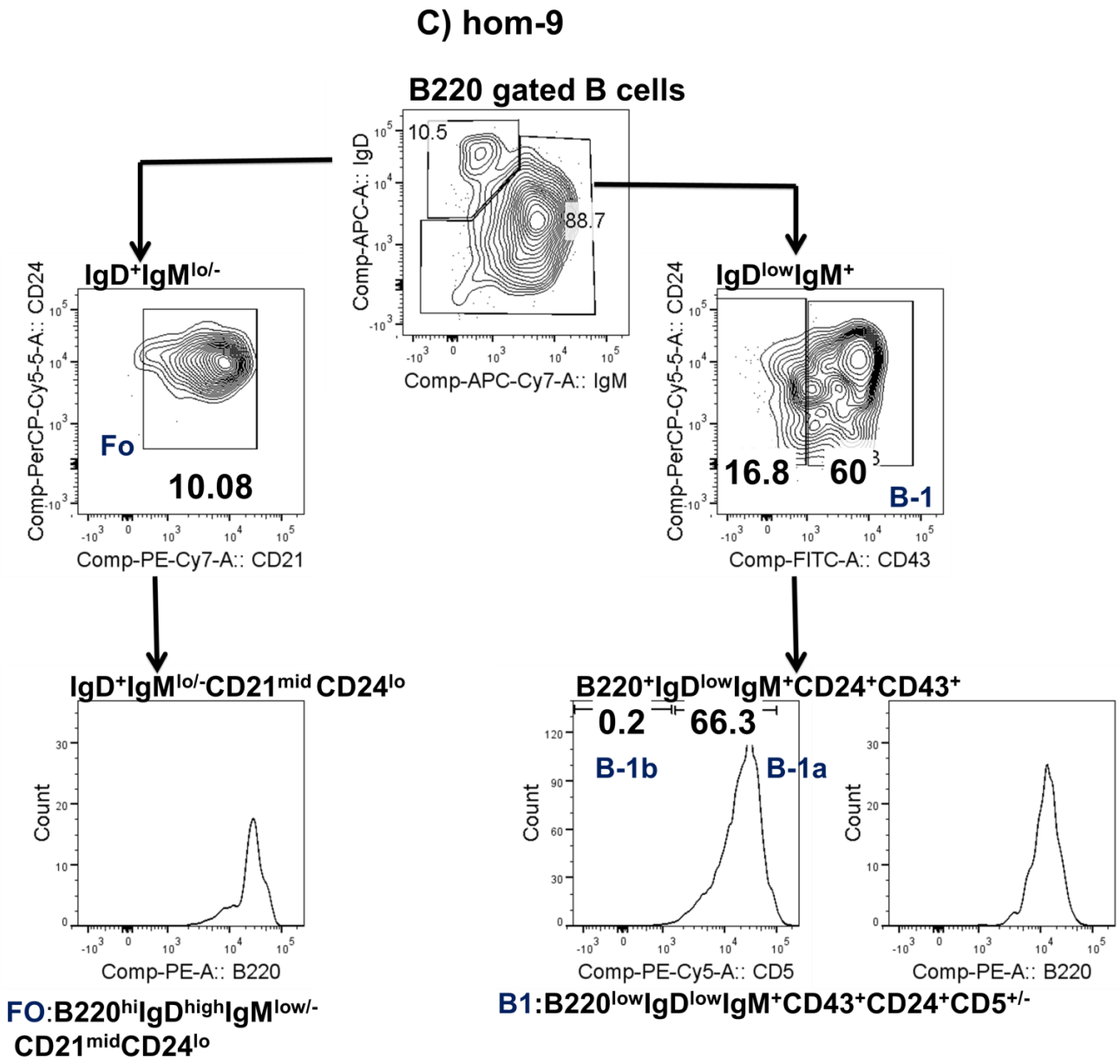

Figure 5-19. FACS analysis of peritoneal B cells in Eμ-PKCβII tg and wild type mice. Single cell suspensions of peritoneal cells were prepared from Eμ-PKCβII tg and wild type mice, and were stained with a cocktail of antibodies described in Figure 5-18. This was followed by flow cytometry. The FACS was performed in the mice **(A)** Peritoneal cells from a wild type littermate control mouse (6-2), **(B)** Peritoneal cells from a wild type non-littermate control mouse (sp-5), **(C)** Peritoneal cells from a Eμ-PKCβII transgenic mouse (hom-9).

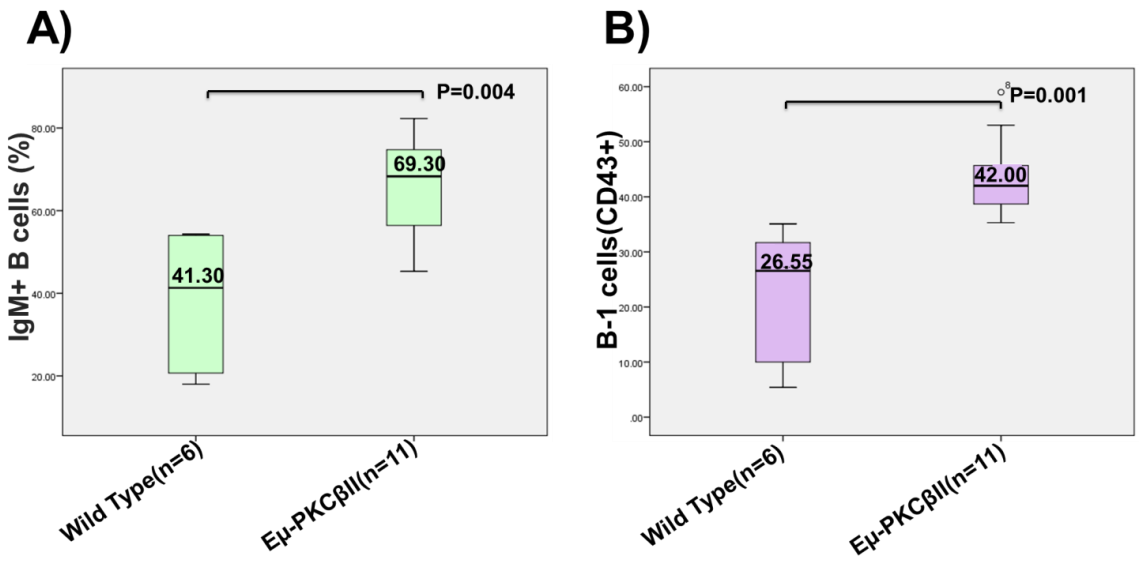

Figure 5-20. Statistical comparison of IgM$^+$ and B-1 B cells in wild type and Eμ-PKCβII tg mice. Box plot representation comparing percentage of **A)** IgM$^+$ B cells, and **B)** B-1 cells in the B220$^+$ population of cells isolated from peritoneum of 6 wild type and 11 11 Eμ-PKCβII tg mice. Statistical significance was assessed using a Mann-Whitney U test.

5.4.3 Peripheral Blood

B cell characterisation in peripheral blood followed the same protocol as for spleen and peritoneum, that is, I gated on live lymphocytes that were B220+. I then did two separate analysis; one analysing the expression of IgD and IgM and a second measuring CD5 expression on B220+ cells. I did this because the antibody I used split the analysis so that simultaneous analysis of IgM and CD5 was not possible. For this analysis littermate control mice were unavailable and so all comparisons are made using the non-littermate wild type mice.

Figure 5-21 shows the FACS traces of the analysis I performed, comparing a single non-littermate wild type mouse with two homozygous PKCβII transgenic mice. The most striking observation is the large increase in percentage of IgD^{dim}IgM$^{+/-}$ B cells in transgenic compared to wild type mice (Figure 5-21A). This increase of IgD^{dim}IgM$^{+/-}$ B cells in transgenic mice corresponded with a significant decrease in the percentage of IgD^{hi}IgM$^-$ cells compared to wild type mice (Figure 5-21B). These data show that B cell

subpopulations differ in the peripheral blood of wild type and transgenic mice, and suggest that it is overexpression of PKCβII that forces this shift.

Further analysis of B220+ cells using CD5 expression showed that transgenic mice have an increase in the numbers of CD5+/B220+ cells (Figure 5-21). These CD5+/B220+ cells are likely to be B-1a cells because of the lower expression of B220 compared to the $CD5^{-}/B220^{sharp}$ cells located in the lower right hand corner of the FACS trace (Figure 5-21). An informative statistical comparison of CD5+/B220+ cells was not possible between transgenic and wildtype mice because of insufficient numbers of wildtype mice. However, the boxplots shown in Figure 5-22 suggests the populaton of immature B cells ($IgD^{dim}IgM^{+/-}$) was significanly increased (part B) whereas the FO B cells ($IgD^{+}IgM^{-}$) was significantly decreased (part A). Thus, the B-1a B cell population was expanded in transgenic mice and this is supported by the significant expansion of $IgD^{dim}IgM^{+/-}$B cells in these mice. B-1 cells are typically $IgD^{dim}IgM^{+/-}$ (Hua Gu 2004). Thus, transgenic expression of PKCβII results in a shift in peripheral blood B cells towards a B-1a phenotype.

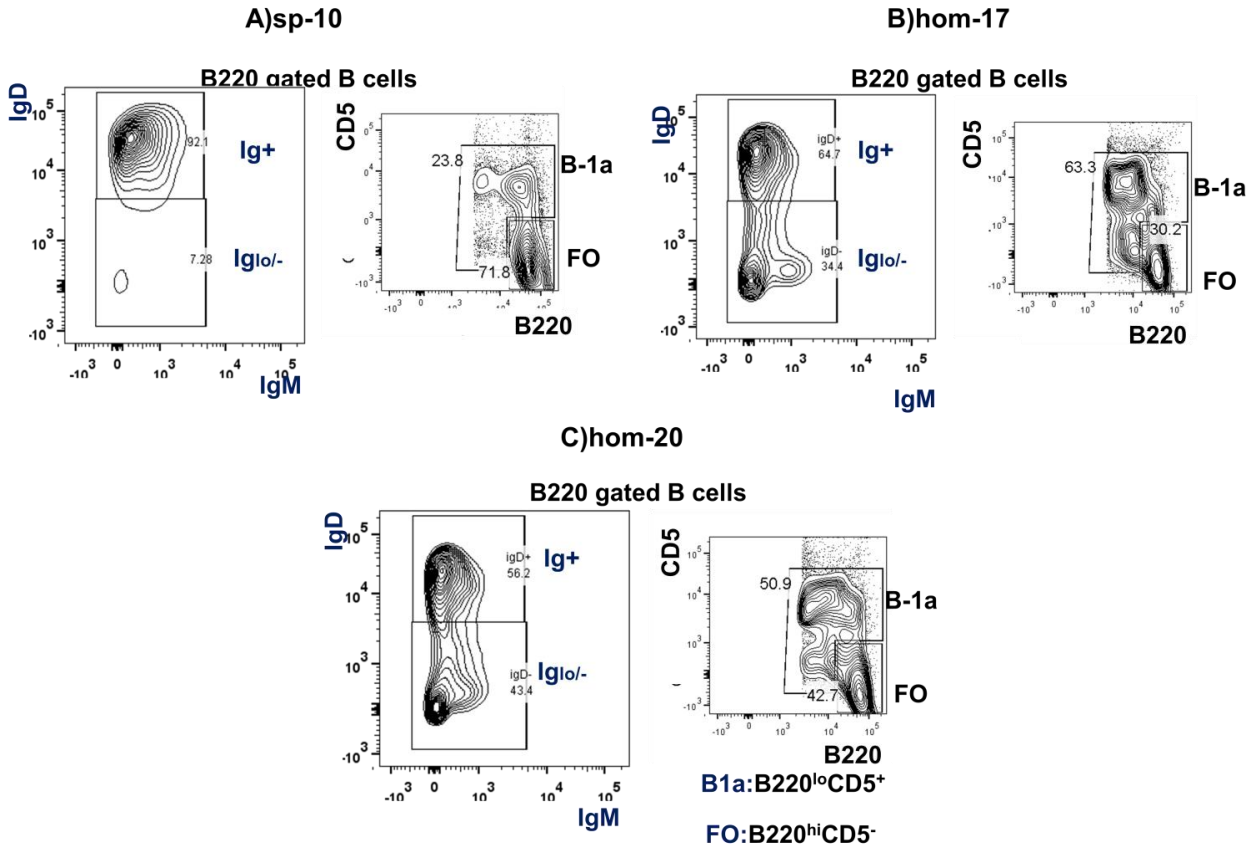

Figure 5-21. FACS analysis of peripheral blood B cells in wild type and Eμ-PKCβII tg mice. The purpose of the FACS analysis of peripheral blood B cells was to detect (**FO**) B cells ($B220^{+}IgM^{low}IgD^{high}$) and **B-1** cells ($B220^{+}IgM^{+}IgD^{lo}CD5^{+/-}$) in the wild type and Eμ-PKCβII tg mice. Thus, the single cell suspension of peripheral blood cells was prepared from Eμ-PKCβII tg and wild type mice, and then, the samples were stained with B220, IgM, IgD and CD5 markers. This was followed by flow cytometry analysis. **(A)** Peripheral blood cells from a wild type non-littermate control mouse (sp-10), **(B)** and **(C)** Peripheral blood cells from Eμ-PKCβII tg mice hom-17 and hom-20.

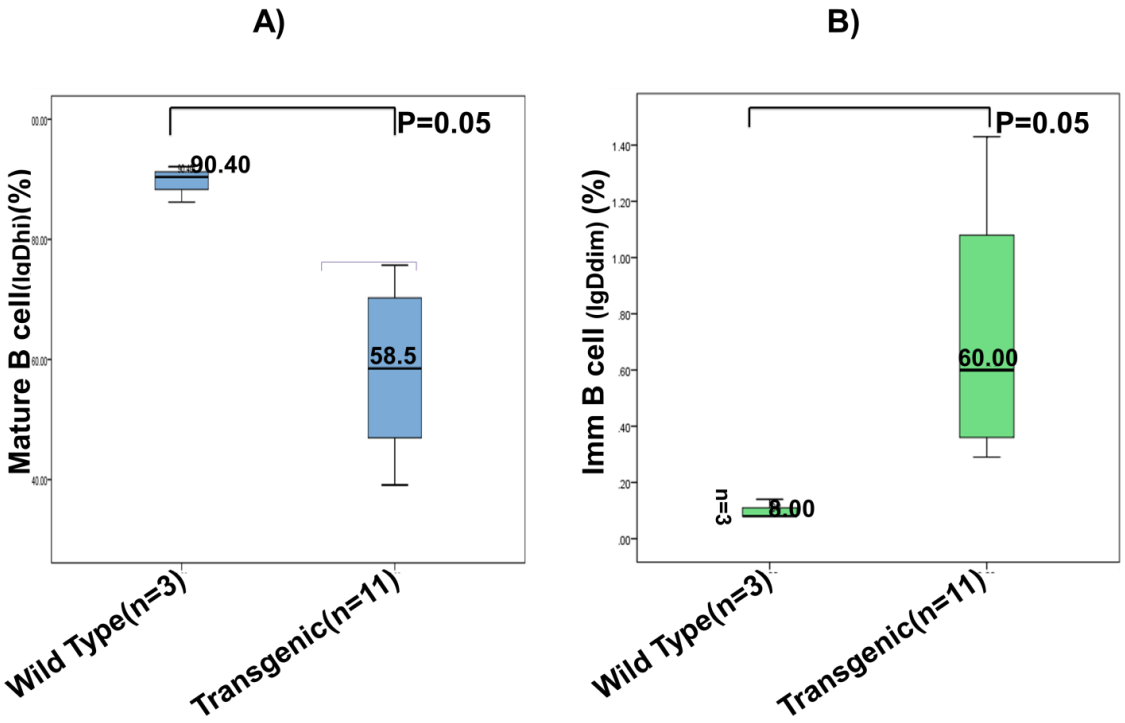

Figure 5-22. Statistical comparison of mature and immature B cell populations in peripheral blood of wild type and Eμ-PKCβII tg mice. Box plot representation comparing percentage of **A)** mature B cells ($IgD^{+}IgM^{-}$), and **B)** immature B cells ($IgD^{dim}IgM^{+/-}$) in the $B220^{+}$ population of cells isolated from peripheral blood of 3 wild type and 11 Eμ-PKCβII tg mice. Statistical significance was assessed using a Mann-Whitney U test.

5.4.4 Bone Marrow

The bone marrow has a more complex compartment of B cell subsets and consists of pro B cells, pre B cells, immature B cells and mature naïve B cells. It was not possible to identify these compartments using the antibody staining protocol that was available. Because B-1 cells are highly represented in the peritoneum and peripheral blood of transgenic mice, I reasoned that these cells may be also highly represented in the bone marrow. Figure 5-23 shows the trace associated with my FACS analysis, and compares a non-littermate wild type control mouse with 2 homozygous EμPKCβII tg mice. I initially analysed for B220 and CD43 expression. From this analysis two populations of cells were visible; the first population consisted of $B220^{sharp}$ cells which

were CD43 negative, and a second population that were $B220^{low}$ that also showed some degree of CD43 positivity. Further analysis of the $B220^{low}$ cells showed that they were largely CD5 and IgM positive, indicating that they were B-1a cells. The $B220^{hi}$ cells were also analysed for IgD and IgM expression.

A comparison of percentage B-1a cells in wild type and EμPKCβII tg mice showed that this population increased in the transgenic mice. Statistical analysis was not possible because of insufficient numbers of control mice. However, the percentage of B-1a cells in the wild type animals is in line with reported values (Hardy and Hayakawa 2001, Hua Gu 2004) . Therefore, the increased percentage of these cells in transgenic mice is likely to reflect a shift in population, particularly because we observe a similar shift in the peritoneum and peripheral blood. Therefore, from this result I suggest that transgenic expression of PKCβII results in a shift in B cell development favouring the formation of B-1a cells.

A comparison of IgD and IgM expression on the $B220^{sharp}$ population of cells between wild type and EμPKCβII tg mice also showed a difference. Thus, the EμPKCβII tg mice saw the emergence of a IgM^{+}/IgD^{dim} population of B cells that was not present in the wild type mouse. This particular comparison was only done once and further investigation is necessary to draw a strong conclusion. Nevertheless, it still provides support for my conclusion that transgenic expression of PKCβII induces a shift in B cell populations.

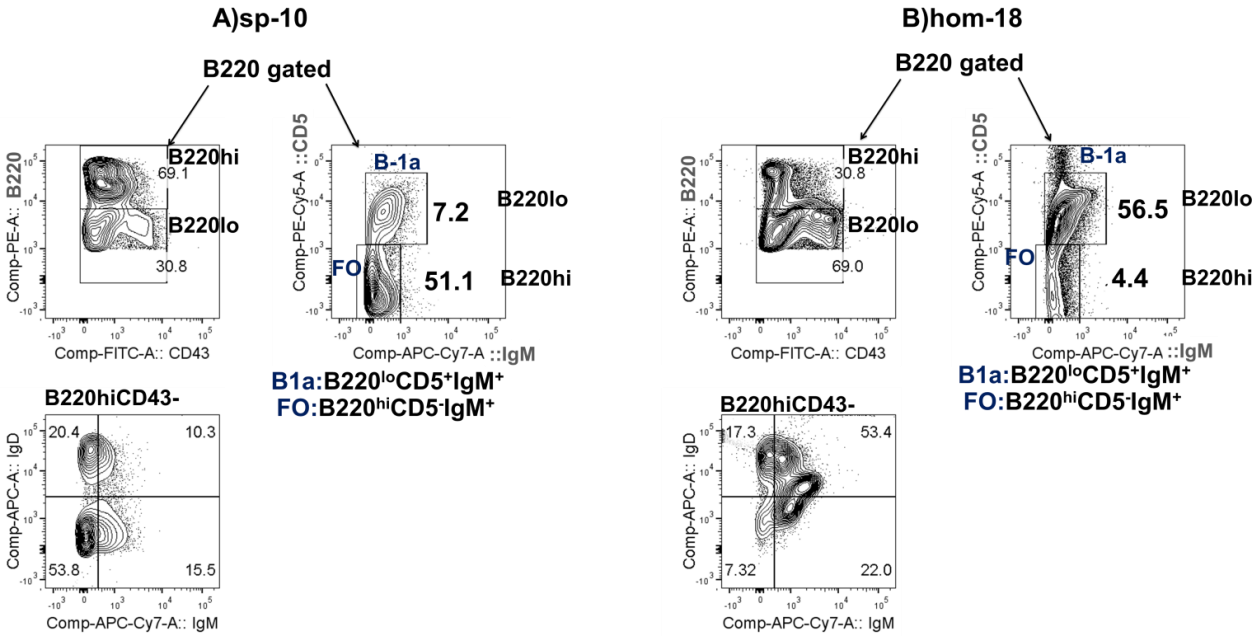

Figure 5-23. FACS analysis of bone marrow B cells in wild type and Eμ-PKCβII tg mice. The purpose of the FACS analysis of bone marrow B cells was to detect (**FO**) B cells ($B220^{+}IgM^{low}IgD^{hi}$) and **B-1a** cells ($B220^{+}IgM^{+}IgD^{lo}CD5^{+}CD43^{+}$) in the wild type and Eμ-PKCβII tg mice. Thus, the single cell suspension of bone marrow cells was prepared from Eμ-PKCβII tg and wild type mice, and then the samples were stained with B220, IgM, IgD, CD5 and CD43 markers. This was followed by flow cytometry analysis. **(A)** Bone marrow cells from a wild type non-littermate control mouse (sp-10), **(B)** bone marrow cells from Eμ-PKCβII tg mice hom-18.

5.4.5 Comparison of old and young PKCβII transgenic mice

So far my analysis has concentrated on comparing EμPKCβII tg mice with wild type controls. However, I generated a cohort of aged transgenic mice (14 months) and young transgenic mice (6 months). Here I analyse only splenic tissue. FACS analysis of splenic cells isolated from these mice showed that the population of $IgD^{low}IgM^{+}$ cells were more highly represented in older than in younger EμPKCβII tg mice. However, analysis of CD43 expression on $IgD^{low}IgM^{+}$ cells showed a significant shift in the older EμPKCβII tg mice (Figure 5-24), suggesting that in these animals the spleen was being colonised with B-1 cells. Importantly, the number of $IgD^{low/-}IgM^{+}CD43^{+}$ cells in EμPKCβII

tg mice was always greater than that observed in the littermate control mice (Figure 5-24). Also, in young EμPKCβII tg mice there is a distinct presence of MZ B cells (See section 5.4.1). Taken together, these results therefore suggest that as EμPKCβII tg mice age there is a shift towards colonisation of the spleen with B-1 cells.

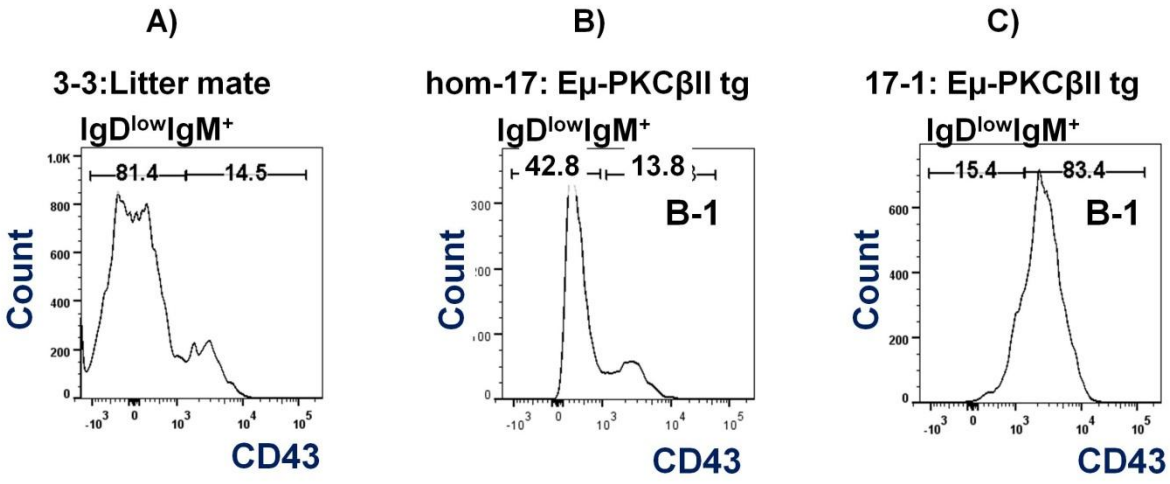

Figure 5-24. FACS analysis of splenic B cells of young, old Eμ-PKCβII tg and wild type mice. This figure shows FACS analysis of cell suspensions prepared from splenic tissue of wild type and Eμ-PKCβII tg mice, with the purpose of identifying B-1 cells ($IgD^{low/-}IgM^{+}CD43^{+}$) in cells already gated for $IgD^{low}IgM^{+}$. **(A)** Splenic cells from a wild type littermate control mouse (3-3, 14 month old). **(B)** Splenic cells from a young Eμ-PKCβII tg mouse (hom-17, 6 months old). **(C)** Splenic cells from a old Eμ-PKCβII tg mouse (17-1 14 month old).

5.5 Functional Assay

So far my characterisation of the EμPKCβII tg mouse shows that transgenic expression of PKCβII in B cells causes changes in the B cell populations of the spleen, peritoneum, peripheral blood and bone marrow. The next important question that needed to be addressed was whether transgenic PKCβII was functional. One role of PKCβII in B cells is to interact and regulate channel-mediated Ca^{2+} entry in B cells during antigen receptor (B cell receptor, BCR) engagement(Numaga*, et al* 2010). To

measure intracellular Ca^{2+} in splenic cells isolated from wild type and EμPKCβII tg mice I used the green-fluorescent calcium indicator Fluo-4. To identify B cells within the splenic cells I gated on CD20+ cells. Figure 5-25 shows a comparison of basal Fluo-4 expression in splenic $CD20^{+}$ cells isolated from EμPKCβII tg and wild type mice. What is clear is the increased level of basal fluorescence associated with cells isolated from EμPKCβII tg mice. This shift was reproducible across 4 EμPKCβII tg mice compared to 2 wild type mice. Fluo-4 is not suitable for absolute quantification of intracellular calcium levels in cells. This suggests that basal calcium levels may be higher in cells over-expressing PKCβII.

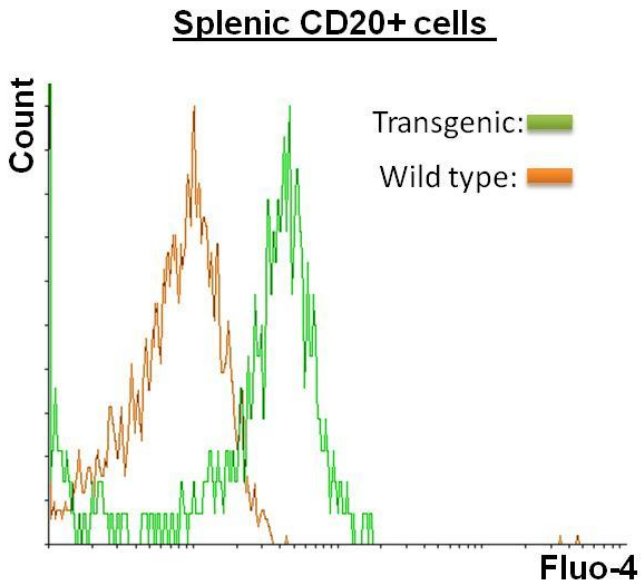

Figure 5-25. Intracellular Ca^{2+} levels in CD20+ cells isolated from splenic tissue of Eμ-PKCβII tg and wild type mice. Intracellular Ca^{2+} in CD20+ splenic cells was measured using the green-fluorescent calcium indicator Fluo-4. This figure is an overlay histogram comparing fluorescence associated with Fluo-4 detection of calcium in cells from Eμ-PKCβII tg (**green line**) and wild type mice (**brown line**). This figure is representative of measurements in cells from 4 Eμ-PKCβII tg and 2 wild type mice.

5.6 PKCβII expression in the MDR-KO mouse model of CLL

In this final section of my thesis I analysed the MDR-KO mouse model for expression of PKCβII. This has not until now been previously done and is important to understand the role in PKCβII in the pathogenesis of the CLL like disease in these mice. In total, four MDR-KO mice were analysed and one of them developed splenomegaly (Figure 5-26A). FACS analysis of live lymphocytes derived from MDR-KO and age-matched control wild type mice showed that the population of CD5+ B-1 B cells was expanded in the spleen, peritoneum and peripheral blood of the MDR-KO mice confirming the results of the original paper(Figure 5-26B). Analysis of protein lysates prepared from spleen tissue of four MDR-KO mice and two aged matched control wild type mice by Western blot showed that PKCβII was more highly expressed in MDR-KO mice than in the wild type mice (Figure 5-26C and D). To conclude, these data show that PKCβII expression is up-regulated in MDR-KO mice and suggest a parallel with human CLL where PKCβII is also overexpressed.

This completes the characterization of the EμPKCβtg mouse I have generated. The implications of my findings regarding the phenotype of this mouse I will now discuss in the general discussion of this thesis.

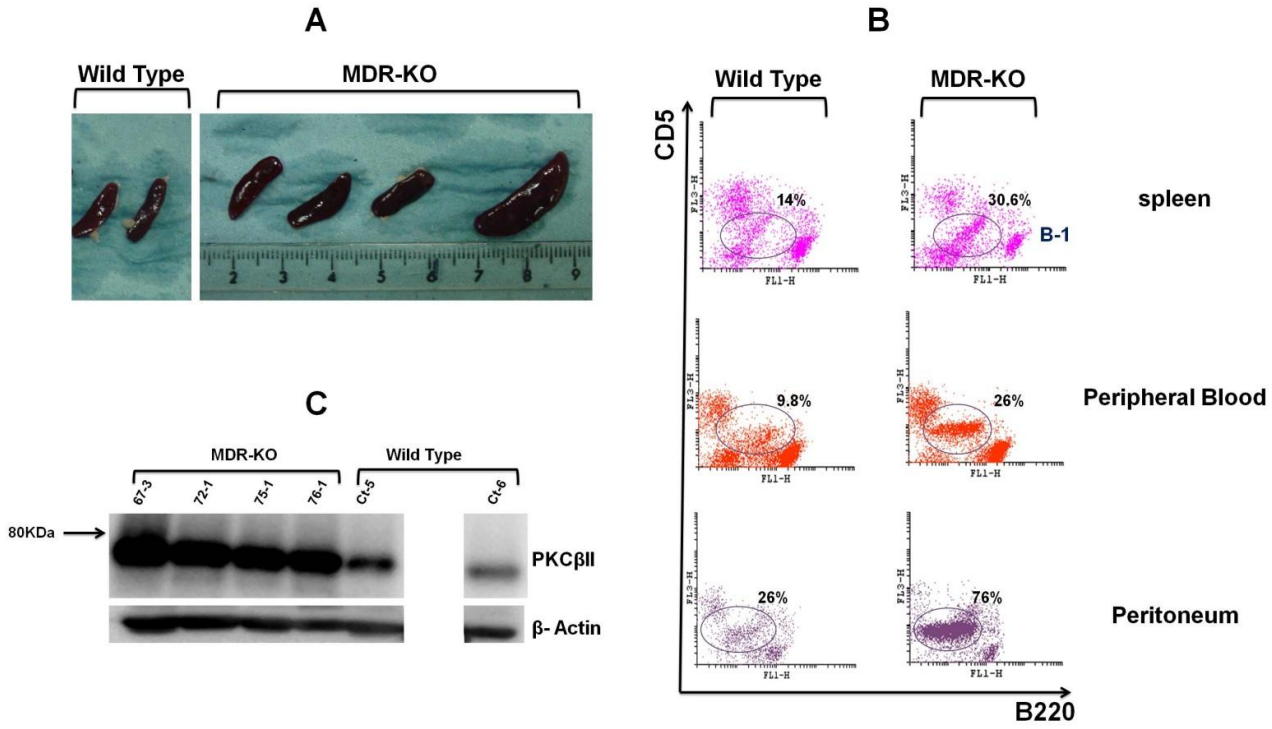

Figure 5-26. PKCβII expression in MDR-KO mice. (A) A photograph taken from the spleen tissues isolated from 4 MDR-KO and 2 age-matched wild type mice. **(B)** FACS analysis of live lymphocytes derived from spleen, peripheral blood and peritoneum of MDR-KO and age-matched wild type mice for the detection of B-1 cells ($B220^{lo}CD5^{+}$). **(C)** Western blot analysis of protein lysates of splenic tissue isolated from four MDR-KO mice and two aged matched wild type mice for detection of the PKCβII protein.

6 Chapter VI: General discussion

Genetic engineering of mice by transgene insertion and deletion is a powerful approach in the investigation of gene function in mouse development and disease pathogenesis. In particular, mice with particular transgenic changes have been used to model human disease and as preclinical platforms for the testing of new drugs. With respect to CLL there are several mouse models, with each exploiting a different pathological feature of human CLL cells. For instance, mice that are transgenic for the gene Tcl-1 develop an aggressive form of CLL (Bichi*, et al* 2002), whereas transgenic mice that have had the genes coding for miR-15a/16-1 deleted have a more indolent disease (Klein*, et al* 2010). Interestingly, the strain of New Zealand Black mice that spontaneously develops CLL also has defects in the expression of miR-15a/16-1 (Raveche*, et al* 2007). In almost all CLL mouse models, the CLL-like malignancy develops from an initial expansion of IgM^+CD5^+ B-1 cells (Oppezzo 2012). This is important because in human CLL it is proposed that the malignant cells develop from a similar expansion of B-1 cells (Chiorazzi and Ferrarini 2003, Seifert*, et al* 2012). Importantly, the malignant cells in both human and the mouse models of CLL congregate in lymphoid tissues such as the spleen and in peritoneum, and eventually lymphocytosis is observed in the peripheral blood (Chiorazzi*, et al* 2005, Oppezzo 2012).

Previous work from this Department has shown that the malignant cells from patients with CLL express high levels of PKCβII compared to peripheral blood B cells isolated from normal age-matched subjects (Abrams*, et al* 2007). In the present thesis I have found that this PKC isoform is highly expressed in the malignant cells of MDR mice, indicating that overexpressed PKCβII is also a feature of this mouse model of CLL. PKCβII may contribute to the pathogenesis of CLL because it plays an important role in regulating BCR signaling and because BCR signaling plays a role in the pathogenesis of this disease (Burger and Chiorazzi 2013, Oppezzo and Dighiero 2013). This hypothesis is supported by a study showing that when the Tcl-1 transgenic mouse is crossed with PKCβII knock-out mice, CLL-like disease does not develop (Holler*, et al* 2009). The failure to develop disease in this Tcl1tg/PKCβ-KO model could be because IgM^+CD5^+ B-1 cells from which the malignant cells develop are not present due to the disruption of

PKCβ expression, and/or because the microenvironment does not support growth of the malignant clone as has been suggested in a recent study by Luzny et al (Lutzny G 2013).

The aim of this thesis was to generate a PKCβII transgenic mouse in which (over) expression of PKCβII occurs specifically in B cells. Because of the role of PKCβ in regulating BCR signaling, and because B-1 cells are specifically deleted in mice where the gene coding for PKCβ has been disrupted (Holler*, et al* 2009), I hypothesized that specific overexpression of PKCβII in B cells would lead to expansion of the B-1 cell compartment in transgenic mice, and possibly to the development of CLL at a later stage.

In Chapter 3, I describe construction of the expression construct I used to generate Eμ-PKCβII tg mice. This construct contained an Eμ promoter so that expression of the gene would only occur in B cells. The genes to be expressed under the control of the Eμ promoter were PKCβII and mCherry. Transgenic PKCβII was tagged with HA so that I would be able to discriminate transgenic from endogenous protein. The gene coding for mCherry fluorescent protein was including for imaging purposes, and the PKCβIIHA and mCherry genes were separated from each other by an internal ribosomal entry site (IRES) so that both genes would be expressed from the Eμ promoter. This expression construct was then tested in a mouse B cell line (A20 cells), and it was shown to be functional; both PKCβIIHA and mCherry were expressed in the cell line that was generated. Thus, my expression construct was ready for injection into fertilized egg cells to generate founder mice.

Chapter 4 describes establishment of a homozygous Eμ-PKCβII tg mouse line. I injected the Eμ-PKCβIIHA-IRES-mCherry construct into fertilized mouse egg cells, and transferred these cells into the oviduct of recipient foster mice. The mouse pups born from these recipient mice were screened for the presence of the transgene using two techniques, Southern blotting and PCR detection of the transgene. Both techniques are complementary and reduce the chance of a false positive or negative. One founder mouse, a female, was detected. An approximation of the number of transgene copies inserted into her genome was made and determined to be between 5 and 10. This

mouse was then used to back-cross with wild type mice in order to generate F-1 progeny. F-1 progeny were screened for presence of the transgene, again using PCR and Southern blotting, and those animals carrying the transgene in their genomic DNA were kept and used for inter-crossing and generation of homozygous Eμ-PKCβII tg mice within the F-2 progeny. With respect to the generation of the F-2 progeny I expected a Mendelian ratio of 25% wild type: 50% heterozygous Eμ-PKCβII tg: 25% homozygous Eμ-PKCβII tg. My screening of the F-2 progeny showed that this was in fact the case suggesting that my transgene was inserted at a single site within the autosomal chromosomes. Here I additionally used quantitative PCR to distinguish between heterozygous and homozygous Eμ-PKCβII tg mice. Detected homozygous Eμ-PKCβII tg mice were confirmed by crossing these animals with wild type mice. The litters of these crossings were expected to be all heterozygous for the transgene. I found that most of the animals I had designated homozygous for the transgene were, in fact, homozygous. Thus, I had generated a homozygous Eμ-PKCβII tg mouse line which was now ready for phenotypic analysis.

Chapter 5 of my thesis describes the phenotype of the Eμ-PKCβII tg mouse line I generated, and the rest of this section of my thesis will discuss what I found. Importantly, although the animals were allowed to age for 14 months there was no notable development of disease, CLL-like or otherwise. This could be because development of disease in this model is indolent, and the detection of disease may have required more animals than were available to me. In all CLL mouse models that have been generated so far, CLL-like disease takes at least 12 months to develop with models of indolent disease taking longer. In the model of indolent CLL developed by Klein et al detection of disease required a comparison of 34 homozygous with 23 wild type mice(Klein*, et al* 2010). For my thesis I was only able to age 4 homozygous and 3 heterozygous Eμ-PKCβII tg mice, and 3 wild type littermate controls to 14 months. Generation of a larger cohort of older mice was unavailable due to structural changes of the animal holding facilities at the University of Liverpool, and to mistakes made by the staff of the holding facility. Thus, the rest of this Chapter is concerned with discussing the phenotype of mice where PKCβII is overexpressed within B cells.

The first step in my analysis of the phenotype of Eμ-PKCβII tg mice was to detect expression of the transgene. I prepared protein lysates of splenic tissue from Eμ-PKCβII tg and wild type mice, and probed these lysates by Western blot for the presence of PKCβIIHA and mCherry. Whereas I could detect PKCβIIHA both as HA-tagged protein and as overexpressed PKCβII, I could not easily detect mCherry. A possible explanation for the failure to detect mCherry comes from a recent review about variability of expression when genes are separated within a plasmid by an IRES sequence. This review argues that expression of the secondary gene was not always efficient because of variable transcription from the IRES sequence. (Kozak 2005).When building the Eμ-PKCβIIHA-IRES-mCherry expression construct I ensured it was functional within a mouse B cell line, and I determined that PKCβIIHA and mCherry proteins were expressed. However, expression of genes following an IRES sequence might be cell specific, and mCherry was only very weakly expressed in the differentiating B cells of the transgenic mouse I generated.

In contrast to mCherry, PKCβIIHA was expressed in B cell-rich tissues of the Eμ-PKCβIIHA tg mouse. This determination was made by comparing Western blots of protein lysates prepared from spleen and liver; splenic tissue expressed PKCβIIHA protein and liver tissue did not. Immunohistochemistry was used to confirm expression of PKCβIIHA in B cell-rich tissues. Here, staining for either HA or for PKCβII showed that high expression of these epitopes in splenic tissue of Eμ-PKCβII tg mice located to the white pulp, and specifically to the follicular region. I used sequential slices of splenic tissue to show that HA and high expression of PKCβII was co-localized. This is important because endogenously-expressed PKCβII in splenic tissue needs to be differentiated from transgenic PKCβIIHA, and demonstration of overexpressed PKCβII co-localizing with HA staining indicates specificity with respect to expression of the transgene, and demonstrates successful generation of a mouse which expresses transgenic PKCβII.

The central hypothesis of this thesis is that over-expression of PKCβII in developing B cells will shift development to favour the generation of transitional B cells

and expand the B-1 and MZ B cell populations. This hypothesis is based on a paradigm whereby Btk determines B cell developmental fate through its role in regulating BCR signaling (Cariappa*, et al* 2001, Pillai and Cariappa 2009), and on findings reported by Leitges et al who have generated a mouse model in which the gene encoding for PKCβII was disrupted. Disruption of PKCβ expression results in the generation of mice which showed a reduction of splenic B-cells, a reduction of serum IgM and a significant decrease in $IgM^{+}CD5^{+}$ B-1 cells in the peritoneum (Leitges*, et al* 1996). This phenotype and impaired B-cell activation are reminiscent of both X-linked immunodeficiency (XID) in mice in which a single amino acid substitution introduced into the pleckstrin homology domain of Btk blocks its membrane association and effective activation (Kerner*, et al* 1995), and mice in which Btk expression has been genetically (Maas and Hendriks 2001) disrupted (Khan*, et al* 1995). This similarity links PKCβ to the regulation of Btk function, and to a B cell developmental pathway.

Where Btk is important in determining B cell fate in bone marrow is at the first immune tolerance checkpoint. Here, auto-reactive B cells become susceptible to apoptosis because of strong BCR engagement, and Btk plays a very important role in providing pro-apoptotic signaling as demonstrated in studies of Btk containing a E41K gain-of-function mutation. This mutation results in a structural change in Btk that allows constitutive association with the plasma membrane leading to activation of the kinase (Li*, et al* 1995, Varnai*, et al* 1999). In transgenic mice where expression of Btk (E41K) is controlled by the promoter for CD19, B cell development is arrested at the stage where immature B cells that are IgM^{low} differentiate to IgM^{hi} B cells. The reason why all B cell development is impaired at this point is because the constitutive activity of Btk (E41K) mimics strong antigen receptor engagement (Maas*, et al* 1999, Maas and Hendriks 2001).

PKCβ is linked to Btk function through an ability to phosphorylate serine 180 within the Tec homology domain of Btk and promote its dissociation from the plasma membrane, an action which leads to down regulation of Btk activity (Kang*, et al* 2001) . Thus, in the absence of PKCβ BCR signaling is stronger due to release of feedback inhibition of Btk (Kang*, et al* 2001). The reason why the phenotype in PKCβ KO mice

resembles that of Btk KO or *Xid* mice is unclear. A greater proportion of developing B cells should be deleted at the first immune tolerance checkpoint (Paul 2003) because the increased strength of Btk signaling in PKCβ KO mice would lead (Abrams*, et al* 2010 Paul 2003) to a greater degree of negative selection. However, transitional B cells emerging from the bone marrow further develop in the spleen where BCR signaling strength is required for the generation of B cell subsets. Here, strong BCR signals lead to the development of follicular B cells, weak BCR signals lead to the development of MZ and B-1 B cells (that are derived from bone marrow progenitors) and cells in which BCR signaling is absent would undergo apoptosis due to neglect (Cariappa*, et al* 2001, Maas and Hendriks 2001). In this environment the absence of PKCβ would lead to favoured development of follicular B cells. Generation of B-1 B cells in PKCβ KO mice could also be affected at an earlier stage in their development. Although it is known that B-1 cells mainly derive on the foetal liver during embryogenesis, the processes involved have not been studied (Kantor*, et al* 1992, Montecino-Rodriguez and Dorshkind 2012).

This model where PKCβ affects Btk activity agrees with a "strength of signal" model proposed by Cariappa et al (Cariappa*, et al* 2001) (illustrated in Figure 6-1). Within this model, transitional B cells in the spleen respond to relatively strong or "triggered" signals delivered via the BCR with commitment to follicular B cell differentiation. Transitional B cells receiving weaker or "tickled" signals from the BCR differentiate into MZ B cells. Thus, the strength of BCR signaling is inversely related to the generation and survival of MZ B cells (Cariappa*, et al* 2001). The data I provide in Chapter 5 support this model. Overexpression of PKCβII should weaken BCR signaling in Transitional B cells, and lead to the preferred development of MZ B cells in the spleen. This is exactly what I observe and is shown in Figures 5.4.2 and 5.4.4. Thus, in the EμPKCβII tg mice I observe a reduction in the proportion of follicular B cells and an increase in the proportion of MZ B cells. This expansion of MZ B cells is not only observed using flow cytometry, but is also apparent in H&E stains indicating an enlarged MZ (See Section 5.3.1) within the structure of the spleen, and in IgM stains showing that this expanded MZ consists mainly of IgM+ cells (see section 5.3.1).

I also observe in splenic tissue of EμPKCβII tg mice an expanded population of B-1 cells. Moreover, whereas in the control mice there was an equal distribution of B-1b and B-1a cells, in the EμPKCβII tg mice there was a preference for B-1a cells. Importantly, I observed that the proportion of B-1 cells in the spleen expands as the mouse ages (Figure 5.4.11). It is unclear why B-1a cells are resident in the splenic tissue of EμPKCβII tg mice in greater numbers than is observed in wild type mice. The development of the B-1 cell lineage occurs mainly within foetal tissues such as the yolk sac and then liver. However, B-1 cells can derive from bone marrow progenitors, but are produced at much lower numbers (Montecino-Rodriguez and Dorshkind 2012). Also, it has been recently suggested that B-1 cells can arise from sIgM+CD93+CD23+/- transitional B cells that are predominantly in the spleen of neonatal mice (Montecino-Rodriguez and Dorshkind 2011). Here, this population of B-1 cells dramatically decreases in favour of the B-2 (follicular) population as the mouse ages due to unknown reasons. In EμPKCβII tg mice the overexpressed PKCβII may maintain this neonatal B-1 cell population, and later expand it as the mouse ages.

Expansion of the B-1 cell population was particularly apparent in the peritoneum of Eμ-PKCβII tg mice. Typically, the peritoneum is the area of the body which is rich in B-1 cells, with these cells probably resulting from foetal progenitors. The expanded B-1 cell population I observe in this compartment of the Eμ-PKCβII tg mice may result from favoured production and survival of foetal cell-derived B-1 cells, but may also result from additional favoured production and survival of B-1 cells derived from bone marrow progenitors. The evidence for the latter proposal comes from my observation that there is an apparent expansion of CD5+ B cells in bone marrow of Eμ-PKCβII tg mice compared to wild type mice, and, as discussed above, there is an expansion of B-1a cells in the spleen.

In peripheral blood I observed expansion of a IgM+/IgD^{dim} B cell population and concomitant reduction of IgM+/IgD+ mature B cells in the Eμ-PKCβII tg mice. The IgM+/IgD^{dim} B cells could be transitional B cells that will eventually further differentiate in the spleen to MZ and B-1 cells. A proportion of these IgM+/IgD^{dim} B cells could also be B-1 cells because B-1 cells are typically IgM+/IgD$^{-/dim}$ (Hua Gu 2004). Support for this

assertion comes from a single experiment where I analyzed IgM+ peripheral blood B cells for CD5 expression. I found that B cells that were $IgM^{+}CD5^{+}$ were much better represented in the EμPKCβII tg mice I analyzed (see section 5.4.3).

Taken together, my use of flow cytometry and immunohistochemistry to characterize the phenotype of EμPKCβII tg mice demonstrate favoured development of IgM+ B cells, and, in particular MZ and B-1 B cells. Thus, I conclude that my hypothesis is true. What remains is to discuss potential functional changes in the B cells of these mice resulting from the overexpression of PKCβII.

First, overexpressed PKCβII may affect survival of specific B cell populations through its role in activation of the NFκB pathway in BCR-stimulated cells. Here, PKCβ operates to phosphorylate CARMA1 leading to the assembly of a complex consisting additionally of Bcl10, the ubiquitin E3-ligase MALT1 and the MAP3K TAK1. NFκB pathway activation occurs when the CARMA1-Bcl10-MALT1 complex recruits IKKγ where the ensuing ubiquitination of this latter protein stimulates TAK1-mediated phosphorylation and activation of IKKβ. This, in turn, catalyzes the downstream phosphorylation and degradation of IκBα leading to the translocation of RelA to the nucleus where it is able to stimulate gene transcription (Shinohara*, et al* 2005). Theoretically, I should observe enhanced NFκB pathway activation in the B cells of EμPKCβII tg mice, and this may contribute to the phenotype I observe because maintenance of NFκB pathway signaling is important for B cell development, particularly when transitional B cells are undergoing further differentiation in the spleen (Pillai and Cariappa 2009).

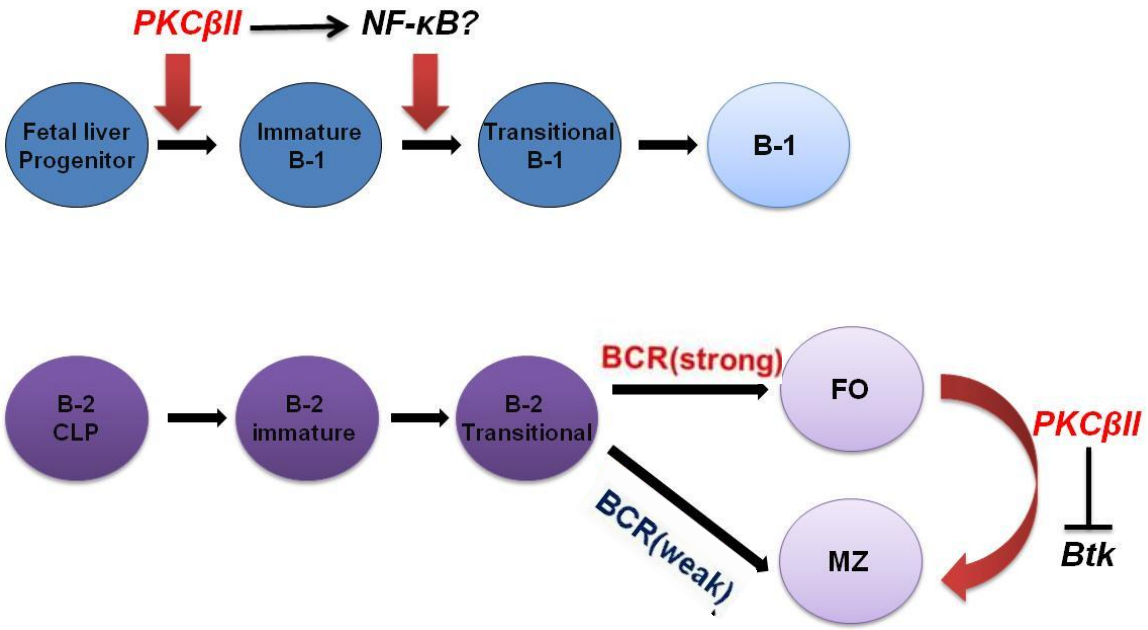

Figure 6-1. Schematic describing possible explanations for the phenotype observed in Eμ-PKCβII tg mice.

Overexpressed PKCβII could additionally play an important role in maintaining calcium homeostasis in B cells (Abrams*, et al* 2007). Obviously, down-regulation of Btk function would limit BCR-induced calcium release from internal stores in B cells. However, PKCβII is also demonstrated to regulate the function of a calcium channel during BCR engagement (Numaga*, et al* 2010), and overexpressed PKCβII may lead to increased intracellular calcium levels in the B cells of EμPKCβII tg mice. My results suggest that B cells isolated from splenic tissue of EμPKCβII tg mice have higher basal intracellular calcium levels than do B cells from wild type mice, and further characterization is necessary to confirm this observation. Nevertheless, higher levels of calcium would potentially result in constitutive NF-AT activity, and possibly support B-1 cell development as is suggested in one study showing that B-1 cells in mice have constitutive activation of NF-AT (Wong*, et al* 2002). Further work characterizing this phenomenon in EμPKCβII tg mice is now necessary.

The EμPKCβII tg mice also potentially reveals a specific role for PKCβII in B cells. The gene for PKCβ is transcribed as two splice variants, PKCβI and PKCβII. These

variants differ from one another in the C-terminus of the protein, particularly in the last 50 amino acids (Ono*, et al* 1986). So far a clear role for either PKCβI or PKCβII in phosphorylation of Btk or CARMA1 has not been demonstrated. An early study of mast cells suggested that PKCβI could down-regulate Btk function (Kawakami*, et al* 2000). A recent second paper examining B cells of mice bearing a mis-sense mutation in *prckb* that results in down-regulated expression of PKCβI has shown this to result in a decreased B-1a cell population in the peritoneum (Teh*, et al* 2013) (Teh*, et al* 2013). These results are at odds with the findings I present in this thesis showing that overexpression of PKCβII leads to expansion of the B-1a cell population. One explanation could be that PKCβII can substitute for PKCβI function where the former is overexpressed. However, further work will be needed, possibly crossing the EμPKCβII tg mice with PKCβ KO mice in order to remove endogenous expression of PKCβI and PKCβII in order to more clearly define the role of PKCβII.

Although I did not observe development of CLL-like disease in the EμPKCβII tg mice I generated, the model I have created still deserves comment with respect to mouse models of CLL. There is now stronger evidence suggesting that human CLL develops from a B-1 lineage, with this evidence coming from genetic array analysis comparison of human CLL cells with a human equivalent of B-1 cells (Seifert*, et al* 2012). Moreover, in virtually all of the existing mouse models of CLL the malignant cells derive from an expansion of B-1 B cells. However, in an earlier review Chiorazzi and Farrarini suggested that the normal counterpart of CLL in humans could derive from MZ B cells because these cells display many key features of mutated and un-mutated CLL cells (Chiorazzi and Ferrarini 2011). In EμPKCβII tg mice both the MZ and B-1 B cell populations are expanded, possibly facilitating the development of CLL if crossed with either the Tcl1tg or MDR-KO mouse models. Support for this notion is supplied by my observation that PKCβII is overexpressed in splenic tissue derived from MDR-KO mice.

In conclusion, this thesis relates the generation of a mouse that overexpresses PKCβII specifically within the B cell compartment. The phenotype that is generated shows expanded populations of IgM+ B cells and a reduction of follicular (mature B cells). Within the IgM+ B cells, there appears to be favoured development of MZ and B-1

B cells in the spleen, and B-1 B cells in the peritoneum, peripheral blood and bone marrow. This mouse may be useful for the study of human CLL because of the potential to accelerate disease development, and would therefore serve as a useful model for drug testing.

Appendix A: Oligonucleotides

Primer	Sequence (5' →3')	Length	GC%	Tm(°C)
PKCP1	AGTGCCAAGTTTGCTGCTTT	20	45	60.06
PKCP2	GAAGGAAGTGAGGCCAATGA	20	50	60.20
PKCP3	TGGCACTCCAGACTACATCG	20	55	59.86
PKCP4	GACCCACAGTGGTCACAAAA	20	50	59.41
PKCP5B	GCTGAAAACTTCGACCGATT	20	45	59.32
5'ClaIPKC	GAGAATCGATCAAGATGGCTGACCCGGC TGCGGGGCC	37	64.9%	>75
3'SalIHAPKC	GAGAGTCGACTCAAAGAGCGTAATCTGG AACATCGTATGGGTAGCTCTTGACTTCGG GTTTTAAA	65	44.6%	>75
5'SalIIRES	GAGAGTCGACCATGCATCTAGGGCGGC CAATTCCGC	36	61.1%	>75
3'BamHIIRES	GAGAGGATCCATGGAAGGTCGTCTCCTT GTGGGTTG	36	55.6%	74.0
mChPROBE-F	GAGGGCACCCAGACCGCCAA	20	70%	65.5
mChPROBE-R	GTCCARGCCGCCGGTGGAGT	20	70%	65.5
pA2	ATTAAAGAGGCCTGCTCAAGG	21	47.6%	57.9
pB2	GACTGTCTGTGTCCTAGCTCATC	23	52.2%	62.4
pD2	TTAGGAACACGTCCTTGTTGG	21	47.6%	57.9
gapdh-F1	CATGGTCTACATGTTCCAGTATGACTCC	28	65.1	46.4%
gapdh-R1	ATGGTGATGGGCTTCCCG	18	58.2	61.1%

Appendix B: Plasmids

i. **pBSVE6BK**: pBSVE6BK (pEμ) plasmid was provided by Dr. Raif Geha (Harvard Medical School, Boston MA, USA). This plasmid is based on a pBluescript-IISK Phagemid backbone that has been modified to include the mouse IgH Promoter and IgH-Eμ enhancer elements, as well as the poly (A) site of Human β-globin gene.

ii. **pCR2.1 (Invitrogen):** a cloning plasmid that is designed to receive PCR products. It uses a commercial cloning strategy designated as a TA cloning® Kit.

iii. **pCEP4 (Invitrogen):** a mammalian expression vector that exploits the CMV promoter to drive over-expression of genes. It carries a gene for ampicillin resistance for cloning purposes, and for Hygromycin resistance for generating stable cell lines expressing the gene of interest.

iv. **pmCherry (Clontech):** a prokaryotic expression vector containing the mCherry gene. mCherry is a fluorescent protein derived from DsRed (a natural fluorescent protein from *Tetrameric diacosoma*). The excitation and emission maxima of mCherry are 587 nm and 610 nm, respectively.

v. **pIRESpuro3:** this plasmid contains an internal ribosome entry site sequence (IRES) of the encephalomycarditis virus (ECMV). The IRES sequence allows the translation of two open-reading frames from a single messenger RNA.

vi. **Phagemid vector pBK-CMV- N-EGFP (pPKCβ-EGFP):** This plasmid encodes a fusion protein, consisting of PKCβII and enhanced green fluorescent (EGFP).EGFP is a red-shifted, human codon-optimized variant of GFP that has been optimised for brighter fluorescence and higher expression in mammalian cells. PPKCβ-EGFP is expressed under the constitutive human CMV immediate-early promoter. Also, the plasmid has a neomycin-resistance cassette (Neo) containing the SV40 early promoter, the Tn5 neomycin/Kanamycin resistance gene and this allows Kanamycin selection in E.coli and neomycin selection in eukaryotic cells.

Appendix C: Antibodies

Antigen	Antibody(Clone)	Source	Host	Concentration	Applications
CD5 conjugated with PerCP	53-7.3	BioLegend	Rat IgG2a, κ	≤ 0.25 μg per 106 cells	FC
CD5 conjugated with PE/Cy5	53-7.3	BioLegend	Rat IgG2a, κ	≤0.25 μg per million cells	FC
CD19 conjugated with FITC	6D5	BioLegend	Rat IgG2a, κ	≤1.0 μg per million cells	FC
CD19 conjugated with PE	6D5	BioLegend	Rat IgG2a, κ	≤ 0.25 μg per 106 cells	FC
FITC Mouse Anti-Human CD20	2H7	BD Pharminge	Mouse IgG2b κ	0.2 μl per rection	FC
CD21/CD35 conjugated with PE/Cy7	7E9	BioLegend	Rat IgG2a, κ	≤0.25 μg per million cells	FC
CD23 conjugated with Pacific Blue™	B3B4	BioLegend	Rat IgG2a, κ	≤ 1.0 μg per 106 cells	FC
CD43 conjugated with FITC	S11	BioLegend	Rat IgG2b	≤0.25 μg per million cells	FC
CD24 conjugated with PerCP/Cy5.5	M1/69	BioLegend	Rat IgG2b, κ	≤0.25 μg per million cells	FC
CD27conjugated with Pacific Blue™	LG.3A10	BioLegend	Armenian Hamster IgG	≤0.25 μg per million cells	FC
CD45R/B220 conjugated with Alexa Fluor® 488	RA3-6B2	BioLegend	Rat IgG2a, κ	≤2.0 μg per million cells	FC
CD45R/B220 conjugated with PE	RA3-6B2	BioLegend	Rat IgG2a, κ	≤0.25 μg per million cells	FC
FITC Rat IgG2b, κ Isotype Ctrl	RTK4530	**BioLegend**	**Rat IgG2b, κ**	**same concentration as your primary antibody**	**FC**
Hemagglutinin Tag (HA)	HA.11 Clone 16B12	COVANCE	mouse monoclonal	1:2000	WB
Hemagglutinin Tag (HA)	C29F4	Cell Signalling	Rabbit monoclonal	1:1000 1:400	WB IHC
Ki67	ab833	abcam	Rabbit polyclonal	1:50	IHC
Living Colors® DsRed (mCherry)	PT3647-2	Clontech	mouse monoclonal	1:5000	WB
IgD conjugated with APC	11-26c.2a	BioLegend	Rat IgG2a, κ	≤0.06 μg per million cells	FC
IgM conjugated with APC/Cy7	RMM-1	BioLegend	Rat IgG2a, κ	≤1.0 μg per million cells	FC
Mouse IgM antibody		Biorbyt	Rabbit IgG	1:200-1000	IHC
PKC βII	F-7	SANTA CRUZ	mouse monoclonal	1:2000	WB
PKC βII	C-18	SANTA CRUZ	Rabbit Polyclonal	1:2000 1:3500	WB IHC

References

Abrams, S.T., et al. (2010) Vascular endothelial growth factor stimulates protein kinase CbetaII expression in chronic lymphocytic leukemia cells. *Blood,* **115,** 4447-4454.

Abrams, S.T., et al. (2007) B-cell receptor signaling in chronic lymphocytic leukemia cells is regulated by overexpressed active protein kinase C beta II. *Blood,* **109,** 1193-1201.

al-Katib, A., et al. (1993) Bryostatin 1-induced hairy cell features on chronic lymphocytic leukemia cells in vitro. *Exp Hematol,* **21,** 61-65.

Alkan, S., et al. (2005) Survival role of protein kinase C (PKC) in chronic lymphocytic leukemia and determination of isoform expression pattern and genes altered by PKC inhibition. *Am J Hematol,* **79,** 97-106.

Allen, J.C., et al. (2011) c-Abl regulates Mcl-1 gene expression in chronic lymphocytic leukemia cells. *Blood,* **117,** 2414-2422.

Altschul, S.F., et al. (1997) Gapped BLAST and PSI-BLAST: a new generation of protein database search programs. *Nucleic Acids Research,* **25,** 3389-3402.

Alvaro, V., et al. (1997) Ectopic expression of a mutant form of PKC alpha originally found in human tumors: Aberrant subcellular translocation and effects on growth control. *Oncogene,* **14,** 677-685.

Aziz, M.H., et al. (2010) Protein kinase Cvarepsilon mediates Stat3Ser727 phosphorylation, Stat3-regulated gene expression, and cell invasion in various human cancer cell lines through integration with MAPK cascade (RAF-1, MEK1/2, and ERK1/2). *Oncogene,* **29,** 3100-3109.

Balatti, V., et al. (2012) NOTCH1 mutations in CLL associated with trisomy 12. *Blood,* **119,** 329-331.

Barragan, M., et al. (2002) Involvement of protein kinase C and phosphatidylinositol 3-kinase pathways in the survival of B-cell chronic lymphocytic leukemia cells. *Blood,* **99,** 2969-2976.

Barragan, M., et al. (2006) Regulation of Akt/PKB by phosphatidylinositol 3-kinase-dependent and -independent pathways in B-cell chronic lymphocytic leukemia cells: role of protein kinase C{beta}. *J Leukoc Biol,* **80,** 1473-1479.

Bellosillo, B., et al. (1997) Involvement of CED-3/ICE proteases in the apoptosis of B-chronic lymphocytic leukemia cells. *Blood,* **89,** 3378-3384.

Bichi, R., et al. (2002) Human chronic lymphocytic leukemia modeled in mouse by targeted TCL1 expression. *Proc Natl Acad Sci U S A,* **99,** 6955-6960.

Binet, J.L., et al. (1977) A clinical staging system for chronic lymphocytic leukemia: prognostic significance. *Cancer,* **40,** 855-864.

Blobe, G.C., et al. (1993) Selective regulation of expression of protein kinase C beta isoenzymes occurs via alternative splicing. *J Biol Chem,* **268,** 10627-10635.

Bononi, A., et al. (2011) Protein kinases and phosphatases in the control of cell fate. *Enzyme Res,* **2011,** 329098.

Bos, N.A., et al. (1989) Serum immunoglobulin levels and naturally occurring antibodies against carbohydrate antigens in germ-free BALB/c mice fed chemically defined ultrafiltered diet. *Eur J Immunol,* **19,** 2335-2339.

Brognard, J. & Newton, A.C. (2008) PHLiPPing the switch on Akt and protein kinase C signaling. *Trends Endocrinol Metab,* **19,** 223-230.

Burger, J.A. & Chiorazzi, N. (2013) B cell receptor signaling in chronic lymphocytic leukemia. *Trends Immunol*.

Byrd, J.C., et al. (2001) UCN-01 induces cytotoxicity toward human CLL cells through a p53-independent mechanism. *Exp Hematol,* **29,** 703-708.

Calin, G.A., et al. (2008) MiR-15a and miR-16-1 cluster functions in human leukemia. *Proc Natl Acad Sci U S A,* **105,** 5166-5171.

Calin, G.A., et al. (2004) MicroRNA profiling reveals distinct signatures in B cell chronic lymphocytic leukemias. *Proc Natl Acad Sci U S A,* **101,** 11755-11760.

Cariappa, A., et al. (2001) The follicular versus marginal zone B lymphocyte cell fate decision is regulated by Aiolos, Btk, and CD21. *Immunity,* **14,** 603-615.

Carsetti, R., et al. (1995) Transitional B cells are the target of negative selection in the B cell compartment. *J Exp Med,* **181,** 2129-2140.

Chen, L., et al. (2005) ZAP-70 directly enhances IgM signaling in chronic lymphocytic leukemia. *Blood,* **105,** 2036-2041.

Chiorazzi, N. & Ferrarini, M. (2003) B cell chronic lymphocytic leukemia: lessons learned from studies of the B cell antigen receptor. *Annu Rev Immunol,* **21,** 841-894.

Chiorazzi, N. & Ferrarini, M. (2011) Cellular origin(s) of chronic lymphocytic leukemia: cautionary notes and additional considerations and possibilities. *Blood,* **117,** 1781-1791.

Chiorazzi, N., et al. (2005) Chronic lymphocytic leukemia. *N Engl J Med,* **352,** 804-815.

Chou, M.M., et al. (1998) Regulation of protein kinase C zeta by PI 3-kinase and PDK-1. *Current Biology,* **8,** 1069-1077.

Damle, R.N., et al. (2002) B-cell chronic lymphocytic leukemia cells express a surface membrane phenotype of activated, antigen-experienced B lymphocytes. *Blood,* **99,** 4087-4093.

Damle, R.N., et al. (1999) Ig V gene mutation status and CD38 expression as novel prognostic indicators in chronic lymphocytic leukemia. *Blood,* **94,** 1840-1847.

Dempsey, E.C., et al. (2000) Protein kinase C isozymes and the regulation of diverse cell responses. *Am J Physiol Lung Cell Mol Physiol,* **279,** L429-438.

Detjen, K.M., et al. (2000) Activation of protein kinase Calpha inhibits growth of pancreatic cancer cells via p21(cip)-mediated G(1) arrest. *J Cell Sci,* **113 (Pt 17),** 3025-3035.

Dutil, E.M., et al. (1994) In vivo regulation of protein kinase C by trans-phosphorylation followed by autophosphorylation. *J Biol Chem,* **269,** 29359-29362.

Endo, T., et al. (2007) BAFF and APRIL support chronic lymphocytic leukemia B-cell survival through activation of the canonical NF-kappaB pathway. *Blood,* **109,** 703-710.

Fischer, M., et al. (1997) Molecular single-cell analysis reveals that CD5-positive peripheral blood B cells in healthy humans are characterized by rearranged Vkappa genes lacking somatic mutation. *J Clin Invest,* **100,** 1667-1676.

Gallegos, L.L., et al. (2006) Targeting protein kinase C activity reporter to discrete intracellular regions reveals spatiotemporal differences in agonist-dependent signaling. *J Biol Chem,* **281,** 30947-30956.

Ganeshaguru, K., et al. (2002) Actions of the selective protein kinase C inhibitor PKC412 on B-chronic lymphocytic leukemia cells in vitro. *Haematologica,* **87,** 167-176.

Gao, T., et al. (2008) The phosphatase PHLPP controls the cellular levels of protein kinase C. *Journal of Biological Chemistry,* **283,** 6300-6311.

Giorgione, J.R., et al. (2006) Increased membrane affinity of the C1 domain of protein kinase Cdelta compensates for the lack of involvement of its C2 domain in membrane recruitment. *J Biol Chem,* **281,** 1660-1669.

Gould, C.M., et al. (2009) The Chaperones Hsp90 and Cdc37 Mediate the Maturation and Stabilization of Protein Kinase C through a Conserved PXXP Motif in the C-terminal Tail. *Journal of Biological Chemistry,* **284,** 4921-4935.

Griner, E.M. & Kazanietz, M.G. (2007) Protein kinase C and other diacylglycerol effectors in cancer. *Nat Rev Cancer,* **7,** 281-294.

Guertin, D.A., et al. (2006) Ablation in mice of the mTORC components raptor, rictor, or mLST8 reveals that mTORC2 is required for signaling to Akt-FOXO and PKC alpha but not S6K1. *Developmental Cell,* **11,** 859-871.

Hamano, Y., et al. (1998) Susceptibility alleles for aberrant B-1 cell proliferation involved in spontaneously occurring B-cell chronic lymphocytic leukemia in a model of New Zealand white mice. *Blood,* **92,** 3772-3779.

Hamblin, T.J., et al. (1999) Unmutated Ig V-H genes are associated with a more aggressive form of chronic lymphocytic leukemia. *Blood,* **94,** 1848-1854.

Hansra, G., et al. (1999) Multisite dephosphorylation and desensitization of conventional protein kinase C isotypes. *Biochem J,* **342 (Pt 2),** 337-344.

Hardy, R.R. (2006) B-1 B cell development. *J Immunol,* **177,** 2749-2754.

Hardy, R.R. & Hayakawa, K. (1991) A developmental switch in B lymphopoiesis. *Proc Natl Acad Sci U S A,* **88,** 11550-11554.

Hardy, R.R. & Hayakawa, K. (2001) B cell development pathways. *Annu Rev Immunol,* **19,** 595-621.

Herling, M., et al. (2009) High TCL1 levels are a marker of B-cell receptor pathway responsiveness and adverse outcome in chronic lymphocytic leukemia. *Blood,* **114,** 4675-4686.

Hewamana, S., et al. (2008) The NF-kappaB subunit, Rel A, is associated with in vitro survival and clinical disease progression in chronic lymphocytic leukaemia and represents a promising therapeutic target. *Br J Haematol,* **141,** 118-119.

Holler, C., et al. (2009) PKC beta is essential for the development of chronic lymphocytic leukemia in the TCL1 transgenic mouse model: validation of PKC beta as a therapeutic target in chronic lymphocytic leukemia. *Blood,* **113,** 2791-2794.

Hua Gu , K.R. (2004) *B Cell Protocols.*

Ikenoue, T., et al. (2008) Essential function of TORC2 in PKC and Akt turn motif phosphorylation, maturation and signalling. *EMBO J,* **27,** 1919-1931.

Janeway., C.A. 5th edition *Immunobology. New York: Garland Science; 2001*

Jiffar, T., et al. (2004) PKC alpha mediates chemoresistance in acute lymphoblastic leukemia through effects on Bcl2 phosphorylation. *Leukemia,* **18,** 505-512.

Joshi, T.M.N.a.S.S. (2010) The Etiology of Chronic Lymphocytic Leukemia: Another Look at the
Relationship Between B1 cells and CLL *The Open Leukemia Journa,* **3, 69-73**.

Kang, S.W., et al. (2001) PKCbeta modulates antigen receptor signaling via regulation of Btk membrane localization. *EMBO J,* **20,** 5692-5702.

Kantor, A.B., et al. (1992) Differential development of progenitor activity for three B-cell lineages. *Proc Natl Acad Sci U S A,* **89,** 3320-3324.

Kawakami, Y., et al. (2000) Regulation of protein kinase CbetaI by two protein-tyrosine kinases, Btk and Syk. *Proc Natl Acad Sci U S A,* **97,** 7423-7428.

Keranen, L.M., et al. (1995) Protein kinase C is regulated in vivo by three functionally distinct phosphorylations. *Current Biology,* **5,** 1394-1403.

Kerner, J.D., et al. (1995) Impaired expansion of mouse B cell progenitors lacking Btk. *Immunity,* **3,** 301-312.

Khan, W.N., et al. (1995) Defective B-Cell Development and Function in Btk-Deficient Mice. *Immunity,* **3,** 283-299.

Kim, K.J., et al. (1979) Establishment and characterization of BALB/c lymphoma lines with B cell properties. *J Immunol,* **122,** 549-554.

Kitada, S., et al. (1999) Bryostatin and CD40-ligand enhance apoptosis resistance and induce expression of cell survival genes in B-cell chronic lymphocytic leukaemia. *Br J Haematol,* **106,** 995-1004.

Kitada, S., et al. (2000) Protein kinase inhibitors flavopiridol and 7-hydroxy-staurosporine down-regulate antiapoptosis proteins in B-cell chronic lymphocytic leukemia. *Blood,* **96,** 393-397.

Klein, U. & Dalla-Favera, R. (2010) New insights into the pathogenesis of chronic lymphocytic leukemia. *Seminars in Cancer Biology,* **20,** 377-383.

Klein, U., et al. (2010) The DLEU2/miR-15a/16-1 cluster controls B cell proliferation and its deletion leads to chronic lymphocytic leukemia. *Cancer Cell,* **17,** 28-40.

Klein, U., et al. (2001) Gene expression profiling of B cell chronic lymphocytic leukemia reveals a homogeneous phenotype related to memory B cells. *J Exp Med,* **194,** 1625-1638.

Kondo, M., et al. (1997) Identification of clonogenic common lymphoid progenitors in mouse bone marrow. *Cell,* **91,** 661-672.

Kozak, M. (2005) A second look at cellular mRNA sequences said to function as internal ribosome entry sites. *Nucleic Acids Research,* **33,** 6593-6602.

Lam, K.P. & Rajewsky, K. (1999) B cell antigen receptor specificity and surface density together determine B-1 versus B-2 cell development. *J Exp Med,* **190,** 471-477.

Lee, G., et al. (1989) Normal B cell precursors responsive to recombinant murine IL-7 and inhibition of IL-7 activity by transforming growth factor-beta. *J Immunol,* **142,** 3875-3883.

Leitges, M., et al. (1996) Immunodeficiency in protein kinase cbeta-deficient mice. *Science,* **273,** 788-791.

Li, T., et al. (1995) Activation of Bruton's tyrosine kinase (BTK) by a point mutation in its pleckstrin homology (PH) domain. *Immunity,* **2,** 451-460.

Lichter, P. (2010) All You Need Is a Mir-acle: The Role of Nontranslated RNAs in the Suppression of B Cell Chronic Lymphocytic Leukemia. *Cancer Cell,* **17,** 3-4.

Loffert, D.e.a. (1997) PCR: Effects of template quality. *Qiagen News,* **1**.

Longo, P.G., et al. (2007) The Akt signaling pathway determines the different proliferative capacity of chronic lymphocytic leukemia B-cells from patients with progressive and stable disease. *Leukemia,* **21,** 110-120.

Lu, D., et al. (2004) Activation of the Wnt signaling pathway in chronic lymphocytic leukemia. *Proc Natl Acad Sci U S A,* **101,** 3118-3123.

Lutzny G, K.T. (2013) Protein kinase c-β-dependent activation of NF-κB in stromal cells is indispensable for the survival of chronic lymphocytic leukemia B cells in vivo. *Cancer Cell,* **23,** 77-92.

Maas, A., et al. (1999) Early arrest in B cell development in transgenic mice that express the E41K Bruton's tyrosine kinase mutant under the control of the CD19 promoter region. *J Immunol,* **162,** 6526-6533.

Maas, A. & Hendriks, R.W. (2001) Role of Bruton's tyrosine kinase in B cell development. *Dev Immunol,* **8,** 171-181.

Martin, F., et al. (2001) Marginal zone and B1 B cells unite in the early response against T-independent blood-borne particulate antigens. *Immunity,* **14,** 617-629.

Martin, P., et al. (2002) Role of zeta PKC in B-cell signaling and function. *EMBO J,* **21,** 4049-4057.

Matsumoto, M., et al. (2001) Inhibition of insulin-induced activation of Akt by a kinase-deficient mutant of the epsilon isozyme of protein kinase C. *J Biol Chem,* **276,** 14400-14406.

Mecklenbrauker, I., et al. (2004) Regulation of B-cell survival by BAFF-dependent PKCdelta-mediated nuclear signalling. *Nature,* **431,** 456-461.

Messmer, B.T., et al. (2004) Multiple distinct sets of stereotyped antigen receptors indicate a role for antigen in promoting chronic lymphocytic leukemia. *J Exp Med,* **200,** 519-525.

Michie, A.M. & Nakagawa, R. (2005) The link between PKC alpha regulation and cellular transformation. *Immunology Letters,* **96,** 155-162.

Michie, A.M., et al. (2007) Murine models for chronic lymphocytic leukaemia. *Biochem Soc Trans,* **35,** 1009-1012.

Montecino-Rodriguez, E. & Dorshkind, K. (2011) Formation of B-1 B cells from neonatal B-1 transitional cells exhibits NF-kappaB redundancy. *J Immunol,* **187,** 5712-5719.

Montecino-Rodriguez, E. & Dorshkind, K. (2012) B-1 B cell development in the fetus and adult. *Immunity,* **36,** 13-21.

Munoz-Chapuli, R., et al. (1999) Differentiation of hemangioblasts from embryonic mesothelial cells? A model on the origin of the vertebrate cardiovascular system. *Differentiation,* **64,** 133-141.

Munzert, G., et al. (2002) Tumor necrosis factor receptor-associated factor 1 gene overexpression in B-cell chronic lymphocytic leukemia: analysis of NF-kappa B/Rel-regulated inhibitors of apoptosis. *Blood,* **100,** 3749-3756.

Murray, N.R., et al. (1999) Overexpression of protein kinase C betaII induces colonic hyperproliferation and increased sensitivity to colon carcinogenesis. *J Cell Biol,* **145,** 699-711.

Nakagawa, R., et al. (2006) Subversion of protein kinase C alpha signaling in hematopoietic progenitor cells results in the generation of a B-cell chronic lymphocytic leukemia-like population in vivo. *Cancer Res,* **66,** 527-534.

Narducci, M.G., et al. (2000) Regulation of TCL1 expression in B- and T-cell lymphomas and reactive lymphoid tissues. *Cancer Res,* **60,** 2095-2100.

Naylor, T.L., et al. (2011) Protein kinase C inhibitor sotrastaurin selectively inhibits the growth of CD79 mutant diffuse large B-cell lymphomas. *Cancer Res,* **71,** 2643-2653.

Neill, G.W., et al. (2003) Loss of protein kinase C alpha expression may enhance the tumorigenic potential of Gli1 in basal cell carcinoma. *Cancer Res,* **63,** 4692-4697.

Newton, A.C. (2003) Regulation of the ABC kinases by phosphorylation: protein kinase C as a paradigm. *Biochemical Journal,* **370,** 361-371.

Newton, A.C. (2010) Protein kinase C: poised to signal. *American Journal of Physiology-Endocrinology and Metabolism,* **298,** E395-E402.

Numaga, T., et al. (2010) Ca2+ influx and protein scaffolding via TRPC3 sustain PKCbeta and ERK activation in B cells. *J Cell Sci,* **123,** 927-938.

Ono, Y., et al. (1986) Two types of complementary DNAs of rat brain protein kinase C. Heterogeneity determined by alternative splicing. *FEBS Lett,* **206,** 347-352.

Oppezzo, E.b.D.P. (2012) *Chronic Lymphocytic Leukemia.* In Tech, Chapters published.

Oppezzo, P. & Dighiero, G. (2013) "Role of the B-cell receptor and the microenvironment in chronic lymphocytic leukemia". *Blood Cancer J,* **3,** e149.

Oster, H. & Leitges, M. (2006) Protein kinase c alpha but not PKC zeta suppresses intestinal tumor formation in Apc(Min/+) mice. *Cancer Res,* **66,** 6955-6963.

Patel, N.A., et al. (2005) Molecular and genetic studies imply Akt-mediated signaling promotes protein kinase CbetaII alternative splicing via phosphorylation of serine/arginine-rich splicing factor SRp40. *J Biol Chem,* **280,** 14302-14309.

Patke, A., et al. (2006) BAFF controls B cell metabolic fitness through a PKC beta- and Akt-dependent mechanism. *Journal of Experimental Medicine,* **203,** 2551-2562.

Paul, W.E. (2003) *Fundamental immunology.* Lippincott Williams & Wilkins, Philadelphia.

Pekarsky, Y., et al. (2000) Tcl1 enhances Akt kinase activity and mediates its nuclear translocation. *Proc Natl Acad Sci U S A,* **97,** 3028-3033.

Pelletier, J. & Sonenberg, N. (1988) Internal initiation of translation of eukaryotic mRNA directed by a sequence derived from poliovirus RNA. *Nature,* **334,** 320-325.

Pepper, C., et al. (2008) Mcl-1 expression has in vitro and in vivo significance in chronic lymphocytic leukemia and is associated with other poor prognostic markers. *Blood,* **112,** 3807-3817.

Phillips, J.A., et al. (1992) The NZB mouse as a model for chronic lymphocytic leukemia. *Cancer Res,* **52,** 437-443.

Pillai, S. & Cariappa, A. (2009) The follicular versus marginal zone B lymphocyte cell fate decision. *Nat Rev Immunol,* **9,** 767-777.

Planelles, L., et al. (2004) APRIL promotes B-1 cell-associated neoplasm. *Cancer Cell,* **6,** 399-408.

Rai, K.R., et al. (2000) Fludarabine compared with chlorambucil as primary therapy for chronic lymphocytic leukemia. *N Engl J Med,* **343,** 1750-1757.

Raveche, E.S., et al. (2007) Abnormal microRNA-16 locus with synteny to human 13q14 linked to CLL in NZB mice. *Blood,* **109,** 5079-5086.

Ringshausen, I., et al. (2006) Mechanisms of apoptosis-induction by rottlerin: therapeutic implications for B-CLL. *Leukemia,* **20,** 514-520.

Ringshausen, I., et al. (2002) Constitutively activated phosphatidylinositol-3 kinase (PI-3K) is involved in the defect of apoptosis in B-CLL: association with protein kinase C8. *Blood,* **100,** 3741-3748.

Rodriguez-Vicente, A.E., et al. (2013) Chronic lymphocytic leukemia: a clinical and molecular heterogenous disease. *Cancer Genet,* **206,** 49-62.

Rossi, D., et al. (2013) Association between molecular lesions and specific B-cell receptor subsets in chronic lymphocytic leukemia. *Blood,* **121,** 4902-4905.

Rozman, C. & Montserrat, E. (1995) Chronic lymphocytic leukemia. *N Engl J Med,* **333,** 1052-1057.

Saito, N., et al. (2002) The family of protein kinase C and membrane lipid mediators. *J Diabetes Complications,* **16,** 4-8.

Sambrook (2000) *Molecular Cloning: A Laboratory Manual,.*

Santanam, U., et al. (2010) Chronic lymphocytic leukemia modeled in mouse by targeted miR-29 expression. *Proc Natl Acad Sci U S A,* **107,** 12210-12215.

Schechtman, D. & Mochly-Rosen, D. (2001) Adaptor proteins in protein kinase C-mediated signal transduction. *Oncogene,* **20,** 6339-6347.

Seifert, M. & Kuppers, R. (2009) Molecular footprints of a germinal center derivation of human IgM+(IgD+)CD27+ B cells and the dynamics of memory B cell generation. *J Exp Med,* **206,** 2659-2669.

Seifert, M., et al. (2012) Cellular origin and pathophysiology of chronic lymphocytic leukemia. *J Exp Med,* **209,** 2183-2198.

Shaw, A.C., et al. (1999) Activated Ras signals developmental progression of recombinase-activating gene (RAG)-deficient pro-B lymphocytes. *Journal of Experimental Medicine,* **189,** 123-129.

Shinohara, H., et al. (2007) IkappaB kinase beta-induced phosphorylation of CARMA1 contributes to CARMA1 Bcl10 MALT1 complex formation in B cells. *Journal of Experimental Medicine,* **204,** 3285-3293.

Shinohara, H., et al. (2005) PKC beta regulates BCR-mediated IKK activation by facilitating the interaction between TAK1 and CARMA1. *Journal of Experimental Medicine,* **202,** 1423-1431.

Snowden, R.T., et al. (2003) Bisindolylmaleimide IX is a potent inducer of apoptosis in chronic lymphocytic leukaemic cells and activates cleavage of Mcl-1. *Leukemia,* **17,** 1981-1989.

Southern, E.M. (1975) Detection of specific sequences among DNA fragments separated by gel electrophoresis. *J Mol Biol,* **98,** 503-517.

Stevenson, F.K. & Caligaris-Cappio, F. (2004) Chronic lymphocytic leukemia: revelations from the B-cell receptor. *Blood,* **103,** 4389-4395.

Tan, S.L. & Parker, P.J. (2003) Emerging and diverse roles of protein kinase C in immune cell signalling. *Biochem J,* **376,** 545-552.

Teh, C.E., et al. (2013) Heterozygous mis-sense mutations in Prkcb as a critical determinant of anti-polysaccharide antibody formation. *Genes and Immunity,* **14,** 223-233.

Thomas, A., et al. (2004) Bryostatin induces protein kinase C modulation, Mcl-1 up-regulation and phosphorylation of Bcl-2 resulting in cellular differentiation and resistance to drug-induced apoptosis in B-cell chronic lymphocytic leukemia cells. *Leuk Lymphoma,* **45,** 997-1008.

Totterman, T.H., et al. (1980) Phorbol ester-induced differentiation of chronic lymphocytic leukaemia cells. *Nature,* **288,** 176-178.

Varnai, P., et al. (1999) Phosphatidylinositol 3-kinase-dependent membrane association of the Bruton's tyrosine kinase pleckstrin homology domain visualized in single living cells. *J Biol Chem,* **274,** 10983-10989.

Weill, J.C., et al. (2009) Human marginal zone B cells. *Annu Rev Immunol,* **27,** 267-285.

Wesemann, D.R., et al. (2013) Microbial colonization influences early B-lineage development in the gut lamina propria. *Nature,* **501,** 112-115.

Wiestner, A., et al. (2003) ZAP-70 expression identifies a chronic lymphocytic leukemia subtype with unmutated immunoglobulin genes, inferior clinical outcome, and distinct gene expression profile. *Blood,* **101,** 4944-4951.

Witt, C.M., et al. (2003) Activated Notch2 potentiates CD8 lineage maturation and promotes the selective development of B1 B cells. *Mol Cell Biol,* **23,** 8637-8650.

Wong, S.C., et al. (2002) Peritoneal CD5(+) B-1 cells have signaling properties similar to tolerant B cells. *Journal of Biological Chemistry,* **277,** 30707-30715.

Yan, X.J., et al. (2006) B cell receptors in TCL1 transgenic mice resemble those of aggressive, treatment-resistant human chronic lymphocytic leukemia. *Proc Natl Acad Sci U S A,* **103,** 11713-11718.

Zapata, J.M., et al. (2004) TNF receptor-associated factor (TRAF) domain and Bcl-2 cooperate to induce small B cell lymphoma/chronic lymphocytic leukemia in transgenic mice. *Proc Natl Acad Sci U S A,* **101,** 16600-16605.

Zapata, J.M., et al. (2007) Targeting TRAfs for therapeutic intervention. *Adv Exp Med Biol,* **597,** 188-201.

Zenz, T., et al. (2010) From pathogenesis to treatment of chronic lymphocytic leukaemia. *Nat Rev Cancer,* **10,** 37-50.

Zhang, Z., et al. (2000) A greedy algorithm for aligning DNA sequences. *Journal of Computational Biology,* **7,** 203-214.

zum Buschenfelde, C.M., et al. (2010) Recruitment of PKC-betaII to lipid rafts mediates apoptosis-resistance in chronic lymphocytic leukemia expressing ZAP-70. *Leukemia,* **24,** 141-152.

Zwiebel, J.A. & Cheson, B.D. (1998) Chronic lymphocytic leukemia: staging and prognostic factors. *Semin Oncol,* **25,** 42-59.